Friedrich-Schiller-Universität Jena

Chemisch-Geowissenschaftliche Fakultät

Anthraquinone based redox-active polymers for organic batteries

Dissertation

(kumulativ)

zur Erlangung des akademischen Grades

doctor rerum naturalium (Dr. rer. nat.)

vorgelegt dem Rat der Chemisch-Geowissenschaftlichen Fakultät

der Friedrich-Schiller-Universität Jena

von Dipl.-Chem. Daniel Schmidt

geboren am 13.10.1986 in Suhl

Gutachter:

1. Prof. Dr. Ulrich S. Schubert, Friedrich-Schiller-Universität Jena
2. Prof. Dr. Philipp Adelhelm, Friedrich-Schiller-Universität Jena

Tag der öffentlichen Verteidigung: 06.07.2016

Table of Contents

Documentation of authorship 4

1. Introduction 8

2. Photo-rechargeable electric energy storage systems 12

3. Redox-active polymers for organic batteries 19

3.1. Synthesis and characterization of poly(*N*,*N'*-dicyanoanthraquinone diimine) as a new redox-active polymer 19

3.2. Poly(exTTF): Utilization of a new redox-active material as cathode material in lithium-organic batteries 24

4. Tuning the redox potential by an unsymmetrical substitution of anthraquinone 28

4.1. Investigations on redox-active polymers based on 10-(1,3-dithiol-2-ylidene)anthracen-9(10*H*)-one derivatives 28

4.2. Application of poly[*N*-(10-oxo-2-vinylanthracen-9(10*H*)-ylidene)cyanamide] as cathode material for lithium-organic batteries 34

5. Summary 40

6. Zusammenfassung 43

7. References 46

List of abbreviations 51

Curriculum vitae 54

Publication list 55

Acknowledgements / Danksagung 57

Declaration of authorship / Selbstständigkeitserklärung 59

Publications **P1**-**P5** 60

Documentation of authorship

This section contains a list of individual authors' contributions to the publications reprinted in this thesis.

P1) "Photo-rechargeable electric energy storage systems" D. Schmidt,[1] M. D. Hager,[2] U. S. Schubert,[3] *Adv. Energy Mater.* **2016**, 6: 1500369. DOI: 10.1002/aenm.201500369.			
Autor	1	2	3
Conception of the manuscript	X		
Preparation of the manuscript	X		
Correction of the manuscript		X	X
Supervision of D. Schmidt		X	X
Proposal for crediting publication equivalents	0.5		

P2) "Poly(DCAQI): Synthesis and characterization of a new redox-active polymer" D. Schmidt,[1] B. Häupler,[2] M. D. Hager,[3] U. S. Schubert,[4] *J. Polym. Sci., Part A: Polym. Chem.* **2016**, *54*, 1998–2003.				
Autor	1	2	3	4
Conceptual contribution	X			
Synthesis of monomers and polymers	X			
Cyclic voltammetry	X	X		
Preparation of the manuscript	X			
Correction of the manuscript		X	X	X
Supervision of D. Schmidt			X	X
Proposal for crediting publication equivalents	1.0			

P3) "Poly(exTTF): A novel redox-active polymer as active material for Li-organic batteries"

B. Häupler,[1] R. Burges,[2] C. Friebe,[3] T. Janoschka,[4] D. Schmidt,[5] A. Wild,[6] U. S. Schubert,[7] *Macromol. Rapid Comm.* **2014**, *35*, 1367–1371.

Autor	1	2	3	4	5	6	7
Synthesis of polymers	X	X			X		
Electrochemical investigations	X		X	X			
Electrode preparations	X						
Battery performance investigations	X			X			
Preparation of the manuscript	X						
Correction of the manuscript			X		X	X	X
Supervision of D. Schmidt						X	X
Proposal for crediting publication equivalents	1.0				0.5		

This publication was also discussed in the Dissertation of Bernhard Häupler, Friedrich Schiller University, 2015 in Chapter 4.2.

P4) "Synthesis and characterization of new redox-active polymers based on 10-(1,3-dithiol-2-ylidene)anthracen-9(10H)-one derivatives"

D. Schmidt,[1] B. Häupler,[2] C.Friebe,[3] M. D. Hager,[4] U. S. Schubert,[5] *Polymer* **2015**, *68*, 321–327.

Autor	1	2	3	4	5
Synthesis	X				
Cyclic voltammetry	X	X			
UV-vis-NIR spectroelectrochemical experiments	X		X		
Preparation of the manuscript	X				
Correction of the manuscript		X	X	X	X
Supervision of D. Schmidt				X	X
Proposal for crediting publication equivalents	1.0				

P5) "Poly[*N*-(10-oxo-2-vinylanthracen-9(10H)-ylidene)cyanamide] as a novel cathode material for Li-organic batteries" D. Schmidt,[1] B. Häupler,[2] C. Stolze,[3] M. D. Hager,[4] U. S. Schubert,[5] *J. Polym. Sci., Part A: Polym. Chem.* **2015**, *53*, 2517–2523.					
Autor	1	2	3	4	5
Synthesis of monomer polymers	X				
Electrochemical investigations	X	X			
Electrode preparations	X				
Battery performance investigations	X	X			
Impedance spectroscopy			X		
Preparation of the manuscript	X		X		
Correction of the manuscript		X	X	X	X
Supervision of D. Schmidt				X	X
Proposal for crediting publication equivalents	1.0				

Jena, den 18.07.2016

Erklärung zu den Eigenanteilen des Promovenden/der Promovendin sowie der weiteren Doktoranden/Doktorandinnen als Koautoren an den Publikationen und Zweitpublikationsrechten bei einer kumulativen Dissertation

Für alle in dieser kumulativen Dissertation verwendeten Manuskripte liegen die notwendigen Genehmigungen der Verlage („Reprint permissions") für die Zweitpublikation vor.

Die Co-Autoren der in dieser kumulativen Dissertation verwendeten Manuskripte sind sowohl über die Nutzung, als auch über die oben angegebenen Eigenanteile der weiteren Doktoranden/Doktorandinnen als Koautoren an den Publikationen und Zweitpublikationsrechten bei einer kumulativen Dissertation informiert und stimmen dem zu (es wird empfohlen, diese grundsätzliche Zustimmung bereits mit Einreichung der Veröffentlichung einzuholen bzw. die Gewichtung der Anteile parallel zur Einreichung zu klären).

Die Anteile der Promovenden/der Promovendinnen sowie der weiteren Doktoranden/Doktorandinnen als Koautoren an den Publikationen und Zweitpublikationsrechten bei einer kumulativen Dissertation sind in der Anlage aufgeführt.

Daniel Schmidt	18.07.2016	Jena

Ich bin mit der Abfassung der Dissertation als publikationsbasiert, d.h. kumulativ, einverstanden und bestätige die vorstehenden Angaben. Eine entsprechend begründete Befürwortung mit Angabe des wissenschaftlichen Anteils des Doktoranden/der Doktorandin an den verwendeten Publikationen werde ich parallel an den Rat der Fakultät der Chemisch-Geowissenschaftlichen Fakultät richten.

Prof. Dr. Ulrich S. Schubert	18.07.2016	Jena

1. Introduction

The utilization and application of mobile and portable electronic devices in our modern society becomes more and more present in our daily life.[1] Additionally, the demand for smaller, thinner and sometimes even flexible devices has strongly increased. A new generation of portable electronic devices is under current development, such as smart packaging, functional smart clothes or the “Internet of Things”, where every small electronic device is connected to the internet.[2,3] For all these devices and applications a rechargeable energy source is mandatory. Secondary batteries represent one suitable possibility, where the required energy can be released independently from a stationary energy source, which is obligatory, in particular for mobile devices.

An additional feature is the combination of secondary batteries with solar cells, the so called solar batteries, which in theory enable independent recharging of the secondary battery using the power of the sun light, resulting in an independently rechargeable portable electronical energy storage device.[4,5] Dependent on the aimed application, battery systems need to meet the following demands: High capacity, high cell voltage and a good charge/discharge performance as well as safety, low cost, low weight, sustainability and environmental friendliness.[6] In particular, small and thin mobile devices (*i.e.*, portable electronics), smart packaging or functional textiles require thin, lightweight and flexible battery systems.[7] The technology for these systems is already investigated and the concept of batteries is based on a simple principle: Two electrodes with different electrochemical potentials are connected by an ionically conductive electrolyte.[1] However, current batteries are the limiting part to obtain thin, light-weight and flexible devices. Present battery systems such as nickel-metal hydride or lithium-ion batteries have conquered the market of energy storage systems mainly due to their electrochemical properties such as high capacity and promising charge/discharge stability. However, the fabrication of flexible secondary batteries reaches the limits of the current systems due to their hard and brittle electrode materials. Additionally, these materials mainly consist of sometimes toxic metals, which are produced by mining in a limited availability and are difficult to dispose.[8] A promising approach to overcome these drawbacks is the utilization of organic compounds as electrode materials.

The setup of an organic battery is identical to the common battery setup: It contains two electrodes, separated by an ion-conducting electrolyte. In particular, the cathode of organic batteries consists of a material, which possess a high redox potential and the anode is built of a material featuring a lower redox potential. The potential gap of the active electrode materials results in the specific cell voltage of the battery. The electrolyte is an ionically conductive material (*e.g.*, a solution of $LiClO_4$ or $LiPF_6$ in acetonitrile or organic carbonates), which provides the charge balance (Figure 1.1). During the charging process an external current forces the oxidation of the cathode material as well as the reduction of the anode material. The ions of the electrolyte rebalance the emerging charges. During discharging, the opposite process is taking place, whereas the anode is oxidized and the cathode is reduced.[9]

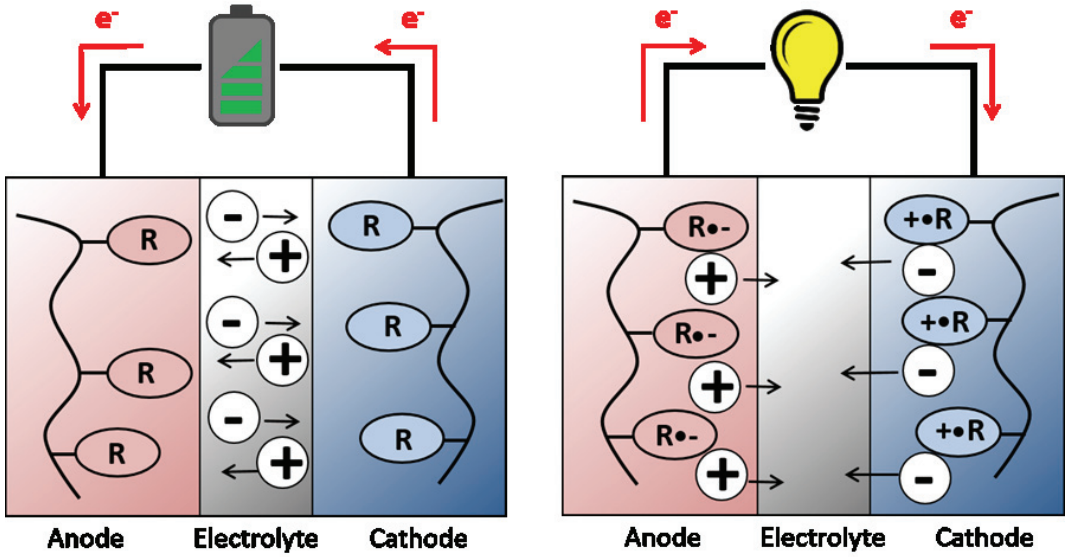

Figure 1.1: Schematic representation of the setup of an organic battery consisting of cathode, anode and electrolyte.

The utilization of organic compounds as active materials in batteries features many advantages such as their production in low-temperature processes, in special cases even from recycled[10] or renewable resources, and the materials can be processed by roll-to-roll technologies, resulting in high flexibility, low toxicity and low weight.[7] Furthermore, the redox potential of the electrode materials and, as a consequence, the cell potential can be tailored by the choice of the appropriate redox system. Up to now, numerous different redox-active compounds have been applied as active electrode materials, such as stable organic radicals[11,12] or carbonyl

compounds.[13] In particular, anthraquinonide structures are of high interest. Due to their two-electron redox reaction a promising charge to mass ratio is obtained, resulting in comparably high theoretical capacities. In general, 1,2-diones possess higher redox potentials than 1,4-diones. Additionally, the potentials can be tailored by two major strategies. The first approach is the introduction of appropriate substituents to influence the redox potential. Thereby, electron donating/withdrawing groups such as cyano,[14] chloro,[14] hydroxyl,[15] lithoxy,[16,17] fluorinated and non-fluorinated alkyl and alkoxy groups,[15,18–20] thiophene,[21] pyridine,[22] pyrazine[22] and lithium *resp.* sodium salts of carboxylic[23] or sulfonic acids are often used.[24] The second procedure is the modification of the redox-active carbonyl group to dicyanomethane[25,26] or 1,3-dithiolane groups, whose redox mechanisms are based on one two-electron reaction.[27]

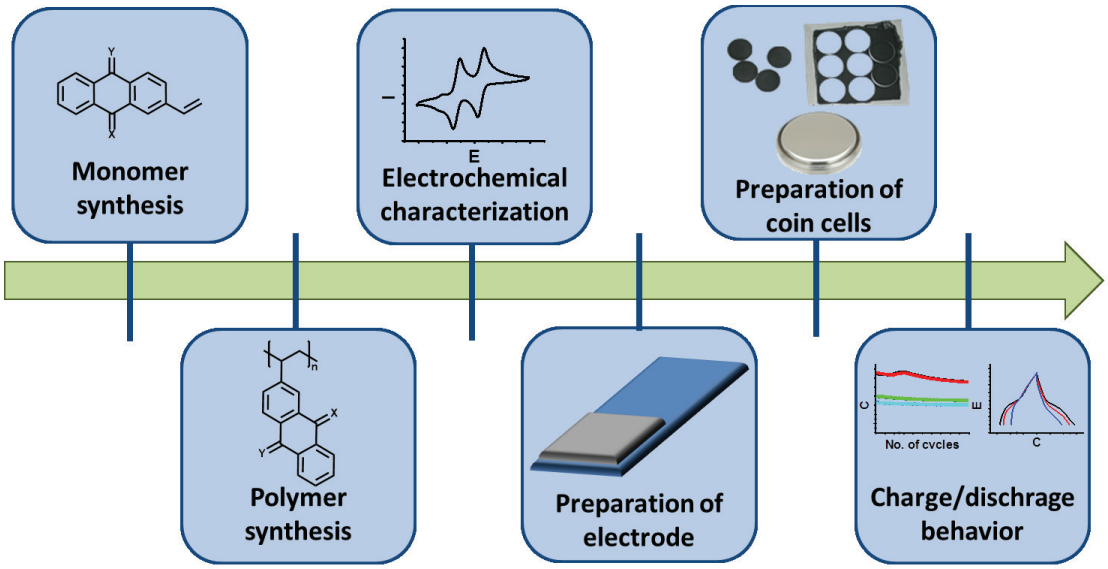

Figure 1.2: Schematic overview of the key steps, which are accomplished in this thesis.

However, the application of organic compounds as active electrode material requires the insolubility of all occurring redox states of the active material in the applied electrolytes. The most promising and straightforward approach, which is also applied in this thesis, is the incorporation of the redox-active units into a polymeric environment, resulting in an insoluble, but swellable electro-active material.[28,29]

The goal of this thesis is the synthesis of new redox-active monomers and polymers as well as their electrochemical characterization. The suitable polymers should be used as active material

in a composite electrode for organic batteries, which charge/discharge behavior will be investigated (Figure 1.2).

The investigated polymers are based on anthraquinone derivatives, whereby the carbonyl groups are transformed to oxidizable or other reducible moieties and their influence will be analyzed. In Chapter 3, anthraquinone derivative are shown, where both carbonyl groups are substituted with another reducible moiety (Chapter 3.1) and an oxidizable group (Chapter 3.2). The influence of the unsymmetrically substitution of the carbonyl groups on the electrochemical behavior is shown in Chapter 4. By the modification of the carbonyl groups with both an oxidizable group and a reducible group leads to bipolar compounds with interesting electrochemical behavior (Chapter 4.1). The redox potentials of the monomer and the polymer can be fine-tuned by a modification of one carbonyl group by another reducible group (Chapter 4.2).

2. Photo-rechargeable electric energy storage systems

Parts of this chapter have been published in P1) D. Schmidt, M. D. Hager, U. S. Schubert, *Adv. Energy Mater.* **2016**, 6: 1500369. DOI: 10.1002/aenm.201500369.

As described in Chapter 1, the main challenge of the utilization of renewable energy sources such as solar or wind energy is the storage of the generated electricity to compensate the fluctuating availability of the energy sources and the actual energy demand. One of the most powerful, efficient and environmental friendly energy sources is the sun, which provides power in unlimited quantity with no running costs and no waste materials are produced.[30–34] Every hour, about 100,000 TW of solar power are received by the earth's surface, which is more power than humans need in an entire year.[35,36] The key technology is the creation of independent electrical energy sources by the combination of solar cells and effective energy storage systems, *e.g.*, batteries or supercapacitors.[4,34,37–41] Usually, the generated solar energy is stored by external batteries, *e.g.*, lithium ion or nickel/metal hydride batteries, which are connected to the solar cell(s) by wires.[40,42,43] Unfortunately, due to the relatively long distance between both parts the energy storage efficiency is low.[40] One approach to avoid this problem is the merging of the photo conversion and the energy storage system in one device. Thereby, the stored energy can be released and used all day even if the sun is not shining.[31,44,45] Many types of electrochemical storage applications such as rechargeable batteries, electrochemical supercapacitors as well as redox flow batteries (RFB) are available, which can be combined with charge generation assemblies like dye-sensitized solar cells (DSSC) or organic photovoltaics (OPV).[11,45–47]

A solar rechargeable battery generates electric energy from the sun light, which is directly stored by an integrated storage.[48] These devices consist of a photoanode, a counter electrode as well as a charge storage electrode (Figure 2.1). Under light illumination of the photoanode, the photo active material is excited to form an electron hole pair. The electrons move to the charge storage electrode, which will be negatively charged, and are stored in the electrode. The holes in the photoanode are counterbalanced by electrons of the counter electrode and the device is charged. During the discharging process the electrons move back from the charge storage electrode to the counter electrode. A membrane separates the counter electrode from the charge storage electrode and provides the counterbalance.

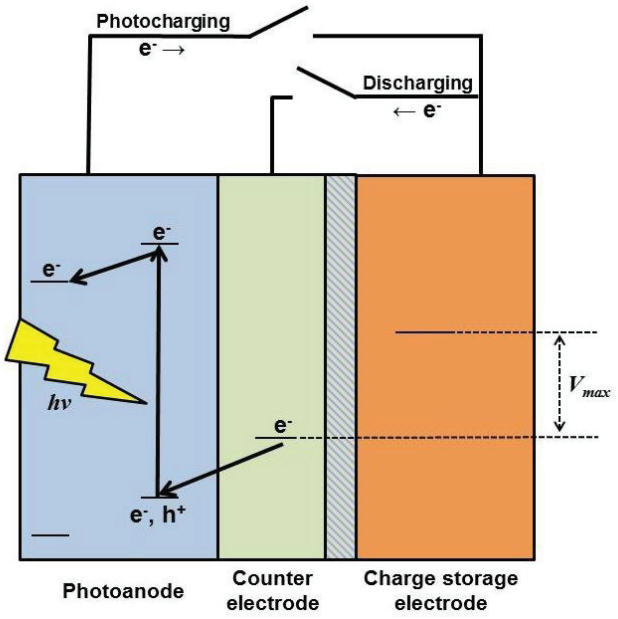

Figure 2.1: Schematic representation of the setup of a solar rechargeable battery, consisting of a photoanode, in which the charge carriers are generated, a charge storage electrode and a counter electrode; both are utilized for energy storage.

The combination of a supercapacitor and a DSSC is the most frequently investigated hybrid device in the field of photo-rechargeable energy storage systems, resulting in an energy-storable dye-sensitized solar cell (ES-DSSC). Supercapacitors can be utilized for flexible electronic systems and are distinguished by high power output densities, high specific capacitance, fast charge/discharge rates, as well as long lifetimes.[49–51] DSSCs are very efficient, environmental friendly and can be fabricated by roll-to-roll processes, which leads to light-weight and flexible devices.[52–54] They are furthermore very powerful even under diffuse and low intensity light conditions.[55] A wide range of different materials are suitable for capacitor devices. Miyasaka *et al.* investigated an ES-DSSC with a two-electrode system using activated carbon. The energy is in this case directly stored as double-layer charges. In the charged state, the photocapacitor achieved a voltage value of 0.45 V and a discharge capacity of 75 mC/cm^2 due to the incorporation of LiI into the TiO_2 layer. Due to the utilization of LiI, the values are 15 times higher than the result of the LiI-free ES-DSSC.[56] An improvement revealed a lower internal resistance by the utilization of a three-electrode photocapacitor, resulting in a five times larger energy output.[57] Carbon nanotubes (CNT) represent other important materials for photo chargeable batteries. DSSC with CNT films as counter

electrodes reveal similar high performance (*e.g.*, a specific capacitance of 54 F/g) like common platinum electrodes.[58] One representative device utilizing CNTs reached a photoelectric conversion efficiency of 6.1%, a specific capacitance of 48 F/g and a storage efficiency of about 84% with an entire photoelectric conversion and storage efficiency of about 5.12%. The specific capacitance can be increased to 208 F/g by the incorporation of poly(aniline) (PANI) into the CNT. However, the overall photoelectric conversion and storage efficiency drops to 4.3% due to a lower energy storage efficiency.[40] The described devices feature a planar structure and by changing it into a wire shaped structure, the flexibility of the ES-DSSC can be enhanced. Peng *et al*. developed a wire shaped device utilizing CNT/Ti wire composites, whereby the Ti wire was modified with perpendicular aligned TiO_2 nanotubes on the surface and horizontally aligned CNT. These nanotubes offer an effective pathway for the charge transport resulting in a photoelectric conversion efficiency of 2.7% and an energy storage efficiency of 75.7%.[59] An electric energy wire with energy conversion in the sheath and energy storage in the core using aligned CNT achieved a photoelectric conversion and storage efficiency of up to 1.8%.[60] Another ES-DSSC wire using a PANI coated stainless steel wire as current collector and a Ti wire, covered with TiO_2 and the dye N719 (*cis*-diiso-thiocyanato-*bis*(2,2'-bipyridyl-4,4'-dicarboxylato)ruthenium(II)*bis*(tetrabutylammonium)), as photoanode reached an overall efficiency of 2.1%.[44] An ES-DSSC with an efficiency of 3.7% was developed utilizing a dye N719 containing photoanode and poly(vinylidene fluoride) (PVDF)/ZnO nanowires as counter electrode.[41] A single fiber device only with ZnO nanowires and a DSSC, which was immobilized onto a copper mesh achieved an entire energy conversion efficiency of only 0.02%, presumably due to the utilization of the copper mesh, which suffers from a low transparency resulting in a significant lower absorption and transfer of the light to the dye (Figure 2.2).[49] Moreover, WO_3 represents another suitable material for ES-DSSC due to its unique optical and electrical performance by reversible intercalation of alkali metal ions[61] and due to the lower conduction band compared to TiO_2.[62] A supercapacitor using WO_3 coated CNT in combination with a DSSC consisting of a TiN/Ti mesh as electro-catalytic electrode where the reduction of I_3^- to I^- took place achieved a photo-charge efficiency of up to 69.5%.[63] Furthermore, also organic conjugated polymers have been applied as capacitor materials. Segawa *et al.* published *e.g.* an ES-DSSC in which the charge-storage electrode consisted of the conjugated polymer poly(pyrrole), which was coated by Nafion®. In combination with a common DSSC, the entire photoelectric conversion efficiency

was 3.2% with a maximum discharge capacity of 37.8 mC/cm^2 and a stability of about 70 cycles.[64] Another three-electron system, which used also poly(pyrrole) films on an indium tin oxide (ITO) slide as charge storage electrode, achieved charge storage efficiencies of up to 22%, dependent on the amount of poly(pyrrole).[65] The total photoelectric conversion and storage efficiency was about 0.1% using a bifunctional TiO_2/poly(3,4-ethylenedioxythiophene) (PEDOT) photoanode.[39]

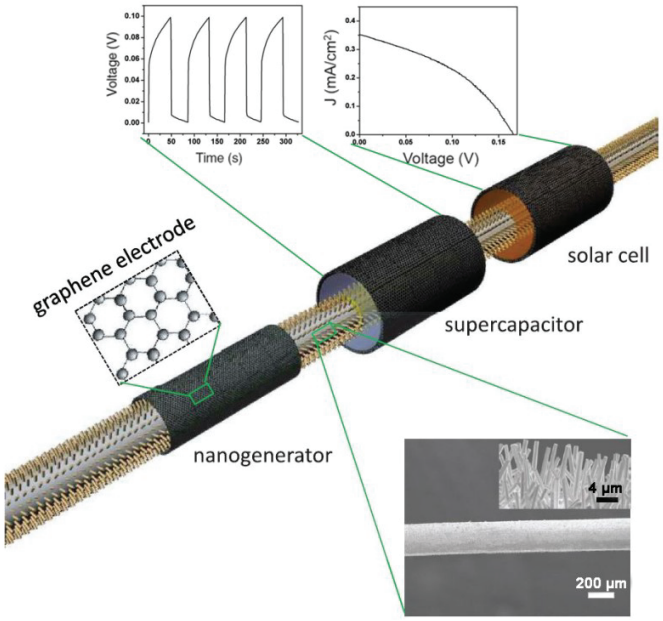

Figure 2.2: Schematic configuration of a fiber-based multi-energy device, consisting of a nanogenerator, a DSSC and a supercapacitor. Adapted with permission.[49]

Next to supercapacitors, other energy storage devices are possible such as Redox flow batteries (RFB). A RFB consists of two parts of liquid electrolyte (catholyte and anolyte) containing one or more dissolved redox-active species. The two segments are connected by an ion exchange membrane, which separates the electrolytes to prevent from cross-mixing while the counterbalance of the charge carriers can take place.[66–68] The advantages of RFB are high lifetime, flexibility, high reliability and the potential to store a large amount of energy.[67–69] Gao *et al.* developed an ES-DSSC, where one part of the RFB consisted of a DSSC. The catholyte consisted of a solution of LiI in propylene carbonate (PC) and the dye N719 coated TiO_2 film was placed on the electrode (photoanode). The anolyte contained Li_2WO_4 and $LiClO_4$ in water and a Pt/Ti mesh was placed as working electrode into the electrolytes. The so

constructed three-electrode device reached a voltage of 0.76 V and a discharge capacity of 0.015 mAh/mL (Figure 2.3).[70] A total energy conversion efficiency of 1.2% was reached by changing the anolyte to an aqueous solution of quinoxaline and its derivatives. This device revealed a good stability and electrochemical activity.[71]

A DSSC with an aqueous $CH_3NH_3Br \cdot PbBr_2$ electrolyte is able to store the generated energy with a power conversion efficiency of 8.6% and a faraday efficiency of up to 81.6%.[72] At the TiO_2 electrode, Pb^{2+} is reduced to Pb and Pb^{2+} is oxidized at the Pt electrode resulting in a charge storage due to the difference of the redox potentials. A three-electrode DSSC using indoline dye-adsorbed TiO_2 layer as photo-anode, poly(viologen) as electron storage anode, a Pt mesh as cathode and an aqueous solution of 1-oxyl-2,2,6,6-tetramethyl-4-hydroxypiperidine (TEMPOL) as electrolyte featured an ES-DSSC with a charge supply after irradiation at a voltage of 0.4 V and a discharge capacity of about 75%.[73]

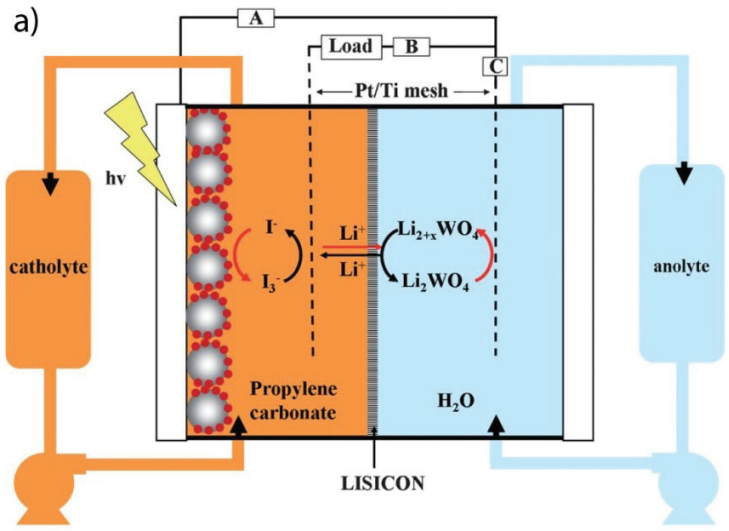

Figure 2.3: Schematic setup and working principle of a solar rechargeable RFB. Reproduced with permission.[70]

An alternative solar cell device represents OPV systems, in particular bulk heterojunction (BHJ) solar cells, which are easy to fabricate by roll-to-roll, printing or coating processes resulting in low cost, flexible and light-weight devices.[74–78] BHJ solar cells consist of an transparent electrode, an hole conducting layer (*e.g.*, PEDOT/poly(styrene sulfonate) (PSS)), the active layer as well as a second electrode to collect the charges. The active layer is a bulky mixture of a conjugated polymer as donor (*e.g.,* poly(3-hexylthiophene) (P3HT)) and a

acceptor material like phenyl-C61-butyric acid methyl ester (PCBM).[79,80] A wire shaped combination of BHJ solar cell and capacitor was developed by Peng *et al*. utilizing a titania nanotube-modified Ti wire as core, P3HT/PCBM as active material and a PEDOT/PSS layer reached an energy conversion efficiency of up to 1.0%. The energy storage part, consisting of CNT and a poly(vinyl alcohol)/H_3PO_4 electrolyte, achieved a storage efficiency of 65.6%, resulting in the entire photoelectric conversion and storage efficiency of up to 0.8%.[81]

Next to the previous presented systems for photo rechargeable batteries, some other charge storage possibilities are available, *e.g.*, solar cells with a battery effect. For instance, a solar cell consisting only of the donor material (*i.e.*, first generation cationic cyanine dendrimer), was utilized as a photo-rechargeable battery. The battery effect results from charge trapping sites within the active layer by an internal charge transfer from the counter anion to the cationic cyanine. Using a film with a thickness of 150 nm, the total storage capacity was 0.20 mAh/g with an output voltage of 0.35 V. A higher film thickness of the active material resulted in a higher discharge current due to more trapping sites within the film.[82] Additionally, due to high energy densities, air batteries features interesting possibilities for photo-rechargeable batteries.[83] The group of Nishide developed a solar-rechargeable air battery consisting of a poly(anthraquinone) based anode and a MnO_2/carbon composite cathode, which catalyze the reduction of oxygen. A boron-dipyrromethene (BODIPY) derivative was adsorbed to the anthraquinone polymer to avoid a rapid decrease in the voltage under dark due to a back electron transfer from the anthraquinone to the oxygen. The battery reached a discharge voltage of 0.63 V, a charging capacity of 166 mAh/g and a capacity of 143 mAh/g for discharging (72% and 62% of the theoretically capacity, respectively) for over 50 cycles (Figure 2.4).[84]

In summary, the main focus of photo-rechargeable energy storage systems is on hybrids of DSSC with supercapacitors. However, all devices have, up to now, low efficiencies or capacities compared to their inorganic counterparts, due to the focus on the development and fabrication of prototypes and, as a consequence, no or less optimization on the overall efficiency was performed. Consequently, the mismatch of the different energy conversion and storage parts limits the efficiency of the devices. For example, OPV systems, which offer a voltage of about 0.8 V, require a corresponding battery with fitting voltage. For this reason, the development of new materials, in particular, organic polymers features a high potential due

to relative simple tuning of the redox potentials and, as a consequence, the voltage of the storage device. Only the group of Nishide utilized the advantages of organic polymers for the development of solar-rechargeable batteries.[73,84] Furthermore, by integration of organic battery materials into supercapacitors, the performance of the capacitors can be improved, resulting in a fast charging and high capacity device.

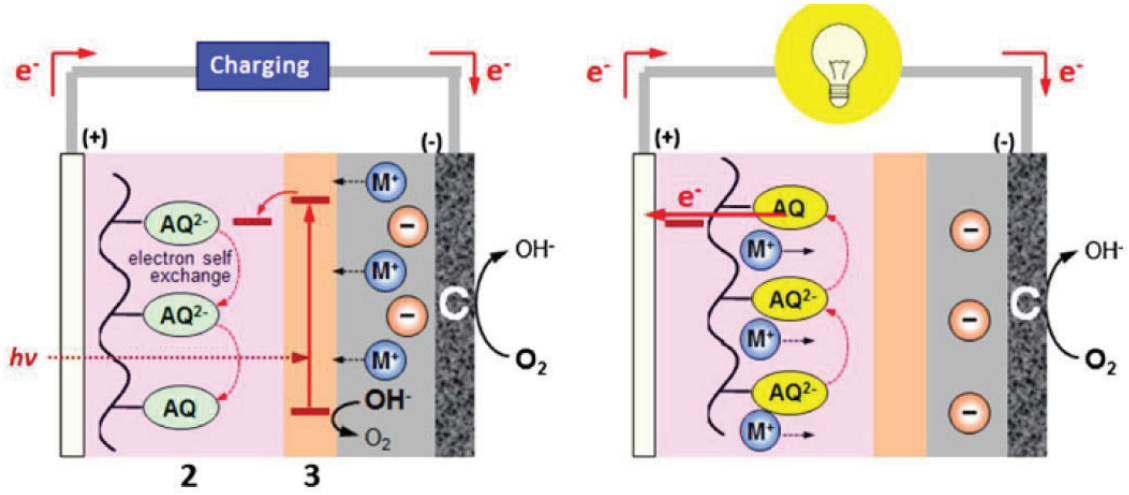

Figure 2.4: Schematic setup and working mechanism of a solar rechargeable air battery. Reproduced with permission.[84]

3. Redox-active polymers for organic batteries

Parts of this chapter have been or will be published in P2) D. Schmidt, B. Häupler, M. D. Hager, U. S. Schubert, *J. Polym. Sci., Part A: Polym. Chem.* **2016**, *54*, 1998–2003; P3) B. Häupler, R. Burges, C. Friebe, T. Janoschka, D. Schmidt, A. Wild, U. S. Schubert, *Macromol. Rapid Comm.* **2014**, *35*, 1367-1371.

Anthraquinone containing polymers are of high interest for organic battery application because they feature a redox reaction involving two electrons, which results in a good electron to mass ratio and, as a consequence, comparably high theoretical capacities. By modification of the redox-active carbonyl groups, the redox potential and consequently the cell potential of the battery can be tailored.

3.1. Synthesis and characterization of poly(*N*,*N'*-dicyanoanthraquinone diimine) as a new redox-active polymer

The transformation of the carbonyl groups of the anthraquinone into *N*-cyanoimine moieties, which possess stronger electron accepting properties, results in a shift of the redox potential to a higher voltage. As a consequence, two novel redox-active monomers were synthesized, which can be polymerized by free radical and rhodium-catalyzed polymerization, respectively.

The *N*,*N'*-dicyanoanthraquinone diimine (DCAQI) synthesis was performed in a straightforward three step procedure according to a modified literature route (Scheme 3.1).[85] 2-Iodanthraquinone (**1)** was synthesized from commercially available 2-aminoanthraquinone utilizing a *p*-toluene sulfonic acid supported Sandmeyer reaction. The polymerizable vinyl group was introduced by a palladium-catalyzed C-C cross coupling reaction at 2-position. The best result was obtained using the Hiyama reaction providing 2-vinylanthraquinone (**2**) in high yield (80%). The carbonyl groups were transformed into *N*-cyanoimine groups utilizing titanium(IV) chloride and *bis*(trimethylsilyl)-carbodiimide. Monomer **3** could be obtained in moderate yields (52%) due to its low stability on silica gel during the purification process.[86] Subsequently, **3** was polymerized by free radical polymerization technique with azo*bis*(isobutyronitrile) (AIBN) as initiator using different solvents (1,2-dichloroethane,

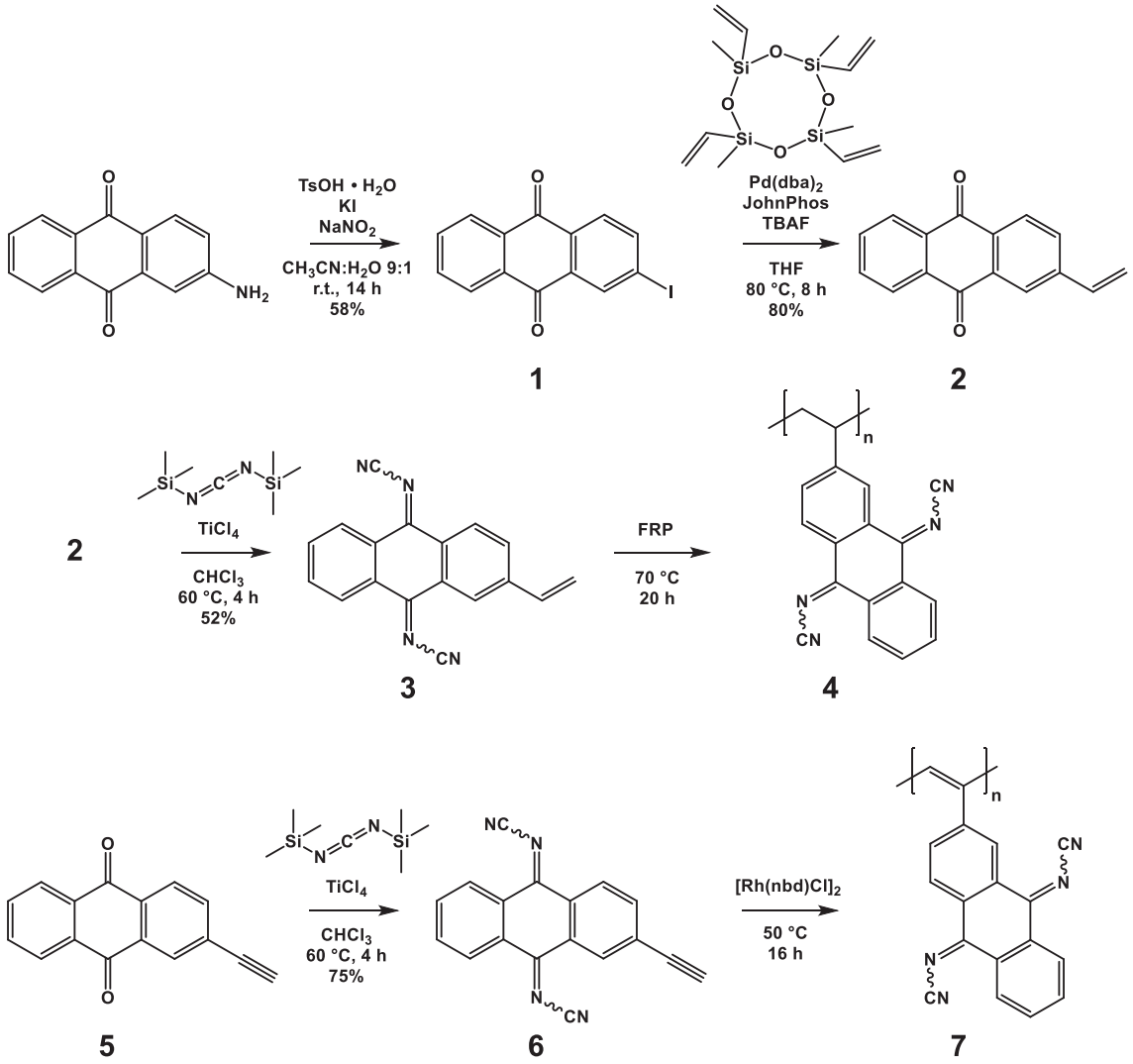

Scheme 3.1: Schematic representation of the synthesis of the monomers **2** and **6** as well as the polymers **4** and **7**.

N-methyl-2-pyrrolidone (NMP), dimethylsulfoxide (DMSO), *N*,*N*-dimethylformamide (DMF) and *N*,*N*-dimethylacetamide (DMAc)). The most promising polymers in terms of high molar masses were obtained in DMSO with a yield of 77% and a high molar mass (M_n) of 16,800 g/mol (Table 3.1). All other solvents led to poor yields (up to 40%) and lower M_n values (7,300 to 10,400 g/mol), presumably due to chain terminating reactions. Furthermore, rhodium-catalyzed polymerization of an ethynyl-based monomer was applied to enable milder reaction conditions (*e.g.*, room temperature conditions). Monomer **6** was synthesized from 2-ethynylanthraquinone **5**, which was prepared in a straightforward two-step procedure from the commercial available 2-bromoanthraquinone.[84] The carbonyl groups were transformed in a

similar manner into *N*-cyanoimine groups using titanium(IV) chloride and *bis*(trimethylsilyl)carbodiimide in good yield (75%) (Scheme 3.1). However, **6** revealed only poor solubility in organic solvents such as dichloromethane and tetrahydrofuran (THF), which are commonly used for the rhodium-catalyzed polymerization of phenylacetylene derivatives.[87] As a consequence, polar aprotic solvents were used for the rhodium-catalyzed polymerization. The utilization of DMF leads to polymers in good yields (63%) but with low molar masses (M_n) of around 4,400 g/mol. Utilizing DMSO as solvent, the molar mass (M_n) could be increased to 10,900 g/mol. However, the polymerization suffered from lower yield of

Table 3.1: Selected reaction conditions and analytical data for polymers **4** and **7** prepared by the free radical polymerization (FRP) technique and Rh-catalyzed polymerizations, respectively.

Polymer	Solvent	Conc. [mol/L]	Temp. [°C]	M_n[a] [g/mol]	Đ[a]	Yield [%]
4a	1,2-Dichloroethane	0.51	70	7,300	1.36	20
4b	NMP	1.00	70	7,700	1.27	7
4c	DMSO	1.00	70	16,800	1.98	77
4d	DMF	1.00	70	10,400	1.40	40
4e	DMAc	1.00	70	8,600	1.28	33
7a	DMF	0.10	50	4,400	1.33	63
7b	DMSO	0.10	50	10,900	3.06	48
7c[b]	DMF	0.20	50	*n/d*[c]	*n/d*[c]	97
7d[b]	DMSO	0.20	50	*n/d*[c]	*n/d*[c]	90
7e[b]	1,2-Dichloroethane	0.10	50	*n/d*[c]	*n/d*[c]	77
7f[b]	DMSO	0.10	r.t.	*n/d*[c]	*n/d*[c]	93

[a] Determined by SEC (DMAc, 0.21% LiCl, poly(styrene) standard, RI detector). [b] Addition of triethylamine (0.1 eq.) to the reaction mixture. [c] SEC measurements could not be performed due to the insolubility of the polymers in the mobile phase.

around 48%. The addition of 0.1 eq. of triethylamine as co-catalyst and elevated reaction temperatures (50 °C) improved the yield to 77% in 1,2-dichloroethane and to 90% and 97% in DMSO and DMF, respectively. Thereby, triethylamine dissociates the dimeric rhodium catalyst to its active monomeric form, which is increasing the initiation efficiency.[88,89] The yield of the polymerization in DMSO at room temperature was only slightly higher (93%). However, all poly(phenylacetylene)-based polymers precipitated during the polymerization reaction and were completely insoluble in common organic solvents (*e.g.*, methanol, DMF, DMSO or DMAc) after purification. Consequently, no detailed analytical investigations could be performed.

The electrochemical behavior of the monomers **3** and **6** as well as of the polymers **4** and **7** was investigated by cyclic voltammetry. In particular, the influence of the electrolyte cations on the redox potential was examined. For this purpose, solutions of 0.1 M $LiClO_4$ and 0.1 M tetrabutylammonium perchlorate ($TBAClO_4$) in DMF were utilized as electrolyte (Figure 3.1). In the lithium ion based electrolyte, monomer **3** features two reversible one-electron reduction steps at $E^1_{1/2} = -0.63$ V and $E^2_{1/2} = -1.03$ V *vs.* Fc^+/Fc. These redox potentials are in good agreement with literature reports of the unsubstituted DCAQI ($E^1_{1/2} = -0.68$ V and $E^2_{1/2} = -1.04$ V *vs.* Fc^+/Fc)[90] indicating that the vinyl group has no influence on the redox behavior of the monomer. Furthermore, the electron acceptance of the *N*-cyanoimine functionality is increased compared to the carbonyl group and the reduction of the monomer to the radical anion and to the dianion occurs at a more positive potential compared to anthraquinone ($E^1_{1/2} = -1.19$ V and $E^2_{1/2} = -1.68$ V *vs.* Fc^+/Fc).[91] The utilization of $TBAClO_4$ as electrolyte salt shifts the redox signals to $E^1_{1/2} = -0.65$ V and $E^2_{1/2} = -1.16$ V *vs.* Fc^+/Fc. Monomer **6** exhibits also two reversible reductions at $E^1_{1/2} = -0.59$ V and $E^2_{1/2} = -0.99$ V *vs.* Fc^+/Fc utilizing $LiClO_4$ as electrolyte salt, which indicates no significant influence of the ethynyl group on the redox behavior. The redox behavior of **6** in $TBAClO_4$ is similar to the behavior in $LiClO_4$. The redox signals are located at $E^1_{1/2} = -0.59$ V and $E^2_{1/2} = -1.09$ V *vs.* Fc^+/Fc. In general, the shift of the second reduction peak of both monomers is slightly influenced by the cation of the electrolyte. This can be explained by the stronger coordination of the lithium ions to the *N*-cyanoimine groups, resulting in a shift of the redox potential to more positive values.[21,91]

The cyclic voltammogram of polymer **4** in DMF, 0.1 M $LiClO_4$ reveals the expected redox signals at $E^1_{1/2} = -0.60$ V and $E^2_{1/2} = -0.97$ V *vs.* Fc^+/Fc, corresponding to the reduction to the radical anion and to the dianion, respectively (Figure 3.2 left). However, an additional redox signal appears at $E^3_{1/2} = -1.26$ V *vs.* Fc^+/Fc. This signal can be presumably assigned to the reduction of the carbonyl group of the *N*-(10-oxo-anthracen-9(10*H*)-ylidene)cyanamide

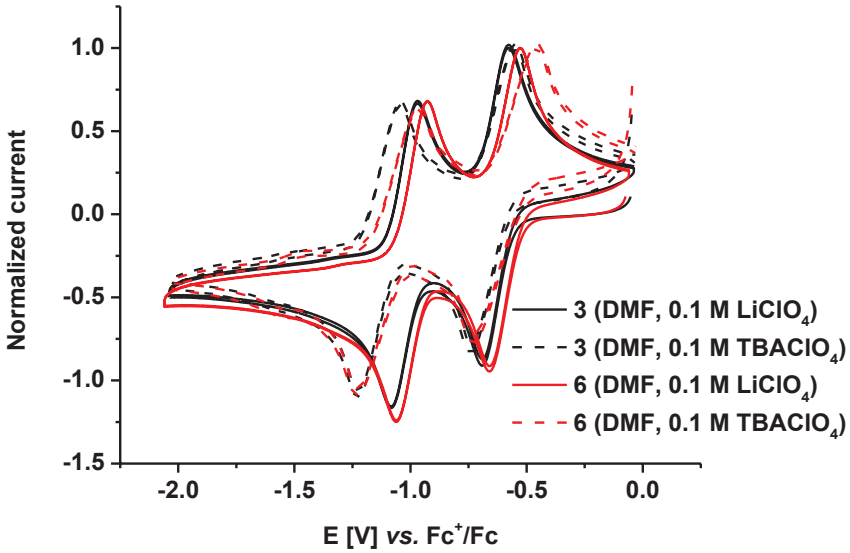

Figure 3.1: Normalized cyclic voltammograms of monomer **3** (c = 0.6 mg/mL; black line) and **6** (c = 1.0 mg/mL; red line) in DMF, 0.1 M $LiClO_4$ (solid line) and $TBAClO_4$ (dashed line), respectively, 500 mV/s, 1st and 2nd cycle, WE: glassy carbon, RE: $AgNO_3/Ag$ in CH_3CN, CE: Pt.

(*cf.* Chapter 4.2), which is most likely formed by a partial hydrolysis of *N*-cyanoimine moieties to carbonyl groups (Figure 3.2 right). The first redox reaction of this unit is presumably overlapped by the signal of the DCAQI unit. However, due to the bad solubility of polymer **4**, a detailed analysis of its composition and the potential side reactions is not possible. However, IR spectroscopy of the monomer and polymer, respectively, indicates a hydrolysis of the monomer during polymerization. In spite of the synthesis of poly(DCAQI) under milder conditions by using rhodium-catalyzed polymerization, the cyclic voltammogram of polymer **7** displays a similar redox behavior and comprises three reduction peaks, indicating that the conjugated backbone has no influence on the redox behavior. The redox signals of the DCAQI moieties appear at $E^1_{1/2} = -0.63$ V and $E^2_{1/2} = -0.96$ V *vs.* Fc^+/Fc. However, an

additional reduction signal at $E^3_{1/2} = -1.20$ V *vs.* Fc^+/Fc occurs similar to polymer **4**. This indicates that the hydrolysis of the *N*-cyanoimine moieties either takes place despite milder reaction conditions during the polymerization at room temperature or a side reaction occurs during the electrochemical redox reaction. IR spectroscopy of the **6** and **7**, respectively, indicates also a hydrolysis of the monomer during polymerization. However, the redox signals are stable and reversible.

A further investigation of polymer **4** and **7** as electrode material in lithium-organic batteries is not meaningful due to their instability. However, monomer **3** and **6** feature interesting electrochemical properties.

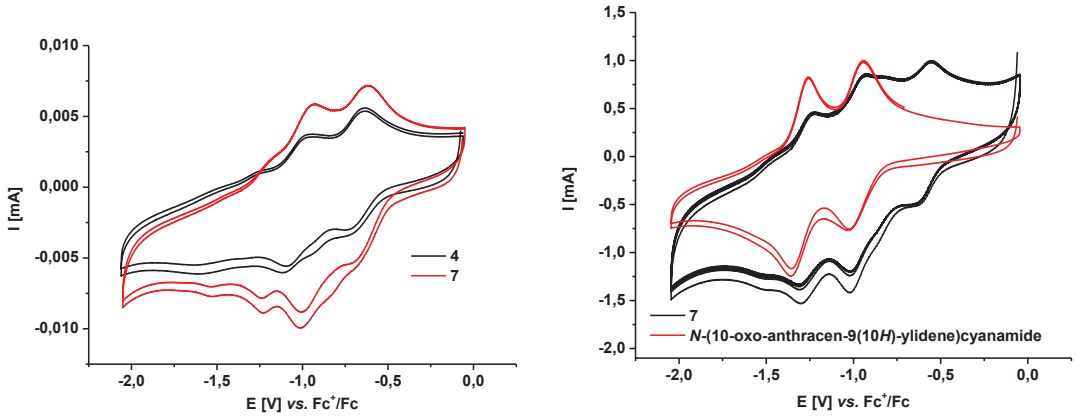

Figure 3.2: Cyclic voltammograms of polymer **4** (c = 0.8 mg/mL) and **7** (c = 1.0 mg/mL) in DMF, 0.1 M $LiClO_4$, 500 mV/s, 1st and 2nd cycle, WE: glassy carbon, RE: $AgNO_3$/Ag in CH_3CN, CE: Pt (left) and the comparison of the cyclic voltammograms of polymer **7** and *N*-(10-oxo-anthracen-9(10*H*)-ylidene)cyanamide (right).

3.2. Poly(exTTF): Utilization of a new redox-active material as cathode material in lithium-organic batteries

π-Extended tetrathiafulvalene systems (*e.g.*, 9,10-di(1,3-dithiol-2-ylidene)-9,10-dihydroanthracene (exTTF)) feature promising structures for electroactive materials, which are oxidizable and, therefore, act as good electron donor.[92–94] These compounds possess good electrical and optical properties due to the extended π-electron delocalization and, as a consequence, have been applied for organic electronics such as molecular wires, artificial photosynthetic systems

or solar cells.[95] For the application of exTTF in organic batteries, a suitable monomer was developed by the introduction of a polymerizable group.[96]

The monomer synthesis starts from commercially available 2-aminoanthraquinone yielding 2-vinylanthraquinone (**2**). Subsequently, the carbonyl groups were transformed into 1,3-dithiol-2-ylidene moieties by Horner-Wadsworth-Emmons reaction resulting in monomer **8** in 51% yield (Scheme 3.2), which was polymerized to **9** utilizing free radical polymerization. AIBN served as initiator and due to the limited solubility of both monomer and polymer, a limited range of polar and aprotic solvent could be used. In detail, the utilization of 1,2-dichloroethane led to a low molar mass polymer in poor yields (2,330 g/mol, 37%), which is similar to the polymerization behavior of monomer **4**. The polymerization in DMF and DMAc revealed a higher molar mass (M_n) with 3,090 and 5,360 g/mol, respectively, with a high yield of 73%. The best result was obtained in DMSO. The polymer exhibited the highest M_n value of 6,020 g/mol with a yield of 60%. Compared with the polymerization of **4**, the molar masses are much lower presumably due to a lower reactivity of monomer **8**. The size exclusion chromatography (SEC) spectra of the polymers reveal two distributions, which are presumably caused by recombination reactions.

The electrochemical behavior of the monomer was investigated by cyclic voltammetry and a solution of 0.1 M $LiClO_4$ in acetonitrile was utilized as electrolyte. The monomer reveals a stable and reversible redox signal at $E_{1/2} = -0.2$ V *vs.* Fc^+/Fc, which can be assigned to the oxidation of the exTTF units to the dicationic species (Figure 3.3). This redox potential displays the large influence of the substitution of the carbonyl groups, whereby an electron

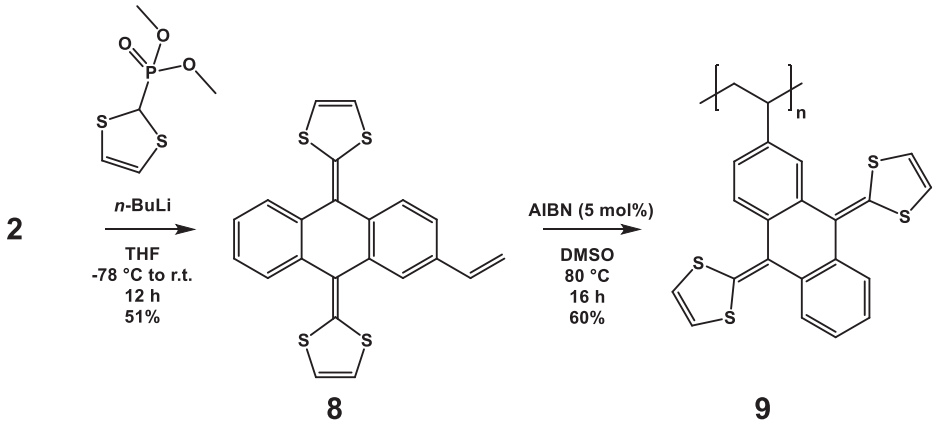

Scheme 3.2: Schematic representation of the synthesis of monomer **8** and polymer **9**.

donating group shifts the redox signal to higher redox potential values compared to electron accepting groups like *N*-cyanoimine groups (*cf.* Chapter 3.1: $E^1_{1/2} = -0.6$ V and $E^2_{1/2} = -1.0$ V *vs.* Fc^+/Fc). The release of the second electron during the oxidization process is promoted due to the planar low-energy conformation associated with the rearomatization of the oxidized dicationic product.[97] Furthermore, UV-*vis*-NIR spectroscopy was performed, revealing a stable and defined electrochemical process. An isosbestic point, indicating the presence of only two species and the high reversibility of the redox process prove the high stability of the redox reaction. The electrochemical behavior of the polymer in the solid state and also its suitability as electrode material for organic batteries was investigated as composite electrode consisting of **9**/PVDF/vapor grown carbon fibers (VGCF) 1/1/8 (*w*/*w*/*w*) on a graphite sheet. A solution of 0.1 M $LiClO_4$ in dimethoxyethane (DME)/PC 4/1 (*v*/*v*) served as electrolyte. Cyclic voltammetry revealed a stable and reversible redox reaction at a potential of $E_{1/2} = -0.2$ V *vs.* Fc^+/Fc, indicating that the polymeric environment and the carbon material have no significant influence on the redox behavior (Figure 3.4).

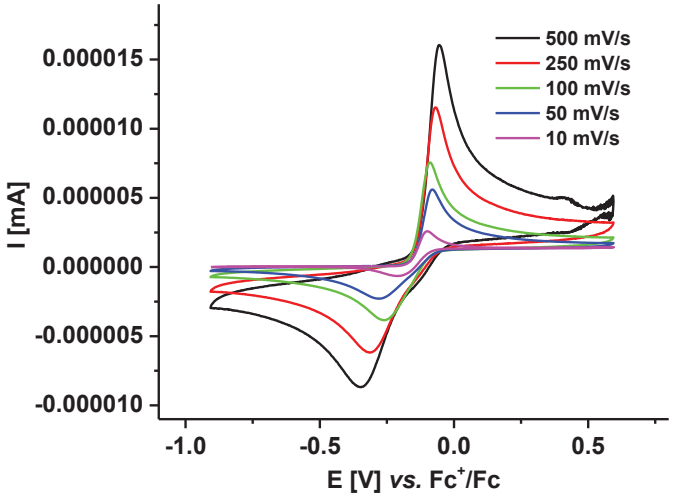

Figure 3.3: Cyclic voltammogram of monomer **8** in CH_3CN, 0.1 M $LiClO_4$, at different scan rates, 1st cycle, WE: glassy carbon, RE: $AgNO_3$/Ag in CH_3CN, CE: Pt.

As a consequence of the stable redox behavior, a lithium-organic battery was fabricated to investigate the charge/discharge properties of polymer **9**. For this purpose, a coin cell was prepared by sandwiching a composite electrode **9**/PVDF/VGCF 1/1/8 (*w*/*w*/*w*) and a lithium foil separated by a porous membrane. A solution of 0.1 M $LiClO_4$ in DME/PC 4/1 (*v*/*v*) was

used as electrolyte. The charge/discharge property revealed a plateau at a cell potential of 3.5 V for charging and 3.1 V for discharging, which is in line with the redox behavior of the composite electrode *vs.* Li^+/Li. The initial capacity of the battery is 108 mAh/g, corresponding to 82% of the theoretical capacity. The capacity drops down to 82 mAh/g during the first 20 cycles (61% of the theoretical capacity), which can be reasoned by the dissolution of low molar mass polymer chains into the electrolyte. The charge/discharge capacity remains stable for the next 230 cycles with a coulombic efficiency of 99% (Figure 3.4).

Poly(exTTF) features a redox-active polymer with a high electrochemical stability resulting in a good charge/discharge performance. The theoretical capacity is high (132 mAh/g) due to the involvement of one two-electron redox reaction.

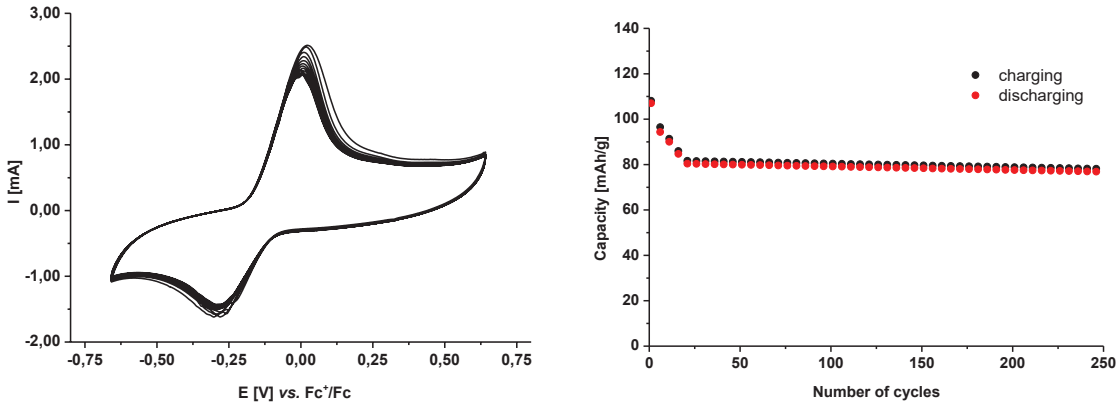

Figure 3.4: Cyclic voltammogram of composite electrode (**9**/PVDF/VGCF 1/1/8 (*w*/*w*/*w*)) in DME/PC 4/1 (*v*/*v*), 0.1 M $LiClO_4$, 5 mV/s, 50 cycles, RE: $AgNO_3$/Ag in CH_3CN, CE: Pt (left) and the charge/discharge cycles of a lithium ion battery of polymer **9** in DME/PC 4/1 (*v*/*v*), 0.1 M $LiClO_4$ (250 cycles, 1C) (right). The cathode is a composite of **9**/PVDF/VGCF 1/1/8 (*w*/*w*/*w*).

4. Tuning the redox potential by an unsymmetrical substitution of anthraquinone

Parts of this chapter have been published in P4) D. Schmidt, B. Häupler, C. Friebe, M. D. Hager, U. S. Schubert, *Polymer* **2015**, *68*, 321–327; P5) D. Schmidt, B. Häupler, C. Stolze, M. D. Hager, U. S. Schubert, *J. Polym. Sci., Part A: Polym. Chem.* **2015**, *53*, 2517–2523.

The polymers described in Chapter 3 bear anthraquinones with a complete substitution of the carbonyl groups. However, the redox potential and, as a consequence, the voltage of the resulting battery can be fine-tuned by unsymmetrical substitution such as the substitution of only one carbonyl group or the substitution of both carbonyl groups with different substituents. In particular by the second approach by the substitution of the carbonyl groups with both an electron donor and an electron acceptor group, the redox potential of both redox reactions can be split into two independent redox reactions with a large potential gap.

4.1. Investigations on redox-active polymers based on 10-(1,3-dithiol-2-ylidene)anthracen-9(10*H*)-one derivatives

In Chapter 3.2 poly(exTTF) is described, consisting of an anthraquinone bearing two electron donating 1,3-dithiol-2-ylidene moieties, featuring one two-electron redox reaction with a potential at $E_{1/2} = -0.2$ V *vs.* Fc^+/Fc. However, by exchange of one 1,3-dithiol-2-ylidene group to an electron accepting moiety, the resulting monomers and polymers feature a bipolar redox behavior and can undergo both an oxidation and a reduction reaction. These unique electrochemical properties make these polymers suitable as potential electrode materials for poleless organic batteries.

The key intermediate of the monomer synthesis is 3-bromoanthracen-9(10*H*)-one (**10**), which could be successfully synthesized by a three-step procedure starting from 1,3-dibromobenzene and 2-formylbenzoic acid (Scheme 4.1).[98] A direct bromination of 9(10*H*)-anthracenone at 3-position led always to a mixture of multibrominated compounds. The bromine group, which is in one of the next steps transformed to the desired polymerizable group was introduced in 3-position to avoid steric hindrance during the polymerization. The 1,3-dithiol-2-ylidene group

of **11** was inserted utilizing 2-methylthio-1,3-dithiolium tetrafluoroborate, dissolved in a mixture of acetic acid and pyridine 5/1 (*v*/*v*). A larger amount of pyridine resulted in longer reaction times and in the formation of side products. In the next synthetic step, the polymerizable vinyl group was introduced in good yields using the Suzuki cross coupling reaction. Subsequently, three different derivatives were synthesized by straightforward one-step modification of the carbonyl group of **12**. The substituents are *N*-cyanoimine, dicyanomethylene as well as thione and possess different electron acceptor strengths, which

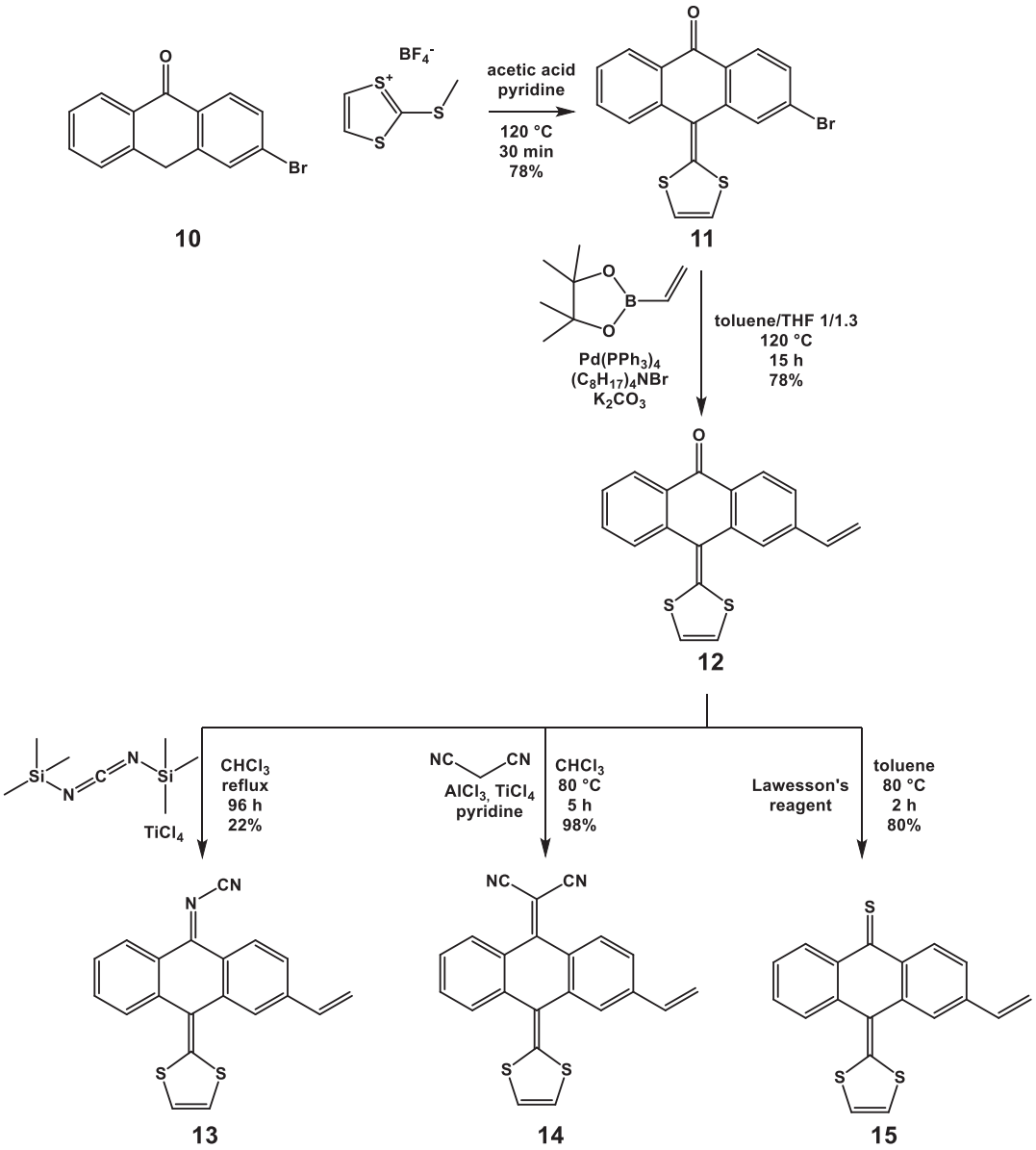

Scheme 4.1: Schematic representation of the synthesis of monomers **13**, **14** and **15**.

influences the redox potentials. The *N*-cyanoimine group of monomer **13** was achieved by the reaction of **12** with titanium(IV) chloride and *bis*(trimethylsilyl)carbodiimide in low yields (22%). Monomer **14** was obtained by a Knoevenagel condensation using malononitrile, pyridine as base and aluminum chloride as well as titanium(IV) chloride as Lewis acid. The product was obtained in a very high yield (98%). The thione group of monomer **15** was introduced by the utilization of Lawesson's reagent and the product was obtained with a yield of 80%.

All resulting monomers were polymerized using the free radical polymerization with AIBN or *tert*-butyl hydroperoxide (TBHP) as initiator (Scheme 4.2). The analytical data of the polymers are summarized in Table 4.1. The polymerization of **12** could be performed in a restricted range of solvents (*i.e.*, 1,2-dichloroethane, NMP or DMSO) due to their limited solubility. The best results were obtained for **16** in DMSO with a molar mass (M_n) of 15,600 g/mol, a polydispersity index (Đ) value of 2.7 and 92% yield. Chlorinated solvents such as 1,2-dichloroethane led to chain-terminating reactions resulting in a lower yield (60%) and larger Đ value (3.0). As a consequence, all other polymerization reactions were performed in DMSO as the monomers **13**, **14** and **15** reveal a similar solubility behavior. Polymer **19** was obtained in 58% yield and with a high average molar mass (M_n) of 24,300 g/mol (Đ = 1.7). The average molar mass and the yield of **17** were comparably low (M_n = 6,500 g/mol, Đ = 1.3, 36%), possibly due to steric hindrance of the specious redox unit during the chain growth reaction. The AIBN initiated polymerization of monomer **14**, which is sterically more

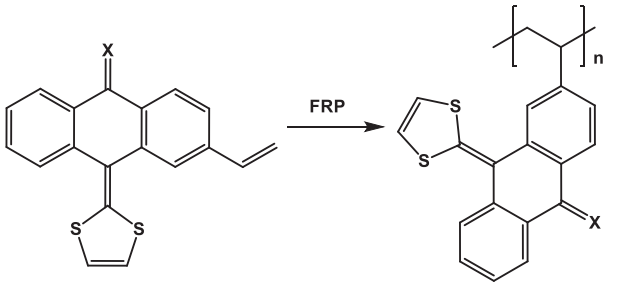

12 X = O
13 X = N-CN
14 X = $C(CN)_2$
15 X = S

16 X = O
17 X = N-CN
18 X = $C(CN)_2$
19 X = S

Scheme 4.2: Schematic representation of the synthesis of the polymers **16** to **19**.

Table 4.1: Selected synthetic and analytical data for polymers **16** to **19** prepared by FRP.

Polymer	Monomer	Initiator	Solvent	M_n[a] [g/mol]	Đ[a]	Yield [%]
16	**12**	AIBN	1,2-Dichloroethane	19,000	3.0	60
16	**12**	AIBN	NMP	10,500	2.3	92
16	**12**	AIBN	DMSO	15,600	2.7	92
17	**13**	AIBN	DMSO	6,500	1.3	36
18	**14**	TBHP	DMSO	23,400	1.7	67
19	**15**	AIBN	DMSO	24,300	1.7	58

[a] Determined by SEC (DMAc, 0.21% LiCl, poly(styrene) standard, RI detector).

demanding, led only to oligomers with a very low yield. As a consequence, the reaction temperature was increased to 130 °C and TBHP was chosen as initiator. Polymer **18** could be obtained with a high average molar mass (M_n = 23,400 g/mol, Đ = 1.7) and acceptable yield (58%).

The electrochemical properties of all monomers were investigated by cyclic voltammetry utilizing a solution of 0.1 M $TBAClO_4$ in acetonitrile as electrolyte (Table 4.2). All monomers, except monomer **13**, show a reversible oxidation process in the range of $E^1_{1/2}$ = 0.4 and $E^2_{1/2}$ = 0.5 V *vs.* Fc^+/Fc. This is attributed to the oxidation of the 1,3-dithiol-1-ylidene moiety to its radical cation, indicating the electron donating property of the group, which was previously shown for monomer **8** (Figure 4.1). The reduction of monomer **12** occurs at the most negative redox potential ($E^{red}_{1/2}$ = – 1.8 V *vs.* Fc^+/Fc), due to the poor electron accepting properties of the carbonyl group. However, its acceptor ability is decreased compared to anthraquinone.[99] Equal to the electrochemical behavior of monomer **3**, the electron acceptance of the *N*-cyanoimine functionality is higher compared to the carbonyl group and, therefore, the reduction of **13** to the radical anion takes place at higher potential ($E_{1/2}$ = – 1.5 V *vs.* Fc^+/Fc). However, the oxidation of **13** at $E_{1/2}$ = 0.3 V *vs.* Fc^+/Fc reveals to be partly irreversible and an additional irreversible signal occurs at $E_{1/2}$ = – 0.6 V *vs.* Fc^+/Fc, indicating presumably a side reaction of the formed radical cation. The malononitrile group of

Table 4.2: Cyclic voltammetric data of monomers **12** to **15** and of polymers **16** to **19**.

Compound	$E^{ox}_{1/2}$ [V *vs.* Fc^+/Fc]	$E^{red}_{1/2}$ [V *vs.* Fc^+/Fc]
12	0.39	– 1.84
13	0.32[a)]	– 1.45
14	0.49	– 1.33; – 1.66
15	0.49	– 1.33; – 1.64
16	0.44[a)]	– 1.31
17	0.37[a)]	– 1.43
18	0.43[a)]	– 1.39
19	0.44[a)]	– 1.37; – 1.70
4[b]	–	– 0.60; – 0.97; – 1.26
9[c]	– 0.15	–

[a] Irreversible. [b] *Cf.* Chapter 3.1. [c] *Cf.* Chapter 3.2.

14 and the thione group of **15** reveal an even stronger electron accepting property resulting in a higher reduction potential of $E_{1/2} = -1.3$ V *vs.* Fc^+/Fc. A further one-electron reduction signal occurs at $E_{1/2} = -1.7$ V *vs.* Fc^+/Fc, corresponding presumably to the reduction of the aromatic skeleton. Due to the low solubility of the polymers **16** to **19** in acetonitrile, the electrochemical investigations were performed in a 0.1 M $TBAClO_4$ solution in DMF as electrolyte. However, the electrochemical behavior of the polymers is surprisingly different compared to the monomers (Figure 4.2). All polymers feature an irreversible oxidation process at about 0.4 V *vs.* Fc^+/Fc, indicating a side reaction of the formed radical cation. The reduction processes are all reversible and depend, similar to those of the monomers, in the substitution pattern of the acceptor moiety. In detail, the reduction of **16** occurs at a potential of $E_{1/2} = -1.3$ V *vs.* Fc^+/Fc. The potential is shifted to higher potentials compared to the results of the corresponding monomer. Similar findings are already published in literature.[100] A second reduction reaction occurs at the edge of the electrochemical stability of the DMF based

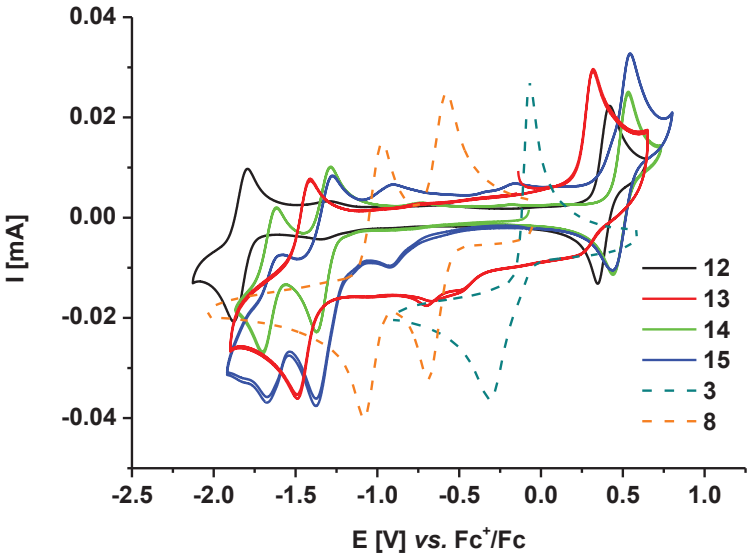

Figure 4.1: Cyclic voltammogram of the monomers **12** to **15** (c = 1 mg/mL) in CH_3CN, 0.1 M $TBAClO_4$, 250 mV/s, 1st cycle, WE: glassy carbon, RE: $AgNO_3$/Ag in CH_3CN, CE: Pt (solid line) and cyclic voltammogram of the monomers **3** and **8** (*cf.* Chapter 3) (dashed line).

electrolyte ($E_{1/2} = -2.1$ *vs.* Fc^+/Fc), which can be assigned to the reduction of the anthracene core of the monomeric units. In contrast, the redox behavior of **17** is in good agreement with monomer **13**, ($E^{red}_{1/2} = -1.4$ V and $E^{ox}_{1/2} = 0.4$ V *vs.* Fc^+/Fc) indicating, that the polymeric backbone has no significant influence on the redox behavior. These results are in line with the electrochemical behavior of **18** and **19**. The reduction process of **18** occurs at $E_{1/2} = -1.4$ V *vs.* Fc^+/Fc and is slightly shifted to lower potential. Similar to **15**, the electrochemical behavior of **19** reveals two one-electron reductions at $E_{1/2} = -1.4$ V and $E_{1/2} = -1.7$ V *vs.* Fc^+/Fc, which can be assigned to the reduction of the thione moiety and the aromatic core to the corresponding anions.

In summary, the redox behavior of the monomers and polymers can be tuned by the choice of the substituent. In detail, the redox potential of the reduction can be tailored in a broad range from – 1.3 to – 1.8 V *vs.* Fc^+/Fc by straightforward one-step modifications of the carbonyl group.

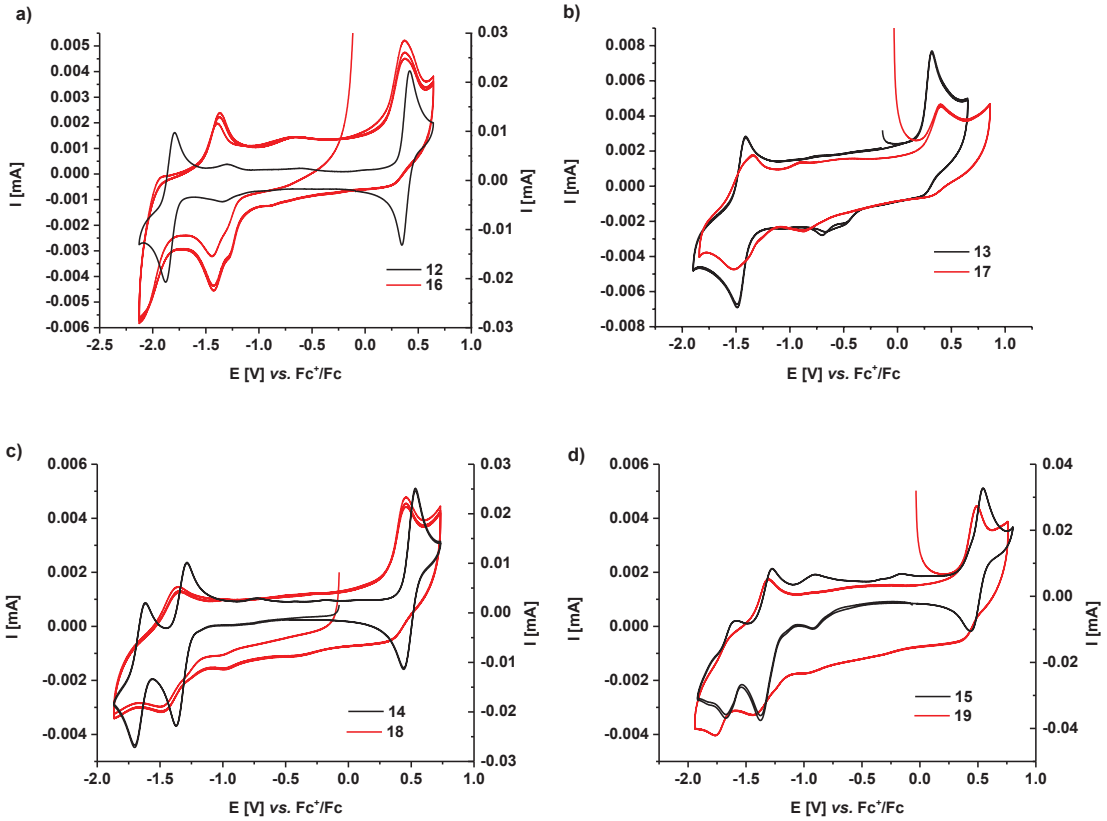

Figure 4.2: Cyclic voltammograms of the polymers **16** (a), **17** (b), **18** (c) and **19** (d) (red line) compared with the corresponding monomer **12** (a), **13** (b), **14** (c) and **15** (d) (black line) in DMF (polymers) and acetonitrile (monomers), 0.1 M $TBAClO_4$ at 250 mV/s, c(polymer) = 0.5 mg/mL, c(monomer) = 1 mg/mL, cycle 1 to 3, WE: glassy carbon, RE: $AgNO_3$/Ag in CH_3CN, CE: Pt.

4.2. Application of poly[*N*-(10-oxo-2-vinylanthracen-9(10*H*)-ylidene)cyanamide] as cathode material for lithium-organic batteries

The introduction of an electron donating group and an electron accepting group in one monomeric unit features a redox-active bipolar system, whose oxidation and reduction reaction occurs independently from each other. In this chapter, one electron accepting carbonyl group from the anthraquinone unit is exchanged by a stronger electron accepting moiety resulting in an unsymmetrically substituted reducible substance. As a consequence, the redox behavior is shifted to higher redox potentials but to lower redox potentials compared to the di-substituted compound in Chapter 3.1. This leads to a straightforward method for fine-

tuning the redox behavior. The resulting substance can be utilized as cathode material in a lithium-organic battery.

Monomer **20** was synthesized from 2-vinylanthraquinone (**2**) by modification of one carbonyl group into a *N*-cyanoimine group utilizing titanium(IV)-chloride and *bis*(trimethylsilyl)carbodiimide (Scheme 4.3). The substitution of only one carbonyl group is preferred due to the specific ratio of these educts and **20** was obtained as an isomeric mixture because of the similar reactivity of both carbonyl groups. The isomers were not separated as they possess the same electrochemical properties. **20** was polymerized using free radical and nitroxide mediated polymerization techniques to obtained eight linear (**21a** to **21h**) and two cross-linked polymers (**21i** and **21j**). The FRP was performed with AIBN as initiator in a limited range of different solvents (*i.e.*, 1,2-dichloroethane, NMP, DMSO, DMF and DMAc) due to the poor solubility of **20**. The best results were obtained in DMSO with a yield of 54%. However, the molar mass was rather low with M_n = 4,500 g/mol (Đ = 1.37). The molar masses (M_n) of the polymers are also much lower compared to the polymers bearing the di-substituted anthraquinone. As a consequence, the reaction temperature was increased to 130 °C, which is possible due to the temperature stability of the monomer and, therefore, other initiators were chosen. The polymerization reaction with TBHP as initiator led to a low molar mass polymer (M_n = 2,600 g/mol) in 33% yield. The average molar mass as well as the yield could be increased by the utilization of di-*tert*-butyl peroxide (DTBP) as initiator (M_n = 5,900 g/mol; 83%). Additionally, *N*-*tert*-butyl-*O*-[1-[4-(chloromethyl)phenyl]ethyl]-*N*-(2-methyl-1-phenylpropyl)hydroxylamine (CMSt-TIPNO) was chosen as initiator to avoid side products and to increase the molar mass of the polymer. As a consequence, polymer **21h** was obtained with a high average molar mass (M_n) of 10,200 g/mol in 66% yield. However, the SEC measurement

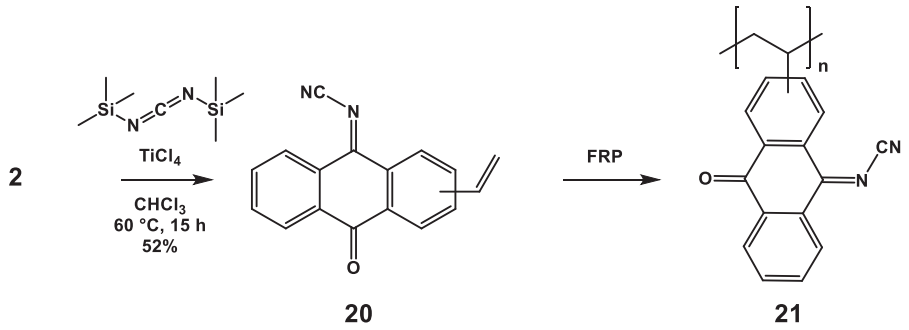

Scheme 4.3: Schematic representation of the synthesis of monomer **20** and polymer **21**.

Table 4.3: Selected reaction conditions and analytical data for polymers **21** prepared by FRP and NMP, respectively.

Polymer	Solvent	Initiator	Temp. [°C]	M_n[a] [g/mol]	Đ[a]	Yield [%]
21a	1,2-Dichloroethane	AIBN (2mol%)	70	5,800	1.24	4
21b	NMP	AIBN (2mol%)	70	5,200	1.23	2
21c	DMSO	AIBN (2mol%)	70	4,500	1.37	54
21d	DMF	AIBN (2mol%)	70	5,100	1.32	2
21e	DMAc	AIBN (2mol%)	70	4,800	1.28	12
21f	DMSO	TBHP (5mol%)	130	2,600	1.37	33
21g	DMSO	DTBP (5mol%)	130	5,900	2.39	83
21h	DSMO	CMSt-TIPNO (5mol%)	130	10,200	16.12	66
21i[b]	DMSO	DTBP (5mol%)	130	8,000[d]	4.57[d]	83
21j[c]	DMSO	DTBP (5mol%)	130	278,900[d]	1.54[d]	85

[a] Determined by SEC (DMAc, 0.21% LiCl, poly(styrene) standard, RI detector). [b] Cross-linked polymer synthesized with divinylbenzene (2 mol%). [c] Cross-linked polymer synthesized with divinylbenzene (5mol%). [d] SEC measurements were performed with the soluble part of the polymers.

revealed a multimodal distribution due to a poor control of the polymerization presumably by chain transfer to the solvent. Two cross-linked polymers were synthesized with divinylbenzene as cross-linker, because of the good solubility of the polymers in standard electrolyte solutions, such as ethylene carbonate (EC) and dimethyl carbonate (DMC). The obtained polymers are mainly insoluble in organic solvents and, as a consequence, SEC data were determined using the soluble part of the polymers, resulting in an average molar mass of up to M_n = 278,900 g/mol. However, the average molar mass of polymer **21j** could not be determined exactly due to the reached exclusion limit of the SEC column.

The electrochemical behavior of monomer **20** and polymer **21c** were investigated by cyclic voltammetry in a solution of 0.1 M $LiClO_4$ in DMF as electrolyte due to the good solubility of both the monomer and the polymer (Figure 4.3). Monomer **20** features two reversible and stable one-electron reduction processes at $E^1_{1/2} = -0.9$ V and $E^2_{1/2} = -1.3$ V *vs.* Fc^+/Fc. The electron acceptance of the *N*-cyanoimine group is increased compared to carbonyl group and, as a consequence, the reduction of the monomer to the radical anion and to the dianion occurs at a more positive potential compared to anthraquinone[91] and at a more negative potential compared to the DCAQI monomer (*cf.* Chapter 3.1). The incorporation of the monomer into a polymeric environment led to a slight shift of the first reduction signal to $E_{1/2} = -1.0$ V *vs.* Fc^+/Fc. The second reduction step is not influenced by the polymeric backbone. The shift of the first reduction signal is presumably caused by π-π-stacking of the monomeric units in the polymer, which requires a higher energy to break these interactions. The first reduction state is negatively charged and due to repulsion of the monomer units, the π-π-stacking interactions are revoked and, as a consequence, the second reduction process is comparable to the reduction of the monomer. In contrast to polymer **7**, no additional redox signal appears, which indicates a high stability of the redox-active units. Additionally, the polymer was further investigated electrochemically as composite electrode on a graphite sheet as current collector. Therefore, the current collector was coated with a slurry of **21**/PVDF/multi-walled carbon nanotubes (MWCNT) 1/1/8 (*w*/*w*/*w*) utilizing a doctor blading method. The electrode was immersed in a solution of 0.1 M $LiClO_4$ in EC/DMC 1/4 (*v*/*v*). The cyclic voltammogram of the composite electrode revealed a reversible and stable redox reaction at $E_{1/2} = -1.02$ V *vs.* Fc^+/Fc, indicating that the carbon material has no significant influence on the reduction behavior. However, both reduction signals are coalesced to one broad redox wave, which can be assigned to slow kinetics due to slow diffusion processes in the electrode as well as to the massive geometrical changes of the redox active units during the redox processes.

Subsequently, the charge/discharge properties of polymer **21** were further investigated in lithium-organic batteries. For this purpose, the high molar mass polymer (**21h**) as well as both cross-linked polymer (**21i** and **21j**) were used due to their insolubility in the applied electrolyte. Therefore, coin cells were prepared under inert atmosphere by sandwiching a composite electrode **21**/PVDF/MWCNT 1/1/8 (*w*/*w*/*w*) and a lithium foil separated by a porous membrane. The best results were obtained with a solution of 1 M $LiClO_4$ in EC/DMC

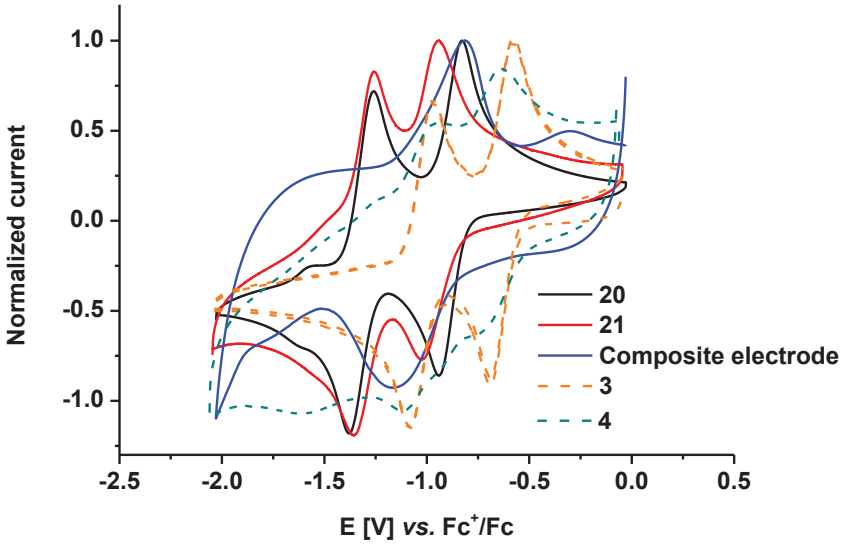

Figure 4.3: Normalized cyclic voltammograms of monomer **20** (c = 0.6 mg/mL), polymer **21c** (c = 0.2 mg/mL) (in DMF, 0.1 M $LiClO_4$, 100 mV/s) and composite electrode (**21h**/PVDF/MWCNT 1/1/8 (*w*/*w*/*w*)) in EC/DMC 1/4 (*v*/*v*), 1 M $LiClO_4$, 5 mV/s, 1st cycle, WE: glassy carbon, RE: $AgNO_3$/Ag in CH_3CN, CE: Pt (solid line) and cyclic voltammograms of monomer **3** and polymer **4** (*cf.* Chapter 3.1) (dashed line).

1/4 (*v*/*v*) as electrolyte. The charge/discharge behavior of all coin cells revealed a plateau at a cell potential of 2.3 V for charging and at 2.3 V for discharging, which corresponds to the characteristic overpotential of the coin cells (total ohmic resistance of 218 Ω). To investigate the influence of the different polymeric environments, the charge/discharge properties of the polymers **21h**, **21i** and **21j** were analyzed (Figure 4.4). The highest capacity values were obtained at the coin cells containing **21h** as active material. The initial capacity is about 130 mAh/g and drops down to 112 mAh/g (15% capacity loss) after 100 cycles. A further swelling of the polymer within the first cycles results in a slight increase of the capacity after about 20 cycles. The cross-linked polymer revealed a lower decrease of the capacity after 100 cycles of only 12% and 6% for polymer **21i** and **21j**, respectively, due to lower solubility of the polymers. However, the initial capacity is low with about 80 mAh/g and 62 mAh/g (31% and 26% active material), respectively. Polymer **21h** was further investigated in detail, because of its high capacity and the good cycling stability (Figure 4.4). The battery exhibits an initial capacity of 137 mAh/g (53% material activity), which drops down to 118 mAh/g (45% of the theoretical capacity), presumably due to dissolution of shorter polymer chains into the

electrolyte or side reaction during the charging/discharging cycles. Furthermore, the influence of the charging speed was investigated during the first 80 cycles. At a charge/discharge rate of 2C, the capacity decreases to 127 mAh/g (5% capacity loss), which decreases by further 18% to 94 mAh/g at a cycling speed of 5C. The charging speed is not significantly influenced by the charge/discharge speed. However, the discharge potential drops down from 2.33 V (1C) to 2.10 V (5C). The coulombic efficiency is high with over 96% at all charging speeds.

The redox behavior of the monomer and the polymer can be fine-tuned by mono-substitution of anthraquinone unit. The resulting polymers are applicable for lithium-organic batteries with a theoretical capacity of 207 mAh/g and a good cycling stability for 100 cycles.

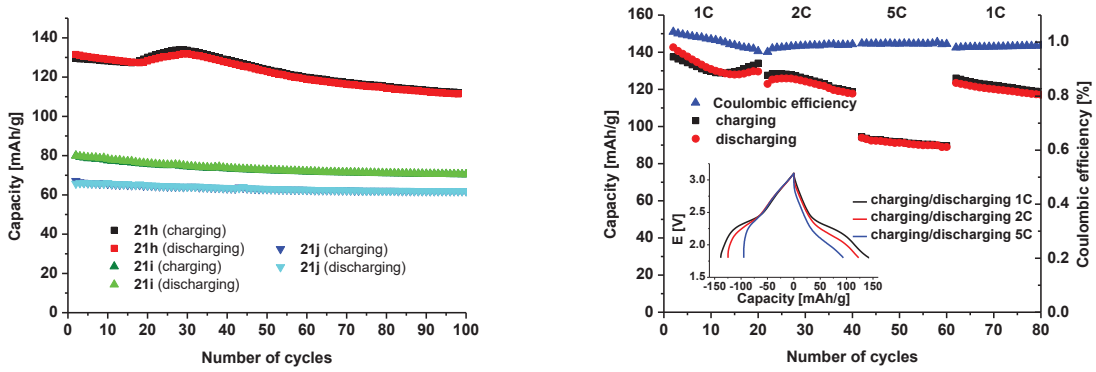

Figure 4.4: Charge/discharge cycles of a lithium organic battery of polymer **21h**, **21i** and **21j** in EC/DMC 1/4 (*v*/*v*), 1 M $LiClO_4$ (100 cycles, 5C). The anode is lithium metal, the cathode is a composite of (**21h**, **21i** or **21j**/PVDF/MWCNT 1/1/8 (*w*/*w*/*w*) (left) and charge/discharge cycles of a lithium organic battery (80 cycles) of **21h** at different C rates in EC/DMC 1/4 (*v*/*v*), 1 M $LiClO_4$. Coulombic efficiency of 80 charge/discharge cycles (blue triangle) (left). First charge/discharge curves (potential *vs.* capacity) at different C rates (insert, left).

5. Summary

The development of new materials for energy storage systems plays an increasingly important role to compensate the growing demand for portable and flexible electronics. Redox-active organic compounds, in particular polymers, represent promising materials featuring many advantages such as flexibility, light-weight and being environmental friendly. Moreover, organic redox-active polymers can be produced at low temperature procedures from renewable or recycled resources and can be processed utilizing efficient and low-cost techniques (*e.g.*, printing techniques). Anthraquinone-based polymers represent promising redox-active materials for the application in organic batteries or solar-rechargeable electric energy storage systems. The redox potential of anthraquinones can be tailored to the desired potential by straightforward modification of the carbonyl groups to electron donating or accepting groups (*i.e.*, 1,3-dithiol-2-ylidene, *N*-cyanoimine, *N*,*N*-dicyanomethylene and thione group) (Figure 5.1). Furthermore, a good charge-to-mass ratio is obtained due to the two electrons redox behavior, which results in comparably high theoretical capacities from 132 to 207 mAh/g. The introduction of low molar mass polymerizable groups, such as vinyl or ethynyl results in anthraquinone monomers that can be polymerized by straightforward polymerization techniques like free radical and rhodium-catalyzed polymerization, respectively.

The one-step modification of anthraquinone to the DCAQI system elevates the redox potentials to about $E^1_{1/2} = -0.6$ V and $E^2_{1/2} = -1.0$ V *vs.* Fc^+/Fc. Additionally, the polymerizable group does not affect the redox potentials. The monomers can be polymerized by free radical polymerization and rhodium-catalyzed polymerization, respectively. However, the *N*-cyanoimine groups are partially hydrolyzed presumably during the polymerization step and degenerate to carbonyl groups, leading to an additional redox reaction at $E^3_{1/2} = -1.3$ V *vs.* Fc^+/Fc.

Additionally, the redox potentials of the anthraquinone can be fine-tuned by mono-modification of one carbonyl group to a *N*-cyanoimine group. The reduction potentials are located at $E^1_{1/2} = -0.9$ V and $E^2_{1/2} = -1.3$ V *vs.* Fc^+/Fc, which results in a small increase compared to anthraquinone, but in a decrease compared to DCAQI. The resulting polymer features a reversible and stable redox behavior, which is not significantly affected by the

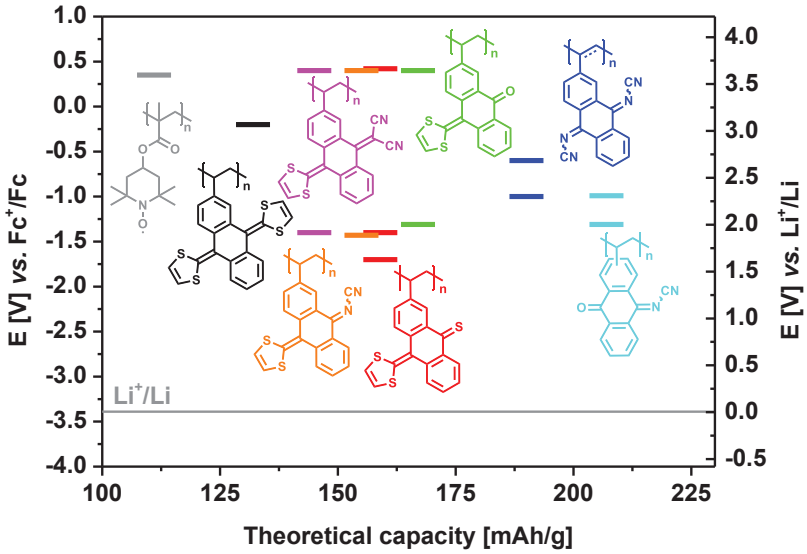

Figure 5.1: Overview of the investigated redox-active polymers in this thesis with their corresponding redox potentials and theoretical capacity.

polymeric environment. The produced polymers are employed as active material in a composite electrode in lithium-organic batteries. These batteries display good cycle stability over 100 cycles, which can be further increased by cross-linked polymers. However, the linear polymer reveals the highest capacity of 137 mAh/g (53% of the theoretical capacity). The capacity of the battery is additionally influenced by the charge/discharge speed, which is slightly decreased at higher rates. Nevertheless, the coulombic efficiency remains over 96% independent on cycling speed, indicating a stable redox behavior.

Bipolar monomers and polymers bearing both oxidizable and reducible moieties are of high interest due to their potential application as both anode and cathode material in organic batteries. An attempt to make a bipolar material starting from anthraquinone is the modification of one carbonyl group to an oxidizable moiety. In detail, one carbonyl group of the anthraquinone is transformed to a 1,3-dithiol-2-ylidene moiety, which is able to undergo a reversible one-electron redox reaction at about 0.4 V *vs.* Fc^+/Fc. The redox potential of the reduction can be tailored in a broad range (–1.3 V to –1.8 V *vs.* Fc^+/Fc) by straightforward one-step transformation of the second carbonyl group to different redox active moieties, resulting in a potential gap in the range of 1.8 V to 2.2 V *vs.* Fc^+/Fc. However, the polymers possess limited reversibility of the redox reaction. In particular, after the oxidation of the 1,3-

dithiol-2-ylidene group, a side reaction presumably of the resulting radical cation with neighboring redox-active units occurs.

The introduction of two oxidizable 1,3-dithiol-2-ylidene groups to the anthracene core leads to a compound with one two-electron oxidation reaction at $E_{1/2} = -0.2$ V *vs.* Fc^+/Fc involving two electrons forming a dicationic species in one step. The monomer can be polymerized by free radical polymerization and the polymeric environment has no influence on the redox behavior. Based on the stable and reversible redox behavior, the polymer can be utilized as cathode material for lithium-organic batteries revealing a capacity of 82 mAh/g, corresponding to 61% of the theoretical capacity. The battery shows a high stability for over 250 charge/discharge cycles at a constant cell potential of 3.5 V.

The future plans imply the introduction of a more spacious polymerizable group such as norbornene, which leads to a larger distance between the redox-active monomer units within the polymer structure and presumably fewer interactions between the units.

In summary, in this thesis it could be shown that polymers bearing redox-active anthraquinone derivatives represent attractive and promising active materials for organic electronics, such as organic batteries. The present results contribute to the understanding of the relationship between structure and electrochemical behavior and show new perspectives for the development of polymers with tailor-made redox potentials for novel redox-active materials in organic electronics.

6. Zusammenfassung

Die Entwicklung neuer Materialien für Energiespeichersysteme spielt eine wichtige und immer größer werdende Rolle um den wachsenden Bedarf an tragbaren und flexiblen elektronischen Geräten zu kompensieren. Redoxaktive organische Verbindungen, vor allem Polymere, stellen vielversprechende Materialien mit vielen Vorteilen wie Flexibilität, geringes Gewicht und Umweltfreundlichkeit dar. Zudem können organische redoxaktive Polymere unter Niedrigtemperaturverfahren von erneuerbaren oder recycelten Rohstoffen produziert und mittels effizienten und kostengünstigen Techniken (z.B. Drucktechniken) verarbeiten werden. Anthrachinon-basierende Polymere stellen vielversprechende redoxaktive Materialien für die Verwendung in organischen Sekundärbatterien oder in solar-aufladbaren elektrischen Energiespeichersystemen. Das Redoxpotential von Anthrachinonen kann durch direkte Modifikation der Carbonylgruppe zu elektronschiebenden oder elektronziehenden Gruppen (z.B. 1,3-Dithiol-2-yliden-, *N*-Cyanoimin-, *N*,*N*-Dicyanomethylen- und Thiongruppe) auf das gewünschte Potential eingestellt werden (Figure 6.1). Darüber hinaus bieten diese Verbindungen durch ihr Zweielektron-Redoxverhalten ein gutes Ladung/Masse-Verhältnis, was in vergleichbar hohe theoretische Kapazitäten von 132 bis 207 mAh/g resultiert. Die Einführung einer polymerisierbaren Gruppe mit niedriger molaren Masse, wie Vinyl oder Ethinyl, führt zu einem Anthrachinonmonomer, welches durch direkte Polymerisationstechniken wie freie radikalische oder Rhodium-katalysierte Polymerisation polymerisiert werden kann.

Die Einstufen-Modifikation des Anthrachinons zum DCAQI-System erhöht das Redoxpotential auf ungefähr $E^1_{1/2} = -0{,}6$ V und $E^2_{1/2} = -1{,}0$ V *vs.* Fc^+/Fc. Zusätzlich beeinflusst die polymerisierbare Gruppe das Redoxpotential nicht. Das Monomer kann durch freie radikalische und Rhodium-katalysierte Polymerisation polymerisiert werden. Die *N*-Cyanoimingruppen hydrolisieren jedoch teilweise vermutlich während des Polymerisationsschrittes und zerfallen zu Carbonylgruppen, was zu einer zusätzlichen Redoxreaktion bei $E^3_{1/2} = -1{,}3$ V *vs.* Fc^+/Fc führt.

Weiterhin kann das Redoxpotential des Anthrachinons durch Monomodifikation einer Carbonylgruppe zu einer *N*-Cyanoimingruppe gezielt eingestellt werden. Die Reduktions-

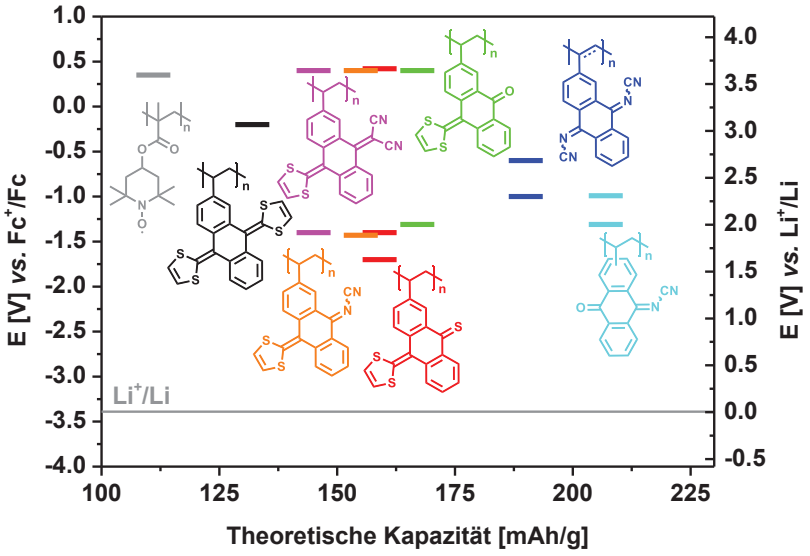

Figure 6.1: Übersicht der in dieser Arbeit untersuchten redoxaktiven Polymere mit deren Redoxpotential und theoretischen Kapazität.

potentiale liegen bei $E^1_{1/2}$ = – 0,9 V und $E^2_{1/2}$ = – 1,3 V *vs.* Fc^+/Fc, was eine leichte Erhöhung im Vergleich zum Anthrachinon und eine leichte Abnahme verglichen mit DCAQI bedeutet. Das resultierende Polymer weist ein reversibles und stabiles Redoxverhalten auf, welches durch die polymere Umgebung nicht signifikant beeinflusst wird. Die hergestellten Polymere wurden als aktives Elektrodenmaterial in Lithium-organischen Sekundärbatterien eingesetzt. Diese Sekundärbatterien zeigen eine gute Zyklenstabilität auf über 100 Zyklen, welche zusätzlich durch die Verwendung quervernetzter Polymere erhöht werden konnte. Jedoch zeigt das lineare Polymer die höchste Kapazität mit 137 mAh/g (53% der theoretischen Kapazität). Die Kapazität der Sekundärbatterie wird zusätzlich von der Lade/Entlade-Geschwindigkeit beeinflusst, welche mit steigender Geschwindigkeit leicht abnimmt. Die Coulomb-Effizienz bleibt unabhängig von der Lade/Entlade-Geschwindigkeit bei über 96%, was auf ein stabiles Redoxverhalten hinweist.

Bipolare Monomere und Polymere, welche sowohl eine oxidierbare als auch eine reduzierbare Gruppe tragen, sind von hohem Interesse, da sie sowohl als Anoden- als auch als Kathodenmaterial in organischen Sekundärbatterien eingesetzt werden können. Ein Ansatz zur Herstellung bipolarer Materialien aus Anthrachinonen ist die Modifikation einer reduzierbaren Carbonylgruppe zu einer oxidierbaren Gruppe. Im Detail heißt das, dass eine Carbonylgruppe

des Anthrachinons in eine 1,3-Dithiol-2-ylidengruppe überführt wurde, welche eine reversible Einelektron-Redoxreaktion bei ungefähr 0,4 V *vs.* Fc^+/Fc eingehen kann. Das Redoxpotential der Reduktion kann durch direkte Einstufenmodifikationen der zweiten Carbonylgruppe in einer breiten Spanne eingestellt werden (–1,3 V bis –1,8 V *vs.* Fc^+/Fc). Dadurch ergibt sich eine Potentialspanne von 1,8 V bis 2,2 V *vs.* Fc^+/Fc. Jedoch weisen die Polymere eine begrenzte Reversibilität der Redoxreaktion auf. Im Besonderen tritt während der Oxidation der 1,3-Dithiol-2-ylidengruppe eine Nebenreaktion auf, vermutlich zwischen dem erzeugten Radikalkation und den benachbarten redoxaktiven Einheiten.

Die Einführung von zwei oxidierbaren 1,3-Dithiol-2-ylidengruppen an dem Anthracenkern führt zu einer Verbindung, die eine Zweielektronen-Oxidation bei $E_{1/2} = -0{,}2$ V *vs.* Fc^+/Fc eingeht, wobei unter Einbeziehung zweier Elektronen die Dikation-Spezies in einem Schritt gebildet wird. Das Monomer kann mittels freier radikalischer Polymerisation hergestellt werden und das Redoxverhalten wird nicht von der polymeren Umgebung beeinflusst. Basierend auf dem stabilen und reversiblen Redoxverhalten wurde das Polymer als Kathodenmaterial für Lithium-organische Sekundärbatterien eingesetzt. Die erhaltene Sekundärbatterie erreicht eine Kapazität von 82 mAh/g, was 61% der theoretischen Kapazität entspricht. Diese Sekundärbatterie zeigt eine hohe Stabilität auf über 250 Lade/Entlade-Zyklen bei einer konstanten Zellspannung von 3,5 V.

In Zukunft könnten großräumigere polymerisierbare Gruppen wie Norbornene eingefügt werden, was zu einem größeren Abstand zwischen den redoxaktiven Monomereinheiten innerhalb der Polymerstruktur und dadurch wahrscheinlich zu geringeren Wechselwirkungen zwischen den Einheiten führen kann.

Zusammenfassend konnte in dieser Arbeit gezeigt werden, dass Polymere, welche Anthrachinonderivate tragen, attraktive und vielversprechende Aktivmaterialien für organische Elektronik wie organische Sekundärbatterien sind. Die vorliegenden Ergebnisse tragen zum Verständnis des Zusammenhangs zwischen Struktur und elektrochemischem Verhalten bei und zeigen neue Perspektiven für die Entwicklung von Polymeren mit maßgeschneiderten Redoxpotentialen für neue redoxaktive Materialien in organischer Elektronik.

7. References

[1] M. Armand, J.-M. Tarascon, *Nature* **2008**, *451*, 652–657.

[2] J. D. MacKenzie, C. Ho, *Proc. IEEE* **2015**, *103*, 535–553.

[3] Z. Abbas, W. Yoon, *Sensors* **2015**, *15*, 24818–24847.

[4] G. Dennler, S. Bereznev, D. Fichou, K. Holl, D. Ilic, R. Koeppe, M. Krebs, A. Labouret, C. Lungenschmied, A. Marchenko, D. Meissner, E. Mellikov, J. Méot, A. Meyer, T. Meyer, H. Neugebauer, A. Öpik, N. Sariciftci, S. Taillemite, T. Wöhrle, *Sol. Energy* **2007**, *81*, 947–957.

[5] F. C. Krebs, T. D. Nielsen, J. Fyenbo, M. Wadstrøm, M. S. Pedersen, *Energy Environ. Sci.* **2010**, *3*, 512.

[6] P. Poizot, F. Dolhem, *Energy Environ. Sci.* **2011**, *4*, 2003–2019.

[7] H. Nishide, K. Oyaizu, *Science* **2008**, *319*, 737–738.

[8] B. A. Andersson, I. Råde, *Transport. Res. D* **2001**, *6*, 297–324.

[9] K. Oyaizu, H. Nishide, *Adv. Mater.* **2009**, *21*, 2339–2344.

[10] M. Armand, S. Grugeon, H. Vezin, S. Laruelle, P. Ribière, P. Poizot, J.-M. Tarascon, *Nat. Mater.* **2009**, *8*, 120–125.

[11] T. Janoschka, M. D. Hager, U. S. Schubert, *Adv. Mater.* **2012**, *24*, 6397–6409.

[12] T. Jähnert, M. D. Hager, U. S. Schubert, *J. Mater. Chem. A* **2014**, *2*, 15234–15251.

[13] B. Häupler, A. Wild, U. S. Schubert, *Adv. Energy Mater.* **2015**, *5*, 1402034.

[14] Y. Hanyu, Y. Ganbe, I. Honma, *J. Power Sources* **2013**, *221*, 186–190.

[15] R. Zeng, L. Xing, Y. Qiu, Y. Wang, W. Huang, W. Li, S. Yang, *Electrochim. Acta* **2014**, *146*, 447–454.

[16] J. Xiang, C. Chang, M. Li, S. Wu, L. Yuan, J. Sun, *Cryst. Growth Des.* **2008**, *8*, 280–282.

[17] R.-h. Zeng, X.-p. Li, Y.-c. Qiu, W.-s. Li, J. Yi, D.-s. Lu, C.-l. Tan, M.-q. Xu, *Electrochem. Commun.* **2010**, *12*, 1253–1256.

[18] M. Yao, H. Senoh, M. Araki, T. Sakai, K. Yasuda, *ECS Trans.* **2010**, *28*, 3–10.

[19] M. Yao, H. Ando, T. Kiyobayashi, *Energy Proc.* **2013**, *34*, 880–887.

[20] T. Yokoji, H. Matsubara, M. Satoh, *J. Mater. Chem. A* **2014**, *2*, 19347–19354.

[21] B. Häupler, T. Hagemann, C. Friebe, A. Wild, U. S. Schubert, *ACS Appl. Mater. Interfaces* **2015**, *7*, 3473–3479.

[22] A. Shimizu, Y. Tsujii, H. Kuramoto, T. Nokami, Y. Inatomi, N. Hojo, J.-i. Yoshida, *Energy Tech.* **2014**, *2*, 155–158.

[23] A. Shimizu, H. Kuramoto, Y. Tsujii, T. Nokami, Y. Inatomi, N. Hojo, H. Suzuki, J.-i. Yoshida, *J. Power Sources* **2014**, *260*, 211–217.

[24] W. Wan, H. Lee, X. Yu, C. Wang, K.-W. Nam, X.-Q. Yang, H. Zhou, *RSC Adv.* **2014**, *4*, 19878–19882.

[25] B. Häupler, R. Burges, T. Janoschka, T. Jähnert, A. Wild, U. S. Schubert, *J. Mater. Chem. A* **2014**, *2*, 8999–9001.

[26] S. Nishida, Y. Yamamoto, T. Takui, Y. Morita, *ChemSusChem* **2013**, *6*, 794–797.

[27] M. Kato, K.-i. Senoo, M. Yao, Y. Misaki, *J. Mater. Chem. A* **2014**, *2*, 6747–6754.

[28] Z. Song, H. Zhan, Y. Zhou, *Chem. Commun.* **2009**, *5*, 448–450.

[29] T. Nokami, T. Matsuo, Y. Inatomi, N. Hojo, T. Tsukagoshi, H. Yoshizawa, A. Shimizu, H. Kuramoto, K. Komae, H. Tsuyama, J.-i. Yoshida, *J. Am. Chem. Soc.* **2012**, *134*, 19694–19700.

[30] T. Song, B. Sun, *ChemSusChem* **2013**, *6*, 408–410.

[31] T. Chen, L. Qiu, Z. Yang, Z. Cai, J. Ren, H. Li, H. Lin, X. Sun, H. Peng, *Angew. Chem. Int. Ed.* **2012**, *51*, 11977–11980.

[32] H. J. Snaith, L. Schmidt-Mende, *Adv. Mater.* **2007**, *19*, 3187–3200.

[33] B. C. Thompson, J. M. J. Fréchet, *Angew. Chem. Int. Ed.* **2008**, *47*, 58–77.

[34] M. Graetzel, R. A. J. Janssen, D. B. Mitzi, E. H. Sargent, *Nature* **2012**, *488*, 304–312.

[35] Q. Schiermeier, J. Tollefson, T. Scully, A. Witze, O. Morton, *Nature* **2008**, *454*, 816–823.

[36] N. S. Lewis, *Science* **2007**, *315*, 798–801.

[37] K. Wang, H. Wu, Y. Meng, Y. Zhang, Z. Wei, *Energy Environ. Sci.* **2012**, *5*, 8384–8389.

[38] L. Li, Z. Wu, S. Yuan, X.-B. Zhang, *Energy Environ. Sci.* **2014**, *7*, 2101–2122.

[39] P. Liu, H. Yang, X. Ai, G. Li, X. Gao, *Electrochem. Commun.* **2012**, *16*, 69–72.

[40] Z. Yang, L. Li, Y. Luo, R. He, L. Qiu, H. Lin, H. Peng, *J. Mater. Chem. A* **2012**, *1*, 954–958.

[41] X. Zhang, X. Huang, C. Li, H. Jiang, *Adv. Mater.* **2013**, *25*, 4093–4096.

[42] N. A. Kelly, T. L. Gibson, *J. Power Sources* **2011**, *196*, 10430–10441.

[43] T. L. Gibson, N. A. Kelly, *J. Power Sources* **2010**, *195*, 3928–3932.

[44] Y. Fu, H. Wu, S. Ye, X. Cai, X. Yu, S. Hou, H. Kafafy, D. Zou, *Energy Environ. Sci.* **2013**, *6*, 805–812.

[45] T. R. Cook, D. K. Dogutan, S. Y. Reece, Y. Surendranath, T. S. Teets, D. G. Nocera, *Chem. Rev.* **2010**, *110*, 6474–6502.

[46] P. Liu, Y.-l. Cao, G.-R. Li, X.-P. Gao, X.-P. Ai, H.-X. Yang, *ChemSusChem* **2013**, *6*, 802–806.

[47] T. Janoschka, N. Martin, U. Martin, C. Friebe, S. Morgenstern, H. Hiller, M. D. Hager, U. S. Schubert, *Nature* **2015**, *527*, 78–81.

[48] M. Sharon, P. Veluchamy, C. Natarajan, D. Kumar, *Electrochim. Acta* **1991**, *36*, 1107–1126.

[49] J. Bae, Y. J. Park, M. Lee, S. N. Cha, Y. J. Choi, C. S. Lee, J. M. Kim, Z. L. Wang, *Adv. Mater.* **2011**, *23*, 3446–3449.

[50] A. Burke, *J. Power Sources* **2000**, *91*, 37–50.

[51] L. L. Zhang, X. S. Zhao, *Chem. Soc. Rev.* **2009**, *38*, 2520–2531.

[52] J.-H. Yum, P. Chen, M. Grätzel, M. K. Nazeeruddin, *ChemSusChem* **2008**, *1*, 699–707.

[53] H.-W. Chen, C.-Y. Hsu, J.-G. Chen, K.-M. Lee, C.-C. Wang, K.-C. Huang, K.-C. Ho, *J. Power Sources* **2010**, *195*, 6225–6231.

[54] S. Zhang, X. Yang, Y. Numata, L. Han, *Energy Environ. Sci.* **2013**, *6*, 1443–1464.

[55] P. G. Bomben, J. Borau-Garcia, C. P. Berlinguette, *Chem. Commun.* **2012**, *48*, 5599–5601.

[56] T. Miyasaka, T. N. Murakami, *Appl. Phys. Lett.* **2004**, *85*, 3932–3934.

[57] T. N. Murakami, N. Kawashima, T. Miyasaka, *Chem. Commun.* **2005**, 3346–3348.

[58] C. Yu, C. Masarapu, J. Rong, B. Wei, H. Jiang, *Adv. Mater.* **2009**, *21*, 4793–4797.

[59] X. Chen, H. Sun, Z. Yang, G. Guan, Z. Zhang, L. Qiu, H. Peng, *J. Mater. Chem. A* **2014**, *2*, 1897–1902.

[60] Z. Yang, J. Deng, H. Sun, J. Ren, S. Pan, H. Peng, *Adv. Mater.* **2014**, *26*, 7038–7042.

[61] G. A. Niklasson, C. G. Granqvist, *J. Mater. Chem.* **2006**, *17*, 127–156.

[62] Y. Saito, S. Uchida, T. Kubo, H. Segawa, *Thin Solid Films* **2010**, *518*, 3033–3036.

[63] N. F. Yan, G. R. Li, G. L. Pan, X. P. Gao, *J. Electrochem. Soc.* **2012**, *159*, A1770-A1774.

[64] Y. Saito, A. Ogawa, S. Uchida, T. Kubo, H. Segawa, *Chem. Lett.* **2010**, *39*, 488–489.

[65] H. Nagai, H. Segawa, *Chem. Commun.* **2004**, 974–975.

[66] S.-H. Shin, S.-H. Yun, S.-H. Moon, *RSC Adv.* **2013**, *3*, 9095–9116.

[67] Y. Wang, P. He, H. Zhou, *Adv. Energy Mater.* **2012**, *2*, 770–779.

[68] H. Chen, T. N. Cong, W. Yang, C. Tan, Y. Li, Y. Ding, *Prog. Nat. Sci.* **2009**, *19*, 291–312.

[69] M. Duduta, B. Ho, V. C. Wood, P. Limthongkul, V. E. Brunini, W. C. Carter, Y.-M. Chiang, *Adv. Energy Mater.* **2011**, *1*, 511–516.

[70] N. F. Yan, G. R. Li, X. P. Gao, *J. Mater. Chem. A* **2013**, *1*, 7012–7015.

[71] N. F. Yan, G. R. Li, X. P. Gao, *J. Electrochem. Soc.* **2014**, *161*, A736-A741.

[72] Q. Wang, H. Chen, E. McFarland, L. Wang, *Adv. Energy Mater.* **2015**, *5*, 1501418.

[73] M. Suzuka, S. Hara, T. Sekiguchi, K. Oyaizu, H. Nishide, *Polymer* **2015**, *68*, 353–357.

[74] G. Wee, T. Salim, Y. M. Lam, S. G. Mhaisalkar, M. Srinivasan, *Energy Environ. Sci.* **2011**, *4*, 413–416.

[75] M. A. Green, *Philos. T. R. Soc. A* **2013**, *371*, 20110413.

[76] P. M. Beaujuge, J. M. J. Fréchet, *J. Am. Chem. Soc.* **2011**, *133*, 20009–20029.

[77] J. K. Lee, W. L. Ma, C. J. Brabec, J. Yuen, J. S. Moon, J. Y. Kim, K. Lee, G. C. Bazan, A. J. Heeger, *J. Am. Chem. Soc.* **2008**, *130*, 3619–3623.

[78] F. C. Krebs, T. Tromholt, M. Jørgensen, *Nanoscale* **2010**, *2*, 873–886.

[79] C. Deibel, V. Dyakonov, *Rep. Prog. Phys.* **2010**, *73*, 096401.

[80] M. Jørgensen, K. Norrman, S. A. Gevorgyan, T. Tromholt, B. Andreasen, F. C. Krebs, *Adv. Mater.* **2012**, *24*, 580–612.

[81] Z. Zhang, X. Chen, P. Chen, G. Guan, L. Qiu, H. Lin, Z. Yang, W. Bai, Y. Luo, H. Peng, *Adv. Mater.* **2014**, *26*, 466–470.

[82] A. K. Pandey, P. C. Deakin, R. D. Jansen-Van Vuuren, P. L. Burn, I. D. W. Samuel, *Adv. Mater.* **2010**, *22*, 3954–3958.

[83] F. Cheng, J. Chen, *Chem. Soc. Rev.* **2012**, *41*, 2172–2192.

[84] K. Oyaizu, Y. Niibori, A. Takahashi, H. Nishide, *J. Inorg. Organomet. Polym. Mater.* **2013**, *23*, 243–250.

[85] M. C. Díaz, B. M. Illescas, C. Seoane, N. Martín, *J. Org. Chem.* **2004**, *69*, 4492–4499.

[86] N. Martín, P. de Miguel, C. Seoane, A. Albert, F. H. Cano, *J. Mater. Chem.* **1997**, *7*, 25–29.

[87] M. A. Casado, A. Fazal, L. A. Oro, *Arab. J. Sci. Eng.* **2013**, *38*, 1631–1646.

[88] J. Liu, Lam, Jacky W Y, B. Z. Tang, *Chem. Rev.* **2009**, *109*, 5799–5867.

[89] W. Yang, M. Tabata, S. Kobayashi, K. Yokota, A. Shimizu, *Polym. J.* **1991**, *23*, 1135–1138.

[90] K. Takahashi, K. Kobayashi, *J. Org. Chem.* **2000**, *65*, 2577–2579.

[91] D. Pletcher, H. Thompson, *Faraday Trans.* **1998**, *94*, 3445–3450.

[92] C. S. Wang, M. R. Bryce, A. S. Batsanov, Howard, J. A. K., *Chem. Eur. J.* **1997**, *3*, 1679–1690.

[93] F. Vilela, P. J. Skabara, C. R. Mason, T. D. J. Westgate, A. Luquin, S. J. Coles, M. B. Hursthouse, *Beilstein J. Org. Chem.* **2010**, *6*, 1002–1014.

[94] G. Fernández, E. M. Pérez, L. Sánchez, N. Martín, *J. Am. Chem. Soc.* **2008**, *130*, 2410–2411.

[95] F. G. Brunetti, J. L. López, C. Atienza, N. Martín, *J. Mater. Chem.* **2012**, *22*, 4188–4205.

[96] B. Häupler, *Dissertation,* Friedrich Schiller University, Jena, **2015**.

[97] D. M. Guldi, L. Sánchez, N. Martín, *J. Phys. Chem. B* **2001**, *105*, 7139–7144.

[98] T. Itoh, M. Matsuno, E. Kamiya, K. Hirai, H. Tomioka, *J. Am. Chem. Soc.* **2005**, *127*, 7078–7093.

[99] T. Yamamoto, H. Etori, *Macromolecules* **1995**, *28*, 3371–3379.

[100] A. Zon, M. Palys, Z. Stojek, H. Sulowska, T. Ossowski, *Electroanal.* **2003**, *15*, 579–585.

List of abbreviations

AIBN	Azo*bis*(isobutyronitrile)
BHJ	Bulk heterojunction
n-BuLi	*n*-Butyllithium
CMSt-TIPNO	*N*-*tert*-Butyl-*O*-[1-[4-(chloromethyl)phenyl]ethyl]-*N*-(2-methyl-1-phenylpropyl)hydroxylamine
CNT	Carbon nanotubes
Conc.	Concentration
Đ	Dispersity
DCAQI	*N*,*N'*-Dicyanoanthraquinone diimine
DMAc	*N*,*N*-Dimethylacetamide
DMC	Dimethyl carbonate
DME	1,2-Dimethoxyethane
DMF	*N*,*N*-Dimethylformamide
DMSO	Dimethyl sulfoxide
DSSC	Dye-sensitized solar cell
DTBP	Di-*tert*-butyl peroxide
EC	Ethylene carbonate
eq.	Equivalents
ES-DSSC	Energy-storable dye-sensitized solar cell
ex(TTF)	9,10-Di(1,3-dithiol-2-ylidene)-9,10-dihydroanthracene

Fc	Ferrocene
FRP	Free radical polymerization
IR	Infrared
ITO	Indium tin oxide
M	Molar concentration
M_n	Number average molar mass
MWCNT	Multi-walled carbon nanotubes
nbd	2,5-Norbornadiene
NMP	*N*-methyl-2-pyrrolidone
NMP	Nitroxide mediated polymerization
OPV	Organic photovoltaic system
ox	Oxidation
P3HT	Poly(3-hexylthiophene)
PANI	Poly(aniline)
PC	Propylene carbonate
PCBM	Phenyl-C61-butyric acid methyl ester
PEDOT	Poly(3,4-ethylenedioxythiophene)
PSS	Poly(styrene sulfonate)
PVDF	Poly(vinylidene fluoride)
red	Reduction
RFB	Redox flow battery
RI	Refractive index

r.t.	Room temperature
SEC	Size exclusion chromatography
$TBAClO_4$	Tetrabutylammonium perchlorate
TBHP	*tert*-Butyl hydroperoxide
Temp.	Temperature
TEMPOL	1-Oxyl-2,2,6,6-tetramethyl-4-hydroxypiperidine
THF	Tetrahydrofuran
TsOH	*para*-Toluenesulfonic acid
VGCF	Vapor grown carbon fibers

Curriculum vitae

13/10/1986	Born in Suhl, Germany
1993 – 1997	Elementary School in Suhl and Sonneborn, both Germany
1997 – 2005	Arnoldischule Gotha, Germany
24/06/2005	University entrance certification at Arnoldischule Gotha, Germany
10/2005 – 03/2006	Basic military service at the German Federal Armed Forces, Armored reconnaissance Battalion 13, Gotha, Germany
10/2006 – 03/2012	Study of chemistry at Friedrich Schiller University Jena, Germany
03/2011 – 03/2012	Diploma thesis under the supervision of Prof. Dr. Ulrich S. Schubert, Jena, Germany Topic: “Synthesis and Characterization of Conjugated Low Band Gap Donor-Acceptor-Copolymer Libraries”
28/03/2012	Diploma
Since 05/2012	PhD student at the Laboratory of Macromolecular and Organic Chemistry (IOMC) at the Friedrich Schiller University Jena under the supervision of Prof. Dr. Ulrich S. Schubert, Jena, Germany

Jena, 18.07.2016

_____

Daniel Schmidt

Publication list

Peer-reviewed publications

[1] B. Häupler, R. Burges, C. Friebe, T. Janoschka, D. Schmidt, A. Wild, U. S. Schubert, "Poly(exTTF): A novel redox-active polymer as active material for Li-organic batteries", *Macromol. Rapid Comm.* **2014**, *35*, 1367-1371.

[2] D. Schmidt, M. D. Hager, U. S. Schubert, "Photo-rechargeable electric energy storage systems", *Adv. Energy Mater.* **2016**, *6*, 1500369.

[3] D. Schmidt, B. Häupler, C. Friebe, M. D. Hager, U. S. Schubert, "Synthesis and characterization of new redox-active polymers based on 10-(1,3-dithiol-2-ylidene)anthracen-9(10H)-one derivatives", *Polymer* **2015**, *68*, 321-327.

[4] D. Schmidt, B. Häupler, C. Stolze, M. D. Hager, U. S. Schubert, "Poly[*N*-(10-oxo-2-vinylanthracen-9(10*H*)-ylidene)cyanamide] as a novel cathode material for Li-organic batteries", *J. Polym. Sci., Part A: Polym. Chem.* **2015**, *53*, 2517–2523.

[5] D. Schmidt, B. Häupler, M. D. Hager, U. S. Schubert, "Poly(DCAQI): Synthesis and characterization of a new redox-active polymer", *J. Polym. Sci., Part A: Polym. Chem.* **2016**, *54*, 1998–2003.

[6] B. Häupler, C. Rössel, A. M. Schwenke, J. Winsberg, D. Schmidt, A. Wild, U. S. Schubert, "Aqueous-based hybrid zinc-organic polymer battery with high rate performance and ultra-long life time.", *NPG Asia Mater.* **2016**, *8*, e283, DOI: 10.1038/am.2016.82.

Poster presentations

[1] D. Schmidt, B. Häupler, M. D. Hager, U. S. Schubert, "Development of a new redox-active polymer as cathode material for Li-organic batteries", ***European Polymer Congress***, June 21 - 26, **2015**, Dresden, Germany.

[2] D. Schmidt, M. D. Hager, U. S. Schubert, “Synthesis and characterization of new conjugated low band gap donor-acceptor-copolymer libraries”, ***ORCHEM***, September 24 - 26, **2012**, Weimar, Germany.

Acknowledgements / Danksagung

This thesis would not have been possible without the continuous help, support and advice of a lot of people.

First of all, I would like to thank Prof. Dr. Ulrich. S. Schubert for giving me the opportunity to prepare this work in his group that constitutes the foundation for this thesis. He offered me a very interesting interdisciplinary topic.

I want to thank all the contributing people, since without their support the majority of the achievements in this thesis could not have been accomplished. Many thanks appertain to my direct supervisor Martin Hager for having always an open ear during and a lot of helpful hints also in difficult times of my work. I would like to thanks in particular Bernhard Häupler for his continues support, help and productive discussions, which were crucial for the success of this work as well as for correcting all our publications.

Additionally, I want to thank Wolfgang Günther, Peter Bellstedt, Gabrielle Sentis, Uwe Köhn, Franca Frister, Simone Burchardt, Sylvia Braunsdorf, Grit Festag, Sandra Köhn, Beate Lentvogt, Renzo Paulus, Steffi Stumpf and René Burges for all the service measurements and administrative management.

I also would like to thank Robert Bolney, Benedikt Suchland, Thomas Kutschin, Thomas Berthold, Daniel Costabel, Maria Strumpf and René Burges for support for the synthesis work as well as Christian Friebe and Christian Stolze for sharing your electrochemical knowledge and support with electrochemical experiments.

Furthermore I want to thank Julia Kötteritzsch, Ronny Tepper, Robert Schroot, Kevin Barthelmes and especially Tina Schlotthauer for the supply with cake during long working days and the nice coffee breaks.

Further gratitude goes to my lab college Bernhard Häupler and René Burges for the nice work atmosphere and helpful discussions.

I grateful tank my parents, my sister and my brother who supported me throughout all the years of my studies.

Dear Fatima, I would like to thank you for your unconditional support. During the years I made this thesis, I never heard one word of reproach, although I was in a bad mood.

Declaration of authorship / Selbstständigkeitserklärung

Ich erkläre, dass ich die vorliegende Arbeit selbständig und unter Verwendung der angegebenen Hilfsmittel, persönlichen Mitteilungen und Quellen angefertigt habe.

I certify that the work presented here is, to the best of my knowledge and belief, original and the result of my own investigations, except as acknowledged, and has not been submitted, either in part or whole, for a degree at this or any other university.

Jena, 18.07.2016

_____

Daniel Schmidt

Publications P1-P5

Publication 1

"Photo-rechargeable electric energy storage systems"

Daniel Schmidt, Martin D. Hager, Ulrich S. Schubert

Adv. Energy Mater. **2016**, 6: 1500369. DOI: 10.1002/aenm.201500369.

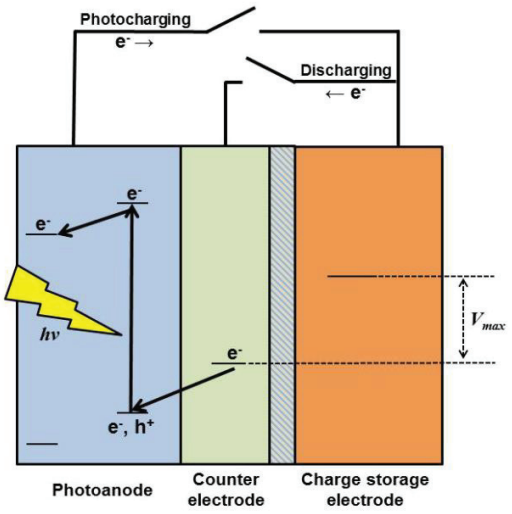

Photo-Rechargeable Electric Energy Storage Systems

*Daniel Schmidt, Martin D. Hager, and Ulrich S. Schubert**

The global energy demand is increasing at the same time as fossil fuel resources are dwindling. Consequently, the search for alternative energy sources is a major topic worldwide. Solar energy is one of the most promising, effective and emission-free energy sources. However, the energy has to be stored to compensate the fluctuating availability of the sun and the actual energy demand. Photo-rechargeable electric energy storage systems may solve this problem by immediately storing the generated electricity. Different combinations of solar cells and storage devices are possible. High efficiencies can be achieved by the combination of dye-sensitized solar cells (DSSC) and capacitors. However, other hybrid devices including DSSCs or organic photovoltaic systems and redox flow batteries, lithium ion batteries and metal air batteries are playing an increasing role in this research field. This Progress Report reviews the state of the art research of photo-rechargeable batteries based on organic solar cells, as well as storage modules.

1. Introduction

Currently, the total energy consumption of the world is about 1.04×10^8 GWh per year.[1] But until now, fossil fuels have still by far the highest share in the global mix, with 82%. However, fossil fuels are not available in unlimited quantities (e.g., "peak oil"), and their utilization leads inherently to a production of more than 10 gigatons of carbon dioxide every year, which is considered to be a greenhouse gas which results in a global warming.[1,2] As a consequence, alternative electricity generation from renewable resources plays an increasingly important role.[3,4] One of the most powerful, efficient and eco-friendly solutions is the usage of solar energy.[5–8] The sun represents an unlimited and effective energy source, which is available with no running costs, and no waste materials are produced. About 100,000 TW of solar power are received by the earth's surface every hour. This is more power than humans consume in an entire year.[2,9] Several technologies are already available for the use of solar energy, e.g., solar collectors, and concentrated solar thermal systems, as well as solar cells. Due to increasing manufacturing capacities and lower costs, the installed capacities of solar cells has grown massively in recent years. In 2012, the capacity of installed solar cells rose over the level of 100 GW worldwide.[10]

The major drawback of solar power is that electricity generation is directly coupled to the availability of the sun (e.g., day and night, weather). This dependence of solar energy does not comply with the actual energy demand and requires a solution. The key technology is the combination of solar cells and effective energy storage systems, e.g., batteries or supercapacitors, to create independent electrical energy sources.[8,11–15] Usually, the generated photovoltaic energy is stored by external batteries (e.g., Li ion or nickel/metal hydride batteries), which are directly connected to the solar cells by wires.[13,16,17] As a consequence, the relatively long distance between both parts lowers the energy storage efficiency.[13] One approach to avoid this problem is the integration of the photo conversion system and the energy storage part within one device, for an effective storage of the excess energy.[6,18] The stored energy can be released and used throughout the day, and at different places, even if the sun is not shining.[18,19] Different possibilities for storing large amounts of energy are available, e.g., pumped hydroelectric energy storage or compressed air energy storage as large-scale, centralized systems.[19] Moreover, photo generated electricity can be stored as chemical energy. The best known system for conversion and storage of solar energy as chemical energy is the photosynthesis of plants, algae and bacteria, in which organic material and oxygen are generated by water and carbon dioxide under sunlight illumination.[20] Water splitting represents an artificial way,[19,21] where hydrogen and oxygen are produced by utilization of photo catalysts[22] or semiconducting electrodes.[23] Photo-electrochemical energy can be efficiently stored by using two vanadium based redox couples.[24] Other possibilities for storage of solar energy are molecular energy storage systems, where new chemical bonds are formed; phase change materials, where the energy is stored as thermal energy; as well as electrochemical storage systems.[20,25] Many types of electrochemical storage applications such as rechargeable batteries (e.g., lithium ion batteries, high-temperature sodium batteries, or lead acid batteries), organic radical batteries, redox flow batteries, as well as electrochemical supercapacitors are available.[4,19,26]

A solar rechargeable battery uses the solar light to generate electric energy, which is directly stored by an integrated storage

D. Schmidt, Dr. M. D. Hager, Prof. U. S. Schubert
Laboratory of Organic and Macromolecular Chemistry (IOMC)
Friedrich Schiller University Jena
Humboldtstr. 10, 07743 Jena, Germany
E-mail: ulrich.schubert@uni-jena.de

D. Schmidt, Dr. M. D. Hager, Prof. U. S. Schubert
Center for Energy and Environmental Chemistry Jena (CEEC Jena)
Friedrich Schiller University Jena
Philosophenweg 7a, 07743 Jena, Germany

DOI: 10.1002/aenm.201500369

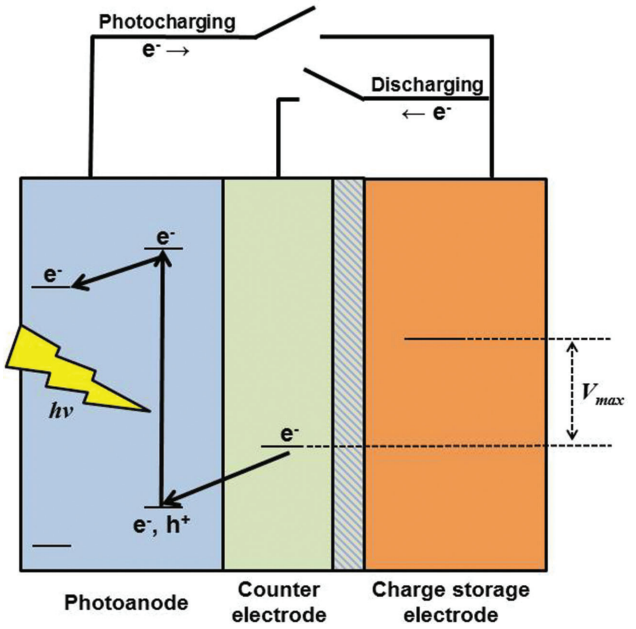

Figure 1. Schematic representation of the setup of a solar rechargeable battery, consisting of a photoanode, in which the charge carriers are generated, a charge storage electrode and a counter electrode. Both are utilizing for energy storage.

assembly.[27] These devices consist of a photoanode, and a counter electrode, as well as a charge storage electrode (**Figure 1**). Under light illumination of the photoanode, the photo-active material is excited to form an electron–hole pair. The electrons move to the charge storage electrode and they are stored in the electrode. The holes in the photoanode will be counterbalanced by the electrons of the counter electrode, and the device will be charged. The electrons move back from the charge storage electrode to the counter electrode during the discharging process. A membrane separates the counter electrode from the charge storage electrode, and provides the counterbalance by the cations.

In this Progress Report, we provide a brief overview of organic-based photo-rechargeable batteries. We focus on the recent developments in hybrid devices between charge generation assemblies like organic photovoltaics, dye-sensitized solar cells, or silicon based solar cells, and charge storage devices like organic radical batteries, redox flow batteries, and lithium ion batteries, as well as supercapacitors.

2. Electric Energy Storage Systems Charged by Silicon Based Solar Cells

The most well-known and established solar cell device is the silicon based solar cell. This technology is predominated by the utilization of crystalline silicon and achieves the highest efficiencies of about 25% and dominates the field of commercial photovoltaic modules.[28–30] However, there are some drawbacks like inflexibility, high weight and high production costs due to the need of a large amount of the expensive raw material. Alternative materials such as amorphous silicon or thin film technologies using other inorganic materials like CdTe are promising approaches to fabricate cheaper and flexible devises, but efficiencies of these setups are lower compared to the crystalline based solar cells.[30,31]

Daniel Schmidt studied chemistry at the Friedrich Schiller University Jena (Germany) where he earned his diploma degree in organic and macromolecular chemistry in 2012. Afterwards, he started his Ph.D. studies in macromolecular chemistry under the supervision of Prof. Ulrich S. Schubert. His research interests are focused on developing new polymer based materials for energy storage systems.

Martin D. Hager studied chemistry at the Friedrich Schiller University Jena (Germany) where he graduated in organic and macromolecular chemistry in 2005. In 2007, he received his Ph.D. in chemistry (Friedrich-Schiller-University Jena, Germany) for work on conjugated rod-coil polymers under supervision of Prof. E. Klemm (scholarship of the Fonds der Chemischen Industrie). Subsequently, in 2007 he joined the group of Prof. U. S. Schubert (Eindhoven University of Technology, the Netherlands and then Friedrich Schiller University Jena, Germany). His research is focused on conjugated polymers for energy applications and self-healing materials.

Ulrich S. Schubert studied chemistry in Frankfurt and Bayreuth (both Germany) and the Virginia Commonwealth University, Richmond (USA). His Ph.D. work was performed at the Universities of Bayreuth and South Florida/Tampa. After a postdoctoral training with Prof. J.-M. Lehn at the University Strasbourg (France), he moved to the TU Munich (Germany) to obtain his habilitation in 1999. From 1999 to 2000 he was a professor at the Center for NanoScience, University of Munich, and from 2000 to 2007 Full-Professor at TU Eindhoven (The Netherlands). Currently, he is Full-Professor at the Friedrich Schiller University Jena (Germany) and Director of the CEEC Jena.

Nevertheless, silicon based solar cells are suitable for photo-rechargeable energy storage systems. A direct conversion and storage of solar energy by using photoelectrochemical and ferroelectric effects was shown by Jiang et al. The authors constructed a device consisting of a transparent electrode, a current collector, a $LiPF_6$ containing electrolyte, ferroelectric PVDF particles, which were bound on silicon particles and a ferroelectric PVDF membrane. The photo-rechargeable battery had a charge storage capacity of 37.62 mC cm^{-2} and after eight hours ≈70% of the initial charge was still stored. The open-circuit output voltage was 0.47 V, which was stable over 24 hours.[32]

Other systems based on silicon cells used a common solar cell, which was connected to a battery by a wire. Kelly and his group used a Li-ion battery with an output voltage of 4.2 V with a capacity of 2.35 Ah and an ultra-thin amorphous silicon solar cell with an efficiency of 15%. The connection of both elements led to a solar energy to charge efficiency of 14.5% by utilizing a 15-cell battery module.[17] The group of Kan discovered that the direct charging of a Li-ion battery by a solar cell took longer times for charging and the capacity of the battery decreased faster than in standard cellular batteries. As a consequence, they investigated the additional introduction of supercapacitors. This buffer function between the solar cell and the battery, at which the energy can be transferred slowly to the battery, prevented the loss of the lifetime as well as the capacity of the battery significantly.[33]

3. Electric Energy Storage Systems Charged by Dye-Sensitized Solar Cells

Due to the still rather high production and installation costs, the high energy consumption during production as well as the missing flexibility of silicon based solar cells, alternative technologies are required. Dye-sensitized solar cells (DSSC) are very prominent, well-understood and suitable systems for converting solar light into electric current. They are very efficient, with energy conversion efficiencies up to 11%,[34] are environmental friendly, can be fabricated by roll-to-roll processes and only require simple materials and equipment, which leads to a low cost alternative to common silicon based solar cells.[35] A DSSC consists of a transparent electrode, which is covered by a dye coated porous TiO_2 layer. The latter electrode and the second electrode (e.g., platinum) are separated by an electrolyte containing a redox couple (e.g., I_2/KI).[36,37] The dye on the TiO_2 film absorb the solar energy and excited dye molecules are formed. Consequently, electrons are injected into the conduction band of the TiO_2 film and are transported towards the transparent electrode. The oxidized dye are regenerated to the neutral state by iodine anions in the electrolyte, which is reproduced by the reduction of I_3^- with the electrons from the counter electrode.[38–41] Due to the low layer thickness of only a few micrometers the solar cells are light-weight and flexible.[18,35] DSSC are very powerful even under diffuse and low intensity light conditions.[36] So called energy-storable dye-sensitized solar cells (ES-DSSC) can be produced by the combination of DSSC with an electron storable device.

3.1. Supercapacitor-DSSC Hybrids

Supercapacitors represent a class of powerful storage device for electric energy which are used typically for flexible electronic systems.[42] They are distinguished by high power output densities, fast charge/discharge rates, as well as long lifetimes.[43] Compared with conventional battery systems, the capacitance is much lower, but the power density is much higher. Furthermore, supercapacitors have a rapid response to the current changes, which can compensate for the variation of the solar light.[5,18,44] Depending on the kind of energy storage, supercapacitors can be classified in electric double layer capacitors (EDLC) and pseudo-capacitors. EDLC consists on two carbon based electrode materials which are separated by an insulator and feature a high power density due to large charge accumulation. The energy is stored by non-faradaic manner. Pseudo-capacitors offer a higher energy density due to a large potential window. The electrostatically storage and faradaic charge transfer occurs at the electrode/electrolyte interface.[45]

A wide range of different materials are suitable for capacitor devices. Miyasaka et al. developed an activated carbon containing ES-DSSC with a two-electrode construction, where the energy is directly stored as double-layer charges. The photocapacitor achieved a voltage value of 0.45 V in the charged state, and a discharge capacity of 75 mC cm^{-2}, due to the incorporation of LiI into the TiO_2 layer. These values are 15 times higher than the results of a LiI-free ES-DSSC.[44] However, this device revealed a high internal resistance. As a consequence, the group of Miyasaka generated a three-electrode photocapacitor with electrodes also covered with activated carbon, which had a five times larger energy output than the two-electrode system.[46]

Another important material for photo chargeable capacitors are carbon nanotubes (CNT). DSSC with a CNT film as the counter electrode have a similar high performance (e.g., a specific capacitance of 54 F g^{-1}) like the common platinum electrodes. Supercapacitors based on electrodes with CNT films reveal also good properties, such as a specific capacitance of 54 F g^{-1}.[47] One device using CNT showed a photoelectric conversion efficiency of 6.1%, a specific capacitance of 48 F g^{-1} and a storage efficiency of about 84%, with an entire photoelectric conversion and storage efficiency of about 5.12%. By incorporation of polyaniline (PANI) into the CNT the specific capacitance increased up to 208 F g^{-1} whereas the energy storage efficiency dropped to ≈70%, with an overall photoelectric conversion and storage efficiency of about 4.29%. This effect was presumably caused by chemical reactions of the CNT-PANI composite during the charge/discharge processes.[13] To enhance the flexibility and lightweight of the ES-DSSC, its planar structure has to changed into a wire shape. Such wires can be easily woven into textiles or other deformable structures for self-powering applications, such as medical biomonitoring devices or implants, safety and construction gear like illuminated vests and wearable electronics.[48] Moreover, Peng et al. utilized CNT/Ti wire composites. The Ti wire was modified with TiO_2 nanotubes, whereas one part of the Ti wire was coated with a photoactive Ru dye (N719—*cis*-diisothiocyanato-*bis*(2,2′-bipyridyl-4,4′-dicarboxylato)ruthenium(II)*bis*(tetrabutylammonium)), and the other part was covered with electrolyte. The wire had a thickness of 10 to 30 μm and achieved an entire photoelectric

conversion and storage efficiency of 1.5% (photoelectric conversion efficiency is 2.2%).[6] An improvement of these wire-shaped energy conversion and storage device was published in 2014 by the same group.[49] The Ti wire substrate, modified with perpendicularly aligned TiO_2 nanotubes on the surface and horizontally aligned CNT, serve as two electrodes in the fiber device. The nanotubes offer a high performance and an effective pathway for the charge transport. The photoelectric conversion efficiency could be increased to 2.73% with an energy storage efficiency of 76%. An electric energy wire with energy conversion in the sheath and energy storage in the core using aligned CNT achieved a photoelectric conversion and storage efficiency of up to 1.83%.[50] Another integrated energy wire was developed by Zou and co-workers. The authors used a PANI coated stainless steel wire as current collector and a Ti wire, which was covered with TiO_2 and the Ru dye N719 as DSSC (photoanode). The so-obtained ES-DSSC wire did not need any Pt to obtain similar performances, which makes the system much cheaper, and the overall efficiency of the device was 2.12%.[18] A higher efficiency of the ES-DSSC of 3.7% was achieved by the group of Jiang. They used a common assemble of a DSSC also with the dye N719 as photoanode and poly(vinylidene fluoride) (PVDF)/ZnO nanowires as counter electrode.[14] An ES-DSSC single-fiber only with ZnO nanowires, and a DSSC, which was immobilized onto a copper mesh, achieved a specific capacitance of 0.4 to 2 mF cm^{-2} with a total energy conversion efficiency of only 0.02%. The authors assumed that the low efficiency is due to the utilization of the copper mesh, which features a too low transparency, resulting in a significantly lower absorption and transfer of the light to the dye (**Figure 2**).[42] Nevertheless,

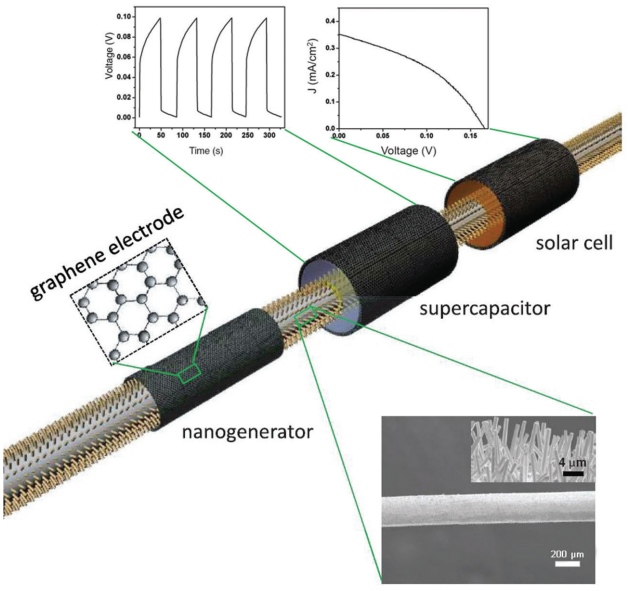

Figure 2. Schematic configuration of a fiber-based multi-energy device consisting of a nanogenerator, a DSSC and a supercapacitor. Radially grown ZnO nanowires are the acting unit of the nanogenerator as well as the core of the solar cell and supercapacitor with large surface area. Graphene serve as cylindrical electrode for all three parts. The nanogenerator converts mechanical energy into electric energy by the piezoelectric property of ZnO, whereby the DSSC converts solar energy into electric energy, which is stored by the supercapacitor. Adapted with permission.[42]

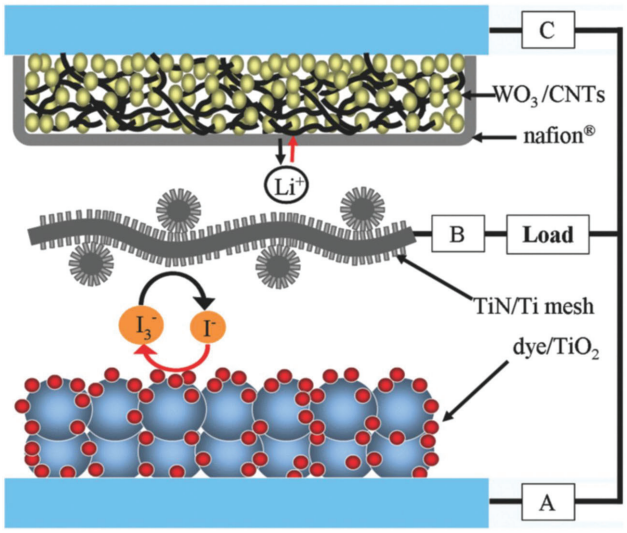

Figure 3. Schematic representation of the setup and the working mechanism of an ES-DSSC. The photoanode (A) and the electron storage electrode (C) are short-circuited during the charging process. The photogenerated electrons from the dye N719 injected into the conduction band of the TiO_2 under light illumination and were stored in the WO_3 electron storage electrode. During the discharging process, the electrocatalytic electrode (B) and the electrode C are short-circuited, while the electrode A is open circuit. The electrons flow to the TiN/Ti mesh, where I_3^- is catalytically reduced to I^-. Reproduced with permission.[53] Copyright 2012, Electrochemical Society.

ES-DSSC wires are suitable for flexible electronics, e.g., in textiles.[6]

Another suitable material for ES-DSSC is WO_3, because of its unique optical and electrical performance due to the reversible intercalation of alkali metal ions (e.g., Li^+ ions).[51] Furthermore, the conduction band is lower compared to TiO_2.[52] A supercapacitor which utilized WO_3 coated CNT as electron storage electrode was constructed by Gao et al. (**Figure 3**). The photoanode was a common DSSC with dye N719, and the electrocatalytic electrode consisted of a TiN/Ti mesh where the reduction of I_3^- to I^- took place catalytically. This three-electrode ES-DSSC revealed a discharge capacity of 0.124 mAh cm^{-2}. Compared with the discharge capacity of 0.200 mAh cm^{-2} by the electrochemical charge process, the photo-charge efficiency was up to 69.5%.[53] It is also possible to use WO_3 without CNT as monoclinic nanocrystalline (nc-WO_3) as well as surface oxidized tungsten oxide (so-WO_{3-x}). This systems reached an output voltage of ≈0.4 V.[52] In a two-electron setup, where the charge storage electrode (transparent conducting electrode) is connected to the photoanode by a WO_3 layer, a capacity of 1.8 C cm^{-2} could be reached.[54]

Moreover, organic conjugated polymers have also been utilized as capacitor materials. Segawa et al. reported an ES-DSSC in which the Pt counter electrode and the charge–storage electrode were connected in two integrated, comb-like electrodes. The charge–storage electrode consisted of the conjugated polymer polypyrrole, which was coated by Nafion. With a common DSSC, the entire photoelectric conversion efficiency was 3.21%, with a maximum discharge capacity of 37.8 mC cm^{-2} and a stability of about 70 cycles.[55] Another three-electron

system, which also used polypyrrole films on an indium tin oxide (ITO) slide as charge–storage electrode, achieved capacitances up to 1.91 mC cm^{-2} and charge storage efficiencies up to 22%, depending on the amount of polypyrrole.[56] By utilizing a bifunctional TiO_2/poly(3,4-ethylenedioxythiophene) (PEDOT) photoanode, the total photoelectric conversion and storage efficiency was about 0.1%.[12] Ho and co-workers used PEDOT and poly(3,4-(2′,2′-diethyl)-propylenedioxythiophene) (PProDOT-Et_2), respectively. The three-electrode device consisted of a DSSC with the dye N719 as photoanode, and two polymer coated Pt-electrodes. The specific capacitance of the PEDOT utilizing ES-DSSC was 0.52 F cm^{-2}.[35] The capacitance could be increased to 5.24 F cm^{-2}, by changing the dye sensitizer to *bis*(isothiocyanato)ruthenium(II)-*bis*-2,2′-bipyridine-4,4′-dicarboxylic acid (N3-dye). PProDOT-Et_2 increased the specific capacitance to 6.52 F cm^{-2} with an energy storage efficiency of about 0.6%.[57]

3.2. Other Energy Storage Systems

Next to supercapacitors as potential energy storage devices for ES-DSSC some other alternatives like redox flow batteries (RFB) or Li-ion batteries are available.

A RFB consists of two parts of liquid electrolyte, which contains one or more dissolved redox species. The two segments are connected by a membrane, which separates the electrolytes to prevent cross-mixing, while the equalization of charge carriers can still take place.[58] The electrolytes are stored externally and are usually pumped through the cathode (catholyte) and anode (anolyte) of the cell. The cell consists of an energy converting unit, where the electrical energy is reversibly converted to chemical energy (charging) or vice versa (discharging). The energy is stored in the electrolyte solution. The advantages of this type of battery are flexibility, high lifetimes, high reliability, relatively low operation costs, as well as the potential to store a large amount of energy. Futhermore, the power and energy output is independent of the storage capacity, which offers an independent control of the energy and the power, resulting in a high flexibility of the system.[59]

Gao et al. demonstrated an ES-DSSC where one part of the RFB consisted of a DSSC. The electrolyte (propylene carbonate) containing LiI and the dye (N719) coated TiO_2 film was placed on the electrode (photoanode). The other electrolyte tank contained Li_2WO_4 and $LiClO_4$ in water. These two electrolytes were connected by a lithium-ion-conducting glass ceramic film. A Pt/Ti mesh was placed as a working electrode into the electrolytes. The so-constructed three-electrode device reached a voltage of 0.76 V and a discharge capacity of 0.015 mA h mL^{-1} (**Figure 4**).[60] Another solar rechargeable redox flow battery was invented by changing the anolyte to an aqueous solution of quinoxaline and its derivatives. This device revealed a good stability and electrochemical activity with a total energy conversion efficiency of 1.2%.[61] Another RFB-DSSC hybrid was described by Yang and coworkers. The authors constructed a two-part ES-DSSC where the DSSC part consisted of the photoanode containing a dye Z709 (*cis*-diisothiocyanato-(2,2′-bipyridyl-4,4′-dicarboxylic acid)-(2,2′-bipyridyl-4,4′-dinonyl)

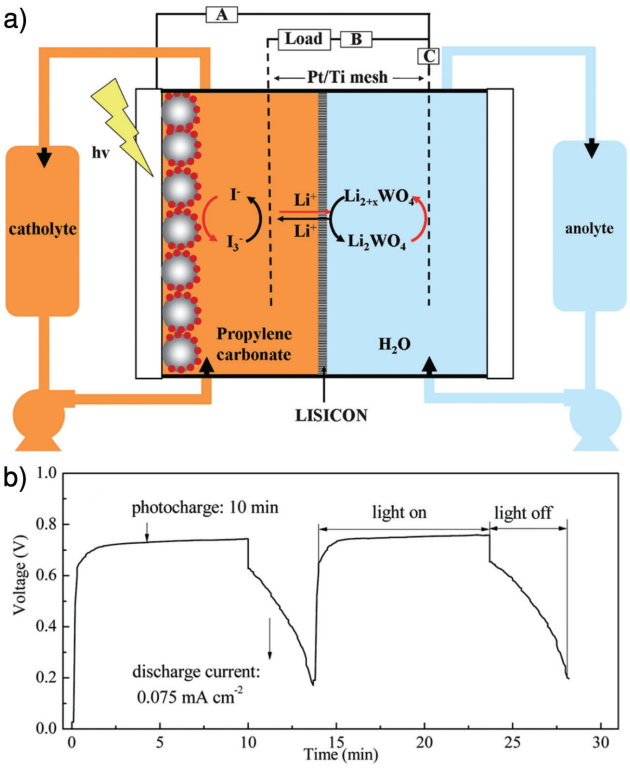

Figure 4. a) Schematic setup and working mechanism of a solar rechargeable redox flow battery, and b) photocharging/discharging curve of the solar rechargeable redox flow battery. Reproduced with permission.[60] Copyright 2013, The Royal Society of Chemistry.

ruthenium(II)) coated TiO_2 layer, a Pt-counter electrode and a separator. The RFB part composed of a Pt working electrode and counter electrode as well as a separator. The separator isolated the two electrolyte circuit loops (I_2 and LiI for the DSSC electrolyte and *bis*(pentamethylcyclopentadienyl)-iron and $LiClO_4$ for the RFB part). The photo-charge capacity and the electrochemical discharge capacity were 108 mA h L^{-1} and 66.6 mA h L^{-1}, respectively. The obtained results indicated that 24.9% of the redox species and 61.6% of the photo-charge capacity had been used.[4]

Another important and prominent battery type is the lithium ion battery, which has a high energy density as well as a long lifetime. However, the power density is lower compared to supercapacitors. During the charging process, lithium ions are reduced to elemental lithium at the anode (e.g., graphite), which is stored in the anode by intercalation. At the discharge process, the lithium is oxidized to lithium ions, which migrate to the cathode (e.g., $LiCoO_2$) and insert into the electrode.[62,63] The major drawback is the formation of lithium dendrites during the charging process, which complicates its application in secondary batteries.[63]

Wang et al. published a hybrid structure consisting of a DSSC and a lithium ion battery. On the Ti electrode, which was be used by both parts, TiO_2 nanotubes were immobilized on both sides. The voltage of the device reached ≈3 V in about eight minutes and the total energy conversion and storage efficiency was 0.82%.[64]

4. Electric Energy Storage Systems Charged by Organic Photovoltaic Devices

Organic photovoltaic systems (OPV) represent a low cost, flexible and light-weight alternative to other solar cell devices. They are easy to fabricate by roll-to-roll as well as by printing and coating processes also on flexible substrates.[3,28,65,66] OPV like bulk heterojunction (BHJ) solar cells consist of a transparent electrode, a hole conducting layer (e.g., PEDOT/poly(styrene sulfonate) (PSS)), and the active layer, as well as a second electrode to collect the charges. The active layer is a bulky mixture of a conjugated polymer and a acceptor material like phenyl-C61-butyric acid methyl ester (PCBM).[67] The absorption of photons by the donor material lead to a formation of excitons (electron-hole-pairs). These excitons diffuse towards the donor-acceptor interface and dissociate via an electron transfer process into the free charge carriers. The electrons are transferred to the acceptor due to its higher electron affinity and the holes are collected in the donor phase.[68] The highest efficiency value of OPV systems is currently 12%.[69]

Srinivasan and co-workers developed a printable device utilizing a BHJ solar cell (poly(3-hexylthiophene (P3HT) with PCBM) and a capacitor. This system showed a 43% reduction of the internal resistance as compared to the separated wire connected systems. The counter electrode was fabricated with CNT coated aluminum layer, and a free-standing CNT network was utilized as the charge storage electrode. This device reached a capacity of 28 F g^{-1}.[3]

A wire shaped photo-rechargeable energy storage device was investigated by Peng et al. utilizing a titania nanotube-modified Ti wire as core. The solar energy conversion part consists of a P3HT:PCBM as well as a PEDOT:PSS layer and achieves an energy conversion efficiency of up to 1.01%. The energy storage part, consisting of CNT and a poly(vinyl alcohol)/H_3PO_4 electrolyte, reaches a storage efficiency of 65.6%. The entire photoelectric conversion ans storage efficiency is up to 0.82%.[70]

Other systems using OPV for light to energy conversion are flexible polymer solar batteries, which used separated solar cells, and battery devices. The group of Wöhrle constructed such a device. The solar cell part contains the active material 2-methoxy-5-(3′,7′-dimethyloctyloxy)-1,4-phenylene-vinylene (MDMO-PPV)/PCBM, which was coated on an ITO film covering a poly(ethylene terephthalate) foil. The solar cell was connected to a flexible lithium polymer battery; the battery had a nominal capacity of 100 mA h at a weight of 3.3 g with high cycle stability.[15]

A flexible and wearable photo-rechargeable battery utilizing an OPV system and a lithium ion battery was investigated by Choi and co-workers (**Figure 5**). The authors coated woven polyester yarn with nickel by the electroless deposition method. This yarn was covered by the battery active layers consisting of the electrode material ($Li_4Ti_5O_{12}$ or $LiFePO_4$), binder, and conductive carbon. The battery was connected to a BHJ solar cell system with the active material poly(*N*-9-hepta-decanyl-2,7-carbazole-*alt*-5,5-(4,7-di-2-thienyl-2,1,3-benzothiadiazole)) (PCDTBT) and $PC_{70}BM$. The power conversion efficiency of the solar cell on a poly(ethylene naphthalene) substrate was 5.49%.

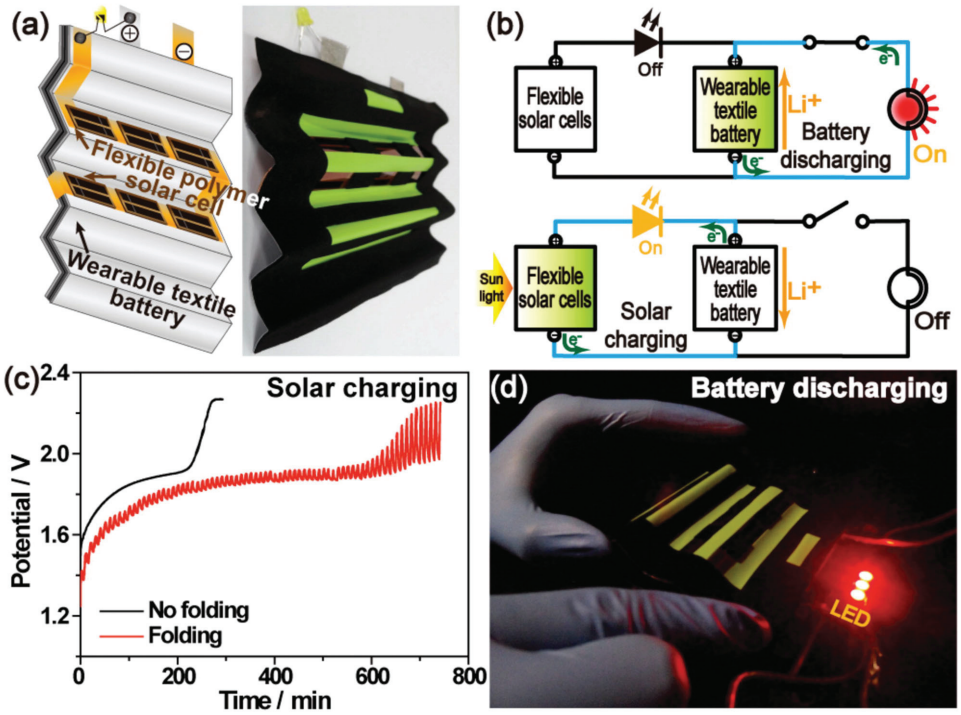

Figure 5. a) Setup and photograph of a flexible polymer solar cell, b) photocharging and discharging circuits of a solar rechargeable textile battery, c) photocharging curves of the device in the present and absence of recurring folding/unfolding motions as well as d) demonstration of the flexible solar rechargeable battery by connection of LED bulbs. Reproduced with permission.[71] Copyright 2013, American Chemical Society.

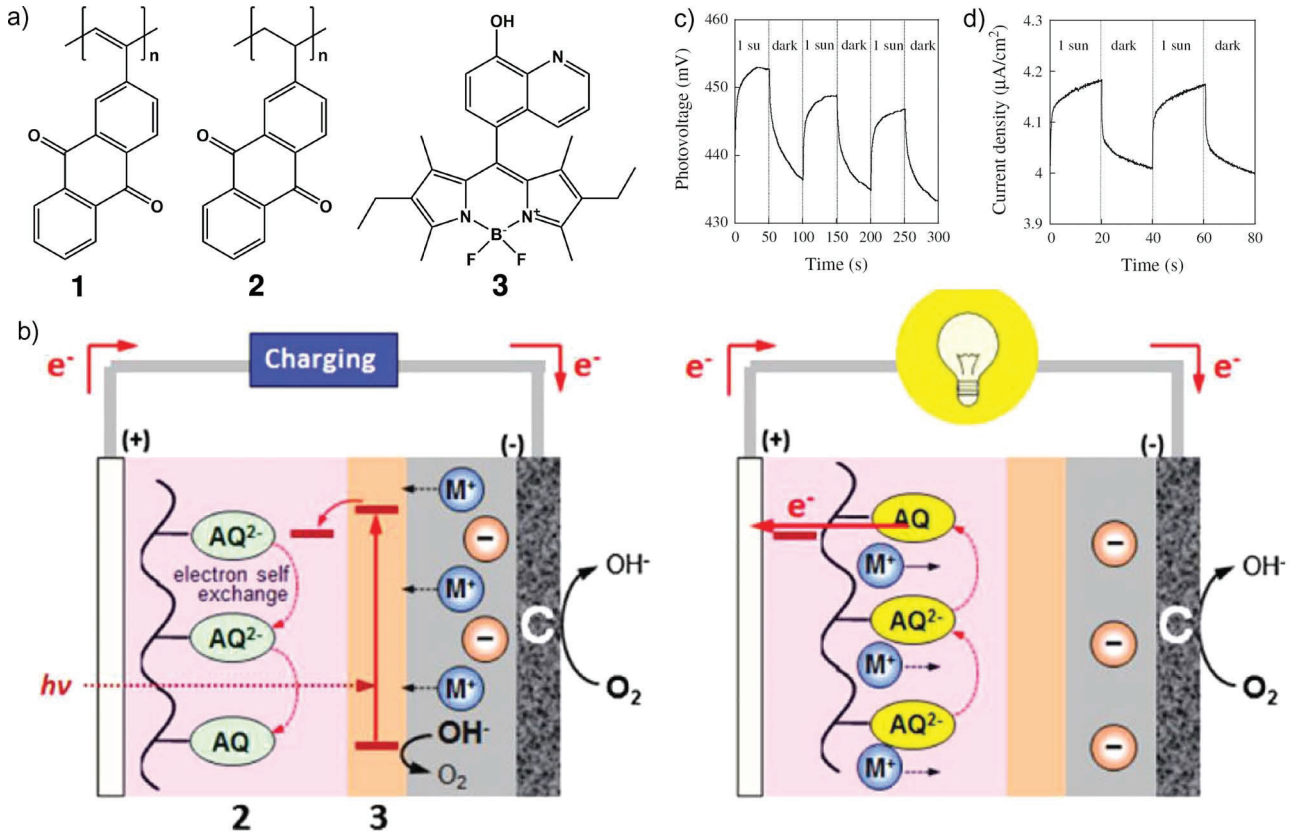

Figure 6. a) Schematic representation of structures of the used anthraquinone polymers **1** and **2** as well as the BODIPY dye **3**, b) schematic setup and working mechanism of a solar rechargeable air battery, c) photo responses of V_{oc} and short-circuit densities, and d) photo responses of V_{oc} and short-circuit densities for a **3**/**2**/ITO photoanode/O_2 cathode battery. Reproduced with permission.[75] Copyright 2013, Springer.

Six solar cells were connected in series to charge the battery, which reached a capacity of about 10 mA h.[71]

5. Different Systems for Solar Rechargeable Battery Systems

Alongside the previously presented systems for photo-rechargeable batteries, some other charge storage possibilities are available, e.g., solar cells with a battery effect. For instance, a solar cell consisting only of the donor material (i.e., first generation cationic cyanine dendrimer), was utilized as a photo-rechargeable battery. The battery effect results from charge trapping sites within the active layer by an internal charge transfer from the counter anion to the cationic cyanine. A higher film thickness of the active material leads to a higher discharge current due to more trapping sites within the film. The total storage capacity of a 150 nm thick film was 0.20 mA h g^{-1}, with an output voltage of 0.35 V.[72]

Another system which reveals battery characteristics was presented by Fujinami et al. The authors constructed a polymer electrolyte bilayer film which was charged by UV light. The layers consisted of an anionically conducting poly(ethyl methacrylate)/tributyl tin halide/tetrabutyl ammonium halide film, in which dibutyl ferrocene and octylviologene were incorporated, respectively. The system reached peak current densities of 39 μA cm^{-2} (one minute storage) and 24 μA cm^{-2} (25 hours storage) with a photo-induced voltage of 0.37 V. This showed that the photo-charged separate state could be held for at least 24 hours.[73]

Currently, air batteries are the focus of research, due to their high energy densities, which could be obtained by these systems.[74] Nishide et al. used anthraquinone containing polymers as active anode material, and a MnO_2/carbon composite as cathode catalyst for the reduction of oxygen. A borondipyrromethene (BODIPY) derivative was adsorbed to the anthraquinone polymer to avoid a rapid decrease in the voltage under dark due to a back electron transfer from the anthraquinone to the oxygen. The battery achieved a discharge voltage of 0.63 V, a charging capacity of 166 mAh g^{-1} and a capacity of 143 mAh g^{-1} for discharging (72% and 62% of the theoretically capacity, respectively) for over 50 cycles (**Figure 6**).[75] An

Table 1. Overview of the number of references regarding the combined device types.

Battery	Organic radical battery	Super-capacitors	Lithium battery	Redox flow battery	Metal air battery
Solar cell					
Dye sensitized solar cell	0	17	1	3	0
Bulk heterojunction solar cell	0	1	2	0	1
Inorganic solar cell	0	0	2	0	1

Table 2. Overview of the various photo-rechargeable energy storage systems with their characteristics and efficiencies.

Solar cell	Energy storage device	Characteristics	Efficiency	Ref.
Silicon based solar cell	Ferroelectric storage	Utilization of photo electrochemical and ferroelectric effects	n/a	[32]
	Lithium ion battery	Solar cell is connected to battery by a wire	$\eta_{conversion} = 15\%$ $\eta_{storage} = 97\%$ $\eta = 14.5\%$	[17]
DSSC	Supercapacitor	Two-electrode setup, with activated carbon	n/a	[43]
		Three-electrode setup, with activated carbon	n/a	[45]
		Utilization of CNT as counter electrode	$\eta_{conversion} = 6.1\%$ $\eta_{storage} = 84\%$ $\eta = 5.12\%$	[13]
		Incorporation of PANI into the CNT	$\eta_{storage} \approx 70\%$ $\eta = 4.29\%$	[13]
		Wire shaped device, utilization of CNT/Ti composites	$\eta_{conversion} = 2.2\%$ $\eta = 1.5\%$	[6]
		Wire shaped device, utilization of Ti modified with perpendicularly aligned TiO_2 nanotubes and horizontally aligned CNT	$\eta_{conversion} = 2.73\%$ $\eta_{storage} = 75.7\%$	[48]
		Wire shaped device, energy conversion in sheath and storage in the core	$\eta = 1.83\%$	[49]
		PANI coated wire	$\eta_{conversion} = 5.41\%$ $\eta_{storage} = 46\%$ $\eta = 2.12\%$	[18]
		PVDF/ZnO nanowires as counter electrode	$\eta_{conversion} = 2.23$ to 4.36% $\eta = 3.7\%$	[14]
		ZnO nanowire	$\eta_{conversion} = 0.02\%$	[40]
		WO_3 coated CNT as electron storage electrode, TiN/Ti mesh as electrocatalytic electrode	$\eta_{conversion} = 69.5\%$	[52]
		Utilization of monoclinic nanocrystalline WO_3 and surface oxidized WO_{3-x}	n/a	[51]
		WO_3 and TiO_2 coated TCO electrode	n/a	[53]
		Polymeric charge storage electrode	$\eta_{conversion} = 3.21\%$	[54]
		Polypyrrole film on ITO slide as charge storage electrode	$\eta_{conversion} = 0.5$ to 1% $\eta_{storage} = 22\%$	[55]
		TiO_2/PEDOT photoanode	$\eta = 0.1\%$	[12]
		PProDOT-Et_2 as photoanode	$\eta_{conversion} = 4.37\%$ $\eta_{storage} = 0.6\%$	[35,56]
	RFB	LiI in propylene carbonate and $Li_2WO_4/LiClO_4$ in water as electrolytes	n/a	[61]
		Quinoxaline derivatives in water as electrolyte	$\eta_{conversion} = 1.2\%$	[62]
		LiI and *bis*(pentamethylcyclopentadienyl)iron/$LiClO_4$ as electrolytes	$\eta_{conversion} = 0.15\%$ $\eta_{storage} > 0.6\%$	[4]
	Lithium ion battery	Ti/TiO_2 electrode	$\eta_{storage} = 41\%$ $\eta = 0.82\%$	[65]
OPV	Supercapacitor	P3HT/PCBM as active material for the OPV device, CNT coated aluminum as charge storage electrode	$\eta_{conversion} = 3.39\%$	[3]
		Wire shaped device with P3HT/PCBM and PEDOT/PSS layers as solar cell device and CNT with PVA/H_3PO_4 electrolyte	$\eta_{conversion} = 1.01\%$ $\eta_{storage} = 65.6\%$ $\eta = 0.82\%$	[71]
	Lithium polymer battery	Separated solar cell and battery devices	$\eta_{conversion} = 1.85\%$	[15]
	Lithium ion battery	Wire shaped battery device, connected to BHJ solar cell	$\eta_{conversion} = 5.49\%$	[72]
	Battery effect	Solar cell consists only of donor material (cationic cyanine dendrimer)	n/a	[73]

Continued

Table 2. Continued

Solar cell	Energy storage device	Characteristics	Efficiency	Ref.
Polymer electrolyte bilayer film with photo-rechargeable characteristics		Layer consists of anionically conducting film	n/a	[74]
Photo-rechargeable metal air battery		Anthraquinone containing polymers as active anode material, MnO_2/carbon composite as cathode material	$\eta_{storage}$ = 62 to 72%	[76]
		Catalytic cathode and a photoanode with $SrTiO_3$	n/a	[77]

inorganic photo-rechargeable air battery was reported by Akuto and Sakurai. The authors constructed a battery with a catalytic cathode and a photoanode, which was made of a metal hydride, and the photo stable n-type semiconductor $SrTiO_3$. The total discharge capacity of this system was about 950 mAh g^{-1}, and by increasing the light irradiation time the discharge time rose significantly.[76]

6. Conclusion

This report offers a brief overview of organic-based solar rechargeable batteries. Currently, only a small number of results were published on this emerging field of research (**Table 1**). The main focus is on hybrids of DSSCs with supercapacitors, but other combinations of OPV systems or silicon solar cells with RFB, lithium ion batteries or organic radical batteries show the high potential of this area of research.

An overview of the different solar-rechargeable energy storage systems and their efficiencies is given in **Table 2**. The highest efficiency of 5.12% was reached by the combination of a DSSC with a capacitor as energy storage. ES-DSSC wires obtain efficiencies up to 3.7%, and combinations of DSSC with other energy storage parts also show good performance. Larger modules with silicon-based solar cells have capacities up to 2.35 Ah. Other combination possibilities, like solar cells with a battery effect, or as hybrid with air batteries, are also available.

All of these devices have, up to now, lower efficiencies or capacities compared to their inorganic counterparts, because the focus is, up to now, on the development and fabrication of prototypes and, as a consequence, no or less optimization on the overall efficiency was performed. Consequently, the different energy conversion and storage parts do not match ideally for an efficient electron transfer. The connection of solar cells and energy storage parts is very difficult, e.g., OPV systems, which offer a voltage of about 800 mV, require a corresponding battery with fitting voltage. Furthermore, geometrical restrictions limit the efficiency of the devices. The size of the solar cell and the battery, respectively, determines the size of the corresponding counterpart, resulting in a possible mismatch. The predetermined size limits for instance the capacity of the battery. Additionally, it is very difficult to improve the capacity and the power of the storage parts simultaneously. Some of the described photo-rechargeable systems are based on a three-electrode setup, i.e. one electrode is the photo-active while also storing the electrons. Consequently, it is necessary to use materials, which can be utilized as good active layer for solar cell and as good electron storage material at once. The best result could be achieved with wire-shaped ES-DSSC using supercapacitors for electron storing, up to now, due to a relatively low mismatch of the different parts. However, supercapacitors can be improved by integration of organic radical batteries into the capacitor, resulting in a fast charging, high capacity storage device. A good possibility to optimize solar-rechargeable batteries is the utilization of a four-electrode setup, whereby the solar cell part and the storage part can be improved separately. In spite of lots of optimization requirements, solar-rechargeable energy storage systems have a high potential for efficient and direct storage of solar energy due to lots of advantages compared with common inorganic devices. In contrast to silicon based solar cells, which production is high expensive due to high material costs and high material demand, the production of OPV devices can be easily scales up by roll-to-roll processes, which makes the fabrication more efficient and decrease the costs significantly.[28,65] RFB can store more energy by simply increasing the electrolyte amounts. Concerning the lifetime of photo-rechargeable energy storage devices, no data are available, up to now, but the different solar cells and storage devices reveal high lifetime potentials.[77] A wide range of potential applications are available, such as electric wires for functional clothes and textiles, as well as portable devices for mobile phones or laptops. OPV systems, combined with supercapacitors or lithium ion batteries are printable and flexible, and can be used as wearable solar batteries. Low power applications like smart packaging are well-suited for these systems. As a consequence, solar-rechargeable batteries provide powerful electronics for daily life applications.

Acknowledgements

The authors thank the European Social Fund (ESF), the Thüringer Aufbaubank (TAB) and the Thuringian Ministry of Economy, Science and Digital Society (TMWWdG) for the financial support.

Received: February 19, 2015
Revised: April 14, 2015
Published online: October 9, 2015

[1] Key World Energy Statistics 2013, International Energy Agency, Paris, **2013**.
[2] Q. Schiermeier, J. Tollefson, T. Scully, A. Witze, O. Morton, *Nature* **2008**, *454*, 816.
[3] G. Wee, T. Salim, Y. M. Lam, S. G. Mhaisalkar, M. Srinivasan, *Energy Environ. Sci.* **2011**, *4*, 413.
[4] P. Liu, Y.-l. Cao, G.-R. Li, X.-P. Gao, X.-P. Ai, H.-X. Yang, *ChemSusChem* **2013**, *6*, 802.
[5] T. Song, B. Sun, *ChemSusChem* **2013**, *6*, 408.

[6] T. Chen, L. Qiu, Z. Yang, Z. Cai, J. Ren, H. Li, H. Lin, X. Sun, H. Peng, *Angew. Chem. Int. Ed.* **2012**, *51*, 11977.
[7] a) H. J. Snaith, L. Schmidt-Mende, *Adv. Mater.* **2007**, *19*, 3187; b) B. C. Thompson, J. M. J. Fréchet, *Angew. Chem. Int. Ed.* **2008**, *47*, 58.
[8] M. Graetzel, R. A. J. Janssen, D. B. Mitzi, E. H. Sargent, *Nature* **2012**, *488*, 304.
[9] N. S. Lewis, *Science* **2007**, *315*, 798.
[10] Renewable Energy World news report, 100 GW of Solar PV Now Installed in the World Today, http://www.renewableenergyworld.com/rea/news/article/2013/02/100-gw-of-solar-pv-now-installed-in-the-world-today (accessed February 2015).
[11] a) K. Wang, H. Wu, Y. Meng, Y. Zhang, Z. Wei, *Energy Environ. Sci.* **2012**, *5*, 8384; b) L. Li, Z. Wu, S. Yuan, X.-B. Zhang, *Energy Environ. Sci.* **2014**, *7*, 2101.
[12] P. Liu, H. Yang, X. Ai, G. Li, X. Gao, *Electrochem. Commun.* **2012**, *16*, 69.
[13] Z. Yang, L. Li, Y. Luo, R. He, L. Qiu, H. Lin, H. Peng, *J. Mater. Chem. A* **2012**, *1*, 954.
[14] X. Zhang, X. Huang, C. Li, H. Jiang, *Adv. Mater.* **2013**, *25*, 4093.
[15] G. Dennler, S. Bereznev, D. Fichou, K. Holl, D. Ilic, R. Koeppe, M. Krebs, A. Labouret, C. Lungenschmied, A. Marchenko, D. Meissner, E. Mellikov, J. Méot, A. Meyer, T. Meyer, H. Neugebauer, A. Öpik, N. Sariciftci, S. Taillemite, T. Wöhrle, *Sol. Energy* **2007**, *81*, 947.
[16] N. A. Kelly, T. L. Gibson, *J. Power Sources* **2011**, *196*, 10430.
[17] T. L. Gibson, N. A. Kelly, *J. Power Sources* **2010**, *195*, 3928.
[18] Y. Fu, H. Wu, S. Ye, X. Cai, X. Yu, S. Hou, H. Kafafy, D. Zou, *Energy Environ. Sci.* **2013**, *6*, 805.
[19] T. R. Cook, D. K. Dogutan, S. Y. Reece, Y. Surendranath, T. S. Teets, D. G. Nocera, *Chem. Rev.* **2010**, *110*, 6474.
[20] J. R. Bolton, D. O. Hall, *Annu. Rev. Energy.* **1979**, *4*, 353.
[21] N. S. Lewis, D. G. Nocera, *Proc. Natl. Acad. Sci. USA* **2006**, *103*, 15729.
[22] a) J. R. McKone, N. S. Lewis, H. B. Gray, *Chem. Mater.* **2014**, *26*, 407; b) F. E. Osterloh, B. A. Parkinson, *MRS Bull.* **2011**, *36*, 17.
[23] a) L. M. Peter, K. G. Upul Wijayantha, *ChemPhysChem* **2014**, *15*, 1983; b) G. Wang, Y. Ling, H. Wang, L. Xihong, Y. Li, *J. Photochem. Photobio. C* **2014**, *19*, 35; c) X. Xia, J. Luo, Z. Zeng, C. Guan, Y. Zhang, J. Tu, H. Zhang, H. J. Fan, *Sci. Rep.* **2012**, *2*, 981.
[24] Z. Wei, D. Liu, C. Hsu, F. Liu, *Electrochem. Commun.* **2014**, *45*, 79.
[25] M. Kenisarin, K. Mahkamov, *Renew. Sust. Energ. Rev.* **2007**, *11*, 1913.
[26] T. Janoschka, M. D. Hager, U. S. Schubert, *Adv. Mater.* **2012**, *24*, 6397.
[27] M. Sharon, P. Veluchamy, C. Natarajan, D. Kumar, *Electrochim. Acta* **1991**, *36*, 1107.
[28] R. Gaudiana, *J. Phys. Chem. Lett.* **2010**, *1*, 1288.
[29] J. Zhao, A. Wang, M. A. Green, F. Ferrazza, *Appl. Phys. Lett.* **1998**, *73*, 1991.
[30] R. Olivares-Amaya, C. Amador-Bedolla, J. Hachmann, S. Atahan-Evrenk, R. S. Sánchez-Carrera, L. Vogt, A. Aspuru-Guzik, *Energy Environ. Sci.* **2011**, *4*, 4849.
[31] a) M. A. Green, *Philos. T. R. Soc. A* **2013**, *371*, 20110413; b) V. V. Tyagi, N. A. Rahim, N. A. Rahim, J. A. Selvaraj, *Renew. Sust. Energ. Rev.* **2013**, *20*, 443.
[32] C.-W. Lo, C. Li, H. Jiang, *AIP Adv.* **2011**, *1*, 042104.
[33] S. Y. Kan, M. Verwaal, H. Broekhuizen, *J. Power Sources* **2006**, *162*, 971.
[34] J.-H. Yum, P. Chen, M. Grätzel, M. K. Nazeeruddin, *ChemSusChem* **2008**, *1*, 699.
[35] H.-W. Chen, C.-Y. Hsu, J.-G. Chen, K.-M. Lee, C.-C. Wang, K.-C. Huang, K.-C. Ho, *J. Power Sources* **2010**, *195*, 6225.
[36] P. G. Bomben, J. Borau-Garcia, C. P. Berlinguette, *Chem. Commun.* **2012**, *48*, 5599.
[37] M. Wang, C. Grätzel, S. M. Zakeeruddin, M. Grätzel, *Energy Environ. Sci.* **2012**, *5*, 9394.
[38] T. V. Arjunan, T. S. Senthil, *Mater. Technol.* **2013**, *28*, 9.
[39] M. Grätzel, *J. Photoch. Photobio. C* **2003**, *4*, 145.
[40] M. K. Nazeeruddin, E. Baranoff, M. Grätzel, *Sol. Energy* **2011**, *85*, 1172.
[41] S. Zhang, X. Yang, Y. Numata, L. Han, *Energy Environ. Sci.* **2013**, *6*, 1443.
[42] J. Bae, Y. J. Park, M. Lee, S. N. Cha, Y. J. Choi, C. S. Lee, J. M. Kim, Z. L. Wang, *Adv. Mater.* **2011**, *23*, 3446.
[43] L. L. Zhang, X. S. Zhao, *Chem. Soc. Rev.* **2009**, *38*, 2520.
[44] T. Miyasaka, T. N. Murakami, *Appl. Phys. Lett.* **2004**, *85*, 3932.
[45] S.-M. Chen, R. Ramachandran, V. Mani, R. Saraswathi, *Int. J. Electrochem. Sci.* **2014**, *9*, 4072.
[46] T. N. Murakami, N. Kawashima, T. Miyasaka, *Chem. Commun.* **2005**, 3346.
[47] C. Yu, C. Masarapu, J. Rong, B. Wei, H. Jiang, *Adv. Mater.* **2009**, *21*, 4793.
[48] K. Jost, G. Dion, Y. Gogotsi, *J. Mater. Chem. A* **2014**, *2*, 10776.
[49] X. Chen, H. Sun, Z. Yang, G. Guan, Z. Zhang, L. Qiu, H. Peng, *J. Mater. Chem. A* **2014**, *2*, 1897.
[50] Z. Yang, J. Deng, H. Sun, J. Ren, S. Pan, H. Peng, *Adv. Mater.* **2014**, *26*, 7038.
[51] G. A. Niklasson, C. G. Granqvist, *J. Mater. Chem.* **2006**, *17*, 127.
[52] Y. Saito, S. Uchida, T. Kubo, H. Segawa, *Thin Solid Films* **2010**, *518*, 3033.
[53] N. F. Yan, G. R. Li, G. L. Pan, X. P. Gao, *J. Electrochem. Soc.* **2012**, *159*, A1770.
[54] A. Hauch, A. Georg, U. O. Krašovec, B. Orel, *J. Electrochem. Soc.* **2002**, *149*, A1208.
[55] Y. Saito, A. Ogawa, S. Uchida, T. Kubo, H. Segawa, *Chem. Lett.* **2010**, *39*, 488.
[56] H. Nagai, H. Segawa, *Chem. Commun.* **2004**, *8*, 974.
[57] C.-Y. Hsu, H.-W. Chen, K.-M. Lee, C.-W. Hu, K.-C. Ho, *J. Power Sources* **2010**, *195*, 6232.
[58] S.-H. Shin, S.-H. Yun, S.-H. Moon, *RSC Adv.* **2013**, *3*, 9095.
[59] a) H. Chen, T. N. Cong, W. Yang, C. Tan, Y. Li, Y. Ding, *Prog. Nat. Sci.* **2009**, *19*, 291; b) M. Duduta, B. Ho, V. C. Wood, P. Limthongkul, V. E. Brunini, W. C. Carter, Y.-M. Chiang, *Adv. Energy Mater.* **2011**, *1*, 511; c) Y. Wang, P. He, H. Zhou, *Adv. Energy Mater.* **2012**, *2*, 770.
[60] N. F. Yan, G. R. Li, X. P. Gao, *J. Mater. Chem. A* **2013**, *1*, 7012.
[61] N. F. Yan, G. R. Li, X. P. Gao, *J. Electrochem. Soc.* **2014**, *161*, A736.
[62] C. M. Hayner, X. Zhao, H. H. Kung, *Annu. Rev. Chem. Biomol. Eng.* **2012**, *3*, 445.
[63] M.-K. Song, S. Park, F. M. Alamgir, J. Cho, M. Liu, *Mat. Sci. Eng. R* **2011**, *72*, 203.
[64] W. Guo, X. Xue, S. Wang, C. Lin, Z. L. Wang, *Nano Lett.* **2012**, *12*, 2520.
[65] P. M. Beaujuge, J. M. J. Fréchet, *J. Am. Chem. Soc.* **2011**, *133*, 20009.
[66] a) J. K. Lee, W. L. Ma, C. J. Brabec, J. Yuen, J. S. Moon, J. Y. Kim, K. Lee, G. C. Bazan, A. J. Heeger, *J. Am. Chem. Soc.* **2008**, *130*, 3619; b) F. C. Krebs, T. Tromholt, M. Jørgensen, *Nanoscale* **2010**, *2*, 873.
[67] a) C. Deibel, V. Dyakonov, *Rep. Prog. Phys.* **2010**, *73*, 096401; b) M. Jørgensen, K. Norrman, S. A. Gevorgyan, T. Tromholt, B. Andreasen, F. C. Krebs, *Adv. Mater.* **2012**, *24*, 580.
[68] Y.-J. Cheng, S.-H. Yang, C.-S. Hsu, *Chem. Rev.* **2009**, *109*, 5868.
[69] Optrics news report, Heliatek achieves 12% organic solar cell efficiency, http://optics.org/news/4/1/36 (accessed February 2015).
[70] Z. Zhang, X. Chen, P. Chen, G. Guan, L. Qiu, H. Lin, Z. Yang, W. Bai, Y. Luo, H. Peng, *Adv. Mater.* **2014**, *26*, 466.

[71] Y.-H. Lee, J.-S. Kim, J. Noh, I. Lee, H. J. Kim, S. Choi, J. Seo, S. Jeon, T.-S. Kim, J.-Y. Lee, J. W. Choi, *Nano Lett.* **2013**, *13*, 5753.
[72] A. K. Pandey, P. C. Deakin, R. D. Jansen-Van Vuuren, P. L. Burn, I. D. W. Samuel, *Adv. Mater.* **2010**, *22*, 3954.
[73] T. Fujinami, *Solid State Ionics* **1996**, *92*, 165.
[74] F. Cheng, J. Chen, *Chem. Soc. Rev.* **2012**, *41*, 2172.
[75] K. Oyaizu, Y. Niibori, A. Takahashi, H. Nishide, *J. Inorg. Organomet. Polym. Mater.* **2013**, *23*, 243.
[76] K. Akuto, Y. Sakurai, *J. Electrochem. Soc.* **2001**, *148*, A121.
[77] a) Y.-F. Chiang, R.-T. Chen, P.-S.Shen, P. Chen, T.-F. Guo, *J. Power Sources* **2013**, *225*, 257; b) R. Roesch, K.-R. Eberhardt, S. Engmann, G. Gobsch, H. Hoppe, *Sol. Energ. Mat. Sol. C* **2013**, *117*, 59; c) M. Wang, D. Le Duong, N. T. Mai, S. Kim, Y. Kim, H. Seo, Y. C. Kim, W. Jang, Y. Lee, J Suhr, J.-D. Nam, *ACS Appl. Mater. Interfaces* **2015**, *7*, 1348.

Publication 2

"Poly(DCAQI): Synthesis and characterization of a new redox-active polymer"

Daniel Schmidt, Bernhard Häupler, Martin D. Hager, Ulrich S. Schubert

J. Polym. Sci., Part A: Polym. Chem. **2016**, *54*, 1998–2003.

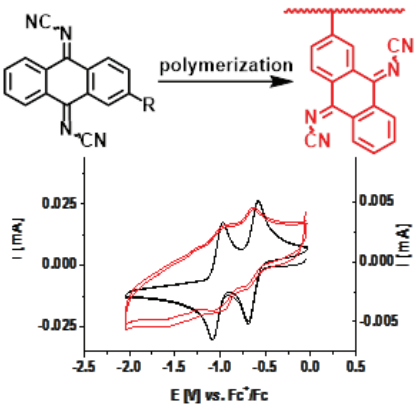

Poly(DCAQI): Synthesis and Characterization of a New Redox-Active Polymer

Daniel Schmidt,[1,2] Bernhard Häupler,[1,2] Martin D. Hager,[1,2] Ulrich S. Schubert[1,2]

[1]Laboratory of Organic and Macromolecular Chemistry (IOMC), Friedrich Schiller University Jena, Humboldtstr. 10, Jena 07743, Germany

[2]Center for Energy and Environmental Chemistry Jena (CEEC Jena), Friedrich Schiller University Jena, Philosophenweg 7a, Jena 07743, Germany

Correspondence to: U. S. Schubert (E-mail: ulrich.schubert@uni-jena.de)

Received 9 December 2015; accepted 18 January 2016; published online 00 Month 2016

DOI: 10.1002/pola.28066

ABSTRACT: Redox-active anthraquinone based polymers are synthesized by the introduction of a polymerizable vinyl and ethynyl group, respectively, resulting in redox-active monomers, which electrochemical behaviors are tailored by the modification of the keto groups to *N*-cyanoimine moieties. These monomers can be polymerized by free radical polymerization and Rh-catalyzed polymerization methods, respectively. The resulting polymers are obtained in molar masses (M_n) of 4,400 to 16,800 g mol^{-1} as well as high yields of up to 97%. The monomers and polymers are furthermore electrochemically characterized by cyclic voltammetry. The monomers exhibit two one-electron redox reactions at about −0.6 and −1.0 V versus Fc^+/Fc. The *N*-cyanoimine units are, however, partially hydrolyzed during the polymerization step or during the electrochemical measurements and degenerate to carbonyl groups, resulting in a new reduction signal at −1.26 V versus Fc^+/Fc. © 2016 Wiley Periodicals, Inc. J. Polym. Sci., Part A: Polym. Chem. **2016**, *00*, 000–000

KEYWORDS: electrochemistry; polymer synthesis; redox polymers; synthesis

INTRODUCTION The application of organic redox-active compounds, in particular polymers, as active materials in organic secondary batteries draw significant interest during the last decade.[1,2] In contrast to inorganic structures, organic materials feature several advantages such as high flexibility,[3] low toxicity,[4] and are producible in low-temperature processes from, in the best case, recycled[5] or renewable resources.[6] Furthermore, the redox potential can be adjusted by the utilization of the available organic redox-active structures and fine-tuned by the introduction of functional substituents. Up to now, different redox-active compounds have been applied as active materials in organic batteries, such as stable organic radicals[7,8] or carbonyl compounds.[9] Quinonide structures are of high interest. Due to the involvement of two electrons in the redox reaction a good charge to mass ratio is obtained, resulting in comparably high theoretical capacities. In general, 1,2-diones possess higher potential than 1,4-diones and their redox potentials can be tailored by two major strategies. The first approach is the introduction of appropriate substituents to influence the redox potential, in particular electron donating/withdrawing groups such as cyano,[10] chloro,[10] hydroxy,[11] lithoxy,[12,13] fluorinated and nonfluorinated alkyl and alkoxy groups,[11,14–16] thiophene,[17] pyridine,[18] pyrazine,[18] and lithium *resp*. sodium salts of carboxylic,[19] or sulfonic acids.[20] The second procedure is to modify the redox-active carbonyl groups to dicyanomethane[21,22] or 1,3-dithiolane groups, whose redox mechanism are based on one two-electron reaction.[23,24] The transformation of the carbonyl groups of the anthraquinone to *N*-cyanoimine groups, which possess stronger electron accepting properties, leading to higher reduction potentials of the compound.[25] However, for the application as active material in organic batteries, insolubility of all occurring redox states of the active material is required in the applied electrolytes, which mostly consist of an electrochemically inert salt and an organic solvent. The most promising and straightforward approach is the incorporation of the redox-active units into a polymeric environment, resulting in an insoluble, but swellable electroactive material.[26,27]

In this contribution, we describe the synthesis and the electrochemical characterization of a new redox-active monomer based on *N*,*N*′-dicyanoanthraquinone diimine (DCAQI). The monomers could be incorporated into a polymeric environment by free radical polymerization and Rh-catalyzed

Additional Supporting Information may be found in the online version of this article.

polymerization of the introduced vinyl and ethynyl substituted monomers, respectively. In contrast to a previously published patent,[28] the polymerization procedures as well as the electrochemical performance of the compounds in solution are investigated in more detail. Furthermore, new insights in the electrochemical behavior in different electrolytes of both monomer and polymer could be revealed.

EXPERIMENTAL

Materials

All solvents were dried according to standard procedures. All starting materials were purchased from commercial sources and were used as obtained unless otherwise noted. 2,2′-Azo*bis*(*iso*-butyronitrile) (AIBN) was recrystallized from methanol prior to use.

2-Vinylanthraquinone (**1**)[29] and 2-ethynylanthraquinone (**4**)[30] were synthesized according to literature procedures. Unless otherwise noted, all reactions were performed under argon atmosphere.

Characterization

The reactions were monitored by TLC on 0.2 mm Merck silica gel plates (60 F254). Flash column chromatography was performed on silica gel 60 (Merck). ^{1}H and ^{13}C NMR spectra were recorded on a Bruker Avance I (400 and 250 MHz) spectrometer at 298 K. Chemical shifts are reported in parts per million (ppm, δ scale) relative to the residual signal of the deuterated solvent. Elemental analyses were carried out using a Vario ELIII-Elementar Euro and an EA-HekaTech. Mass spectrometry was performed using a Finnigan MAT SSQ 710 with EI ionization. ESI-Q-TOF MS measurements (positive ion mode) were carried out using a micrOTOF mass spectrometer from Bruker Daltonics equipped with an automatic syringe pump by KD Scientific for sample injection. The standard electrospray ion (ESI) source was used to generate the ions and the instrument was calibrated in the m/z range 50–3000 using an internal calibration standard (Tunemix solution) from Agilent. Samples with concentrations ranging from 1 to 10 mg mL^{-1} were injected using a constant flow (3 mL min^{-1}) of sample solution. Data and HRMS calculations were processed *via* the Bruker Data Analysis software version 4.0. Cyclic voltammetry experiments were performed using a Biologic VMP 3 potentiostat at room temperature under argon atmosphere. A three electrode setup was utilized (WE: glassy carbon, RE: $AgNO_3$/Ag in CH_3CN, CE: Pt). The redox couple Fc^+/Fc was used as internal standard after each measurement. Size-exclusion chromatography was performed on an Agilent 1200 series system (degasser: PSS, pump: G1310A, autosampler: G1329A, oven: Techlab, DAD detector: G1315D, RI detector: G1362A, eluent: DMAc + 0.21% LiCl, 1 mL min^{-1}, temperature: 40 °C, column: PSS GRAM guard/1000/30 Å).

Synthesis

N,N$_0$-(2-Vinyl-Anthracene-9,10-Diylidene)Dicyanamide (2)

1 (1.5 g, 6.4 mmol) was dissolved in chloroform (45 mL). Titanium(IV) chloride (3.5 mL, 32.0 mmol) followed by *bis*-(trimethylsilyl)carbodiimide (14.5 mL, 42.6 mmol) was added at 0 °C. The solution was stirred at 60 °C for 4 h. After cooling to room temperature, the mixture was cast into ice water and the crude product was extracted with dichloromethane (3 × 100 mL). The combined organic phases were washed with water (2 × 100 mL) and dried over magnesium sulfate. The solvent was removed under reduced pressure and the crude product was purified by flash column chromatography (silica gel 60; dichloromethane) to obtain 0.9 g (3.3 mmol, 52%) as yellow powder. The product-a mixture of E/Z isomers-was stored under argon atmosphere at −20 °C. ^{1}H NMR (400 MHz, CD_2Cl_2, δ): 9.50–8.10 (br, 4H; Ar H), 7.86 (s, 3H, Ar H), 6.87 (m, 1H; vinyl), 6.10 (d, $J = 18$ Hz, 1H; vinyl), 5.62 (d, $J = 11$ Hz, 1H; vinyl); ^{13}C NMR (75 MHz, CD_2Cl_2, δ): 172.2 (C═N), 171.4 (C═N), 144.2, 135.2, 135.0, 132.2, 128.6, 128.0, 125.4, 120.3, 114.2, 114.1; EIMS (m/z (%)): 282 (100) [M^+], 255 (52) [M^+−vinyl], 229 (11) [M^+−vinyl−CN], 175 (12) [M^+−vinyl−2 NCN]; HRMS (ESI, m/z): [2 M + Na]$^+$ calcd. for $C_{18}H_{10}N_4$: 587.1703; found: 587.1700. Anal. calcd. for $C_{18}H_{10}N_4$: C 76.58, H 3.57, N 19.85; found: C 76.31, H 3.55, N 20.10.

General Procedure of Polymerization of 2

A flask was charged with **2** (50 mg, 0.2 mmol), AIBN (0.01 mmol, 5 mol%) and solvent (for detailed information see Table 1). The reaction mixture was degassed by the freeze–pump–thaw method and was stirred at 70 °C for 20 h. Subsequently, the mixture was cooled to room temperature and the polymer was precipitated twice in cold acetone (20 mL each) and collected by centrifugation. The obtained brown powder was dried under vacuum. The polymers were stored under argon atmosphere at −20 °C. ^{1}H NMR (400 MHz, DMSO-d_6, δ): 9.55–6.38 (br, 7H; Ar H), 1.82–0.64 (br, 3H).

N,N′-(2-Ethynyl-Anthracene-9,10-Diylidene) Dicyanamide (5)

4 (100 mg, 0.4 mmol) was dissolved in chloroform (7 mL). Titanium(IV) chloride (0.24 mL, 2.2 mmol) followed by *bis*-(trimethylsilyl)carbodiimide (0.98 mL, 4.3 mmol) was added at 0 °C. The solution was stirred at 50 °C for 4 h. After cooling to room temperature, the mixture was cast into ice water and the crude product was extracted with dichloromethane (3 × 20 mL). The combined organic phases were washed with water (2 × 20 mL) and dried over magnesium sulfate. The solvent was removed under reduced pressure and the crude product was purified by gel filtration (silica gel 60; dichloromethane) to obtain 91 mg (0.3 mmol, 75%) as yellow powder. The product was stored under argon atmosphere at 5 °C. ^{1}H NMR (400 MHz, CD_2Cl_2, δ): 9.58 to 8.09 (br, 4H; Ar H), 7.92 (s, 3H, Ar H), 3.54 (s, 1H; ethynyl); ^{13}C NMR: Not possible due to low solubility; EIMS (m/z (%)): 280 (100) [M^+], 253 (12) [M^+−HCN], 175 (4) [M^+−ethynyl−2 NCN]; HRMS (ESI, m/z): [M + H]$^+$ calcd. for $C_{18}H_8N_4$: 281.0821; found: 281.0816.

TABLE 1 Selected Analytical Data for Polymers **3** and **6** Prepared by the Free Radical Polymerization (FRP) Technique and Rh-Catalyzed Polymerizations, Respectively.

Polymer	Solvent	Concentration (mol L^{-1})	Temperature (°C)	M_n[a] (g mol^{-1})	PDI[a]	Yield (%)
3a	1,2-Dichloroethane	0.51	70	7,300	1.36	20
3b	NMP	1.00	70	7,700	1.27	7
3c	DMSO	1.00	70	16,800	1.98	77
3d	DMF	1.00	70	10,400	1.40	40
3e	DMAc	1.00	70	8,600	1.28	33
6a	DMF	0.10	50	4,400	1.33	63
6b	DMSO	0.10	50	10,900	3.06	48
6c[b]	DMF	0.20	50	n/d[c]	n/d[c]	97
6d[b]	DMSO	0.20	50	n/d[c]	n/d[c]	90
6e[b]	1,2-Dichloroethane	0.10	50	n/d[c]	n/d[c]	77
6f[b]	DMSO	0.10	r.t.	n/d[c]	n/d[c]	93

[a] Determined by SEC (DMAc, 0.21% LiCl, polystyrene standard, RI detector).
[b] Addition of triethylamine (0.1 eq.) to the reaction mixture.
[c] SEC measurements could not be performed due to the insolubility of the polymers in the mobile phase (DMAc, 0.21% LiCl).

General Procedure of Rh-Catalyzed Polymerization of 5

A degassed solution of **5** (30 mg, 0.1 mmol) and triethylamine in 0.4 mL (0.20M) and 0.9 mL (0.10M) of the solvent, respectively, was added to a degassed solution of [Rh(2,5-norbornadiene)Cl]$_2$ (0.005 mmol, 5 mol%) in 0.1 mL of the same solvent (for detailed information see Table 1). The reaction mixture was stirred at room temperature (**6f**) and 50 °C (**6a–6e**), respectively, for 20 h. Subsequently, the mixture was cooled to room temperature and the polymer was precipitated twice in cold acetonitrile (20 mL each) and was

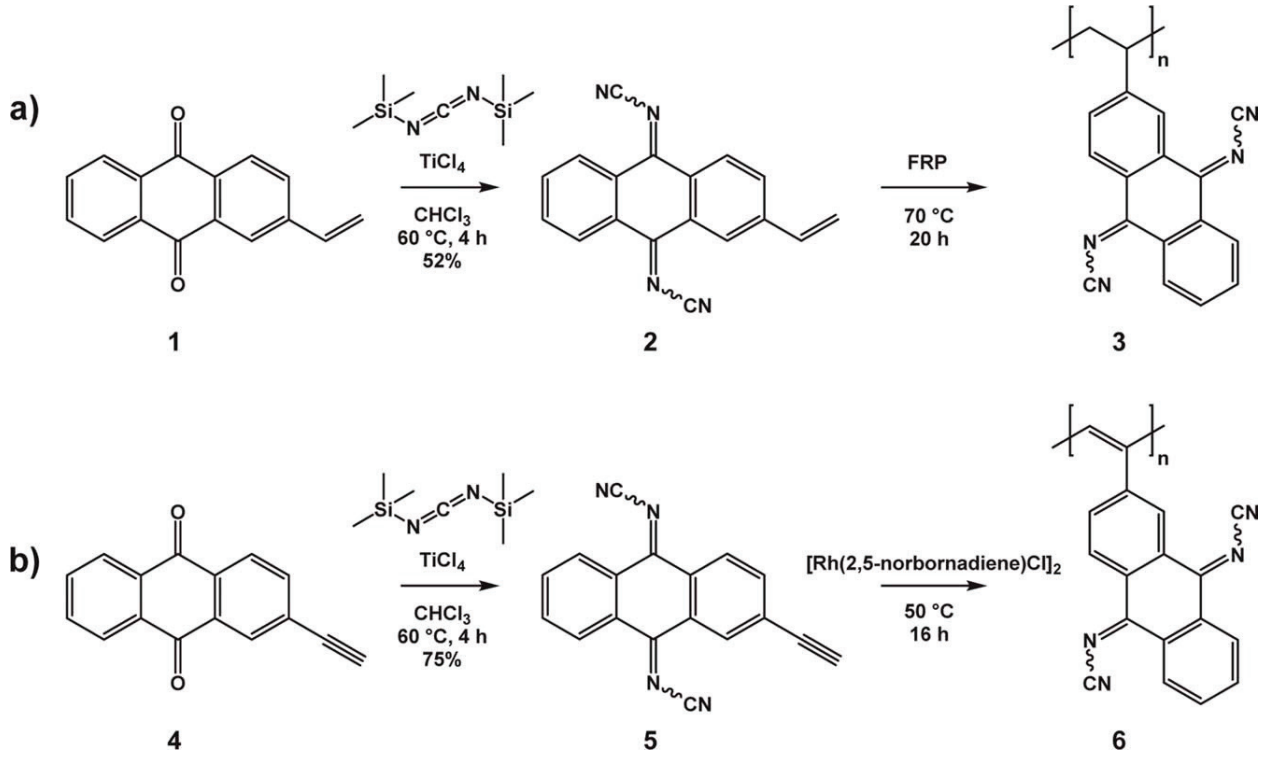

SCHEME 1 Schematic representation of the synthesis of monomer **2** (a) and polymer **3** (a) as well as of monomer **5** (b) and polymer **6** (b).

TABLE 2 Cyclic Voltammetric Data of Monomer **2** and **5**

Compound	E (V vs. Fc^+/Fc)	E (V vs. Fc^+/Fc)
Monomer **2**	−0.63[a]	−1.03[a]
	−0.65[b]	−1.16[b]
Monomer **5**	−0.59[a]	−0.99[a]
	−0.59[b]	−1.09[b]

[a] In DMF, 0.1M $LiClO_4$, 500 mV s^{-1}.
[b] In DMF, 0.1M $TBAClO_4$, 500 mV s^{-1}.

collected by centrifugation. The obtained brown powder was dried under vacuum. The polymers were stored under argon atmosphere at 5 °C. ^{1}H NMR (250 MHz, DMF-d_7, δ): 10.17–7.67 (br, 7H; Ar H), 5.78 (s, 1H).

RESULTS AND DISCUSSION

Synthesis of Monomers and Polymers

The preparation of monomer **2** was carried out from 2-vinylanthraquinone **1** as shown in Scheme 1, which can be straightforwardly obtained in a two-step procedure from the commercially available 2-aminoanthraquinone.[29] Subsequently, the carbonyl groups were transformed into *N*-cyanoimine groups utilizing titanium(IV) chloride and *bis*(trimethylsilyl)carbodiimide. Monomer **2** could only be obtained in moderate yields due to its low stability on silica gel during the purification procedure.[31] Subsequently, **2** was polymerized under different conditions using the free radical polymerization technique and five polymers (**3a** to **3e**) with different molar masses were obtained (Table 1). The polymerization step is important to enhance the electrochemical performance of the organic material in organic electronics, which is dependent on the insolubility of the redox-active material in the electrolyte. Oligomers and low molar mass polymers feature a better solubility, leading to a strong decay of the electrochemical performance in the solid state. As a consequence, high molar mass polymers with a low poly-dispersity index are preferred. The free radical polymerization was performed with AIBN as initiator and due to the low solubility of **2** in the selected solvents [1,2-dichloroethane, *N*-methyl-2-pyrrolidone (NMP), dimethylsulfoxide (DMSO), *N*,*N*-dimethylformamide (DMF) and *N*,*N*-dimethylacetamide (DMAc)]. The obtained polymers were investigated by size exclusion chromatography (SEC) and revealed in all cases a monomodal distribution. The analytical data of the polymers are summarized in Table 1. The most promising polymers in terms of high molar masses were obtained in DMSO with a yield of 77% and a high molar mass of 16,800 g mol^{-1}. All other solvents led to poor yields (up to 40%) and lower molar masses (7300 to 10,400 g mol^{-1}), presumably due to chain terminating reactions.

The ethynyl-based monomer **5** was synthesized from 2-ethynylanthraquinone **4**, which could be prepared in a straightforward two-step procedure from the commercial available 2-bromoanthraquinone.[30] The carbonyl groups were transformed in a similar manner into *N*-cyanoimine groups using titanium(IV) chloride and *bis*(trimethylsilyl) carbodiimide. Monomer **5** could be obtained in a good yield of 75% and features good solubility in polar aprotic solvents like DMF and 1,2-dichloroethane, which were used for the Rh-catalyzed polymerization.[32,33] The use of DMF leads to the polymers in promising yields (63%) but with low molar masses (M_n) of around 4,400 g mol^{-1}, according to SEC (PS standard). Utilizing DMSO as solvent increased the molar mass (M_n) to 10,900 g mol^{-1}. However, the polymerization suffered from a lower yield of around 48%. By addition of 0.1 eq. of trimethylamine as cocatalyst, which acts as promoter to dissociate the Rh-dimer complex to its monomeric form and increases the initiation efficiency,[34,35] the yield could be increased to 77% in 1,2-dichloroethane and to 90 and 97% using DMSO and DMF, respectively, at a reaction temperature of 50 °C. Under milder conditions at room temperature and in DMSO, the yield of the polymerization was slightly lower (93%). However, all poly(acetylene)-based polymers precipitated during the polymerization reaction and were completely insoluble in common organic solvents like methanol, DMF, DMSO, or DMAc. Consequently, no detailed analytical investigations could be performed.

Electrochemical Performance

The electrochemical behavior of monomers **2** and **5** as well as of polymers **3** and **6** was investigated by cyclic voltammetry. In particular, the influence of the electrolyte cations on the redox potential was examined (Table 2). Due to the solubility of both the monomers and polymers and the large stable electrochemical operational window, DMF was chosen as solvent and a solution of 0.1M lithium perchlorate and 0.1M tetrabutylammonium perchlorate ($TBAClO_4$), respectively, in DMF was utilized as electrolyte (Fig. 1). The results are summarized in Table 2. In 0.1M lithium perchlorate in DMF the monomer **2** features two reversible one-electron reduction steps at $E^1_{1/2} = -0.63$ and $E^2_{1/2} = -1.03$ V versus Fc^+/Fc at

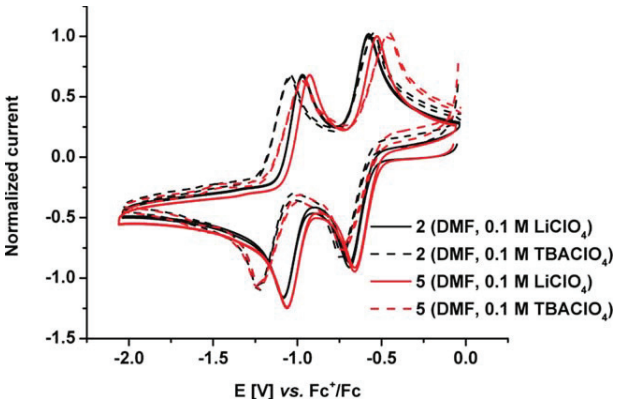

FIGURE 1 Normalized cyclic voltammograms of monomer **2** ($c = 0.6$ mg mL^{-1}) and **5** ($c = 1.0$ mg mL^{-1}) in DMF, 0.1M $LiClO_4$ and $TBAClO_4$, respectively, 500 mV s^{-1}, 1st and 2nd cycle, WE: glassy carbon, RE: $AgNO_3$/Ag in CH_3CN, CE: Pt. [Color figure can be viewed in the online issue, which is available at wileyonlinelibrary.com.]

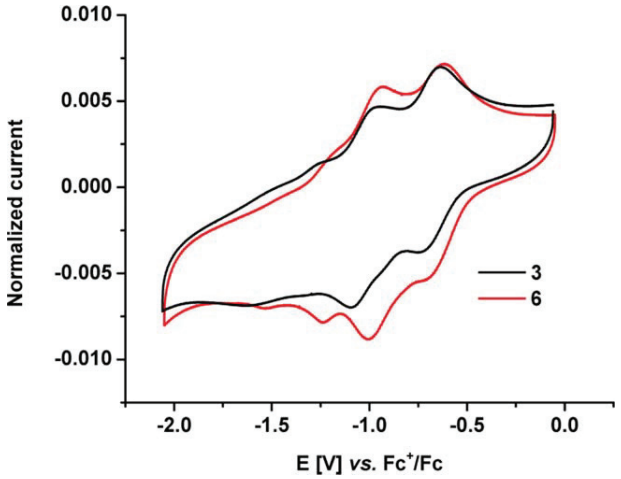

FIGURE 2 Normalized cyclic voltammograms of polymer **3** ($c = 0.8$ mg mL^{-1}) and **6** ($c = 1.0$ mg mL^{-1}) in DMF, 0.1M $LiClO_4$, 500 mV s^{-1}, 1st and 2nd cycle, WE: glassy carbon, RE: $AgNO_3$/Ag in CH_3CN, CE: Pt. [Color figure can be viewed in the online issue, which is available at wileyonlinelibrary.com.]

a scan rate of 500 mV s^{-1}. These redox potentials are in good agreements with literature reports of related small molecules[36] and, as a consequence, the vinyl group has no influence on the redox behavior of the monomer. The electron acceptance of the *N*-cyanoimine functionality is increased compared to the keto group and, therefore, the reduction of the monomer to the radical anion and to the dianion occurs at a more positive potential compared to anthraquinone ($E^1_{1/2} = -1.19$ V and $E^2_{1/2} = -1.68$ V *vs.* Fc^+/Fc)[37] as well as to the monofunctionalized *N*-(10-oxo-2-vinylanthracen-9(10*H*)-ylidene)cyanamide ($E^1_{1/2} = -0.88$ V and $E^2_{1/2} = -1.31$ V *vs.* Fc^+/Fc).[29] The utilization of $TBAClO_4$ as electrolyte salt shifts the redox signals to $E^1_{1/2} = -0.65$ and $E^2_{1/2} = -1.16$ V *vs.* Fc^+/Fc at a scan rate of 500 mV s^{-1}. Monomer **5** exhibits also two reversible redox potentials at $E^1_{1/2} = -0.59$ and $E^2_{1/2} = -0.99$ V *vs.* Fc^+/Fc (500 mV s^{-1} scan rate) utilizing $LiClO_4$ as electrolyte salt, which indicates no significant influence of the ethynyl group on the redox behavior. The redox behavior of monomer **5** in $TBAClO_4$ is similar to the behavior in $LiClO_4$. The redox signals are located at $E^1_{1/2} = -0.59$ and $E^2_{1/2} = -1.09$ V *vs.* Fc^+/Fc at a scan rate of 500 mV s^{-1}. The shift of the second reduction peak of both monomers is slightly influenced by the cation of the electrolyte. Due to the stronger coordination of the lithium ions to the *N*-cyano-imine groups, the redox potential is shifted to more positive values.[17,37]

However, the cyclic voltammogram of polymer **3** in DMF, 0.1M $LiClO_4$ reveals at a scan rate of 500 mV s^{-1} the expected redox signals at $E^1_{1/2} = -0.60$ V and $E^2_{1/2} = -0.97$ V *vs.* Fc^+/Fc, corresponding to the reduction to the radical anion and to the dianion, respectively (Fig. 2). However, an additional redox signal appears at $E^3_{1/2} = -1.26$ V *vs.* Fc^+/Fc. This signal can be presumably assigned to the reduction of the carbonyl group of the *N*-(10-oxo-anthracen-9(10*H*)-ylidene)cyanamide,[29] which is most likely formed by a partial hydrolysis of *N*-cyanoimine moieties to carbonyl groups (Fig. 3). However, it is not quite clear if the monomeric units hydrolyze during the polymerization reaction or during the electrochemically induced reduction. The first redox reaction of this unit is presumably overlapped by the signal of the DCAQI unit. However, due to the low solubility of polymer **3**, a detailed analysis of its composition and degradation is not possible. However, IR spectroscopy of the monomer and polymer, respectively, indicates a hydrolysis of the monomer during polymerization (see Supporting Information for further details). As a consequence, Rh-catalyzed polymerization was applied to enable milder reaction conditions (e.g., at room temperature) and the catalyst features a high functional group tolerance even in polar aprotic solvents. To examine the formation of the carbonyl groups during the polymerization, the Rh-catalyst polymerization was applied to monomer **5**. The cyclic voltammogram of polymer **6** displays a similar redox behavior and comprises three reduction peaks, indicating that the conjugated backbone has no influence on the redox behavior. The redox signals of the *N,N′*-dicyanoimine anthraquinone moieties appear at $E^1_{1/2} = -0.63$ V and $E^2_{1/2} = -0.96$ V *vs.* Fc^+/Fc. However, an additional reduction signal at $E^3_{1/2} = -1.20$ V *vs.* Fc^+/Fc occurs similar to the polymer with the saturated backbone. IR spectroscopy of the **5** and **6**, respectively, indicates also a hydrolysis of the monomer during polymerization (see Supporting Information for further details). This evidence that the hydrolysis of the *N*-cyanoimine moieties takes place despite milder reaction conditions during the polymerization at room temperature. The poor solubility of polymer **6** makes a detailed analysis impossible. However, the redox signals are stable and reversible, but at equal mass loadings the peak area of the redox reactions of the conjugated polymer is slightly larger indicating improved electron transport within the polymer chain.

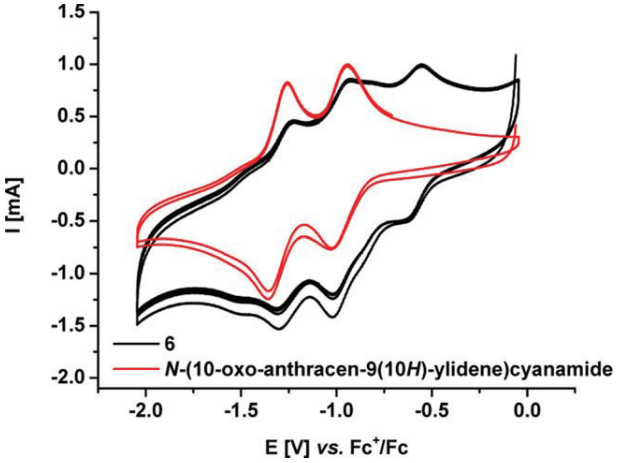

FIGURE 3 Comparison of the cyclic voltammograms of polymer **6** and *N*-(10-oxo-anthracen-9(10*H*)-ylidene)cyanamide. [Color figure can be viewed in the online issue, which is available at wileyonlinelibrary.com.]

CONCLUSIONS

Two new redox-active *N,N'*-dicyanoimine anthraquinone based polymers were synthesized by modification of the carbonyl groups to *N*-cyanoimine groups. The monomer was synthesized in a two-step procedure comprising the introduction of the polymerizable group *via* Pd-catalyzed cross-coupling reactions and the transformation of the carbonyl groups. In this particular case, polymerizable vinyl and ethynyl groups were applied. The monomers were investigated by cyclic voltammetry and both possess two stable and reversible one-electron redox reactions at about -0.6 and -1.0 V *vs.* Fc^+/Fc, which are not significantly affected by the polymerizable group. The redox potentials of the monomers are located at higher potentials compared to the potentials of anthraquinone and *N*-(10-oxo-2-vinyl-anthracen-9(10*H*)-ylidene)cyanamide. The polymerization was carried out utilizing the free radical and the Rh-catalyzed polymerization technique, respectively, and led to redox-active polymers with average molar masses (M_n) of 4,400 to 16,800 g mol^{-1} in high yields (up to 97%). However, the *N*-cyanoimine units were partially hydrolyzed presumably during the polymerization step leading to carbonyl groups. As a consequence, the new reduction signal at -1.26 V *vs.* Fc^+/Fc appeared. However, the synthesized compounds are useful for possible applications like organic energy storage systems.

ACKNOWLEDGMENT

The authors thank the European Social Fund (ESF), the Thüringer Aufbaubank (TAB) and the Thuringian Ministry of Economy, Science and Digital Society (TMWWdG) for the financial support.

REFERENCES AND NOTES

1 Y. Liang, Z. Tao, J. Chen, *Adv. Energy Mater.* **2012**, *2*, 742–769.

2 Z. Song, H. Zhou, *Energy Environ. Sci.* **2013**, *6*, 2280–2301.

3 H. Nishide, K. Oyaizu, *Science* **2008**, *319*, 737–738.

4 T. Janoschka, N. Martin, U. Martin, C. Friebe, S. Morgenstern, H. Hiller, M. D. Hager, U. S. Schubert, *Nature* **2015**, *527*, 78–81.

5 M. Armand, S. Grugeon, H. Vezin, S. Laruelle, P. Ribière, P. Poizot, J. M. Tarascon, *Nat. Mater.* **2009**, *8*, 120–125.

6 P. Poizot, F. Dolhem, *Energy Environ. Sci.* **2011**, *4*, 2003–2019.

7 T. Jähnert, M. D. Hager, U. S. Schubert, *J. Mater. Chem. A* **2014**, *2*, 15234–15251.

8 T. Janoschka, M. D. Hager, U. S. Schubert, *Adv. Mater.* **2012**, *24*, 6397–6409.

9 B. Häupler, A. Wild, U. S. Schubert, *Adv. Energy Mater.* **2015**, *5*, 1402034.

10 Y. Hanyu, Y. Ganbe, I. Honma, *J. Power Sources.* **2013**, *221*, 186–190.

11 R. Zeng, L. Xing, Y. Qiu, Y. Wang, W. Huang, W. Li, S. Yang, *Electrochim. Acta* **2014**, *146*, 447–454.

12 R. Zeng, X. Li, Y. Qiu, W. Li, J. Yi, D. Lu, C. Tan, M. Xu, *Electrochem. Commun.* **2010**, *12*, 1253–1256.

13 J. Xiang, C. Chang, M. Li, S. Wu, L. Yuan, J. Sun, *Crystallogr. Growth Des.* **2008**, *8*, 280–282.

14 M. Yao, H. Senoh, M. Araki, T. Sakai, K. Yasuda, *ECS Trans.* **2010**, *28*, 3–10.

15 M. Yao, H. Ando, T. Kiyobayashi, *Energy Proc.* **2013**, *34*, 880–887.

16 T. Yokoji, H. Matsubara, M. Satoh, *J. Mater. Chem. A* **2014**, *2*, 19347–19354.

17 B. Häupler, T. Hagemann, C. Friebe, A. Wild, U. S. Schubert, *ACS Appl. Mater. Interfaces* **2015**, *7*, 3473–3479.

18 A. Shimizu, Y. Tsujii, H. Kuramoto, T. Nokami, Y. Inatomi, N. Hojo, J. Yoshida, *Energy Tech.* **2014**, *2*, 155–158.

19 A. Shimizu, H. Kuramoto, Y. Tsujii, T. Nokami, Y. Inatomi, N. Hojo, H. Suzuki, J. Yoshida, *J. Power Sources* **2014**, *260*, 211–217.

20 W. Wan, H. Lee, X. Yu, C. Wang, K. W. Nam, X. Q. Yang, H. Zhou, *RSC Adv.* **2014**, *4*, 19878–19882.

21 B. Häupler, R. Burges, T. Janoschka, T. Jähnert, A. Wild, U. S. Schubert, *J. Mater. Chem. A* **2014**, *2*, 8999–9001.

22 S. Nishida, Y. Yamamoto, T. Takui, Y. Morita, *Chem Sus Chem.* **2013**, *6*, 794–797.

23 B. Häupler, R. Burges, C. Friebe, T. Janoschka, D. Schmidt, A. Wild, U. S. Schubert, *Macromol. Rapid Commun.* **2014**, *35*, 1367–1371.

24 M. Kato, K. Senoo, M. Yao, Y. Misaki, *J. Mater. Chem. A* **2014**, *2*, 6747–6754.

25 D. Schmidt, B. Häupler, C. Friebe, M. D. Hager, U. S. Schubert, *Polymer* **2015**, *68*, 321–327.

26 Z. Song, H. Zhan, Y. Zhou, *Chem. Commun.* **2009**, *5*, 448–450.

27 T. Nokami, T. Matsuo, Y. Inatomi, N. Hojo, T. Tsukagoshi, H. Yoshizawa, A. Shimizu, H. Kuramoto, K. Komae, H. Tsuyama, J. Yoshida, *J. Am. Chem. Soc.* **2012**, *134*, 19694–19700.

28 H. Nishiide, K. Oyaizu, T. Yoshimoto, Waseda University, (NISSAN CHEMICAL INDUSTRIES, LTD.). JP 2012190545, October 04, **2012**.

29 D. Schmidt, B. Häupler, C. Stolze, M. D. Hager, U. S. Schubert, *J. Polym. Sci. A: Polym. Chem.* **2015**, *53*, 2517–2523.

30 K. Oyaizu, Y. Niibori, A. Takahashi, H. Nishide, *J. Inorg. Organomet. Polym. Mater.* **2013**, *23*, 243–250.

31 N. Martín, I. Pérez, L. Sánchez, C. Seoane, *J. Org. Chem.* **1997**, *62*, 870–877.

32 I. Saeed, M. Shiotsuki, T. Masuda, *Macromolecules* **2006**, *39*, 5347–5351.

33 I. Saeed, M. Shiotsuki, T. Masuda, *Macromolecules* **2006**, *39*, 8977–8981.

34 J. Liu, Lam, W. Y. Jacky. B. Z. Tang, *Chem. Rev.* **2009**, *109*, 5799–5867.

35 W. Yang, M. Tabata, S. Kobayashi, K. Yokota, A. Shimizu, *Polym. J.* **1991**, *23*, 1135–1138.

36 K. Takahashi, K. Kobayashi, *J. Org. Chem.* **2000**, *65*, 2577–2579.

37 D. Pletcher, H. Thompson, *Farad. Trans.* **1998**, *94*, 3445–3450.

Supporting Information

Poly(DCAQI): Synthesis and Characterization of a New Redox-Active Polymer

D. Schmidt, B. Häupler, M. D. Hager, U. S. Schubert*

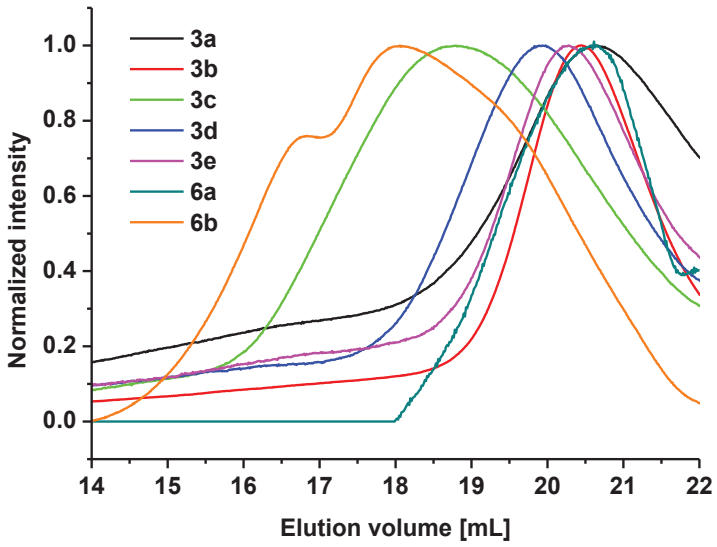

FIGURE S1 Size exclusion chromatograms of the polymers **3a** to **3e** and **6a** to **6b**. Eluent: DMAc, 0.21% LiCl, polystyrene standard, RI detector.

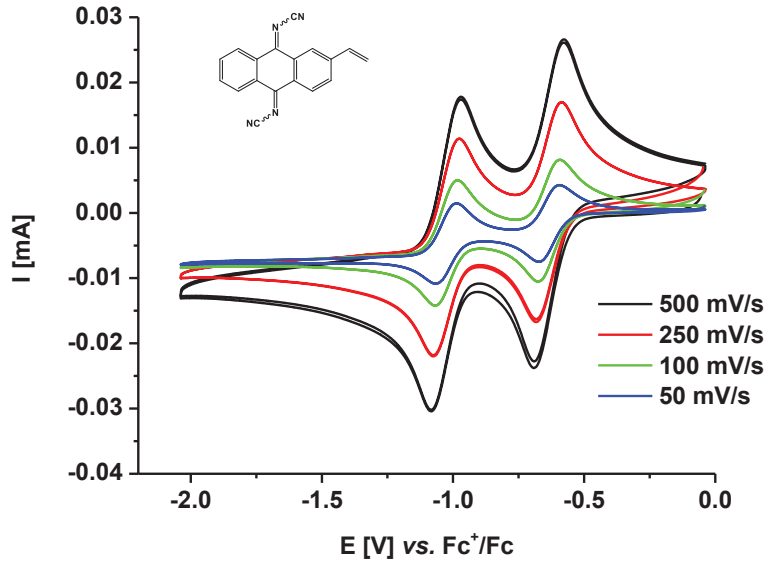

FIGURE S2 Cyclic voltammograms of monomer **2** in DMF, 0.1 M $LiClO_4$, at different scan rates (WE: GC; RE: $AgNO_3$/Ag, in CH_3CN, CE: Pt), c = 0.6 mg mL^{-1}, 1st and 2nd cycle.

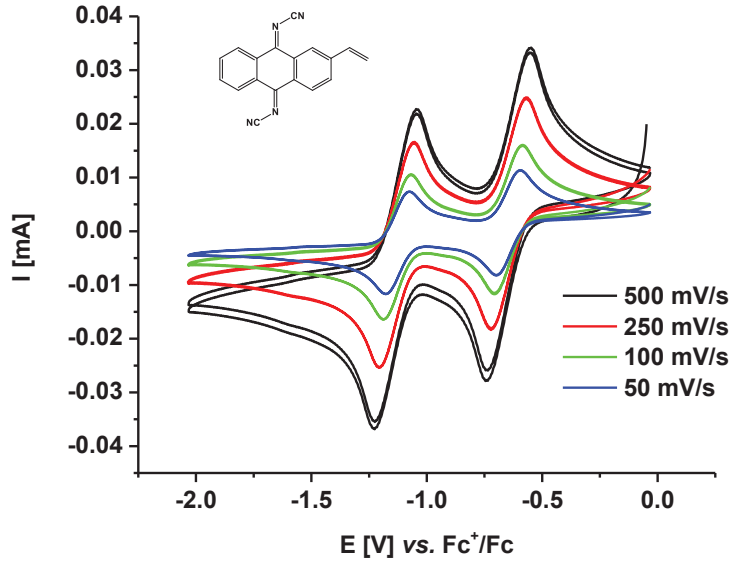

FIGURE S3 Cyclic voltammograms of monomer **2** in DMF, 0.1 M $TBAClO_4$, at different scan rates (WE: GC; RE: $AgNO_3$/Ag, in CH_3CN, CE: Pt), c = 0.6 mg mL^{-1}, 1st and 2nd cycle.

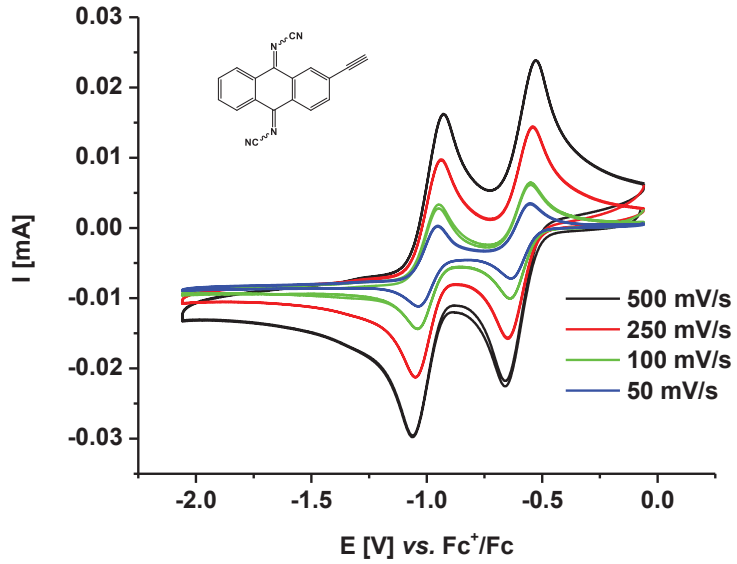

FIGURE S4 Cyclic voltammograms of monomer **5** in DMF, 0.1 M $LiClO_4$, at different scan rates (WE: GC; RE: $AgNO_3$/Ag, in CH_3CN, CE: Pt), c = 1.00 mg mL^{-1}, 1st and 2nd cycle.

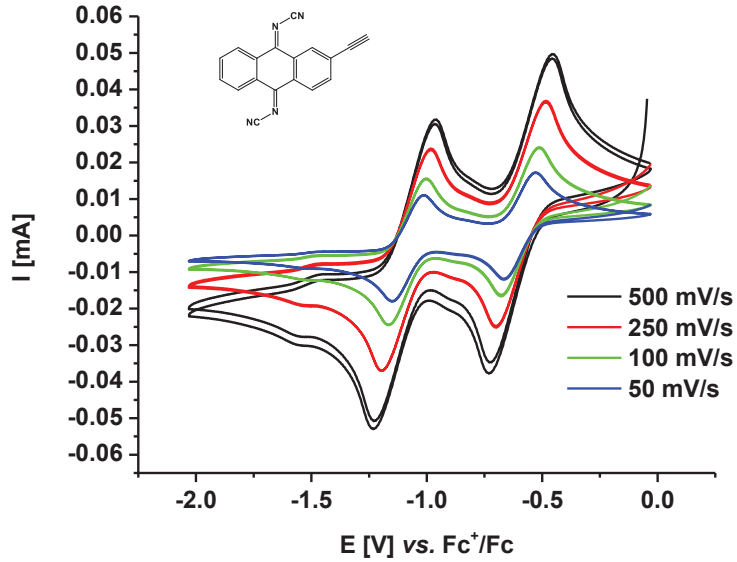

FIGURE S5 Cyclic voltammograms of monomer **5** in DMF, 0.1 M $TBAClO_4$, at different scan rates (WE: GC; RE: $AgNO_3$/Ag, in CH_3CN, CE: Pt), c = 1.00 mg mL^{-1}, 1st and 2nd cycle.

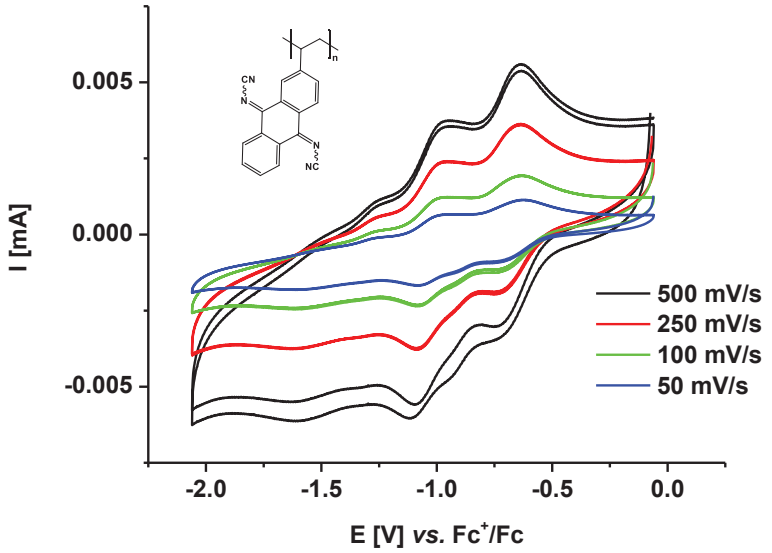

FIGURE S6 Cyclic voltammograms of polymer **3** in DMF, 0.1 M $LiClO_4$, at different scan rates (WE: GC; RE: $AgNO_3$/Ag, in CH_3CN, CE: Pt), c = 0.80 mg mL^{-1}, 1st and 2nd cycle.

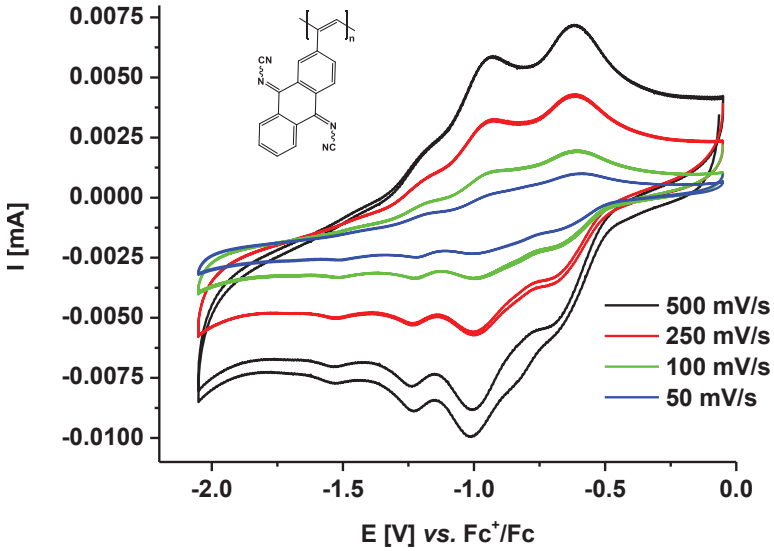

FIGURE S7 Cyclic voltammograms of polymer **6** in DMF, 0.1 M $LiClO_4$, at different scan rates (WE: GC; RE: $AgNO_3$/Ag, in CH_3CN, CE: Pt), c = 1.00 mg mL^{-1}, 1st and 2nd cycle

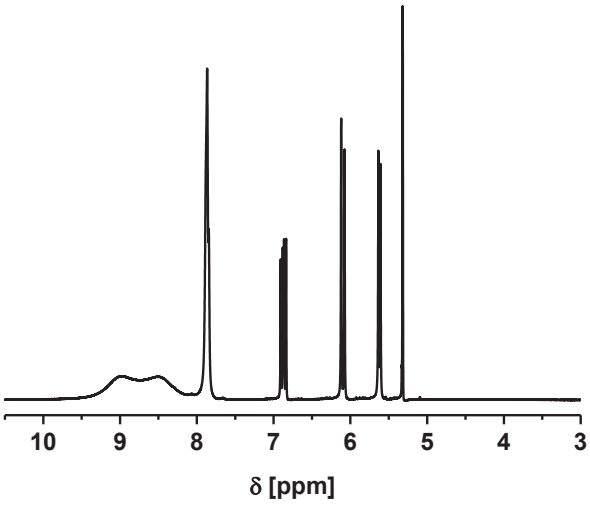

FIGURE S8: ^{1}H-NMR spectra of monomer **2** (400 MHz, CD_2Cl_2).

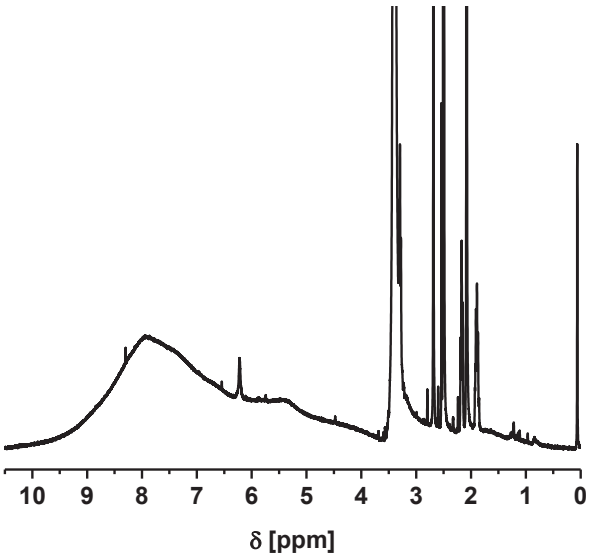

FIGURE S9: ^{1}H-NMR spectra of polymer **3** (400 MHz, DMSO-d_6).

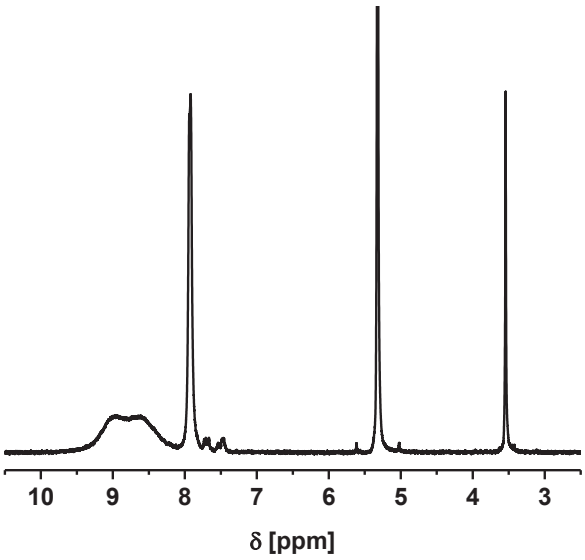

FIGURE S10: ^{1}H-NMR spectra of monomer **5** (300 MHz, CD_2Cl_2).

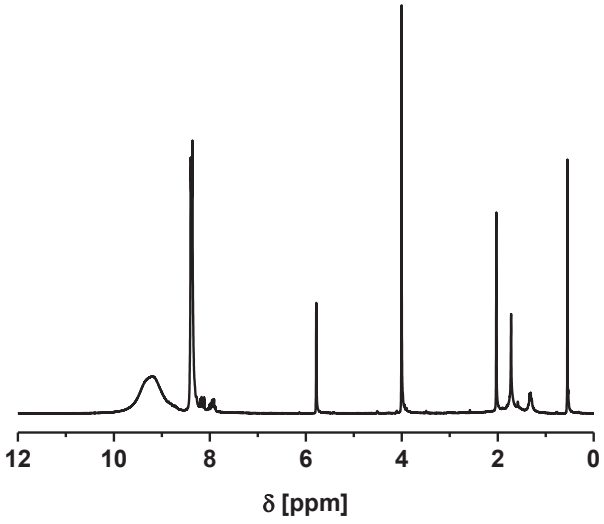

FIGURE S 11: ^{1}H-NMR spectra of polymer **6** (250 MHz, DMF-d_7).

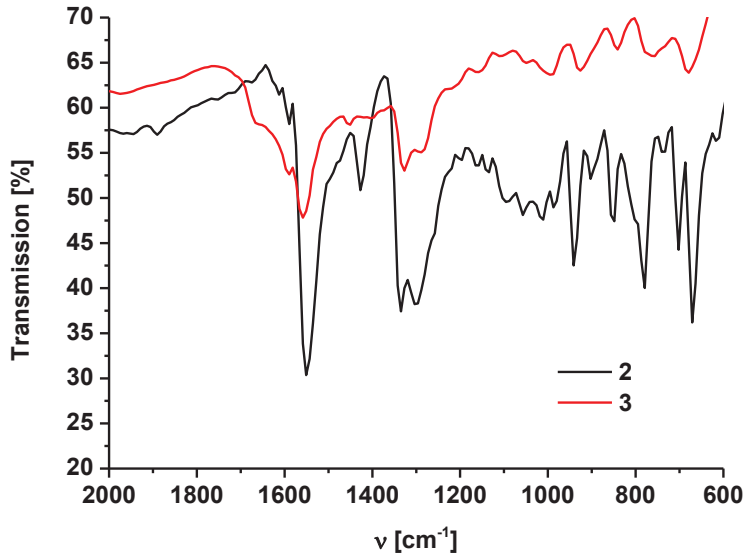

FIGURE S12: IR spectra of monomer **2** and polymer **3**.

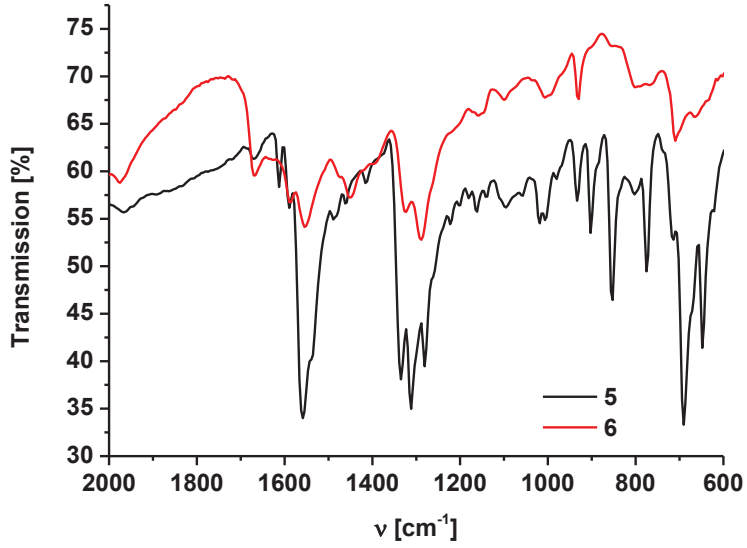

FIGURE S13: IR spectra of monomer **5** and polymer **6**.

Publication 3

"Poly(exTTF): A novel redox-active polymer as active material for Li-organic batteries"

Bernhard Häupler, René Burges, Christian Friebe, Tobias Janoschka, Daniel Schmidt, Andreas Wild, Ulrich S. Schubert

Macromol. Rapid Comm. **2014**, *35*, 1367–1371.

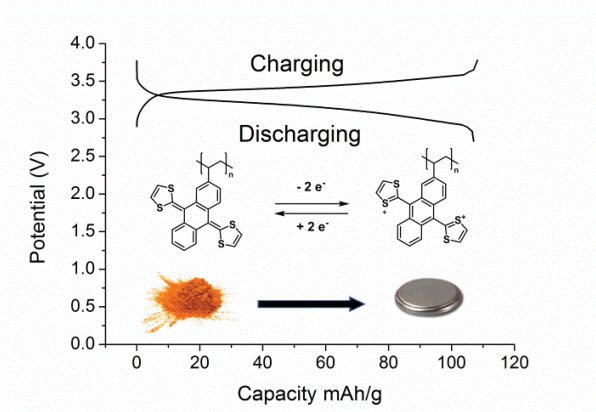

Poly(exTTF): A Novel Redox-Active Polymer as Active Material for Li-Organic Batteries

Bernhard Häupler, René Burges, Christian Friebe, Tobias Janoschka, Daniel Schmidt, Andreas Wild,* Ulrich S. Schubert

The first polymer bearing exTTF units intended for the use in electrical charge storage is presented. The polymer undergoes a redox reaction involving two electrons at –0.20 V vs Fc/Fc^+ and is applied as active cathode material in a Li-organic battery. The received coin cells feature a theoretical capacity of 132 mAh g^{-1}, a cell potential of 3.5 V, and a lifetime exceeding more than 250 cycles.

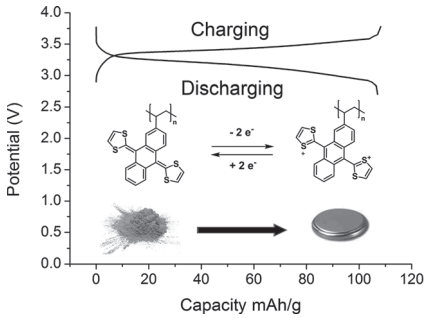

1. Introduction

Redox-active polymers are one of the key elements in the remarkably developing research area of organic electronics, such as organic solar cells, organic light-emitting diodes, polymeric magnets, sensors, and organic electrical charge-storage devices.[1–3] Recently, major attention was attracted by the application of polymers that bear redox-active groups as active electrode material in secondary batteries. They feature beneficial properties such as low toxicity, high flexibility, and light weight, in particular compared to metals, which are normally employed as active charge-storage materials.[4,5] The first approaches of the application of polymers as active material in organic batteries focused on conjugated polymers. However, the resulting batteries displayed a fluctuating cell potential, due to the conjugation of the redox-active groups.[6] The second generation of organic batteries eluded this problem by utilization of polymers with pendant non-conjugated redox-active groups. In particular organic radicals such as nitroxides,[7–11] galvinoxyls,[12,13] nitronyl-nitroxides,[14–16] and arylnitroxides[17] have been studied intensively, but also other redox-active compounds such as triarylamines,[18] carbazoles,[19] or ferrocene[20] were utilized. Most of these compounds possess an ordinary one-electron redox reaction, leading to a single charge/discharge plateau with a constant cell potential. The theoretical capacity is limited by the molar mass of their repeating unit. As a consequence, several approaches were performed to apply polymers bearing redox-active compounds that possess a redox reaction involving two or more electrons, such as quinoid structures,[21,22] viologens,[23] triangulenes,[24] or phthalimides.[25] The disadvantage of these systems is that their redox reactions can depend on each other and, therefore, can occur at different potentials, leading to possible additional undesired charge/discharge plateaus at different cell voltages.

B. Häupler, R. Burges, Dr. C. Friebe, T. Janoschka, D. Schmidt, Dr. A. Wild, Prof. U. S. Schubert
Laboratory of Organic and Macromolecular Chemistry, Friedrich Schiller University Jena, Humboldtstr. 10, 07743 Jena, Germany
Fax: (+)49 3641 948202
E-mail: ulrich.schubert@uni.jena.de
B. Häupler, R. Burges, Dr. C. Friebe, T. Janoschka, D. Schmidt, Dr. A. Wild, Prof. U. S. Schubert
Jena Center for Soft Matter (JCSM), Friedrich Schiller University Jena, Philosophenweg 7, 07743 Jena, Germany

2. Results and Discussion

π-Extended tetrathiafulvalenes systems, namely 9,10-di(1,3-dithiol-2-ylidene)-9,10-dihydroanthracene (exTTF), have been applied within many fields in organic electronics, such as molecular wires, artificial photosynthetic systems, or solar cells, because of their favorable

DOI: 10.1002/marc.201400167

structural and optical properties.[26] Contrary to thetetrathiafulvalenes, which show two well-separated one-electron oxidation processes, exTTF exhibits an oxidation involving two electrons forming a dicationic species in a single step. During the oxidation, the release of the second electron is promoted due to the planar low-energy conformation associated with the rearomatization of the oxidized dicationic product.[27] This unique electrochemical behavior makes polymers with pendant exTFF systems promising candidates for the usage as active electrode material in organic batteries. Thus, we herein present the synthesis and characterization of an exTTF-containing polymer, poly(exTTF), as well as its application in a Li-organic battery. To maintain the high theoretical capacity, we focused on the introduction of a low-molar-mass-polymerizable group, namely vinyl. The monomer **3** was synthesized in three straightforward steps according to a modified literature procedure.[28] Commerically available 2-aminoanthraquinone was transformed into 2-iodoanthraquinone **1** using a *p*-toluenesulfonic-acid-supported Sandmeyer reaction. To avoid toxic organo-tin compounds, different Pd-catalyzed coupling reactions for the introduction the of vinyl group were examined. The best results were achieved with the Hiyama reaction providing 2-vinylanthraquinone **2** in high yields. Subsequently, the carbonyl groups of **2** were transformed into 1,3-dithiol-2-ylidene groups by Horner-Wadsworth-Emmons reaction. The resulting monomer **3** was polymerized using the free radical polymerization technique with 2,2′-azobis(2-methylpropionitrile) (AIBN) as initiator (Scheme 1). The chemical properties of polymer **4** can be influenced by the choice of the appropriate solvent and the amount of initiator. The low solubility of the monomer limited the range of applicable solvents, but DMSO led to high conversions, polymers with high molar mass ($\bar{M}_n = 6.02 \times 10^3$ g mol^{-1}), and a narrow molar mass distribution (PDI = 2.04). The size-exclusion chromatogram of polymer **4** exhibits two distributions, which are probably caused by recombination reactions (see Supporting Information). Polymer **4** is soluble in *N*,*N*′-dimethylformamide (DMF), *N*,*N*′-dimethylacetamide (DMAc), and dimethylsulfoxide (DMSO), as well as insoluble but swellable in common electrolytes.

For the applications of polymer **4** as active material in secondary batteries, stability and insolubility of both redox states have to be ensured. Hence, the electrochemical properties of both monomer in solution and the polymer as composite electrode must be investigated in detail. Cyclic voltammetry of monomer **3** in acetonitrile solution reveals an electrochemical response at $(E_{pa} + E_{pc})/2 = -0.2$ V vs Fc/Fc$^+$, which is ascribed to the oxidation of exTTF units to the dicationic species (Figure 1a). The peak splits are quite large, in particular at high scan rates, and are assigned to the massive geometrical changes during the redox reaction. Therefore, it remains unclear if the redox behavior is based on one two-electron or two one-electron redox reactions. UV-vis-NIR spectroelectrochemical studies of the monomer **3** (Figure 1b) revealed a defined and stable electrochemical process. During oxidation, a significant decrease of the compound's absorption below 500 nm occurs, accompanied by the appearance of a very broad, undefined absorption feature in the long-wavelength region. An isosbestic point emerges at 480 nm, indicating the presence of only two species, i.e., a defined redox process without side products. Applying a re-reducing potential (–0.5 V vs Fc/Fc$^+$) restores the initial spectrum nearly completely, which confirms the electrochemical stability of the system. Due to the low intrinsic conductivity of polymer **4**, the electrochemical properties were examined as composite layer on a graphite sheet as current collector. An electrode slurry of **4**/vapor grown carbonfibers (VGCF)/polyvinylidene fluoride (PVdF) 10/80/10 (m/m/m) in *N*-methylpyrrolidene was sufficiently ground, spread onto the current collector by doctor blading method, and dried under vacuum at 40 °C. The homogeneity of the layer was proven by elemental analysis and scanning electron microscopy (Figure S5, Supporting Information). The electrode was immersed in a solution of 0.1 M $LiClO_4$ in 1,2-dimethoxymethane/propylene carbonate 4/1 (v/v) and cyclic voltammetry at a scan rate of 5 mV s^{-1} revealed

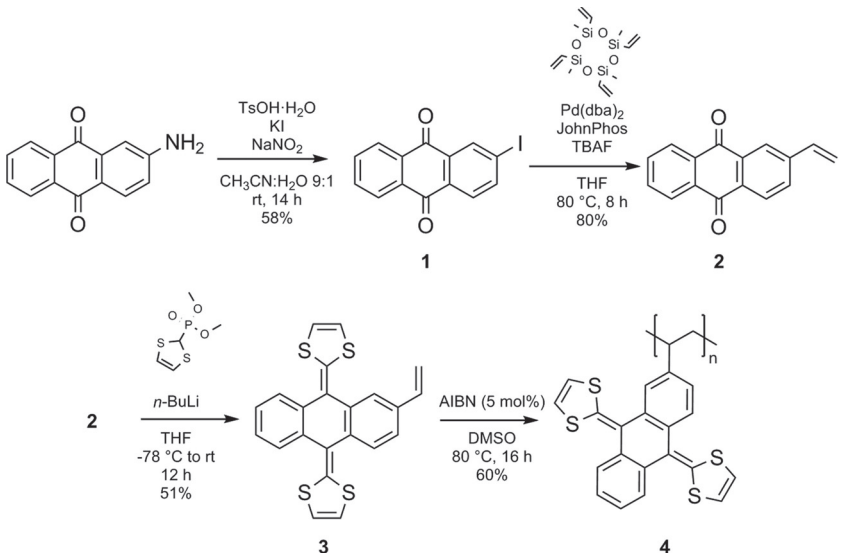

Scheme 1. Schematic representation of the synthesis of poly(exTTF) **4**.

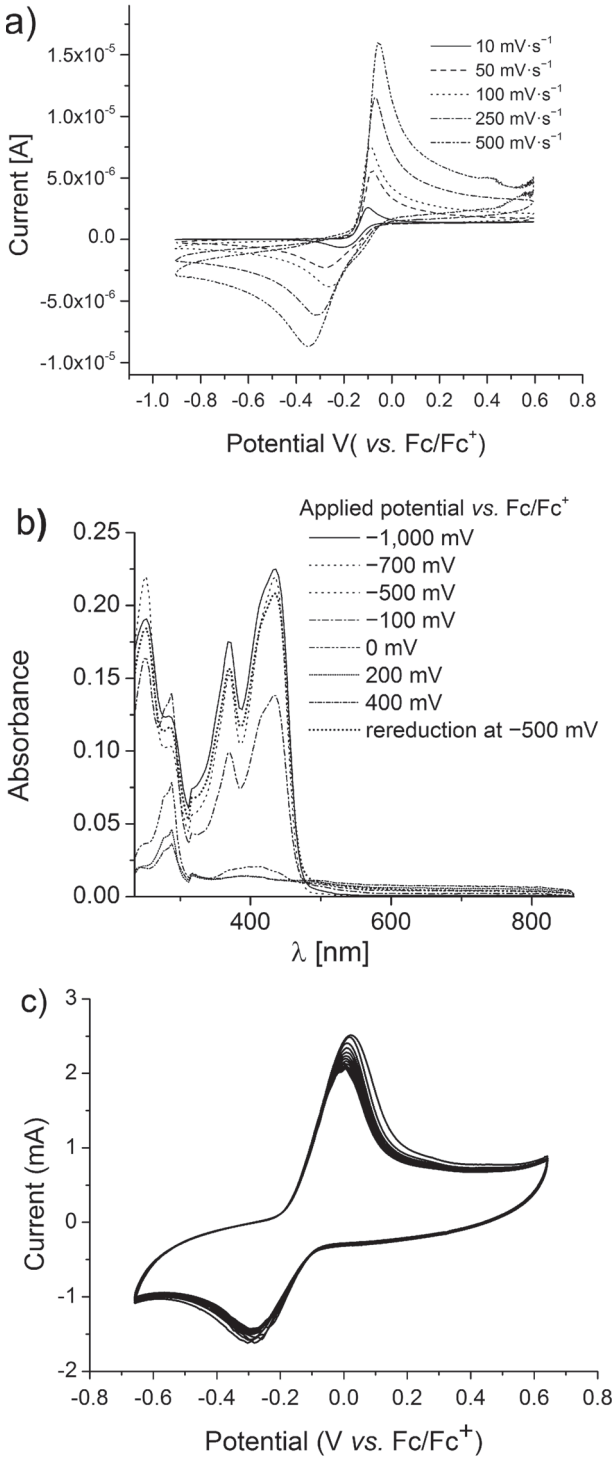

Figure 1. a) Cyclic voltammogram of monomer **3** in acetonitrile, 0.1 M $LiClO_4$ at different scan rates. b) UV-VIS-NIR-Spectroelectrochemistry of monomer **3** in acetonitrile, 0.1 M $LiClO_4$. c) Cyclic voltammogram of a polymer-composite electrode (10/80/10 (m/m/m) **4**/VGCF/PVdF) in 1,2-dimethoxyethane/propylene carbonate 4/1 (v/v), 0.1 M $LiClO_4$, 50 cycles.

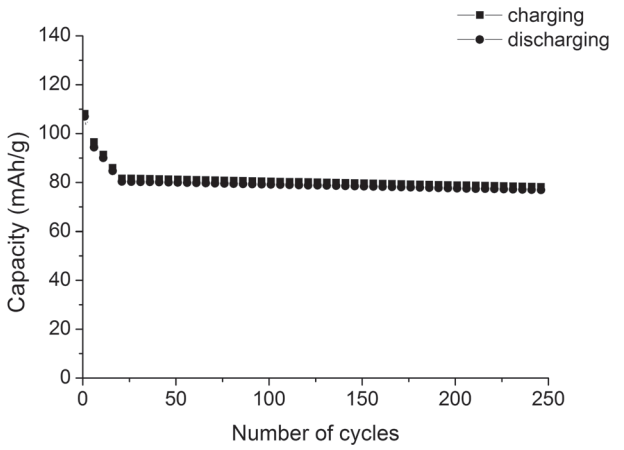

Figure 2. Capacity development during extended charge/discharge cycling (250 cycles) of a Li-organic battery with a composite electrode of **4**/VGCF/PVdF 10/80/10 (m/m/m) in 1,2-dimethoxyethane/propylene carbonate 4/1 (v/v), 0.1 M $LiClO_4$ as active material.

a redox wave at $(E_{pa} + E_{pc})/2 = -0.15$ V vs Fc/Fc^+ (Figure 1c). The intensity of the redox signal slightly decreases during the first 15 cycles, and then remains stable. This is most likely because of the dissolution of some shorter polymer chains in the electrolyte. The redox behavior of the electrode is in good agreement with the one of monomer **3**, demonstrating that binder and conductive additives have negligible influence. The slightly larger peak-to-peak separation (270 mV) can be explained by slower kinetics due to slower diffusion processes in the electrode.

A coin cell was prepared under inert atmosphere by sandwiching a composite electrode **4**/VGCF/PVdF 10/80/10 (m/m/m) and a lithium foil using a separator film. A solution of 0.1 M $LiClO_4$ in 1,2-dimethoxymethane/propylene carbonate 4/1 (v/v) served as electrolyte. The charge/discharge characteristics of the fabricated cell at a constant current of 1 C display a plateau at a cell potential of 3.5 V for charging and at 3.1 V for discharging, which is in accordance to the redox behavior of the composite electrode of **4** vs Li/Li^+. At the first charge/discharge cycle, the battery exhibits a capacity of 108 mAh g^{-1} corresponding to 82% of the theoretical capacity. During the first 20 charge/discharge cycles, the capacity dropped to 82 mAh g^{-1} corresponding to 61% of the theoretical capacity. This is probably because of the dissolution of shorter polymer chains into the electrolyte (Figure 2). The charge/discharge capacity remains stable for the next 230 charge/discharge cycles, at an average coulombic efficiency of 99%. The influence of the charging speed was investigated after 250 cycles. At a charging speed of 2 C, the capacity drops by 10% to 69 mAh g^{-1} and at a charging speed of 5 C, the capacity decreases by around 50% to 38 mAh g^{-1} (Figure 3).

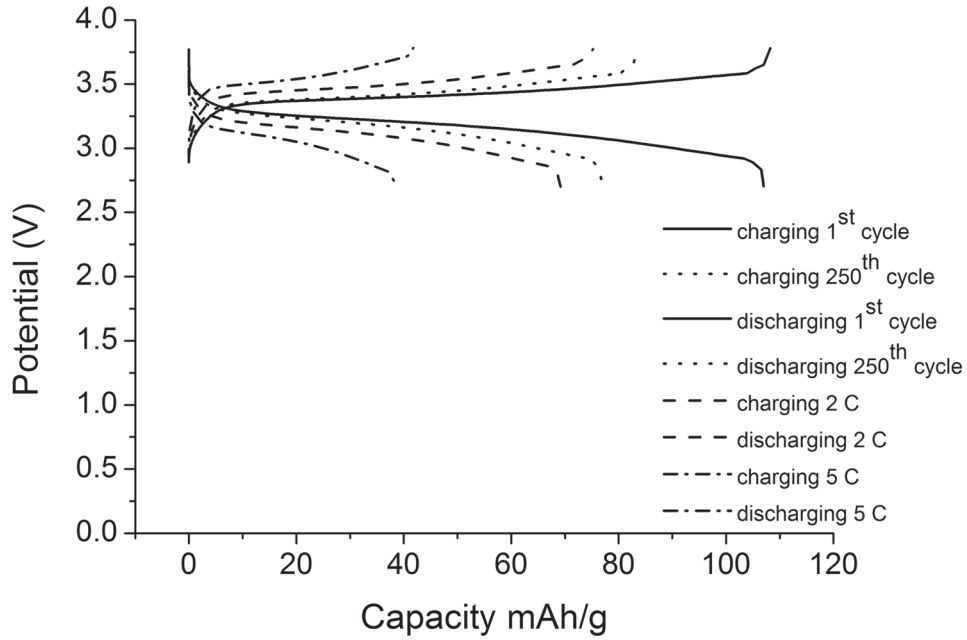

Figure 3. Charge/discharge curves (capacity vs potential) of a Li-organic battery of the first and the 250th cycle and charge/discharge curves at different charging speeds.

3. Conclusions

The free radical polymerization of 2-vinyl(exTTF) leads to poly(2-vinyl(exTTF)), a novel redox-active polymer bearing exTTF units, which undergoes a redox reaction involving two electrons at –0.2 V vs Fc/Fc^+. The exTTF units have proven to be a promising core structure as an active material unit for organic batteries. The application of poly(exTTF) in a Li-organic battery enables charge-storage devices that display a theoretical capacity of 132 mAh g^{-1}, which is higher than the capacity of PTMA (112 mAh g^{-1})[8] and equal to the capacity of PTVE (136 mAh g^{-1})[7] together with a constant cell potential and a long lifetime exceeding 250 cycles. However, charging speeds exceeding 2 C lead to a large capacity drop, probably because of the slow kinetics in the electrode.

Supporting Information

Supporting Information is available from the Wiley Online Library or from the author.

Acknowledgements: The authors thank the Bundesministerium für Bildung und Forschung (project no. 13N11393), the European Social Fund (ESF), the Thüringer Aufbaubank (TAB), the Thuringian Ministry of Economy, Employment and Technology (TMWAT), the Fonds der Chemischen Industrie, as well as the Dutch Polymer Institute (DPI, technology area HTE) for the financial support.

Received: March 19, 2014; Revised: April 29, 2014; Published online: May 23, 2014; DOI: 10.1002/marc.201400167

Keywords: organic battery; polymer; redox chemistry; exTTF

[1] Y. Liang, Z. Tao, J. Chen, *Adv. Energy Mater.* **2012**, *2*, 742.
[2] Z. Song, H. Zhou, *Energy Environ. Sci.* **2013**, *6*, 2280.
[3] T. Janoschka, M. D. Hager, U. S. Schubert, *Adv. Mater.* **2012**, *24*, 6397.
[4] H. Nishide, K. Oyaizu, *Science* **2008**, *319*, 737.
[5] P. Poizot, F. Dolhem, *Energy Environ. Sci.* **2011**, *4*, 2003.
[6] P. Novák, K. Müller, K. S. V. Santhanam, O. Haas, *Chem. Rev.* **1997**, *97*, 207.
[7] K. Oyaizu, T. Kawamoto, T. Suga, H. Nishide, *Macromolecules* **2010**, *43*, 10382.
[8] H. Nishide, S. Iwasa, Y.-J. Pu, T. Suga, K. Nakahara, M. Satoh, *Electrochim. Acta* **2004**, *50*, 827.
[9] T. Suga, H. Konishi, H. Nishide, *Chem. Commun.* **2007**, 1730.
[10] P. Nesvadba, L. Bugnon, P. Maire, P. Novák, *Chem. Mater.* **2010**, *22*, 783.
[11] T. Katsumata, J. Q. Qu, M. Shiotsuki, M. Satoh, J. Wada, J. Igarashi, K. Mizoguchi, T. Masuda, *Macromolecules* **2008**, *41*, 1175.
[12] T. Suga, H. Ohshiro, S. Sugita, K. Oyaizu, H. Nishide, *Adv. Mater.* **2009**, *21*, 1627.
[13] T. Jähnert, B. Häupler, T. Janoschka, M. D. Hager, U. S. Schubert, *Macromol. Chem. Phys.* **2013**, *214*, 2616.
[14] T. Suga, S. Sugita, H. Ohshiro, K. Oyaizu, H. Nishide, *Adv. Mater.* **2011**, *23*, 751.
[15] K. Oyaizu, T. Sukegawa, H. Nishide, *Chem. Lett.* **2011**, *40*, 184.
[16] T. Sukegawa, A. Kai, K. Oyaizu, H. Nishide, *Macromolecules* **2013**, *46*, 1361.
[17] T. Suga, Y.-J. Pu, S. Kasatori, H. Nishide, *Macromolecules* **2007**, *40*, 3167.

[18] J. K. Feng, Y. L. Cao, X. P. Ai, H. X. Yang, *J. Power Sources* **2008**, *177*, 199.
[19] M. Yao, H. Senoh, T. Sakai, T. Kiyobayashi, *J. Power Sources* **2012**, *202*, 364.
[20] K. Tamura, N. Akutagawa, M. Satoh, J. Wada, T. Masuda, *Macromol. Rapid. Commun.* **2008**, *29*, 1944.
[21] Z. Song, H. Zhan, Y. Zhou, *Chem. Commun.* **2009**, 448.
[22] T. Nokami, T. Matsuo, Y. Inatomi, N. Hojo, T. Tsukagoshi, H. Yoshizawa, A. Shimizu, H. Kuramoto, K. Komae, H. Tsuyama, J. Yoshida, *J. Am. Chem. Soc.* **2012**, *134*, 19694.
[23] N. Sano, W. Tomita, S. Hara, C.-M. Min, J.-S. Lee, K. Oyaizu, H. Nishide, *ACS Appl. Mater. Int.* **2013**, *5*, 1355.
[24] Y. Morita, S. Nishida, T. Murata, M. Moriguchi, A. Ueda, M. Satoh, K. Arifuku, K. Sato, T. Takui, *Nat. Mater.* **2011**, *10*, 947.
[25] K. Oyaizu, A. Hatemata, W. Choi, H. Nishide, *J. Mater. Chem.* **2010**, *20*, 5404.
[26] F. G. Brunetti, J. L. López, C. Atienza, N. Martín, *J. Mater. Chem.* **2012**, *22*, 4188.
[27] D. M. Guldi, L. Sánchez, N. Martín, *J. Phys. Chem. B* **2001**, *105*, 7139.
[28] M. C. Díaz, B. M. Illescas, C. Seoane, N. Martín, *J. Org. Chem.* **2004**, *69*, 4492.

Supporting Information

for *Macromol. Rapid Commun.*, DOI: 10.1002/marc.201400167

Poly(exTTF): A Novel Redox-Active Polymer as Active Material for Li-Organic Batteries

Bernhard Häupler, René Burges, Christian Friebe, Tobias Janoschka, Daniel Schmidt, Andreas Wild,* Ulrich S. Schubert

Supporting Information

for *Macromol. Rapid Commun.*, DOI: 10.1002/marc.201400167

Poly(exTTF): A novel redox-active polymer as active material for Li-organic batteries

Bernhard Häupler,[a,b] René Burges,[a,b] Christian Friebe,[a,b] Tobias Janoschka,[a,b] Daniel Schmidt,[a,b] Andreas Wild,[a,b] Ulrich S. Schubert[a,b*]

1.) General remarks

Dichloromethane, tetrahydrofuran, and toluene were dried with a PureSolv-EN™ Solvent Purification System (Innovative Technology). *N*,*N*-Dimethylformamide and benzene were distilled over calcium hydride and stored over mol sieves. 1,2-Dichloroethane was distilled over P_2O_5 and stored over mol sieves.

All starting materials were purchased from commercial sources and were used as obtained unless otherwise noted. 2,2'-Azobis(*iso*-butyronitrile) (AIBN) was recrystallized from methanol prior to use.

Unless otherwise noted, all reactions were performed under inert atmosphere.

Reactions were monitored by TLC on 0.2 mm Merck silica gel plates (60 F254). Column chromatography was performed on silica gel 60 (Merck).

^{1}H and ^{13}C NMR spectra were recorded on a Bruker AC 300 (300 MHz) spectrometer at 298 K. Chemical shifts are reported in parts per million (ppm, δ scale) relative to the residual signal of the deuterated solvent.

Elemental analyses were carried out using a Vario ELIII–Elementar Euro and an EA–HekaTech.

Cyclic voltammetry and galvanostatic experiments were performed using a Biologic VMP 3 potentiostat at room temperature.

Size-exclusion chromatography was performed on an Agilent 1200 series system (degasser: PSS, pump: G1310A, auto sampler: G1329A, oven: Techlab, DAD detector: G1315D, RI detector: G1362A, eluent: DMAc + 0.21% LiCl, 1 mL/min, temperature: 40 °C, column: PSS GRAM guard/1000/30 Å)

2.) Synthesis

Synthesis of 2-iodoanthraquinone (**1**):

A flask was charged with 2-aminoanthraquinone (5.81 g, 26 mmol), *p*-toluenesulfonic acid monohydrate (14.86 g, 78 mmol) and 117 mL acetonitrile. To this mixture a solution of potassium iodide (10.81 g, 65.1 mmol) and sodium nitrite (3.59 g, 52.1 mmol) in water (13.5 mL) was added dropwise over 10 minutes. The reaction mixture was stirred for 16 hours at room temperature. Ethyl acetate (250 mL) was added to the reaction mixture and the mixture was extracted successively with saturated sodium sulfite solution (100 mL), saturated sodium hydrogencarbonate solution (100 mL) and brine. The organic phase was dried over sodium sulfate, filtered and concentrated under reduced pressure. The obtained crude product was purified by column chromatography (silica gel; chloroform) to yield 4.71 g (54%) of 2-iodoanthraquinone as an off white solid. Anal. Calcd for $C_{16}H_{10}I$: C, 50.33; H, 2.11. Found: C, 50.23; H, 2.05. ^{1}H NMR ($CDCl_3$, 300 MHz, ppm): δ 7.81 (t, 1H), 7.82 (t, 1H), 7.99 (d, 1H), 8.15 (d, 1H), 8.30 (m, 2H), 8.65 (d, 1H). ^{13}C NMR ($CDCl_3$, 75 MHz, ppm): δ 193.2, 192.6, 141.2, 135.6, 134.0, 133.8, 133.6, 133.5, 132.5, 128.0, 126.8, 126.5, 99.5.

Synthesis of 2-vinylanthraquinone (**2**):

A flask was charged with 2-iodoanthraquinone (4 g, 11.97 mmol), *bis*(dibenzylideneacetone)palladium(0) (0.138 g, 0.239 mmol), biphenyl-2-yldi-*tert*-butylphosphine (0.143 g, 0.479 mmol), tetrahydrofuran (10.5 mL) and 13.17 mL of a 1 M tetrabutylammonium fluoride solution in tetrahydrofuran. The mixture was purged with nitrogen and 2,4,6,8-tetramethyl-2,4,6,8-tetravinyl-1,3,5,7,2,4,6,8-tetraoxatetrasiloxane (2.07 mL, 5.99 mmol) was added dropwise. The reaction mixture was heated to 60 °C for eight hours under nitrogen atmosphere. The reaction mixture was allowed to cool to room temperature and 100 mL of chloroform were added. The mixture was extracted two times with water (100 mL), once with brine, dried over sodium sulfate, filtered and concentrated under reduced pressure. The crude product was purified by column chromatography (silica gel; chloroform:*n*-heptane, 8:1) and 2.25 g (80% yield) of 2-vinylanthraquinone were obtained.

Anal. Calcd for $C_{16}H_{10}O_2$: C, 81.90; H, 4.30. Found: C, 81.85; H, 4.31. ^{1}H NMR ($CDCl_3$, 300 MHz, ppm): δ 5.54 (d, 1H), 6.05 (d, 1H), 6.87 (dd, 1H), 7.80 (m, 3H), 8.32 (m, 4H). ^{13}C NMR ($CDCl_3$, 75 MHz, ppm): δ 183.2, 182.6, 143.2, 135.4, 134.1, 134.0, 133.8, 133.6, 133.5, 132.5,131.4, 128.3, 127.8, 127.2, 124.8, 118.4.

Synthesis of 2,2'-(2-vinylanthracene-9,10-diylidene)bis(1,3-dihiole) (**3**):

Dimethyl-1,3-dithiol-2-ylphosphonate (733 mg, 3.45 mmol) was dissolved in 10 mL tetrahydrofurane under argon atmosphere and the reaction mixture was cooled to -78 °C. A 2.5 M solution of *n*-butyllithium in *n*-hexane (1.50 mL, 3.75 mmol) was added dropwise to the reaction mixture within five minutes. The mixture was stirred at -78 °C for 2 hours. To the reaction mixture a solution of 2-vinylanthraquinone (352 mg, 1.50 mmol) in 11.5 mL tetrahydrofurane was added dropwise at -78 °C and the reaction mixture was stirred 4 hours at room temperature. Ethyl acetate (50 mL) was added to the reaction mixture and it was extracted twice with water (35 mL) and once with brine (20 mL). The organic layer was dried over sodium sulfate, filtered and concentrated under reduced pressure. The crude product was purified by column chromatography (silica gel; *n*-hexane:toluene, 1:1) to yield 700 mg (2.12 mmol, 51%) as yellow powder. Anal. Calcd for $C_{22}H_{10}N_4$: C, 64.99; H, 3.47, S, 31.54. Found: C, 64.81; H, 3.58, S 30.95. ^{1}H NMR (CD_2Cl_2, 300 MHz, ppm): δ 7.78 (d, 1H), δ 7.74-7.69 (m, 2H), δ 7.67 (s, 1H), δ 7.38 (d, 1H), δ 7.36 (m, 2H), δ 6.81 (dd, 1H), δ 6.39 (s, 2H), δ 6.38 (s, 1H), δ 5.84 (d, 1H), δ 5,33 (d, 1H). ESI-MS, *m/z* 406.00 [M^+],

General procedure for the polymerization of **3**:

A flask was charged with 50 mg of monomer **3** (0.123 mmol) and 0.25 mL of solvent (see Table S1) was added to dissolve the monomer completely. Subsequently, 1.01 mg AIBN (0.00615 mmol, 5 mol %), was added and the reaction mixture purged with argon for 5 minutes. The mixture was heated to 80 °C for 18 hours. After the polymerization, the solution was poured into dichloromethane to precipitate the product, which was purified by reprecipitation from DMF into dichloromethane to yield the polymer **4** as an orange powder. Anal. Calcd for $C_{22}H_{10}N_4$: C, 64.99; H, 3.47, S, 31.54. Found: C, 65.33; H, 3.54, S 30.78. ^{1}H NMR (DMF-d7, 300 MHz, ppm): δ 7.93 to 5.84 (br, 11H), 2.42 to 0.84 (br, 3H).

Table S1: Analytical data for polymers prepared by free radical polymerization of **3**.

Entry	solvent	PDI[a]	M_n [g/mol][a]	yield [%]
1	1,2-dichloroethane	2.88	2.33×10^3	37
2	*N*,*N*-dimethylformamide	1.99	3.09×10^3	73
3	*N*,*N*-dimethylacetamide	1.88	5.36×10^3	73
4	dimethylsulfoxide	1.66	6.02×10^3	60

a) Determined by SEC (DMAc, 0.1% LiCl, PS standard).

Electrochemical analysis:

For cyclic voltammetry a three electrode setup was used (WE: glassy carbon, RE: $Ag/AgNO_3$ in CH_3CN, CE: Pt). The redox couple of Fc/Fc^+ was utilized as internal standard. All electrolytes were degassed with dry argon and all measurements were performed under argon atmosphere. Cyclic voltammograms of the polymers were obtained employing the composite electrode as working electrode (RE: $Ag/AgNO_3$ in CH_3CN, CE: Pt).

Preparation of electrodes:

Electrodes were prepared by adding a solution of poly(exTTF) in NMP (*N*-methyl-2-pyrrolidone) (10 mg/mL) to a mixture of vapor grown carbonfibers (VGCF; Sigma Aldrich) as conducting additives and poly(vinylidenefluoride) (PVDF; Sigma Aldrich) as a binder (ratio: 1/8/1 m/m/m). These materials were mixed in a montar for 10 minutes, and the thus-obtained paste was coated on graphite foil (Alfa Aesar) applying a doctor blading method. Next, NMP was removed heating the electrodes at 100 °C for 24 h. Subsequently, the electrochemical experiments were performed.

Preparation of coin cells:

Electrodes for coin type cells were prepared as follows: A solution of poly(exTTF) in NMP (*N*-methyl-2-pyrrolidone) (10 mg/mL) was added to vapor grown carbonfibers (VGCF; Showa-Denko) as conducting additive and poly(vinylidenefluoride) (PVDF; Sigma Aldrich) as a binder (ratio: 1/8/1 m/m/m). These materials were mixed in a motar for 10 minutes and the thus-obtained paste was coated on aluminium foil (thickness 0.015 mm, MTI Corporation) applying a doctor blading method. Next, the NMP was removed at 100 °C for 24 h. The amount of active material on the electrode was determined on the basis of the weigth of the dried electrodes. The two electrode coin cells (type 2032) were manufactured under argon atmosphere. Suitable round composite electrodes (15 mm diameter) were cut with a MTI Corporation Precision Disc Cutter T-0.6. Thereby, the crude electrode was sandwiched between two sheets of paper. This electrode employed as cathode was placed into the bottom cell case and separated from the lithium anode by a porous polypropylene membrane (celgard, MTI Corporation). On top of the lithium anode a stainless steal space (diameter: 15.5 mm, thickness: 0.3 mm, MTI Corporation) and a stainless steal wave spring (diameter: 14.5 mm, thickness: 5 mm) were placed. The cell was filled with electrolyte (1,2-dimethoxyethane/propylene carbonate 4/1 v/v, 0.1 M lithium perchlorate) and the top cell case was placed onto the electrode. The cell was sealed with an electric crimper machine (MTI Corporation MSK-100D). Electrochemical measurements were performed after an equilibration time of 24 h.

Charge-discharge experiments:

All experiments were performed at room temperature. The charge/discharge capacities were determined based on the weight of poly(exTTF) in the electrode.

Table S2: Peak splits of the cyclo voltammogram of monomer **3** in acetonitrile 0.1 M $LiClO_4$.

scan rate (mV/s)	peak split (mV)
500	0.285
250	0.243
100	0.170
50	0.191
10	0.110

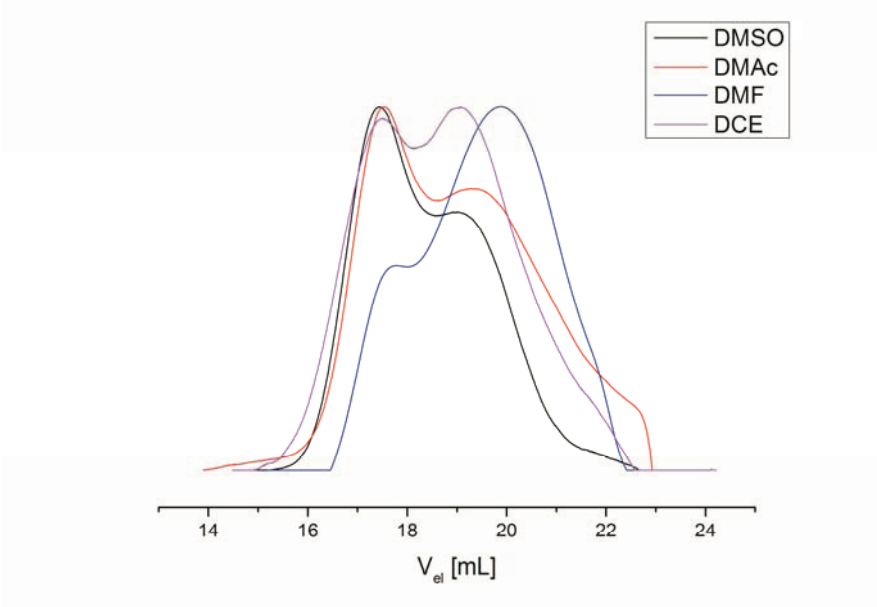

Figure S1: Size-exclusion chromatogram of **4** synthesized with different solvents. Eluent: DMAc, 0.21% LiCl, polystyrene standards, RI detector.

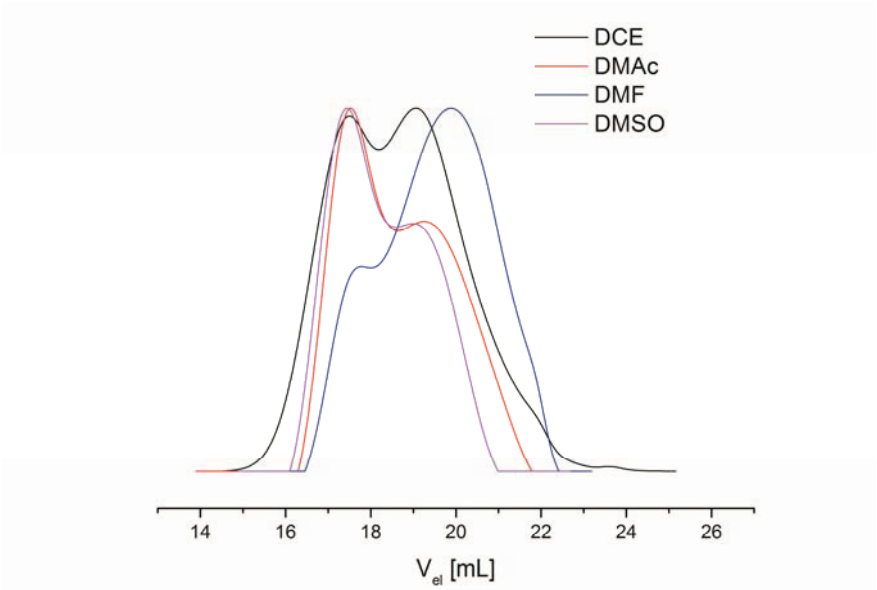

Figure S2: Size-exclusion chromatogram of **4** synthesized with different solvents. Eluent: DMAc, 0.21% LiCl, polystyrene standards, UV-Vis detector 421 nm.

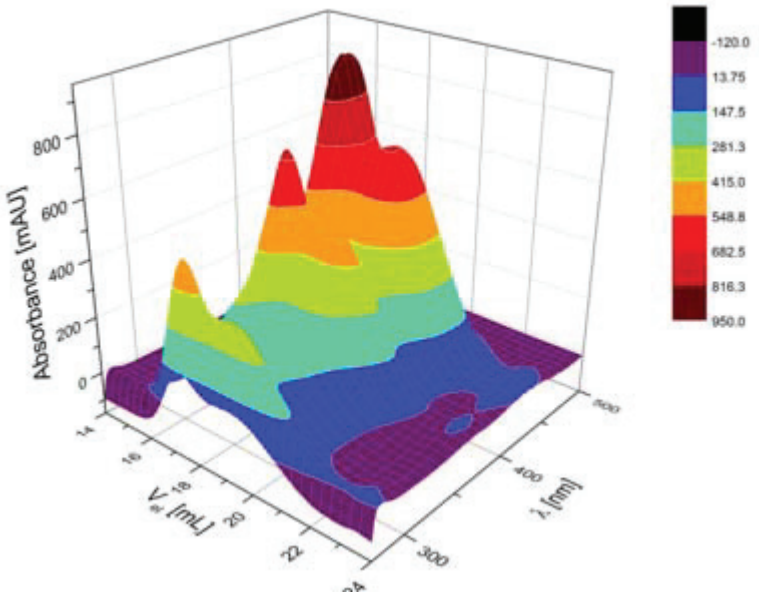

Figure S3: 3D-Size-exclusion chromatrogram of **4** synthesized with dimethylsulfoxide as solvent. Eluent: DMAc, 0.21% LiCl, polystyrene standards.

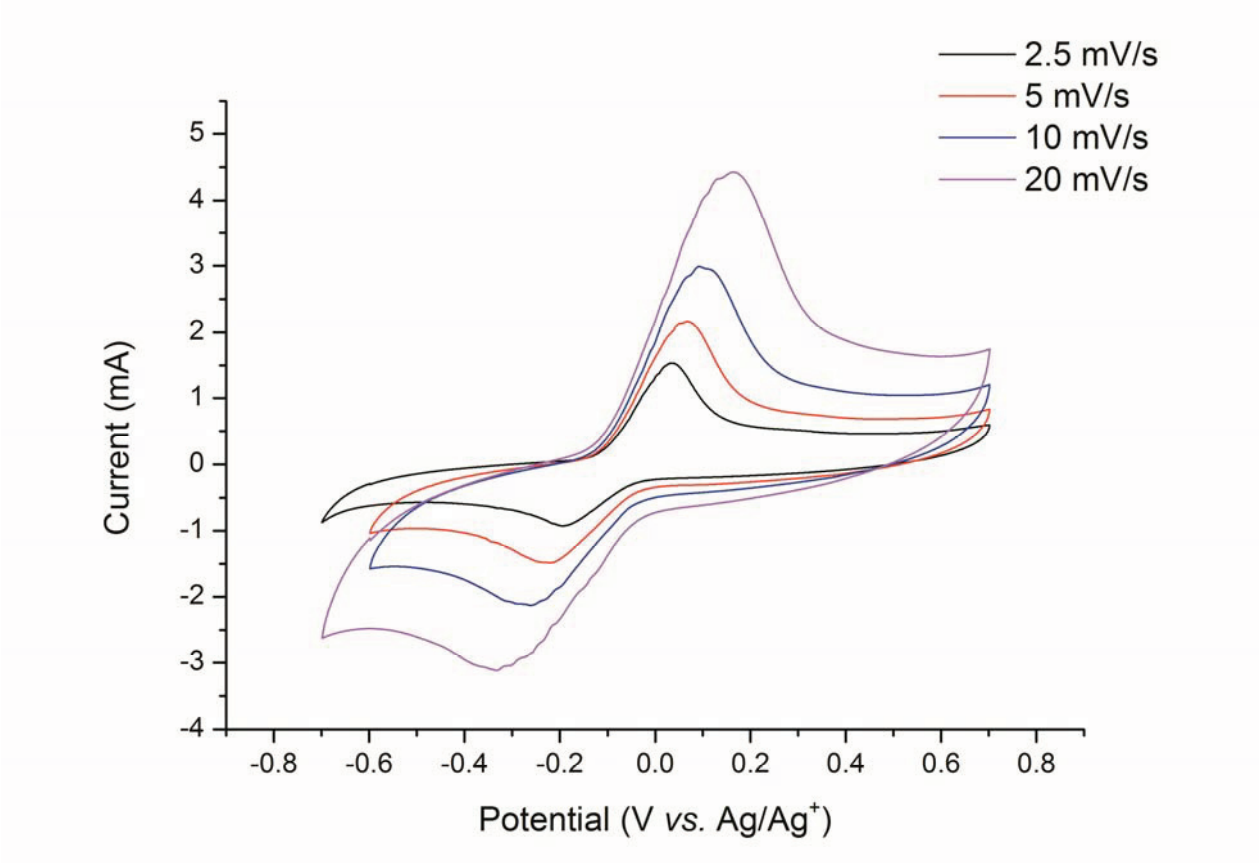

Figure S4: Cyclic voltammogram of a composite electrode (1/8/1 m/m/m) of **4**/VGCF/PVdF at different scan rates; (RE $Ag/AgNO_3$, in CH_3CN, CE: Pt net. Electrolyte: 1,2-dimethoxy-ethane/propylene carbonate 4/1 v/v, 0.1 M $LiClO_4$).

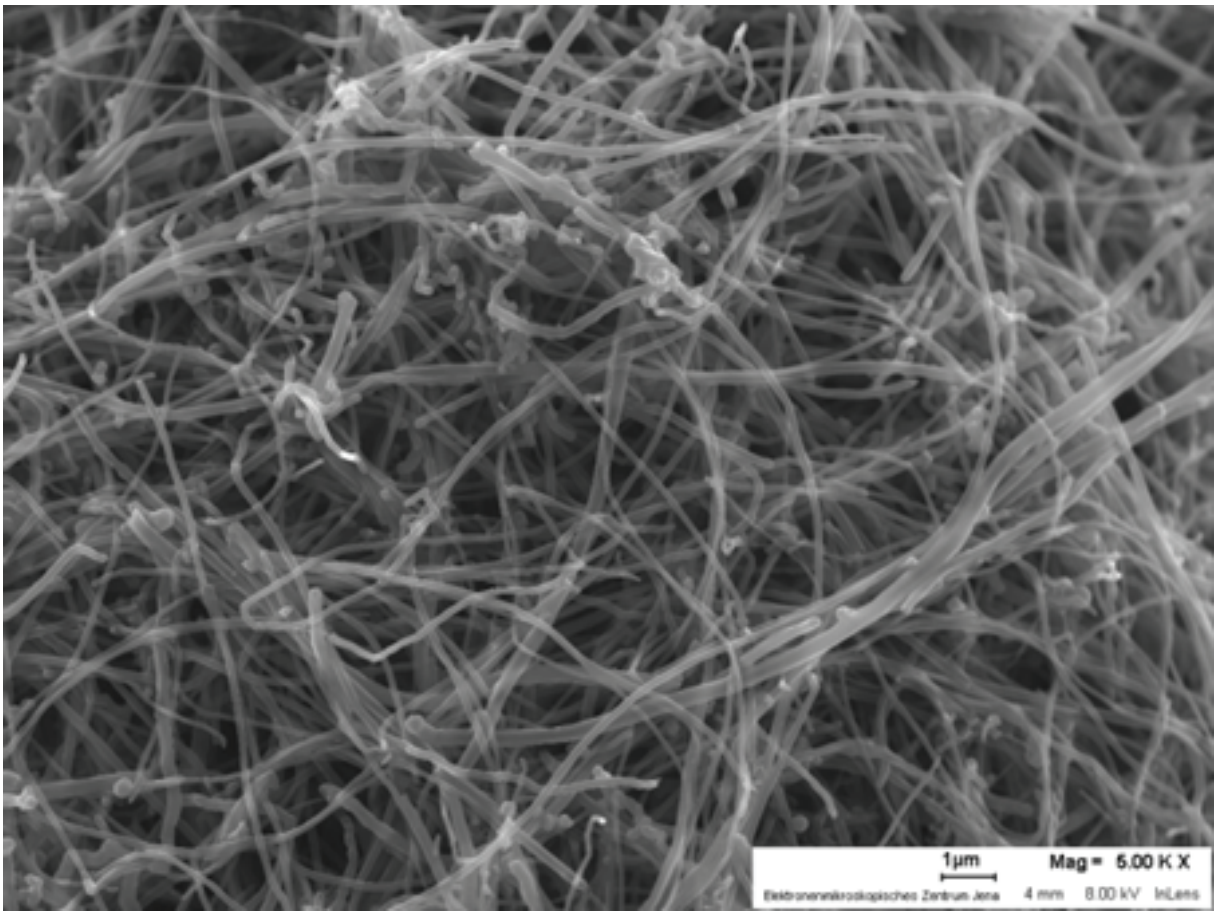

????????

Figure S5: SEM picture of a composite electrode (1/8/1 m/m/m) of **4**/VGCF/PVdF.

??

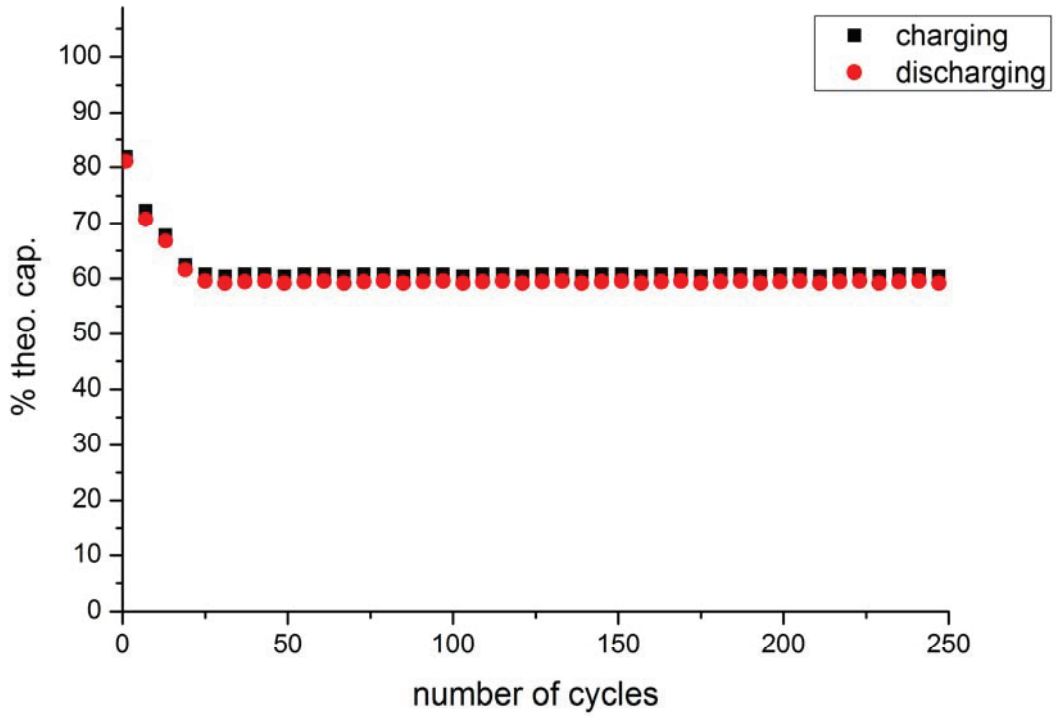

Figure S6: Capacity development during extended charge/discharge cycling (250 cycles) of a Li-organic battery with a composite electrode of **4**/VGCF/PVdF 20/70/10 m/m/m in 1,2-dimethoxyethane/propylene carbonate 4/1, 0.1 M $LiClO_4$ as active material.

Publication 4

"Synthesis and characterization of new redox-active polymers based on 10-(1,3-dithiol-2-ylidene)anthracen-9(10*H*)-one derivatives"

Daniel Schmidt, Bernhard Häupler, Christian Friebe, Martin D. Hager, Ulrich S. Schubert

Polymer **2015**, *68*, 321–327.

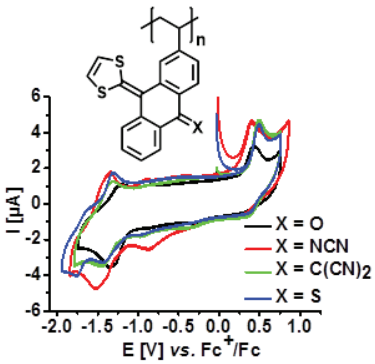

Polymer 68 (2015) 321–327

Contents lists available at ScienceDirect

Polymer

journal homepage: www.elsevier.com/locate/polymer

Synthesis and characterization of new redox-active polymers based on 10-(1,3-dithiol-2-ylidene)anthracen-9(10*H*)-one derivatives

Daniel Schmidt [a, b], Bernhard Häupler [a, b], Christian Friebe [a, b], Martin D. Hager [a, b], Ulrich S. Schubert [a, b, *]

[a] Laboratory of Organic and Macromolecular Chemistry (IOMC), Friedrich Schiller University Jena, Humboldtstr. 10, 07743 Jena, Germany
[b] Center for Energy and Environmental Chemistry Jena (CEEC Jena), Friedrich Schiller University Jena, Philosophenweg 7a, 07743 Jena, Germany

ARTICLE INFO

Article history:
Received 13 March 2015
Received in revised form
13 May 2015
Accepted 14 May 2015
Available online 21 May 2015

Keywords:
Electrochemistry
Redox polymers
Synthesis

ABSTRACT

Redox-active materials based on a 10-(1,3-dithiol-2-ylidene)anthracen-9(10*H*)one core were synthesized by the introduction of a polymerizable vinyl group in 3-position, resulting in a redox-active monomer, which possess both electron donating and electron accepting properties. The electron accepting properties can be tailored by straightforward one-step modifications of the carbonyl functionality to *N*-cyanoimine, dicyanomethylene or thione moieties, respectively, leading to bipolar compounds. These monomers can be polymerized by free radical polymerization. The resulting polymers could be obtained with molar masses of 6,500 to 24,300 g/mol as well as yields of up to 92% and were examined with ^{1}H NMR and SEC. Their electrochemical behavior reveals reversible reductions comparable with the redox properties of the corresponding monomers. After further optimization, these materials could become potentially interesting for applications in organic batteries.

1. Introduction

Organic redox-active compounds, in particular polymers, attracted increasing interest as active material in organic electronics like secondary batteries, semiconductors or organic metals during the last decades [1,2]. In contrast to inorganic structures, organic materials reveal several advantages such as high flexibility [3], low toxicity as well as low temperature synthesis from, in the best case, recycled [4] or renewable resources [5]. Additionally, the redox potential of organic compounds can be tuned by tailor-made structures using different redox-active systems, which are readily available due to the great diversity of organic chemistry [1,6].

Promising structures for electroactive materials in organic electronics are benzoquinonides bearing one or more 1,3-dithiol-2-ylidene moieties, which are oxidizable and, therefore, act as a good electron donors [7]. The most prominent examples are (π-extended) tetrathiafulvalenes (exTTF) having a two-electron oxidation [8]. This compound class possesses good electrical properties due to the extended π-electron delocalization. However, for several applications such as organic memory devices or organic batteries, bipolar materials that can be both reversibly oxidized and reduced are of high interest, as they can be applied as both anode and cathode active material in an organic battery, for example [9]. One promising approach towards these bipolar compounds is replacing one of the 1,3-dithiol-2-ylidene groups by an electron acceptor group. Only a limited number of these unsymmetrical structures have been described so far and none of these structures has a polymerizable group or has been integrated into a polymeric backbone [10–12]. The first compounds were developed by Gompper [13] and the anthraquinonide series was later studied by Bryce and Moore [12,14]. Additionally, other push–pull systems bearing 1,3-dithiol-2-ylidene structures have been described [15], which are stabilized by the aromatization of the benzoquinonide ring [12].

However, in several applications in organic electronics, the redox-active structure needs to be insoluble in the surrounding electrolyte, which normally consists of a salt dissolved in an organic solvent. The most promising approach to gain insolubility but redox activity is the incorporation of the redox-active unit into a polymeric backbone, resulting in an insoluble but swellable electroactive material.

In this contribution, we describe the synthesis and electrochemical characterization of new redox-active polymers based on

* Corresponding author. Laboratory of Organic and Macromolecular Chemistry (IOMC), Friedrich Schiller University Jena, Humboldtstr. 10, 07743 Jena, Germany.
E-mail address: ulrich.schubert@uni-jena.de (U.S. Schubert).

http://dx.doi.org/10.1016/j.polymer.2015.05.028
0032-3861/

the 9,10-anthracenediylidene core bearing a 1,3-dithiol-2-ylidene ring as electron donor unit and a ketone, *N*-cyanoimine, dicyanomethylene or thione groups as electron acceptor unit. The compounds were polymerized by free radical polymerization through the introduced vinyl group.

2. Experimental section

2.1. Materials

Tetrahydrofuran and toluene were dried with a PureSolv-EN™ Solvent Purification System (Innovative Technology). All other solvents were dried according to standard procedures.

All starting materials were purchased from commercial sources and were used as obtained unless otherwise noted. 2,2′-Azobis(*iso*-butyronitrile) (AIBN) was recrystallized from methanol prior to use. 3-Bromoanthracen-9(10*H*)-one (1) [16] and 2-methyl-1,3-dithiolium tetrafluoroborate [17] were synthesized according to literature procedures. Unless otherwise noted, all reactions were performed under inert argon atmosphere. Reactions were monitored by TLC on 0.2 mm Merck silica gel plates (60 F254). Column chromatography was performed on silica gel 60 (Merck). ^{1}H and ^{13}C NMR spectra were recorded on a Bruker AC 300 (300 MHz) spectrometer at 298 K. Chemical shifts are reported in parts per million (ppm, δ scale) relative to the residual signal of the deuterated solvent. Elemental analyses were carried out using a Vario ELIII–Elementar Euro and an EA–HekaTech. Infrared spectroscopy was performed using a Thermo Electron Nicolet FT-IR Avatar 370 DTGS. Cyclic voltammetry experiments were performed using a Biologic VMP 3 potentiostat at room temperature under argon atmosphere. A three-electrode setup was utilized (WE: glassy carbon, RE: $AgNO_3$/Ag in CH_3CN, CE: Pt). The redox couple Fc^+/Fc was used as internal standard after each measurement. UV-vis-NIR spectroelectrochemical experiments were carried out in a quartz cuvette containing the respective electrolyte solution, a platinum grid working electrode, a platinum wire auxiliary electrode, and a $AgNO_3$/Ag reference electrode. The potential was controlled using a Metrohm Autolab PGSTAT30 potentiostat. The redox process was monitored using a PerkinElmer Lambda 750 UV-vis spectrophotometer and considered complete when there was no further spectral change. Size-exclusion chromatography was performed on an Agilent 1200 series system (degasser: PSS, pump: G1310A, auto sampler: G1329A, oven: Techlab, DAD detector: G1315D, RI detector: G1362A, eluent: DMAc + 0.21% LiCl, 1 mL/min, temperature: 40 °C, column: PSS GRAM guard/1000/30 Å).

2.2. Monomer synthesis

2.2.1. 3-Bromo-10-(1,3-dithiol-2-ylidene)anthracen-9(10H)-one (2)

A flask was charged with 3-bromoanthracen-9(10*H*)-one (2.9 g, 10.6 mmol) and 2-methylthio-1,3-dithiolium tetrafluoroborate (12.96 g, 54.9 mmol). Acetic acid (130 mL), followed by pyridine (26 mL) were added and the mixture was stirred for 30 min at 120 °C. The solution was cooled to room temperature and the formed precipitate was filtered off. Subsequently, the solid was washed with water and dried to yield 3.1 g (8.3 mmol, 78%) as orange powder. ^{1}H NMR (300 MHz, CD_2Cl_2, δ): 8.21 (dd, $J = 8$ Hz, 1H, Ar H), 8.10 (m, 2H; Ar H), 7.99 (d, $J = 8$ Hz, 1H; Ar H), 7.70 (m, 1H, Ar H), 7.56 (dd, $J = 7$ Hz, 1H, Ar H), 7.45 (m, 1H, Ar H), 6.58 (s, 2H, SCH); ^{13}C NMR: Not possible due to the low solubility; EIMS *m*/*z* (%): 374 (100) [M^+ + 2], 372 (100) [M^+], 294 (5) [M^+–Br + H], 163 (14); HRMS (ESI) *m*/*z*: [M]$^+$ calcd for $C_{17}H_9BrOS_2$, 371.9273; found, 371.9278.

2.2.2. 3-Vinyl-10-(1,3-dithiol-2-ylidene)anthracen-9(10H)-one (3)

A closed flask was charged with 2 (0.75 g, 2.0 mmol), 4,4,5,5-tetramethyl-2-vinyl-1,3,2-dioxaborolane (0.40 g, 2.6 mmol), tetraoctylammonium bromide (0.22 g, 0.4 mmol), tetrakis (triphenylphosphine)palladium(0) (115 mg, 0.1 mmol, 5 mol%), potassium carbonate (0.83 g, 6 mmol), 2,6-di-*tert*-butyl-4-methylphenol (0.02 g, 0.1 mmol), toluene (9.7 mL), THF (7.5 mL) and water (3.9 mL). The mixture was purged with argon for 20 min and stirred for 15 h at 120 °C. Subsequently, the reaction mixture was cooled to room temperature and water was added. The mixture was extracted with dichloromethane (3 × 20 mL). All collected organic phases were washed with water (3 × 20 mL), dried over magnesium sulfate, filtered and the solvent was evaporated under reduced pressure. The crude product was purified by column chromatography (silica gel 60; dichloromethane) to obtain 0.50 g (1.6 mmol, 78%) as orange powder. ^{1}H NMR (300 MHz, CD_2Cl_2, δ): 8.20 (m, 2H, Ar H), 7.98 (m, 2H; Ar H), 7.68 (t, $J = 8$ Hz, 1H; Ar H), 7.45 (m, 2H, Ar H), 6.89 (m, 1H, CH vinyl), 6.54 (s, 2H, SCH), 5.98 (d, $J = 18$ Hz, 1H, CH_2 vinyl), 5.49 (d, $J = 11$ Hz, 1H, CH_2 vinyl); ^{13}C NMR (75 MHz, CD_2Cl_2, δ): 183.0 (C═O), 146.4, 141.2, 140.2, 139.7, 136.7, 132.1, 131.0, 130.2, 127.7, 127.2, 126.8, 126.5, 124.6, 124.3, 118.6, 118.5, 117.8, 117.3; EIMS *m*/*z* (%): 321 (100) [M^+ + H], 294 (64) [M^+ − CH═CH_2], 189 (100) [$C_{14}H_5O^+$]; HRMS (ESI) *m*/*z*: [2M + Na]$^+$ calcd for $C_{19}H_{12}OS_2$, 663.0551; found, 663.0528.

2.2.3. N-(3-vinyl-10-(1,3-dithiol-2-ylidene)-anthracen-9(10H)-ylidene)cyanamide (4)

3 (100 mg, 0.31 mmol) was dissolved in chloroform (15 mL). Titanium(IV) chloride (0.12 mL, 1.1 mmol) followed by *bis* (trimethylsilyl)carbodiimide (0.21 mL, 0.9 mmol) was added and the mixture was stirred under reflux for 96 h with periodic addition of additional *bis*(trimethylsilyl)carbodiimide (2.5 mL, 11.0 mmol). The reaction mixture was allowed to cool to room temperature and water (10 mL) was added. Subsequently, the mixture was extracted with dichloromethane (3 × 25 mL). The combined organic phases were washed with water (3 × 25 mL), dried over magnesium sulfate, filtered and the solvent was removed under reduced pressure. The crude product was purified by column chromatography (silica gel 60; dichloromethane:*n*-hexane, 2:1) to obtain 24 mg (0.07 mmol, 22%) of a purple solid. ^{1}H NMR (300 MHz, CD_2Cl_2, δ): 8.99 to 8.12 (br, 1H, Ar H), 8.12 to 7.76 (br, 2H; Ar H), 7.70 (m, 1H; Ar H), 7.57 to 7.09 (br, 3H, Ar H), 6.88 (m, 1H, CH vinyl), 6.60 (s, 2H, SCH), 6.01 (d, $J = 18$ Hz, 1H, CH_2 vinyl), 5.53 (d, $J = 11$ Hz, 1H, CH_2 vinyl); ^{13}C NMR: Not possible due to low solubility; EIMS *m*/*z* (%): 344 (100) [M^+], 317 (18) [$M^+ - C_2H_3$], 291 (5) [$M^+ - C_2H_3CN$]. 214 (18), 189 (5) [M+ − C_2H_3CN − $C_2H_3S_2$]; HRMS (ESI) *m*/*z*: [M + Na]$^+$ calcd for $C_{20}H_{12}N_2S_2$, 367.0334; found, 367.0320.

2.2.4. 2-(3-Vinyl-10-(1,3-dithiol-2-ylidene)anthracen-9(10H)-ylidene)malononitrile (5)

Compound 3 (300 mg, 0.94 mmol), malononitrile (620 mg, 9.4 mmol) and aluminum(III) chloride (620 mg, 4.68 mmol) were dissolved in chloroform (20 mL) and then pyridine (0.25 mL, 3.12 mmol) was added. The reaction mixture was stirred at 80 °C for 5 h. Subsequently, titanium(IV) chloride (0.5 mL, 4.7 mmol) was added and the mixture was heated to 80 °C for 15 h. The reaction mixture was cooled to room temperature and water was added. Subsequently, the mixture was extracted with dichloromethane (3 × 25 mL) and the organic phase was dried over magnesium sulfate and filtered. The solvent was removed under reduced pressure and the crude product was purified by column chromatography (silica gel 60; dichloromethane) to obtain 340 mg (0.92 mmol, 98%) of the purple solid. ^{1}H NMR (300 MHz, CD_2Cl_2, δ): 8.11 (t, $J = 8$ Hz, 2H, Ar H), 7.99 (m, 2H; Ar H), 7.61 (t, $J = 8$ Hz, 1H; Ar H), 7.43 (m, 2H, Ar H), 6.84 (m, 1H, CH vinyl), 6.56 (s, 2H, SCH), 5.96

(d, $J = 18$ Hz, 1H, CH_2 vinyl), 5.48 (d, $J = 11$ Hz, 1H, CH_2 vinyl); ^{13}C NMR (75 MHz, CD_2Cl_2, δ): 162.2 (C=O), 146.4, 141.0, 136.7, 136.2, 136.2, 131.7, 127.2, 126.8, 126.7, 125.8, 124.5, 123.4, 118.8, 118.7, 118.3, 117.7, 115.5, 77.3; EIMS m/z (%): 368 (100) [M^+], 342 (12) [$M^+ - CH{=}CH_2 + H$], 305 (4) [$M+ - C(CN)_2 + H$], 265 (23) [$M - C_3H_3S_2$]; HRMS (ESI) m/z: [$M + H]^+$ calcd for $C_{22}H_{12}N_2S_2$, 369.0515; found, 369.0502.

2.2.5. 3-Vinyl-10-(1,3-dithiol-2-ylidene)anthracen-9(10H)-thione (6)

A flask was charged with 3 (100 mg, 0.31 mmol), Lawesson's reagent (189 mg, 0.47 mmol) and toluene (20 mL). The reaction mixture was stirred at 80 °C for 2 h. The mixture was cooled to room temperature and passed through a silica gel plug. The solvent was removed under reduced pressure and the crude product was purified by column chromatography (silica gel 60; dichloromethane:*n*-hexane, 1:1) to obtain 84 mg (0.25 mmol, 80%) of the blue/violet solid. ^1H NMR (300 MHz, CD_2Cl_2, δ): 8.54 (t, $J = 12$ Hz, 2H, Ar H), 7.96 (m, 2H; Ar H), 7.69 (m, 1H; Ar H), 7.39 (m, 2H, Ar H), 6.87 (m, 1H, CH vinyl), 6.59 (s, 2H, SCH), 6.00 (d, $J = 18$ Hz, 1H, CH_2 vinyl), 5.51 (d, $J = 11$ Hz, 1H, CH_2 vinyl); ^{13}C NMR (75 MHz, CD_2Cl_2, δ): 215.3 (C=O), 147.6, 140.9, 238.9, 238.3, 136.7, 136.1, 134.0, 133.5, 131.8, 129.9, 129.3, 127.0, 125.7, 124.7, 123.5, 119.4, 119.2, 117.4; EIMS m/z (%): 336 (100) [M^+], 277 (10) [$M^+ - C_2H_3S$], 234 (9) [$M^+ - C_3H_2S_2^+$]; HRMS (ESI) m/z: [$M + H]^+$ calcd for $C_{19}H_{12}S_3$, 336.0095; found, 336.0085.

2.3. Polymer synthesis

2.3.1. General procedure of polymerization

A flask was charged with the monomer, the initiator and a solvent. The reaction mixture was purged with argon for 15 min and heated for 21 h. Subsequently, the mixture was allowed to cool to room temperature and the polymer was precipitated in acetone. The product was purified by reprecipitation from dichloromethane into methanol.

2.3.2. Poly[3-vinyl-10-(1,3-dithiol-2-ylidene)anthracen-9(10H)-one] (P1)

From monomer 3 (50 mg, 0.16 mmol), AIBN (1.28 mg, 7.8 μmol, 5 mol%) and 1,2-dichloroethane (0.6 mL) at 70 °C. Polymer P1 was obtained as dark orange solid (30 mg, 60%). ^1H NMR (300 MHz, DMF-d7, δ): 7.96 to 5.68 (br, 9H, Ar H), 2.31 to 0.64 (br, 3H).

2.3.3. Poly[3-vinyl-10-(1,3-dithiol-2-ylidene)anthracen-9(10H)-one] (P2)

From monomer 3 (50 mg, 0.16 mmol), AIBN (1.28 mg, 7.8 μmol, 5 mol%) and NMP (0.16 mL) at 70 °C. Polymer P2 was obtained as dark orange solid (46 mg, 92%). ^1H NMR (300 MHz, DMF-d7, δ): 7.94 to 5.68 (br, 9H, Ar H), 2.32 to 0.66 (br, 3H).

2.3.4. Poly[3-vinyl-10-(1,3-dithiol-2-ylidene)anthracen-9(10H)-one] (P3)

From monomer 3 (50 mg, 0.16 mmol), AIBN (1.28 mg, 7.8 μmol, 5 mol%) and DMSO (0.5 mL) at 70 °C. Polymer P3 was obtained as dark orange solid (49 mg, 98%). ^1H NMR (300 MHz, DMF-d7, δ): 7.95 to 5.69 (br, 9H, Ar H), 2.30 to 0.65 (br, 3H).

2.3.5. Poly[N-(3-vinyl-10-(1,3-dithiol-2-ylidene)-anthracen-9(10H)-ylidene)cyanamide] (P4)

From monomer 4 (22 mg, 0.06 mmol), AIBN (0.52 mg, 3.2 μmol, 5 mol%) and DMSO (0.4 mL) at 70 °C. Polymer P4 was obtained as dark purple solid (8 mg, 36%). ^1H NMR (300 MHz, DMF-d7, δ): 7.98 to 5.49 (br, 9H, Ar H), 2.47 to 1.65 (br, 3H).

2.3.6. Poly[2-(3-vinyl-10-(1,3-dithiol-2-ylidene)anthracen-9(10H)-ylidene)malononitrile] (P5)

From monomer 5 (30 mg, 0.08 mmol), 5.5 M solution of *tert*-butyl hydroperoxide in decane (0.75 μL, 4.1 μmol, 5 mol%) and DMSO (0.22 mL) at 130 °C. Polymer P5 was obtained as dark purple solid (20 mg, 67%). ^1H NMR (300 MHz, DMF-d7, δ): 7.97 to 5.53 (br, 9H, Ar H), 2.51 to 1.40 (br, 3H).

2.3.7. Poly[3-vinyl-10-(1,3-dithiol-2-ylidene)anthracen-9(10H)-thione] (P6)

From monomer 6 (60 mg, 0.18 mmol), AIBN (1.46 mg, 8.9 μmol, 5 mol%) and DMSO (0.2 mL) at 70 °C. Polymer P6 was obtained as dark blue solid (35 mg, 58%). ^1H NMR (300 MHz, DMF-d7, δ): 7.93 to 5.43 (br, 9H, Ar H), 2.51 to 1.20 (br, 3H).

3. Results and discussion

3.1. Synthesis of the monomers

The monomer synthesis is depicted in Scheme 1 and started from 3-bromoanthracen-9(10*H*)-one (1). The bromine substituent and later the polymerizable group is introduced in 3-position to avoid steric hindrance during the polymerization. 1 was synthesized in a three-step synthetic route [16], because a direct bromination of the 9(10*H*)-anthracenone at 3-position led to a mixture of multibrominated compounds. To introduce the 1,3-dithio-2-ylidene group, 1 and 2-methylthio-1,3-dithiolium tetrafluoroborate were dissolved in a mixture of acetic acid and pyridine (5:1) and heated for 30 min. A higher ratio of pyridine results in longer reaction times and side products are formed. The product 2 could be obtained in high purity after precipitation and was used for the next reaction step without any further purification. Due to the bromine substituent, different polymerizable groups such as acetylene, norbornene or vinyl can be introduced by Pd-catalyzed C–C cross coupling reactions. The vinyl group was selected to obtain a styrene derivative, which can be polymerized by straightforward free radical polymerization techniques. It was introduced by a Pd-catalyzed Suzuki cross coupling reaction, which yields monomer 3. Subsequently, three different derivatives were synthesized utilizing a one-step modification of the carbonyl group of 3. The substituents are in detail *N*-cyanoimine, dicyanomethylene as well as thione and possess different electron acceptor strengths, which influences the redox potentials. Therefore, the electrochemical behavior of this substance class can be tuned to obtain tailored properties for specific applications. The *N*-cyanoimine group of monomer 4 was achieved by the reaction of 3 with titanium(IV) chloride and *bis*(trimethylsilyl)carbodiimide in moderate yields. Monomer 5 was obtained by a Knoevenagel condensation using malononitrile and pyridine as base. Aluminum chloride as well as titanium(IV) chloride was used as Lewis acid and the product could be obtained in a very high yield (98%). The thione group of monomer 6 was introduced by the utilization of Lawesson's reagent. The product was achieved after a reaction time of 2 h with a yield of 80%.

3.2. Synthesis of the polymers

All resulting monomers were polymerized using the free radical polymerization technique with 2,2′-azo*bis*(2-methylpropionitrile) (AIBN) or *tert*-butyl hydroperoxide as initiator (Scheme 2). The analytical data of the polymers are summarized in Table 1. The polymerization of 3 could be performed in a limited range of solvents (*i.e.* 1,2-dichloroethane, *N*-methyl-2-pyrrolidone (NMP) or dimethylsulfoxide (DMSO)) due to the limited solubility of 3. The best results were obtained for P3 in DMSO with a molar mass of

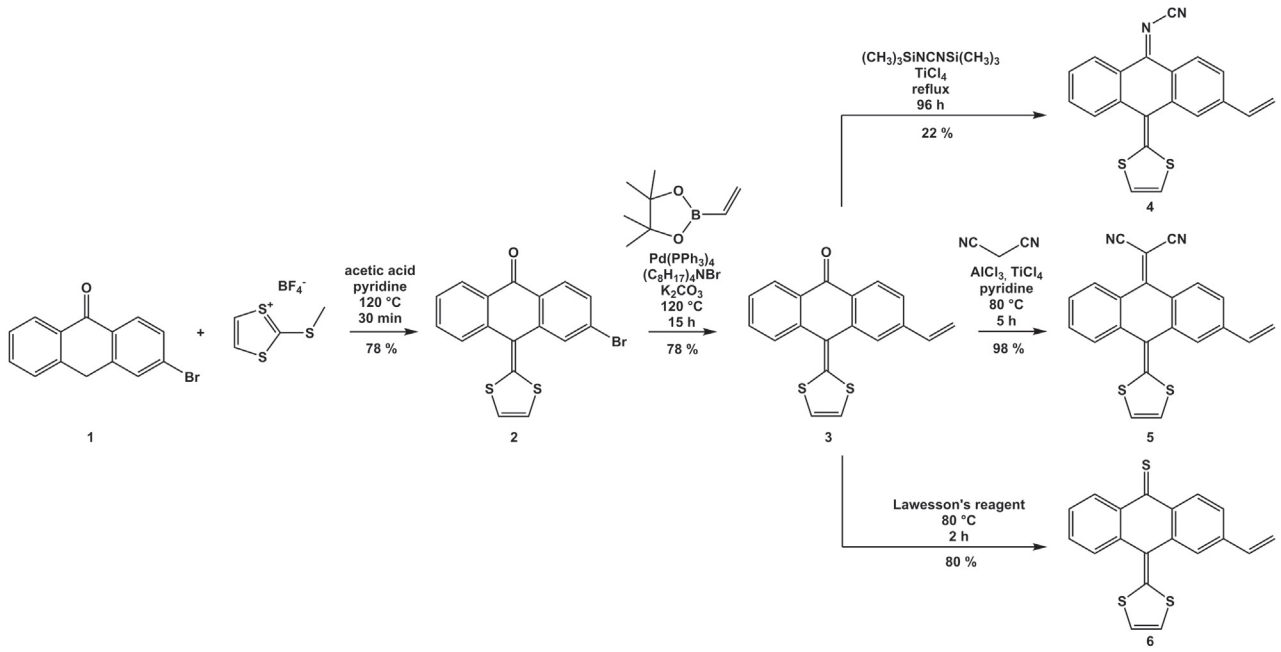

Scheme 1. Schematic representation of the synthesis of the monomers 3 to 6.

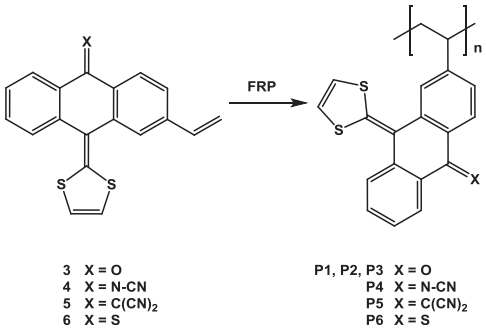

Scheme 2. Schematic representation of the synthesis of the polymers P1 to P6.

M_n = 15,600 g/mol, a PDI value of 2.7 and 92% yield. Chlorinated solvents such as 1,2-dichloroethane led to chain-terminating reactions resulting in a lower yield (60%) and larger PDI value (3.0). As a consequence, all other polymerization reactions were performed in DMSO as the monomers 4, 5 and 6 reveal similar solubility properties. Polymer P6 could be obtained with a 58% yield and a high molar mass (M_n) of 24,300 g/mol (PDI = 1.7) using 5 mol% AIBN as initiator. The molar mass and the yield of P4 were comparably low (M_n = 6,500 g/mol, PDI = 1.3, 36%), possibly due to steric hindrance of the specious redox unit during the chain-growth reaction. The polymerization of monomer 5, which is sterically more demanding, was initiated with AIBN at 70 °C and led only to oligomers with a very low yield. As a consequence for a successful polymerization of 5, the reaction temperature was increased to 130 °C and *tert*-butyl hydroperoxide was chosen as suitable initiator. Polymer P5 could be obtained with a high molar mass (M_n = 23,400 g/mol, PDI = 1.7) and acceptable yield (58%). All polymers were investigated by SEC and revealed a distinct monodisperse distribution (Fig. 1). Furthermore, all polymers were analyzed by FT-IR spectroscopy. Comparison of the spectra of the polymers and the corresponding monomers (Fig. S1) revealed no significant changes. This indicates that no side reactions took place during the polymer synthesis and the functional moieties are attached to the polymer backbone.

3.3. Electrochemistry

The electrochemical behavior of all monomers was investigated by cyclic voltammetry using a solution of 0.1 M tetra-*N*-butylammonium perchlorate ($TBAClO_4$) in acetonitrile as electrolyte. The results are summarized in Table 2. All monomers, except monomer 4, show a reversible redox process attributed to the oxidation of the 1,3-dithiol-2-ylidene moiety forming a radical cation in the range of 0.39 and 0.49 V *vs.* Fc^+/Fc (Fig. 2).

The reduction of monomer 3 occurs at the most negative redox potential, due to its poor electron accepting properties. It reveals a reversible one-electron redox reaction at −1.84 V *vs.* Fc^+/Fc, which is in good agreement with literature reports [11]. However, compared to anthraquinone, its acceptor ability is decreased [18].

Table 1
Selected analytical data of the polymers prepared by free radical polymerization.

Polymer	Monomer	Initiator	Solvent	M_n[a] [g/mol]	M_w[a] [g/mol]	PDI[a]	Yield [%]
P1	3	AIBN	1,2-Dichloroethane	19,000	56,000	3.0	60
P2	3	AIBN	NMP	10,500	23,900	2.3	92
P3	3	AIBN	DMSO	15,600	42,800	2.7	92
P4	4	AIBN	DMSO	6,500	8,600	1.3	36
P5	5	^{t}BuOOH	DMSO	23,400	40,700	1.7	67
P6	6	AIBN	DMSO	24,300	40,800	1.7	58

[a] Determined by SEC (DMAc, 0.21% LiCl, PS standard, RI detector).

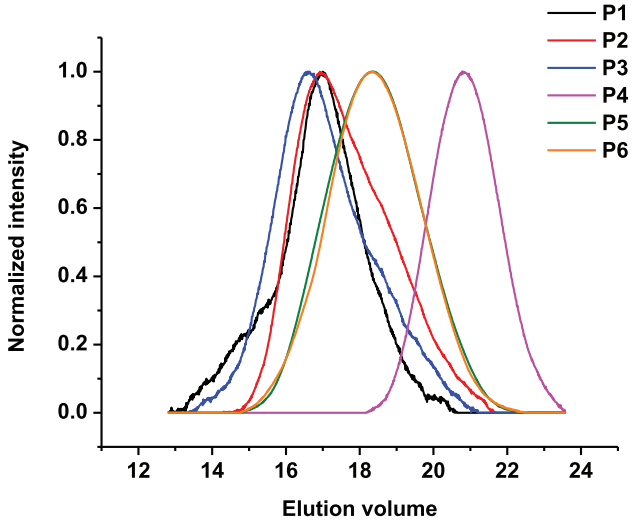

Fig. 1. Size-exclusion chromatogram of the polymers. Eluent: DMAc, 0.21% LiCl, polystyrene (PS) standard, RI detector.

Table 2
Cyclic voltammetric data for monomers 3 to 6 and for polymers P3 to P6.

Compound	E_{ox} [V]	E_{red} [V]
3	0.39	−1.84
4	0.32[a]	−1.45
5	0.49	−1.33; −1.66
6	0.49	−1.33; −1.64
P3	0.44[a]	−1.31
P4	0.37[a]	−1.43
P5	0.43[a]	−1.39
P6	0.44[a]	−1.37; −1.70

[a] Irreversible.

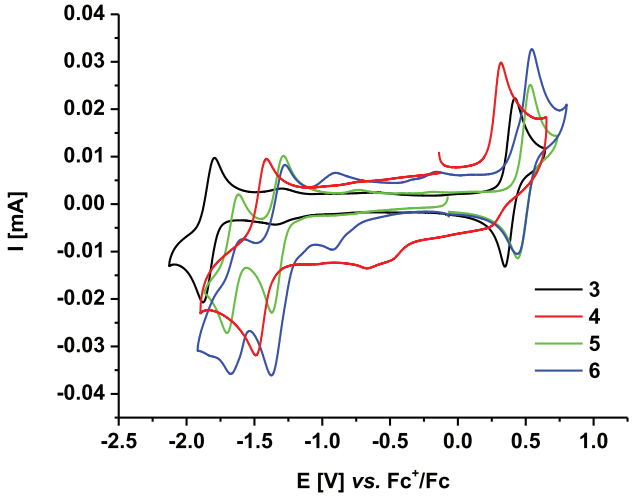

Fig. 2. Cyclic voltammograms of the monomers in acetonitrile, 0.1 M $TBAClO_4$ at a scan rate of 250 mV/s, c(monomer) = 1 mg/mL, 1st cycle.

The electron acceptance of the *N*-cyanoimine functionality is higher compared to the keto group and, therefore, the reduction of monomer 4 to the radical anion occurs at higher potential (−1.45 V *vs.* Fc^+/Fc), which is in line with recent results from Batsanov et al. [12]. In contrast to their findings, the oxidation of monomer 4 (0.32 V *vs.* Fc^+/Fc) revealed to be partly irreversible and an additional irreversible signal occurs at −0.57 V *vs.* Fc^+/Fc, indicating presumably a side reaction of the formed radical cation. The malononitrile group of monomer 5 and the thione group of monomer 6 are even better electron acceptors resulting in a higher reduction potential of −1.33 V *vs.* Fc^+/Fc. The results are conform to recent literature examples [19]. Furthermore, a second one-electron reduction step occurs at around −1.65 V *vs.* Fc^+/Fc, corresponding presumably to the reduction of the aromatic skeleton, which is comparable with the results from literature and similar to the reduction potential of anthracene [11].

The low solubility of the polymers P3 to P6 in acetonitrile directed us to investigate their electrochemical behavior in DMF-based electrolytes (0.1 M $TBAClO_4$); this behavior is surprisingly different compared to the monomers (Fig. 3). All polymers feature an irreversible oxidation process at ca. 0.4 V *vs.* Fc^+/Fc. indicating a side reaction of the formed radical cation. The reduction processes of the polymers are all reversible and depend, similarly to those of the monomers, on the substitution pattern of the acceptor moiety. In detail, the reduction of polymer P3 occurs at a potential of −1.31 V *vs.* Fc^+/Fc, which is shifted to higher potential compared to the reduction potential of the corresponding monomer (Fig. 3a). Similar findings are presented in literature [20]. Another reduction reaction occurs at the edge of the electrochemical stability of the DMF-based electrolyte (−2.1 V *vs.* Fc^+/Fc), which is most likely attributed to the reduction of the aromatic anthracene core of the monomer unit. In contrast, the electrochemical behavior of P4 is in good agreement with monomer 4: A one-electron reduction at −1.43 V *vs.* Fc^+/Fc and an irreversible oxidation at 0.37 V *vs.* Fc^+/Fc, indicating that the polymeric backbone has only a negligible influence on the electron-accepting redox behavior (Fig. 3b). These findings are in line with the electrochemical behavior of P5 and P6. The reductions of P5 are slightly shifted to lower potentials. The reduction of the dicyanomethylene group occurs at −1.39 V *vs.* Fc^+/Fc while the reduction of the aromatic system occurs most probably outside of the stability window of the used electrolyte (Fig. 3c). Similar to monomer 6, the electrochemical behavior of P6 reveals two one-electron reductions at −1.37 and −1.70 V *vs.* Fc^+/Fc, which can be assigned to the reduction of the thione functionality and the aromatic system, respectively, to the corresponding anions (Fig. 3d). Additionally, UV-vis-NIR spectroelectrochemical studies on the polymers were performed. The oxidation process of P3 revealed to be nearly reversible. During the oxidation, the absorption at 470 and 360 nm decreases; after re-reduction of the compound the original spectrum is restored almost completely. The reduction process shows no significant change in the UV-vis-NIR spectrum (Fig. S10). The oxidation of P4 reveals an irreversible redox behavior. The absorption band at 550 nm decreases significantly during oxidation and the initial spectrum could not be restored after re-reduction. The reduction reveals a shift of the absorption band at 550 nm to lower wavelengths and the rise of a second absorption at 360 nm after; the re-oxidation showed a nearly reversible redox behavior (Fig. S11). During the oxidation of P5, the absorption intensity at 550 nm decreases and the absorption band at 350 nm shows a slight, hypsochromic shift; the original spectrum could be observed after re-reduction. The reduction of the polymer reveals also a decrease of the absorption bands at 550 and 340 nm, while a third band is formed at 420 nm. Isosbestic points are present at 396 and 500 nm, indicating the presence of only two species. The re-oxidation reveals closely the original spectrum (Fig. S12). During the oxidation of P6, the absorption band at 550 nm decreases, while the absorption band at 340 nm increases significantly; the initial spectrum could not be restored after re-reduction of the polymer. During reduction, the absorption bands at 550 and 340 nm decrease and the original spectrum is not restored after re-oxidation. During the second reduction, the absorption at 550 and 340 nm decreases further and the absorption

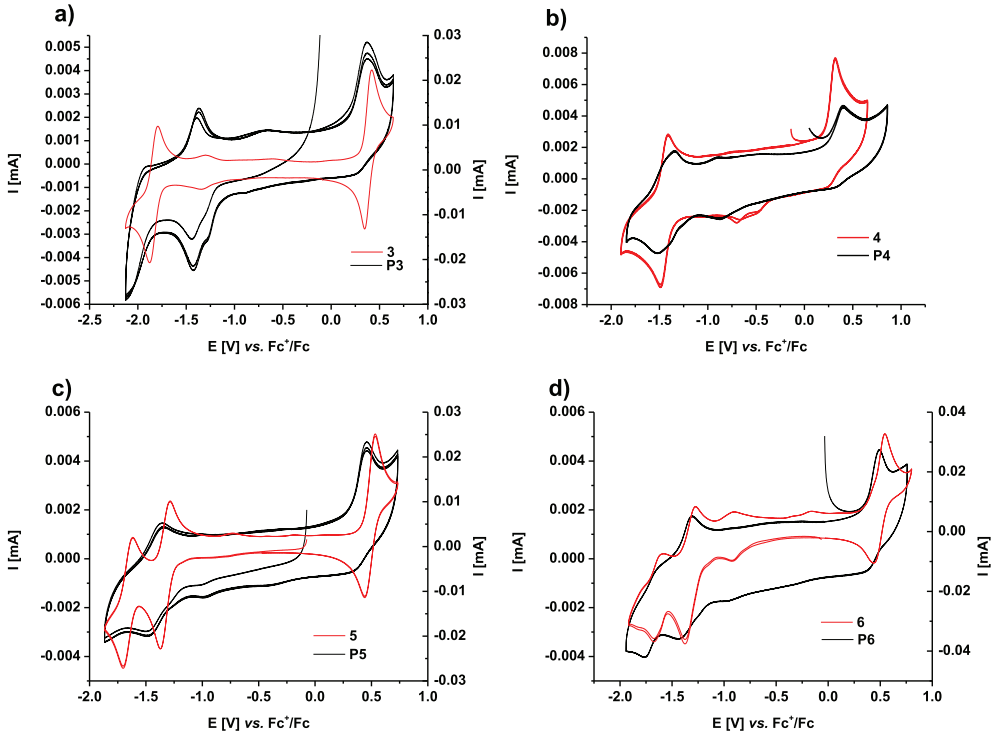

Fig. 3. Cyclic voltammograms of the polymers P3 (a), P4 (b), P5 (c) and P6 (d) (black line) compared with the corresponding monomer 3 (a), 4 (b), 5 (c) and 6 (d) (red line) in DMF (polymers) and acetonitrile (monomers), 0.1 M $TBAClO_4$ at 250 mV/s, c(polymer) = 0.5 mg/mL, c(monomer) = 1 mg/mL, cycle 1 to 3. (For interpretation of the references to color in this figure legend, the reader is referred to the web version of this article.)

band at 550 nm is shifted to lower wavelengths (Fig. S13). These findings suggest that the radical ions, formed by oxidation/reduction, undergo a side reaction such as dimerization or irreversible intermolecular sulfur–sulfur bond formation between neighbored 1,3-dithiol-2-ylidene units during the oxidation [21].

4. Conclusions

In summary, a synthetic route towards redox-active bipolar monomers based on the 10-(1,3-dithiol-2-ylidene)anthracen-9(10*H*)one was developed. The polymerizable group can be altered as desired and is introduced in a straightforward manner *via* Pd-catalyzed cross coupling reactions. In this particular case, a vinyl group was applied, which can by polymerized by the free radical polymerization technique. The electron donating behavior of the monomers relies on the 1,3-dithiol-2-ylidene group, which is able to undergo a reversible one-electron redox reaction at around 0.4 V *vs.* Fc^+/Fc. The redox potential of the reduction can be tailored in a broad range (−1.33 to −1.84 V *vs.* Fc^+/Fc) by straightforward one-step modifications of the carbonyl functionality of the 10-(1,3-dithiol-2-ylidene)anthracen-9(10*H*)one to *N*-cyanoimine, dicyanomethylene or thione enabling bipolar materials with a potential gap in the range of 1.8 to 2.2 V *vs.* Fc^+/Fc. These monomers were polymerized through the vinyl group applying the free radical polymerization technique, leading to redox-active materials with average molar masses in the range of 6,500 to 24,300 g/mol. The reduction processes of these materials are still reversible in solution as shown by cyclic voltammetry. However, limited reversibility is revealed, in particular after oxidation of the 1,3-dithiol-2-ylidene moiety, indicating a side reaction most probably with neighboring redox-active units in the polymeric environment. UV-vis-NIR spectroelectrochemistry measurements reveal partly stable redox process of the polymers. However, the results reflect only the redox behavior of the polymers in solution and can be different in the solid state, *e.g.*, as electrode material. The future plans imply the introduction of a more spacious polymerizable group, such as norbornene, leading to less dense polymer structures and fewer interactions between the redox-active units.

Acknowledgments

The authors thank the European Social Fund (ESF, 2011 FGR 0088), the Thüringer Aufbaubank (TAB) and the Thuringian Ministry of Economy, Science and Digital Society (TMWWdG) for the financial support.

Appendix A. Supplementary data

Supplementary data related to this article can be found at http://dx.doi.org/10.1016/j.polymer.2015.05.028.

References

[1] Liang Y, Tao Z, Chen J. Adv. Energy Mater. 2012;2:742.
[2] Song Z, Zhou H. Energy Environ. Sci. 2013;6:2280.
[3] Nishide H, Oyaizu K. Science 2008;319:737.
[4] Armand M, Grugeon S, Vezin H, Laruelle S, Ribière P, Poizot P, Tarascon J-M. Nat. Mater. 2009;8:120.
[5] Poizot P, Dolhem F. Energy Environ. Sci. 2011;4:2003.
[6] a) Morita Y, Nishida S, Murata T, Moriguchi M, Ueda A, Satoh M, Arifuku K, Sato K, Takui T. Nat. Mater. 2011;10:947.
b) Janoschka T, Hager MD, Schubert US. Adv. Mater. 2012;24:6397.
[7] a) Wang C, Bryce MR, Batsanov AS, Howard JAK. Chem. Eur. J. 1997;3:1679.
b) Vilela F, Skabara PJ, Mason CR, Westgate TDJ, Luquin A, Coles SJ, Hursthouse MB. Beilstein J. Org. Chem. 2010;6:1002.
c) Fernández G, Pérez EM, Sánchez L, Martín N. J. Am. Chem. Soc. 2008;130:2410.
[8] a) Häupler B, Burges R, Friebe C, Janoschka T, Schmidt D, Wild A, Schubert US. Macromol. Rapid Commun. 2014;35:1367.
b) Kato M, Senoo K-i, Yao M, Misaki Y. J. Mater. Chem. A 2014;2:6747.

c) Bryce MR, Murphy LC. Nature 1984;309:119.
d) Brunetti FG, López JL, Atienza C, Martín N. J. Mater. Chem. 2012;22:4188.
[9] Sukegawa T, Kai A, Oyaizu K, Nishide H. Macromolecules 2013;46:1361.
[10] Schaumann E, Winter-Extra S, Kummert K, Scheiblich S. Synthesis 1990:271.
[11] Bryce MR, Chinarro E, Green A, Martín N, Moore AJ, Sánchez L, Seoane C. Synthetic Met. 1997;86:1857.
[12] Batsanov AS, Bryce MR, Coffin MA, Green A, Hester RE, Howard JAK, Lednev IK, Martín N, Moore AJ, Moore JN, Ortí E, Sánchez L, Savirón M, Viruela PM, Viruela R, Ye T-Q. Chem. Eur. J. 1998;4:2580.
[13] Gompper R, Wagner H-U, Kutter E. Chem. Ber. 1968;101:4123.
[14] Moore AJ, Bryce MR. J. Chem. Soc., Perkin Trans. 1 1991:157.
[15] a) Inoue S, Aso Y, Otsubo T. Chem. Commun. 1997:1105.
b) Andreu R, Blesa MJ, Carrasquer L, Garín J, Orduna J, Villacampa B, Alcalá R, Casado J, Ruiz Delgado MC, López Navarrete JT, Allain M. J. Am. Chem. Soc. 2005;127:8835.
[16] Itoh T, Matsuno M, Kamiya E, Hirai K, Tomioka H. J. Am. Chem. Soc. 2005;127:7078.
[17] Khodorkovskii VY, Bite DV, Petrova MV, Neiland OY. Chem. Heterocycl. Compd. 1984;20:574.
[18] Yamamoto T, Etori H. Macromolecules 1995;28:3371.
[19] a) Häupler B, Burges R, Janoschka T, Jähnert T, Wild A, Schubert US. J. Mater. Chem. A 2014;2:8999.
b) Iordache A, Maurel V, Mouesca J-M, Pécaut J, Dubois L, Gutel T. J. Power Sources 2014;267:553.
[20] Zon A, Palys M, Stojek Z, Sulowska H, Ossowski T. Electroanalysis 2003;15:579.
[21] a) de Sorgo M, Wasserman B, Szwarc M. J. Phys. Chem. 1972;76:3468.
b) Musker WK. Acc. Chem. Res. 1980;13:200.
c) Priego EM, Sánchez L, Herranz MA, Martín N, Viruela R, Ortí E. Org. Biomol. Chem. 2007;5:1201.

Supporting Information

Synthesis and characterization of new redox-active polymers based on 10-(1,3-dithiol-2-ylidene)anthracen-9(10*H*)-one derivatives

D. Schmidt, B. Häupler, C. Friebe, M. D. Hager, U. S. Schubert*

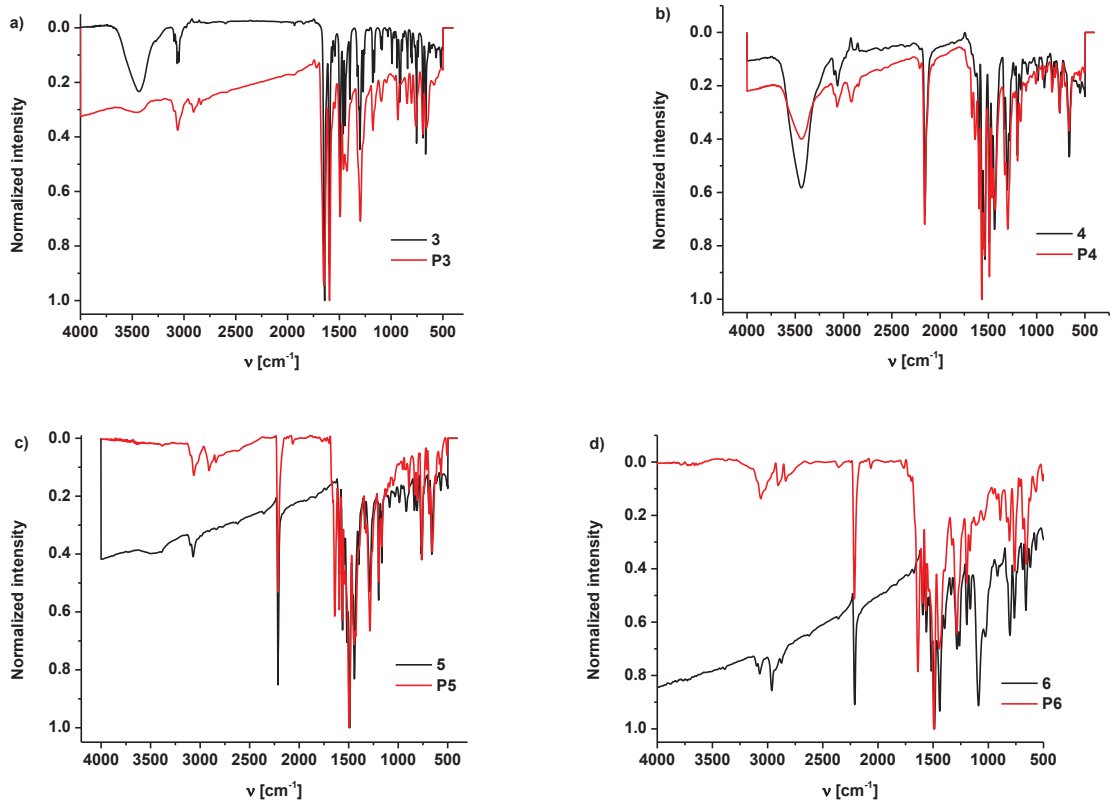

Figure S1. IR spectra of a) **3** and **P3**, b) **4** and **P4**, c) **5** and **P5** and d) **6** and **P6**.

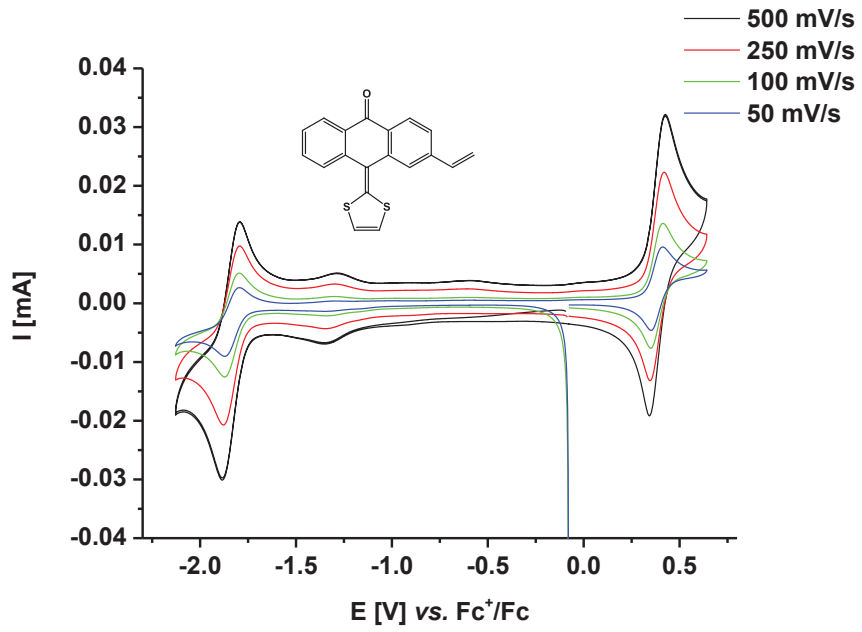

Figure S2. Cyclic voltammograms of monomer **3** in acetonitrile, 0.1 M $TBAClO_4$ at different scan rates (WE: GC; RE: $AgNO_3$/Ag, in CH_3CN; CE: Pt), c = 1 mg/mL, 1st and 2nd cycle.

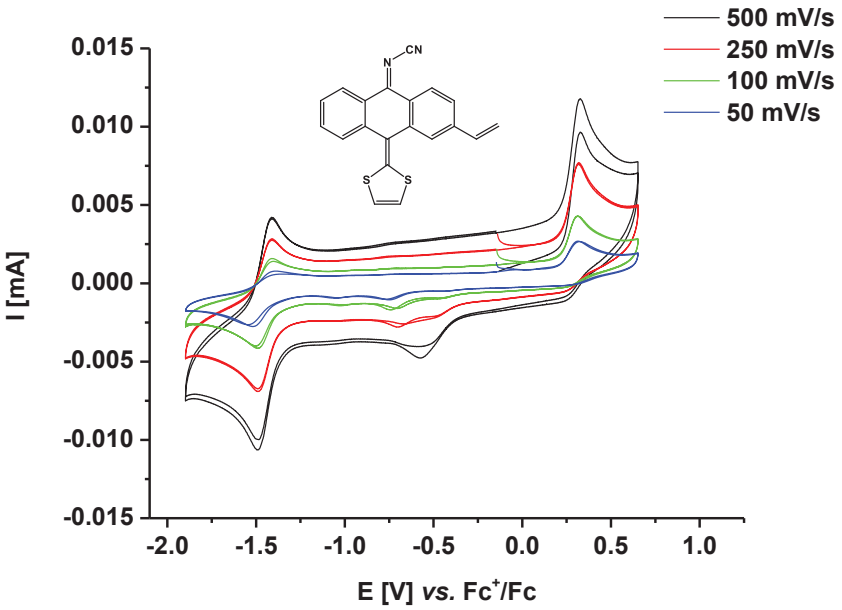

Figure S3. Cyclic voltammograms of monomer **4** in acetonitrile, 0.1 M $TBAClO_4$ at different scan rates (WE: GC; RE: $AgNO_3$/Ag, in CH_3CN; CE: Pt) , c = 1 mg/mL, 1st and 2nd cycle.

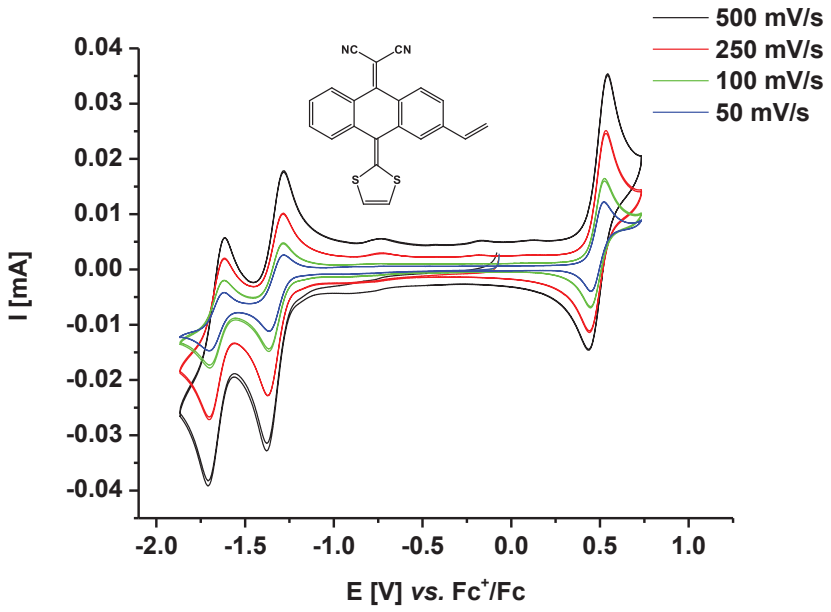

Figure S4. Cyclic voltammograms of monomer **5** in acetonitrile, 0.1 M $TBAClO_4$ at different scan rates (WE: GC; RE: $AgNO_3$/Ag, in CH_3CN; CE: Pt) , c = 1 mg/mL, 1st and 2nd cycle.

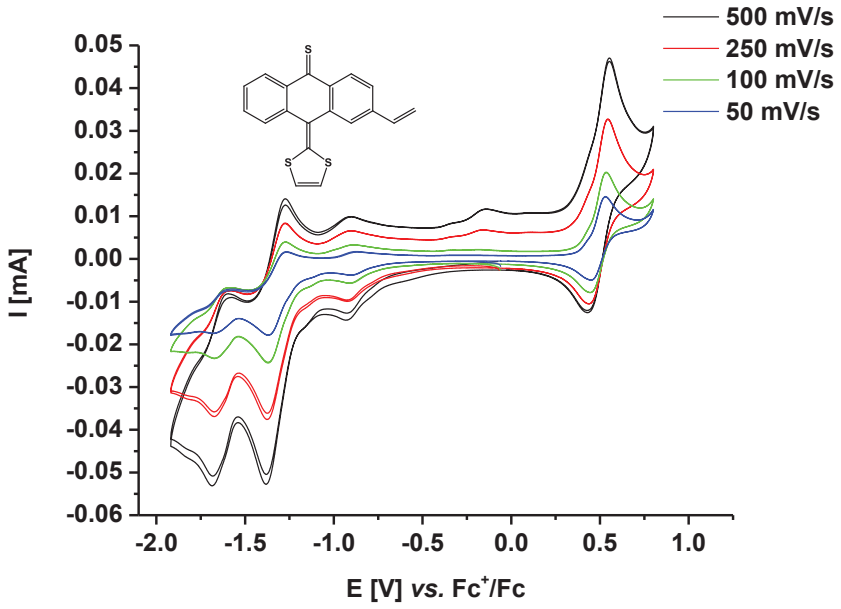

Figure S5. Cyclic voltammograms of monomer **6** in acetonitrile, 0.1 M $TBAClO_4$ at different scan rates (WE: GC; RE: $AgNO_3$/Ag, in CH_3CN; CE: Pt) , c = 1 mg/mL, 1st and 2nd cycle.

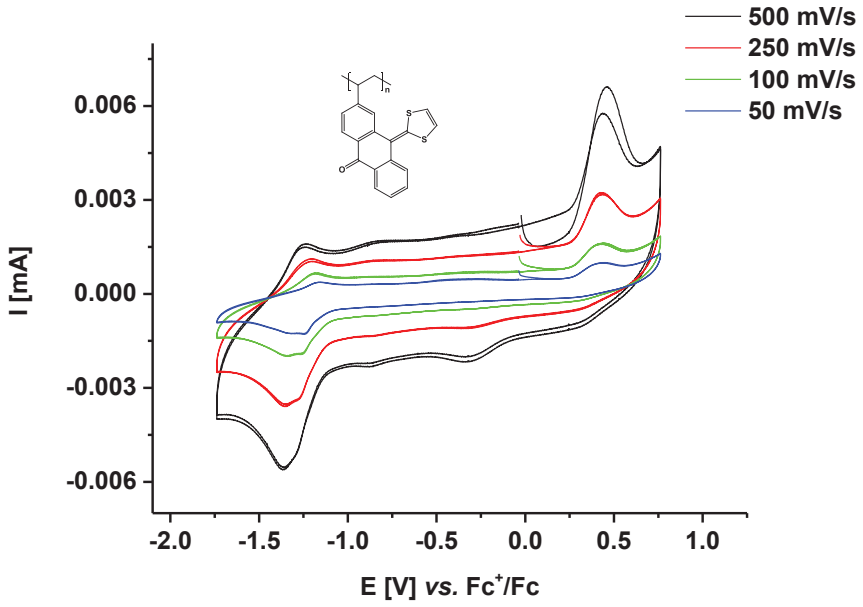

Figure S6. Cyclic voltammograms of polymer **P3** in DMF, 0.1 M $TBAClO_4$ at different scan rates (WE: GC; RE: $AgNO_3$/Ag, in CH_3CN; CE: Pt), c = 0.5 mg/mL, 1st and 2nd cycle.

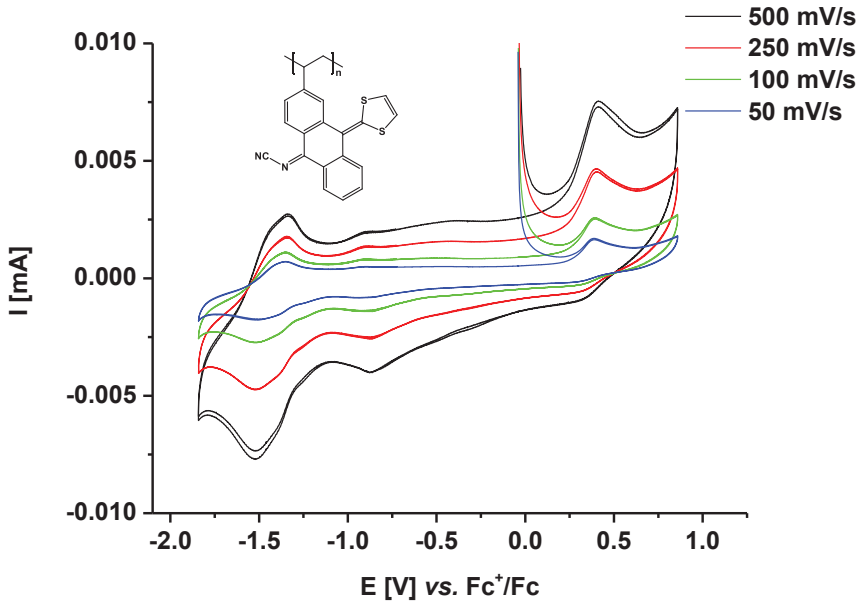

Figure S7. Cyclic voltammograms of polymer **P4** in DMF, 0.1 M $TBAClO_4$ at different scan rates (WE: GC; RE: $AgNO_3$/Ag, in CH_3CN; CE: Pt), c = 0.5 mg/mL, 1st and 2nd cycle.

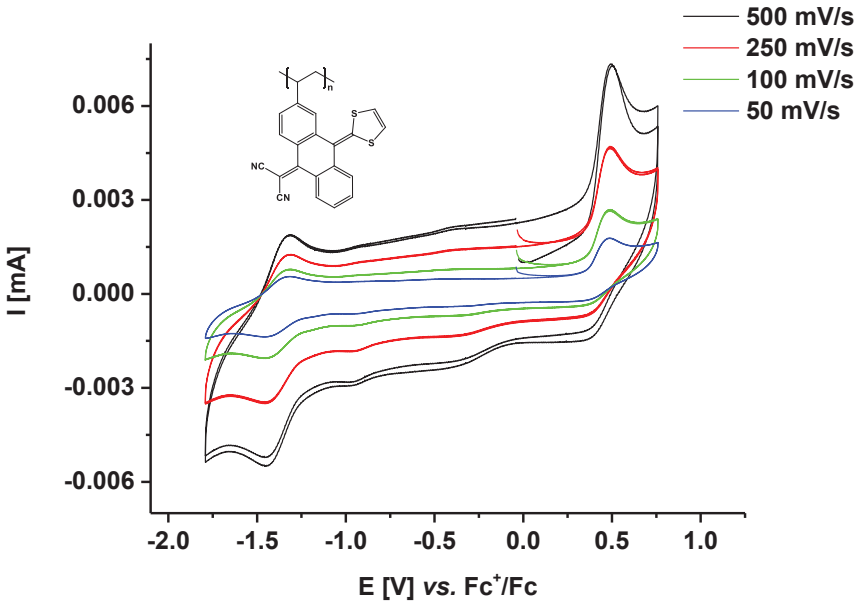

Figure S8. Cyclic voltammograms of polymer **P5** in DMF, 0.1 M $TBAClO_4$ at different scan rates (WE: GC; RE: $AgNO_3$/Ag, in CH_3CN; CE: Pt), c = 0.5 mg/mL, 1st and 2nd cycle.

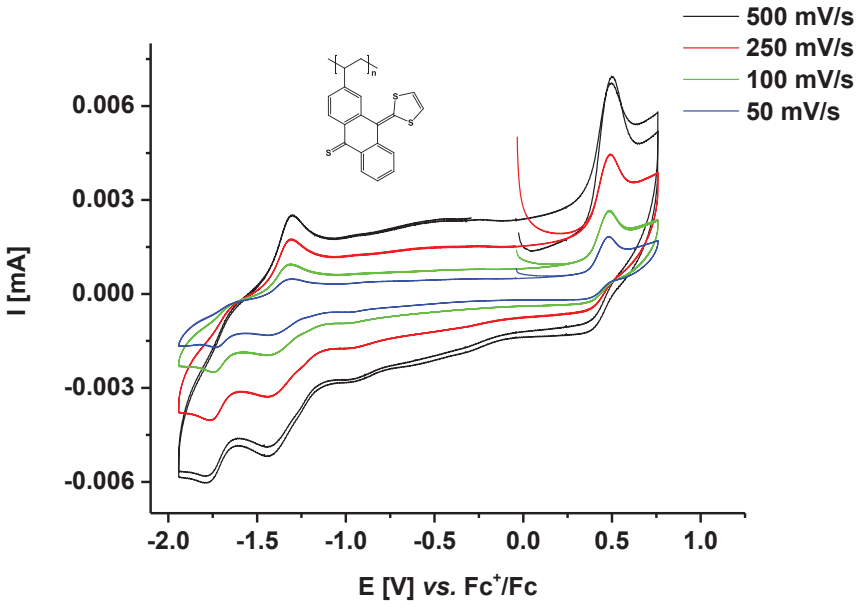

Figure S9. Cyclic voltammograms of polymer **P6** in DMF, 0.1 M $TBAClO_4$ at different scan rates (WE: GC; RE: $AgNO_3$/Ag, in CH_3CN; CE: Pt), c = 0.5 mg/mL, 1st and 2nd cycle.

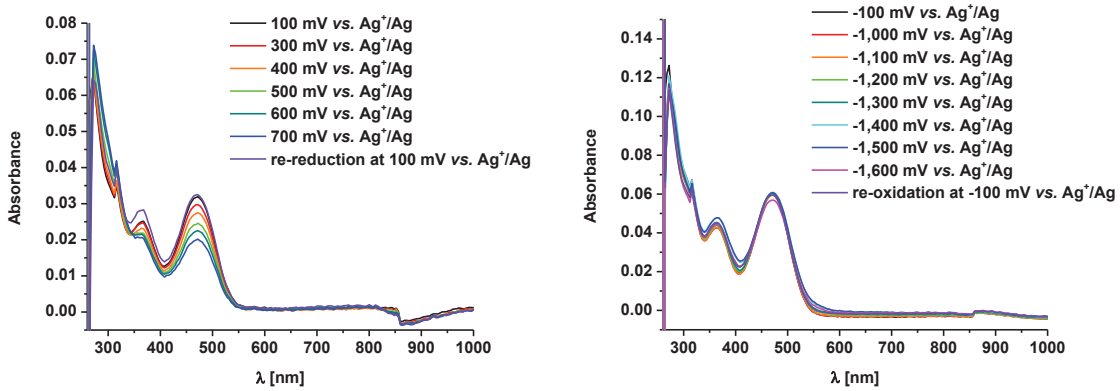

Figure S10. UV-vis-NIR spectroelectrochemistry of **P3** (DMF, 0.1 M $TBAClO_4$. RE: $AgNO_3/Ag$ = 0.08 V *vs.* Fc^+/Fc).

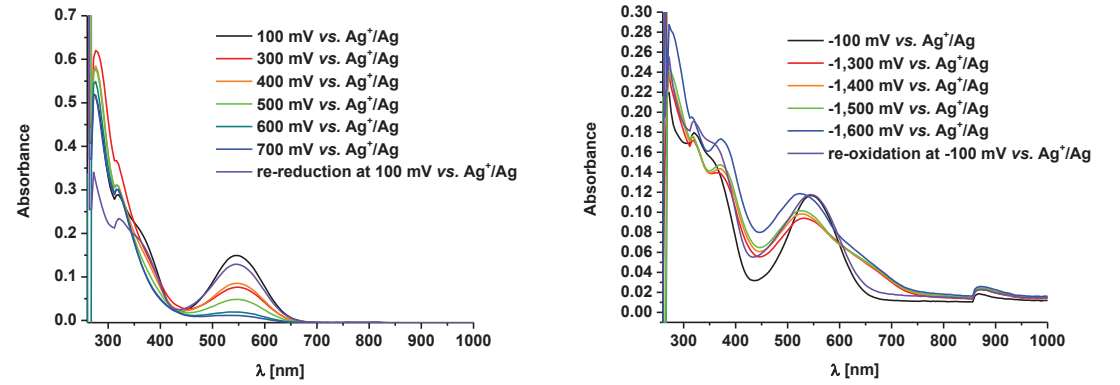

Figure S11. UV-vis-NIR spectroelectrochemistry of **P4** (DMF, 0.1 M $TBAClO_4$. RE: $AgNO_3/Ag$ = 0.08 V *vs.* Fc^+/Fc).

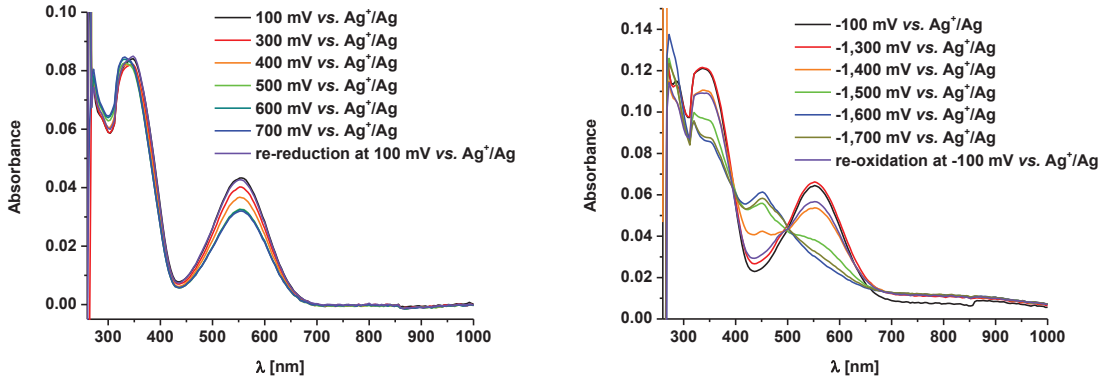

Figure S12. UV-vis-NIR spectroelectrochemistry of **P5** (DMF, 0.1 M $TBAClO_4$. RE: $AgNO_3/Ag$ = 0.08 V *vs.* Fc^+/Fc).

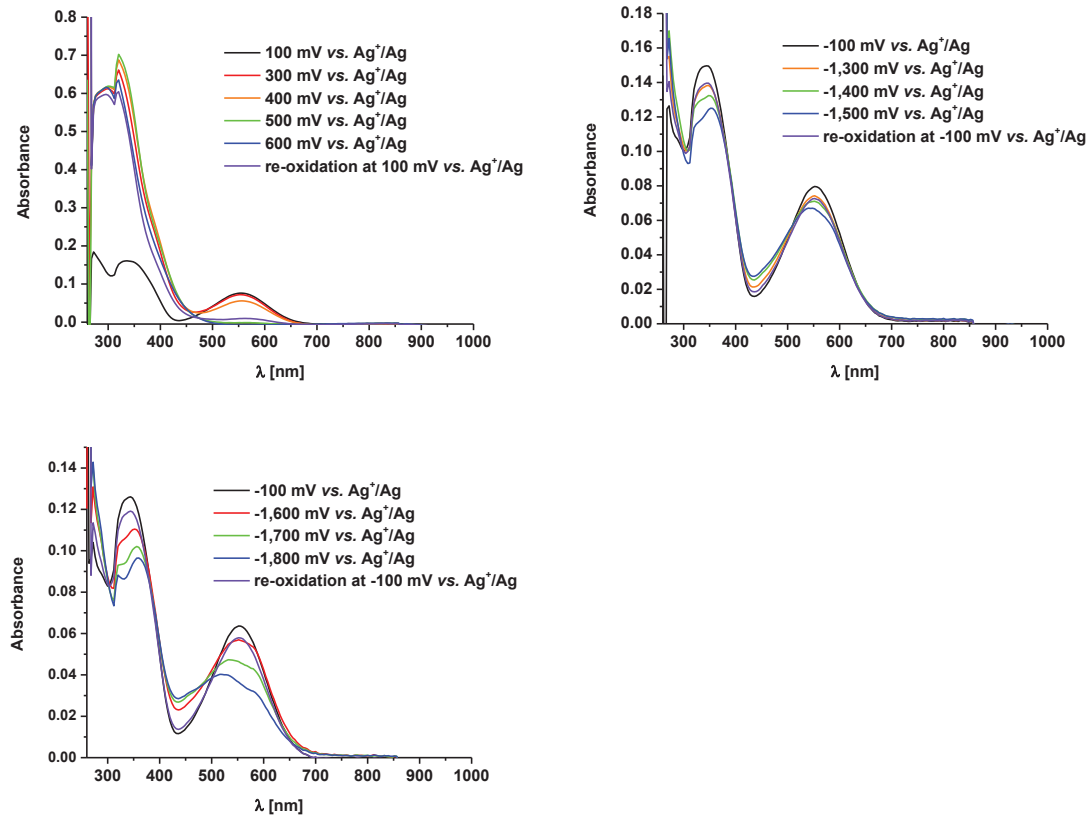

Figure S13. UV-vis-NIR spectroelectrochemistry of **P6** (DMF, 0.1 M $TBAClO_4$. RE: $AgNO_3/Ag$ = 0.08 V *vs.* Fc^+/Fc).

Publication 5

"Poly[*N*-(10-oxo-2-vinylanthracen-9(10*H*)-ylidene)cyanamide] as a novel cathode material for Li-organic batteries"

Daniel Schmidt, Bernhard Häupler, Christian Stolze, Martin D. Hager, Ulrich S. Schubert

J. Polym. Sci., Part A: Polym. Chem. **2015**, *53*, 2517–2523.

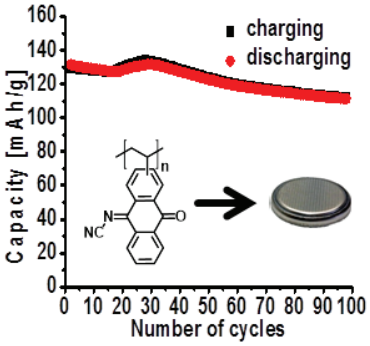

Poly[*N*-(10-oxo-2-vinylanthracen-9(10*H*)-ylidene)cyanamide] as a Novel Cathode Material for Li-Organic Batteries

Daniel Schmidt,[1,2] Bernhard Häupler,[1,2] Christian Stolze,[1,2] Martin D. Hager,[1,2] Ulrich S. Schubert[1,2]

[1]Laboratory of Organic and Macromolecular Chemistry, Friedrich Schiller University Jena, Humboldtstr. 10, 07743 Jena, Germany
[2]Center for Energy and Environmental Chemistry (CEEC Jena), Friedrich Schiller University Jena, Philosophenweg 7a, 07743 Jena, Germany
Correspondence to: U. S. Schubert (E-mail: ulrich.schubert@uni-jena.de)

Received 15 April 2015; revised 26 May 2015; accepted 27 May 2015; published online 17 June 2015
DOI: 10.1002/pola.27716

ABSTRACT: Redox-active polymers draw significant attention as active material in secondary batteries during the last decade. A new anthraquinone-based redox-active monomer was designed, which electrochemical behavior was tailored by mono-modification of one keto group. The monomer exhibits two one-electron redox reactions and has a low molar mass, resulting in a high theoretical capacity of 207 mAh/g. The polymerization of the monomer was optimized by variation of solvent and initiator. Moreover, the electrochemical behavior was studied using cyclic voltammetry and the polymer was used as active material in a composite electrode in lithium organic batteries. The polymer reveals a cell potential of 2.3 V and a promising capacity of 137 mAh/g. During the first 100 cycles, the capacity drops to 85% of the initial value. The influence of the charging speed on the charging/discharging properties of the batteries was further investigated. © 2015 Wiley Periodicals, Inc. J. Polym. Sci., Part A: Polym. Chem. **2015**, *53*, 2517–2523

KEYWORDS: electrochemistry; organic batteries; redox polymers; synthesis

INTRODUCTION The application of redox-active organic compounds, in particular polymers, in secondary batteries, such as lithium or sodium-ion batteries, draw significant attention during the last decade.[1,2] In contrast to inorganic materials, which are usually applied in secondary batteries, organic structures feature several distinct advantages such as being flexible,[3] low-toxic, and are producible in low-temperature processes in special cases from recycled[4] or renewable resources.[5] Moreover, their redox-potential can be tailored by the choice of the appropriate redox system; up to now numerous different redox-active compounds have been applied as active electrode materials, such as stable organic radicals[6,7] or carbonyl compounds.[8] Quinonide structures are of particular interest, because they undergo a redox reaction involving two electrons and possess a comparably low molar mass, resulting in high theoretical capacities. Two major strategies have been developed to tailor the redox potential of quinones (Fig. 1); they can be categorized into two major approaches: Group I consists of quinones, whose redox-potential is tuned by the introduction of appropriate substituents. In general, 1,2-diones possess higher potential than 1,4-diones and their redox potential can be further tailored by the addition of electron pushing/withdrawing substituents such as cyano,[9] chloro,[9] hydroxy,[10] lithoxy,[11,12] fluorinated, and non-fluorinated alkyl and alkoxy groups,[10,13–15] thiophene,[16] pyridine,[17] pyrazine,[17] lithium *resp*. sodium salts of carboxylic[18] or sulfonic acids.[19] Group II represents compounds with modified redox core, such as tetracyanoanthraquinone dimethanes[20,21] or (π-extended) tetrathiafuvalene systems, whose redox mechanism is based on one two-electron reaction.[22,23] However, the major drawback in the application of small quinonide molecules as active electrode material is their solubility in common organic electrolytes, which leads to a rapid capacity decrease within the first charge/discharge cycles. Special battery setups with crystalline electrodes or quasi-solid electrolytes enable battery systems with small quinonide molecules, but their setup end electrolytes are very complex.[9,24,25] A simple and promising approach to overcome these decisive disadvantages is the incorporation of the redox-active unit into a polymeric backbone, resulting in an insoluble, but swellable material that remains electro-active in the solid state.[26,27]

Additional Supporting Information may be found in the online version of this article.

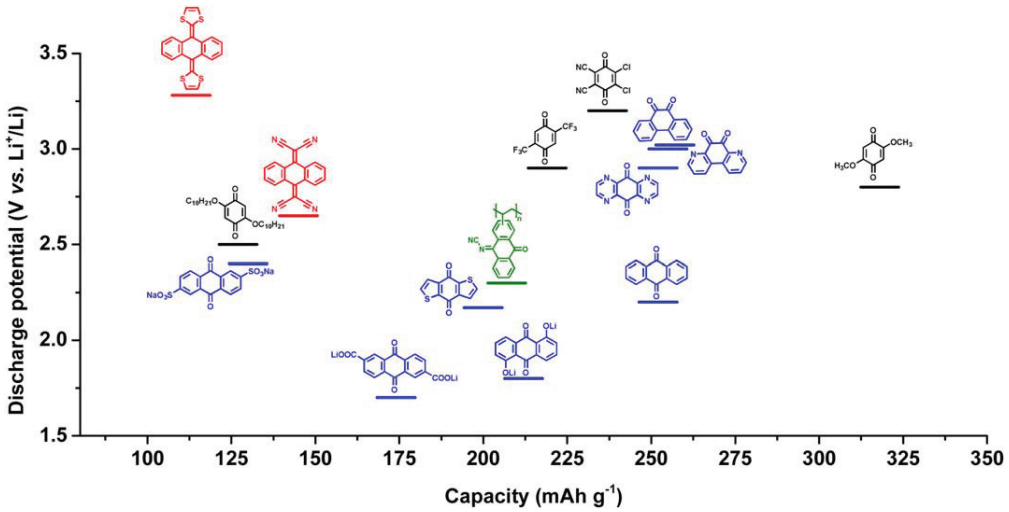

FIGURE 1 Schematic representation of discharge potentials and theoretical capacities of quinone derivatives applied as active cathode material in Li-organic batteries. [Color figure can be viewed in the online issue, which is available at wileyonlinelibrary.com.]

To further extend these approaches we decided to incorporate a mono-modified anthraquinone, where one keto group is replaced by a *N*-cyanoimine group and utilize the resulting polymer as active cathode material in a lithium-organic battery. This electro-active structure reveals a redox reaction at 2.3 V versus Li^+/Li involving two electrons and could be integrated into a polymeric environment by free radical polymerization of the introduced vinyl group.

EXPERIMENTAL

Materials

Tetrahydrofuran and toluene were dried with a PureSolv-EN™ Solvent Purification System (Innovative Technology). All other solvents were dried according to standard procedures. All starting materials were purchased from commercial sources and were used as obtained unless otherwise noted. 2,2′-Azo*bis*(*iso*-butyronitrile) (AIBN) was recrystallized from methanol prior to use. 2-Iodoanthraquinone (**1**) and 2-vinylanthraquinone (**2**) were synthesized according to literature procedures.[22] Unless otherwise noted, all reactions were performed under inert argon atmosphere.

Characterization

The reactions were monitored by TLC on 0.2 mm Merck silica gel plates (60 F254). Column chromatography was performed on silica gel 60 (Merck). ^1H and ^{13}C NMR spectra were recorded on a Bruker AC 300 (300 MHz) spectrometer at 298 K. Chemical shifts are reported in parts per million (ppm, δ scale) relative to the residual signal of the deuterated solvent. Elemental analyses were carried out using a Vario ELIII–Elementar Euro and an EA–HekaTech. Cyclic voltammetry experiments were performed using a Biologic VMP 3 potentiostat at room temperature under argon atmosphere. A three-electrode setup was utilized (WE: glassy carbon, RE: $AgNO_3/Ag$ in CH_3CN, CE: Pt). The redox couple Fc^+/Fc was used as internal standard after each measurement. Electrochemical impedance spectroscopy was carried out using a Biologic VMP 3 potentiostat at room temperature. Size-exclusion chromatography was performed on an Agilent 1200 series system (degasser: PSS, pump: G1310A, auto sampler: G1329A, oven: Techlab, DAD detector: G1315D, RI detector: G1362A, eluent: DMAc + 0.21% LiCl, 1 mL/min, temperature: 40 °C, column: PSS GRAM guard/1000/30 Å).

Synthesis of Monomer

***N*-(10-oxo-vinylanthracen-9-(10H)-ylidene)cyanamide (3)**

2 (3.0 g, 12.8 mmol) was dissolved in chloroform (60 mL). Titanium(IV) chloride (1.4 mL, 12.8 mmol) followed by *bis*(trimethylsilyl)carbodiimide (6.4 mL, 28.2 mmol) was added and the mixture was stirred at 60 °C for 15 h. After cooling to room temperature, the mixture was cast into saturated ammonium chloride solution (50 mL) and the crude product was extracted with dichloromethane (3 × 50 mL). The combined organic phases were dried over magnesium sulfate and the solvent was removed under reduced pressure. The crude product was purified by column chromatography (silica gel 60; dichloromethane) followed by a second column chromatography (silica gel 60; dichloromethane:*n*-hexane, 3:1) to obtain 1.7 g (6.7 mmol, 52%) as ocher powder. ^1H NMR (300 MHz, CD_2Cl_2, δ): 9.75 to 8.02 (br, 4H; Ar H), 7.87 (m, 2H, Ar H), 6.91 (m, 1H; vinyl), 6.10 (m, 1H; vinyl), 5.59 (m, 1H; vinyl); ^{13}C NMR (75 MHz, CD_2Cl_2, δ): 182.2 (C=O), 181.7 (C=O), 172.1 (C=N), 171.4 (C=N), 144.4, 143.8, 135.4, 135.1, 134.7, 134.6, 134.5, 132.8, 132.4, 131.7, 128.2, 127.6, 127.4, 125.7, 125.1, 119.6, 119.2, 114.5 (C≡N), 114.4 (C≡N); EIMS [*m/z* (%)]: 258 (100) $[M^+]$, 331 (23) $[M^+ - CN + H]$, 203 (19) $[C_{16}H_{11}{}^+]$, 176 (13) $[C_{14}H_8{}^+]$, 76 (27) $[C_6H_4{}^+]$; HRMS (ESI, *m/z*): $[M + Na]^+$ calcd. for $C_{17}H_{10}N_2O$: 281.0685; found: 281.0687.

TABLE 1 Selected Analytical Data for Polymers **4** Prepared by Free Radical Polymerization and NMP, Respectively

Polymer	Solvent	Concentration (mol/L)	Initiator	Temperature (°C)	M_n[a] (g/mol)	PDI[a]	Yield (%)
4a	1,2-Dichloromethane	1.00	AIBN (2 mol%)	70	5,800	1.24	4
4b	NMP	1.00	AIBN (2 mol%)	70	5,200	1.23	2
4c	DMSO	1.00	AIBN (2 mol%)	70	4,500	1.37	54
4d	DMF	1.00	AIBN (2 mol%)	70	5,100	1.328	2
4e	DMAc	1.00	AIBN (2 mol%)	70	4,800	1.28	12
4f	DMSO	1.05	TBHP (5 mol%)	130	2,600	1.37	33
4g	DMSO	1.05	DTBP (5 mol%)	130	5,900	2.39	83
4h	DSMO	1.05	CMSt-TIPNO (5 mol%)	130	10,200	16.12	66
4i[b]	DMSO	1.05	DTBP (5 mol%)	130	*8,000*[d]	*4.57*[d]	83
4j[c]	DMSO	1.05	DTBP (5 mol%)	130	*278,900*[d]	*1.54*[d]	85

[a] Determined by SEC (DMAc, 0.21% LiCl, polystyrene standard, RI detector).
[b] Cross-linked polymer synthesized with divinylbenzene (2 mol%).
[c] Cross-linked polymer synthesized with divinylbenzene (5 mol%).
[d] SEC measurements were performed with the soluble part of the polymers.

Synthesis of Polymers

General Procedure of Polymerization of 3

A flask was charged with **3** (50 mg, 0.2 mmol), initiator, divinylbenzene (for **4i** and **4j**), and solvent (for detailed information see Table 1). The reaction mixture was degassed by the freeze-pump-thaw method and heated to 70 and 130 °C, respectively. Subsequently, the mixture was allowed to cool to room temperature and the polymer was precipitated in acetone twice and was collected by centrifugation. The product as an ocher powder was dried under vacuum. ^{1}H NMR (300 MHz, DMSO-d_6, δ): 8.79–6.16 (br, 7H; Ar H), 1.96–0.69 (br, 3H).

Preparation of Composite Electrodes

A solution of polymer **4** and poly(vinylidenefluoride) (PVDF; Sigma Aldrich) as binder in *N*-methyl-2-pyrrolidone (NMP) ($c_{polymer} = 10$ mg/mL) was added to multi-walled carbon nanotubes (MWCNT; Sigma Aldrich) as conducting additives (ratio: polymer/PVDF/MWCNT, 1/1/8, *w*/*w*/*w*). These materials were mixed in a mortar for 10 min and the slurry was coated on graphite foil and aluminum foil, respectively, applying a doctor blade method. Subsequently, NMP was removed by heating the electrodes at 80 °C for 20 h.

Preparation of the Coin Cells

The coin cells (type 2032) were manufactured under argon atmosphere. Suitable round composite electrodes on aluminum foil (15 mm diameter) were cut with a MTI Corporation Precision Disc Cutter T-0.6. The amount of active material on the electrodes was determined on the basis of the weight of the dried electrodes. The electrode, utilized as cathode, was placed into the bottom cell case and separated from the lithium anode by a porous polypropylene membrane (Celgard, MTI Corporation). A stainless steel spacer (diameter: 15.5 mm, thickness: 0.3 mm, MTI corporation) and a stainless steel wave spring (diameter: 14.5 mm, thickness: 5 mm) were placed on top of the lithium anode. The cell was filled with electrolyte and the top cell case was placed onto the electrode. Subsequently, the cell was sealed with an electric crimper machine (MTI Corporation MSK-100D). Electrochemical measurements were performed after an equilibration time of 24 h.

Charge/Discharge Experiments

All experiments were performed at room temperature. The charge/discharge capacities were determined based on the weight of the polymer in the electrode.

RESULTS AND DISCUSSION

Synthesis of Monomer and Polymers

The synthetic route of polymer **4** is depicted in Scheme 1 starting from commercially available 2-aminoanthraquinone, which was transformed to 2-iodoanthraquinone **1** by a *p*-toluene sulfonic acid supported Sandmeyer reaction.[22] Different polymerizable groups such as acetylene, norbornene, or vinyl can be introduced by subsequent palladium catalyzed C–C cross-coupling reactions due to the iodine substituent. The vinyl group was introduced by a palladium catalyzed Hiyama cross-coupling reaction in high yield[22] to obtain monomer **3**, which can be polymerized by metal catalyst free radical polymerization techniques. Subsequently, one of the carbonyl groups was transformed into a *N*-cyanoimine group using titanium (IV) chloride and *bis*(trimethylsilyl)carbodiimide. Monomer **3** could be achieved in moderate yields as an isomeric mixture due to similar reactivity of both carbonyl groups. The isomers were not separated because both isomers reveal similar electrochemical properties. Monomer **3** was polymerized using the free radical and the nitroxide mediated polymerization (NMP) technique to obtain eight linear (**4a** to **4h**) and two cross-linked polymers (**4i** and **4j**). The polymerization step is important to enhance the charge/discharge stability of the organic material, which is dependent on the non-solubility of the active material in the electrolyte. Oligomers and small chain polymers reveal a better solubility, which lead to a capacity decay during the first charge/discharge cycles of the battery. As a consequence,

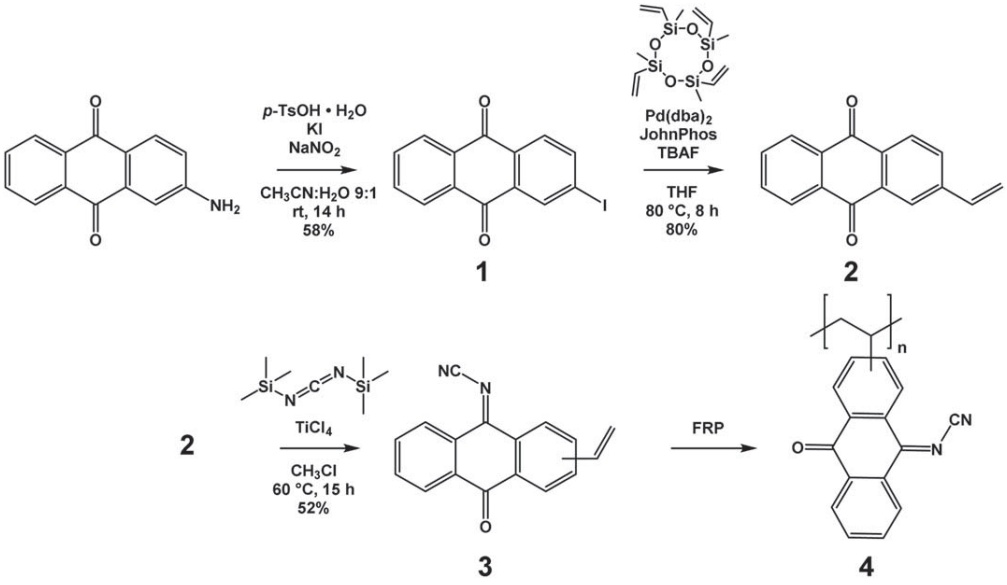

SCHEME 1 Schematic representation of the synthesis of monomer **3** and polymer **4**.

high molar mass polymers without low molar mass oligomers are preferred. An alternative approach is the utilization of cross-linked polymers, which possess a low solubility in the electrolyte. However, this can lead to a completely insoluble material, which complicates the electrode processing and results in a low material activity in the battery. The analytical data of the polymers is summarized in Table 1. All polymers were investigated by size-exclusion chromatography (SEC). The linear polymers synthesized by free radical polymerization reveal a monomodal distribution. The free radical polymerization was performed with AIBN as initiator in a limited range of different solvents [*i.e.,* 1,2-dichloroethane, *N*-methyl-2-pyrrolidone (NMP), dimethylsulfoxide (DMSO), *N*,*N*-dimethylformamide (DMF), and *N*,*N*-dimethylacetamide (DMAc)] due to the poor solubility of **3**. The best results were obtained in DMSO with a yield of 54%. All other solvents led to very poor yield (2–12%) and low molar masses (4,500 to 5,800 g/mol), presumably due to steric hindrance of the *N*-cyanoimine group and chain terminating reactions. As a consequence, the reaction temperature was increased to 130 °C and, therefore, other initiators were chosen. The polymerization with *tert*-butyl hydroperoxide (TBHP) as initiator led to a polymer with a very low molar mass of 2,600 g/mol (PDI = 1.37) in 33% yield. The molar mass as well as the yield could be increased to 5,900 g/mol and 83%, respectively, by the utilization of di-*tert*-butyl peroxide (DTBP) as initiator. However, the PDI value increased to 2.39. Additionally, nitroxide mediated polymerization with the initiator *N*-*tert*-butyl-*O*-[1-[4-(chloromethyl)phenyl]ethyl]-*N*-(2-methyl-1-phenylpropyl)hydroxylamine (CMSt-TIPNO) was performed to avoid side reactions as well as to increase thereby the molar mass. **4h** was achieved in moderate yields and a high molar mass (M_n = 10,200 g/mol, PDI = 16.1, 66%). However, the SEC measurement revealed a multimodal distribution due to a poor control of the polymerization presumably by chain transfer to the solvent, which has no influence on the redox behavior of the polymer. Because of the good solubility of the polymers in standard electrolyte solutions for lithium organic batteries, such as ethylene carbonate/dimethyl carbonate 1/4 (*v*/*v*), two cross-linked polymers were synthesized with divinylbenzene as cross-linker. The polymerizations were performed with *tert*-butyl peroxide as initiator in DMSO with 2 and 5 mol% divinylbenzene, respectively, resulting in mainly insoluble polymers. The SEC data were determined using the soluble part of the polymers, which revealed a molar mass (M_n) of about 8,000 g/mol for the polymer, cross-linked with 2 mol%

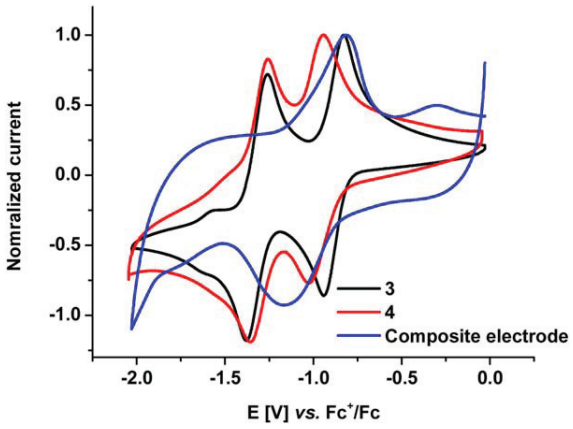

FIGURE 2 Normalized cyclic voltammograms of monomer **3** (c = 0.6 mg/mL), polymer **4c** (c = 0.2 mg/mL) (in DMF, 0.1 M $LiClO_4$, 100 mV/s), and composite electrode (**4h**/PVDF/MWCNT 1/1/8 (*w*/*w*/*w*)) in EC/DMC 1/4 (*v*/*v*), 1 M $LiClO_4$, 5 mV/s, 1st cycle, WE: glassy carbon, RE: $AgNO_3$/Ag in CH_3CN, CE: Pt. [Color figure can be viewed in the online issue, which is available at wileyonlinelibrary.com.]

TABLE 2 Cyclic Voltammetric Data of Monomer **3**, Polymer **4**, and the Composite Electrode

Compound	$E^1_{1/2}$ (V vs. Fc^+/Fc)	$E^2_{1/2}$ (V vs. Fc^+/Fc)
Monomer **3**[a]	−0.88	−1.31
Polymer **4**[a]	−0.99	−1.31
Composite electrode[b]	−1.02	

[a] In DMF, 0.1 M $LiClO_4$, 100 mV/s.
[b] Composite: **4**/PVDF/MWCNT 1/1/8 (*w*/*w*/*w*); in EC/DMC 1/4 (*v*/*v*), 1 M $LiClO_4$, 5 mV/s.

divinylbenzene. As expected, the molar mass distribution of the polymer is very broad (PDI = 4.57). The second cross-linked polymer (5 mol% divinylbenzene) achieved a higher molar mass of about 280,000 g/mol (PDI = 1.54). The molar mass of the polymer could not be determined exactly due to the exclusion limit of the SEC column. The yields of both cross-linked polymers are high with over 80%.

Electrochemical Performances

The electrochemical behavior of monomer **3** and polymer **4c** was investigated by cyclic voltammetry and, therefore, a solution of 0.1 M lithium perchlorate in DMF was utilized as electrolyte due to the good solubility of both the monomer and the polymer (Fig. 2). The results are summarized in Table 2. The monomer **3** features two reversible one-electron reduction steps at −0.88 and −1.31 V versus Fc^+/Fc. The electron acceptance of the *N*-cyanoimine functionality is increased compared to the keto group and, therefore, the reduction of the monomer to the radical anion and to the dianion occurs at a more positive potential compared to anthraquinone ($E^1_{1/2}$ = –1.2 V and $E^2_{1/2}$ = –1.7 V vs. Fc^+/Fc).[18] Furthermore, due to the incorporation of only one *N*-cyanoimine group, the reduction potentials are even lower compared to the difunctionalized *N,N′*-dicyano-9,10-anthraquinonediimine ($E^1_{1/2}$ = –0.68 V and $E^2_{1/2}$ = –1.04 V vs. Fc^+/Fc).[28] The peak splits of both reduction steps are in the range of 74 to 120 mV and decrease with slower scan rates. The incorporation of the monomer in a polymeric environment led to a slight shift of the first reduction potential to −0.99 V versus Fc^+/Fc. The second reduction step is not influenced by the polymeric backbone ($E_{1/2}$ = –1.31 V vs. Fc^+/Fc). The shift of the first reduction potential is presumably due to π-π-stacking of the monomeric units in the polymer, which requires a higher energy to break these interactions. The first reduction state is negatively charged and due to repulsion of the monomer units, the π–π stacking interactions are revoked and, as a consequence, the second reduction step is comparable to the reduction of the monomer. The reduction processes are reversible and stable and their peak splits are also low and decrease with lower scan rates. Additionally, the polymer was further investigated electrochemically as composite electrode on a graphite sheet as current collector (Fig. 2, Table 2). An electrode slurry of **4**/PVDF/MWCNT 1/1/8 (*w*/*w*/*w*) was spread onto the current collector by a doctor blading method and was dried at 80 °C. The electrode was immersed in a solution of 0.1 M $LiClO_4$ in ethylene carbonate/dimethyl carbonate (EC/DMC) 1/4 (*v*/*v*) and cyclic voltammetry revealed a stable and reversible reduction wave at −1.02 V vs. Fc^+/Fc, which proved that the carbon material has no significant influence on the reduction potential. However, both reduction signals are coalesced to one broad redox wave and a large peak-to-peak separation of 0.53 V at 10 mV/s was observed; that can be assigned to slow kinetics due to slow diffusion processes in the electrode, comparable low conductivity of the composite film as well as to the massive geometrical changes of the redox active units during the redox processes. The peak split decreases with lower scan rates.

Coin Cell Studies

Encouraged by the suitable redox activity of polymer **4**, lithium organic batteries were constructed to investigate the charge/discharge properties of the polymers. For this purpose, the high molar mass polymer (**4h**) as well as both cross-linked polymers (**4i** and **j**) were used due to their high insolubility in the used electrolyte. The coin cells were prepared under inert atmosphere by sandwiching a composite electrode **4**/PVDF/MWCNT 1/1/8 (*w*/*w*/*w*) and a lithium foil separated by a porous membrane. Different solvents (e.g., EC, DMC, diethyl carbonate, ionic liquids and their mixtures) were tested as electrolytes. The best results were obtained with a solution of 1 M $LiClO_4$ in EC/DMC 1/4 (*v*/*v*) and, as a consequence, all further studies were carried out with this electrolyte. Self-discharge behavior was investigated by OCV measurements and no significant decrease in the battery's state of charge could be observed within 13 days. The charge/discharge properties of all cells revealed a plateau at a cell potential of 2.33 V for charging and at 2.28 V for discharging, which corresponds to the characteristic overpotential of the coin cell. An electrochemical impedance spectroscopy measurement was carried out to

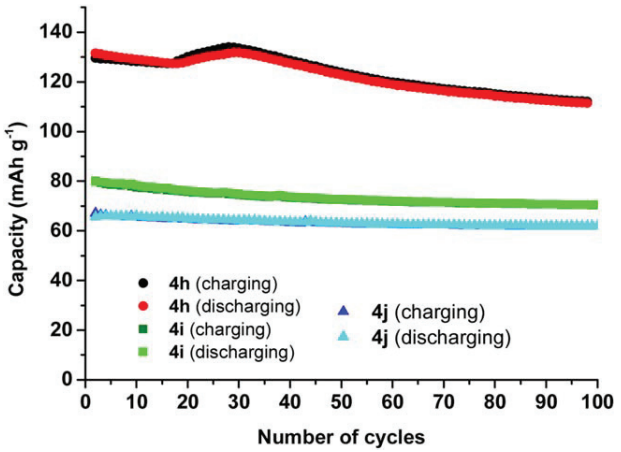

FIGURE 3 Charge/discharge cycles of a lithium organic battery of polymer **4h**, **4i,** and **4j** in EC/DMC 1/4 (*v*/*v*), 1 M $LiClO_4$ (100 cycles, 5C). The anode is lithium metal, the cathode is a composite of (**4h**, **4i,** or **4j**/PVDF/MWCNT 1/1/8 (*w*/*w*/*w*). [Color figure can be viewed in the online issue, which is available at wileyonlinelibrary.com.]

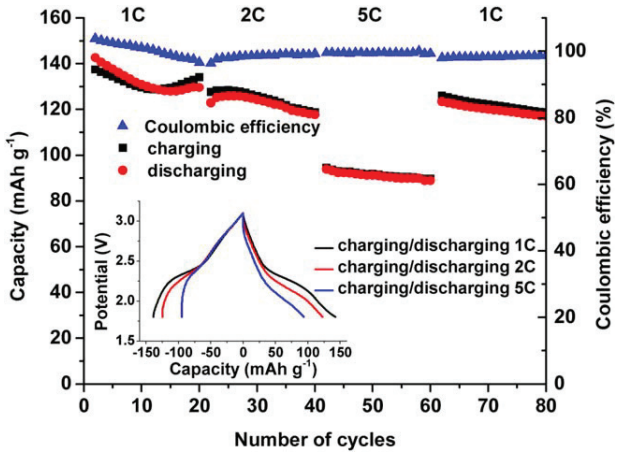

FIGURE 4 Charge/discharge cycles of a lithium organic battery (80 cycles) of **4h** at different C rates in EC/DMC 1/4 (*v*/*v*), 1 M $LiClO_4$. Coulombic efficiency of 80 charge/discharge cycles (blue triangle). First charge/discharge curves (potential vs. capacity) at different C rates (insert). [Color figure can be viewed in the online issue, which is available at wileyonlinelibrary.com.]

investigate the overpotential in detail, resulting in a total ohmic resistance of 218 Ω (see Supporting Information for further details). To analyze the influence of the different polymeric environments, the charge/discharge behavior of the polymers **4h**, **4i** and **4j** were investigated (Fig. 3). The polymers revealed a stable charge/discharge behavior. The coin cell with polymer **4h** had an initial capacity of about 130 mAh/g, which drops down to 112 mAh/g, 15% capacity loss after 100 cycles. A further swelling of the polymer within the first cycles results in a slight increase of the capacity after about 20 cycles. Due to the lower solubility of the cross-linked polymers in the electrolyte, these cells showed a decrease of the capacity of only 12% and 6% for polymer **4i** and **4j**, respectively, after 100 cycles. However, the initial capacity is low with about 80 and 62 mAh/g (31 and 26% active material), respectively. Based on the highest capacity and the good cycle stability, polymer **4h** was further investigated in detail (Fig. 4). At the first charge/discharge cycle, the battery exhibits a capacity of 137 mAh/g, which corresponds to 53% of the theoretical capacity. Within 100 cycles the capacity drops to 118 mAh/g corresponding to 45% of the theoretical capacity. The influence of the charging speed was investigated during the first 80 cycles. The capacity decreases by 5% to 127 mAh/g at a charging speed of 2C and at a charging speed of 5C, the capacity drops by further 18% to 94 mAh/g. The coulombic efficiency is over 96% at all charging speeds. The charging cell potential is not significantly influenced by the charging speed. However, the discharging potential drops from 2.33 V (1C) to 2.10 V (5C).

CONCLUSIONS

A new anthraquinone-based monomer was synthesized and due to the mono-modification the redox behavior of the monomer can be tailored. The monomer was polymerized using free radical polymerization and nitroxide mediated polymerization techniques. The polymerization was optimized to yield **4** in high molar masses as well as in high yields, which allow its application in lithium organic batteries. The electrochemical behavior of both monomer and polymers was investigated by cyclic voltammetry. The monomer possesses two reversible one-electron reductions at −0.88 and −1.31 V versus Fc^+/Fc, that is shifted to −0.99 and −1.31 V versus Fc^+/Fc after incorporation of the monomer into an polymeric environment. The polymeric backbone as well as the conducting and binding materials revealed no significant influence on the electrochemical behavior and, as a consequence, the polymers were employed as active material in a composite electrode for lithium organic batteries. In contrast to the monomer, the polymers showed good cycle stability over 100 cycles. The cross-linked polymers revealed the highest cycle stability but low potential activity. The high molar mass linear polymer revealed the most promising capacity of 137 mAh/g, which corresponds 53% of the theoretical capacity. Furthermore, the influence of the charging speed on the performance of the battery was investigated and exhibited a slight decrease of the capacity with higher charging speed rates of up to 5C.

ACKNOWLEDGMENTS

The authors thank the European Social Fund (ESF), the Thüringer Aufbaubank (TAB), and the Thuringian Ministry of Economy, Science and Digital Society (TMWWdG) for the financial support.

REFERENCES AND NOTES

1 Y. Liang, Z. Tao, J. Chen, *Adv. Energy Mater.* **2012**, *2*, 742–769.

2 Z. Song, H. Zhou, *Energy Environ. Sci.* **2013**, *6*, 2280–2301.

3 H. Nishide, K. Oyaizu, *Science* **2008**, *319*, 737–738.

4 M. Armand, S. Grugeon, H. Vezin, S. Laruelle, P. Ribière, P. Poizot, J.-M. Tarascon, *Nat. Mater.* **2009**, *8*, 120–125.

5 P. Poizot, F. Dolhem, *Energy Environ. Sci.* **2011**, *4*, 2003–2019.

6 T. Jähnert, M. D. Hager, U. S. Schubert, *J. Mater. Chem. A* **2014**, *2*, 15234–15251.

7 T. Janoschka, M. D. Hager, U. S. Schubert, *Adv. Mater.* **2012**, *24*, 6397–6409.

8 B. Häupler, A. Wild, U. S. Schubert, *Adv. Energy Mater.* **2015**. doi:10.1002/aenm.201402034

9 Y. Hanyu, Y. Ganbe, I. Honma, *J. Power Sources* **2013**, *221*, 186–190.

10 R. Zeng, L. Xing, Y. Qiu, Y. Wang, W. Huang, W. Li, S. Yang, *Electrochim. Acta* **2014**, *146*, 447–454.

11 J. Xiang, C. Chang, M. Li, S. Wu, L. Yuan, J. Sun, *Cryst. Growth Des.* **2008**, *8*, 280–282.

12 R.-H. Zeng, X.-P. Li, Y.-C. Qiu, W.-S. Li, J. Yi, D.-S. Lu, C.-L. Tan, M.-Q. Xu, *Electrochem. Commun.* **2010**, *12*, 1253–1256.

13 M. Yao, H. Senoh, M. Araki, T. Sakai, K. Yasuda, *ECS Trans.* **2010**, *28*, 3–10.

14 M. Yao, H. Ando, T. Kiyobayashi, *Energy Proc.* **2013**, *34*, 880–887.

15 T. Yokoji, H. Matsubara, M. Satoh, *J. Mater. Chem. A* **2014**, *2*, 19347–19354.

16 B. Häupler, T. Hagemann, C. Friebe, A. Wild, U. S. Schubert, *ACS Appl. Mater. Interfaces* **2015**, *7*, 3473–3479.

17 A. Shimizu, Y. Tsujii, H. Kuramoto, T. Nokami, Y. Inatomi, N. Hojo, J.-I. Yoshida, *Energy Tech.* **2014**, *2*, 155–158.

18 A. Shimizu, H. Kuramoto, Y. Tsujii, T. Nokami, Y. Inatomi, N. Hojo, H. Suzuki, J.-I. Yoshida, *J. Power Sources* **2014**, *260*, 211–217.

19 W. Wan, H. Lee, X. Yu, C. Wang, K.-W. Nam, X.-Q. Yang, H. Zhou, *RSC Adv.* **2014**, *4*, 19878–19882.

20 B. Häupler, R. Burges, T. Janoschka, T. Jähnert, A. Wild, U. S. Schubert, *J. Mater. Chem. A* **2014**, *2*, 8999–9001.

21 S. Nishida, Y. Yamamoto, T. Takui, Y. Morita, *ChemSusChem* **2013**, *6*, 794–797.

22 B. Häupler, R. Burges, C. Friebe, T. Janoschka, D. Schmidt, A. Wild, U. S. Schubert, *Macromol. Rapid Commun.* **2014**, *35*, 1367–1371.

23 M. Kato, K.-I. Senoo, M. Yao, Y. Misaki, *J. Mater. Chem. A* **2014**, *2*, 6747–6754.

24 M. Lécuyer, J. Gaubicher, A.-L. Barrès, F. Dolhem, M. Deschamps, D. Guyomard, P. Poizot, *Electrochem. Commun.* **2015**, *55*, 22–25.

25 Y. Hanyu, I. Honma, *Sci. Rep.* **2012**, *2*, 453.

26 Z. Song, H. Zhan, Y. Zhou, *Chem. Commun.* **2009**, *5*, 448–450.

27 T. Nokami, T. Matsuo, Y. Inatomi, N. Hojo, T. Tsukagoshi, H. Yoshizawa, A. Shimizu, H. Kuramoto, K. Komae, H. Tsuyama, J.-I. Yoshida, *J. Am. Chem. Soc.* **2012**, *134*, 19694–19700.

28 K. Takahashi, K. Kobayashi, *J. Org. Chem.* **2000**, *65*, 2577–2579.

Supporting Information

Poly[*N*-(10-oxo-2-vinylanthracen-9(10*H*)-ylidene)cyanamide] as a novel cathode material for Li-organic batteries

D. Schmidt, B. Häupler, C. Stolze, M. D. Hager, U. S. Schubert*

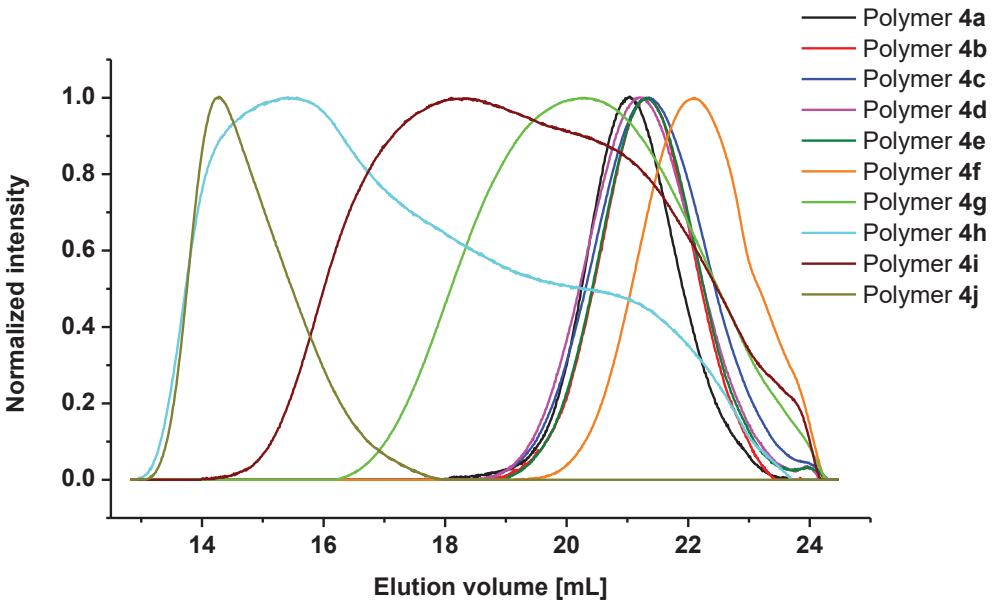

FIGURE S1 Size exclusion chromatograms of the polymers **4a** to **4j**. Eluent: DMAc, 0.21% LiCl, polystyrene standard, RI detector.

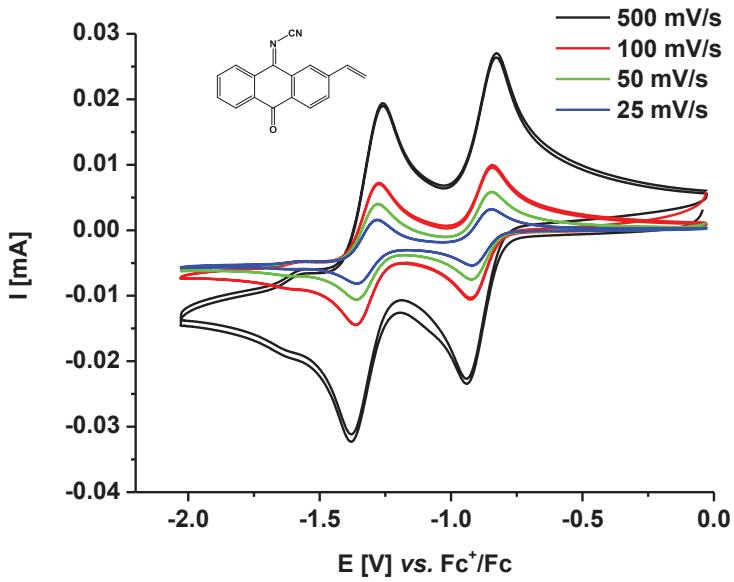

FIGURE S2 Cyclic voltammograms of monomer **3** in DMF, 0.1 M $LiClO_4$ at different scan rates (WE: GC; RE: $AgNO_3$/Ag, in CH_3CN, CE: Pt), c = 0.6 mg mL^{-1}, 1st and 2nd cycle.

TABLE S1 Peak split of the cyclic voltammograms of monomer **3** in DMF 0.1 M $LiClO_4$.

Scan rate (mV s^{-1})	Peak split [$E^1_{1/2}$ = -0.88 V *vs.* Fc^+/Fc] (mV)	Peak split [$E^1_{1/2}$ = -1.31 V *vs.* Fc^+/Fc] (mV)
500	110	120
100	84	87
50	75	82
25	74	78

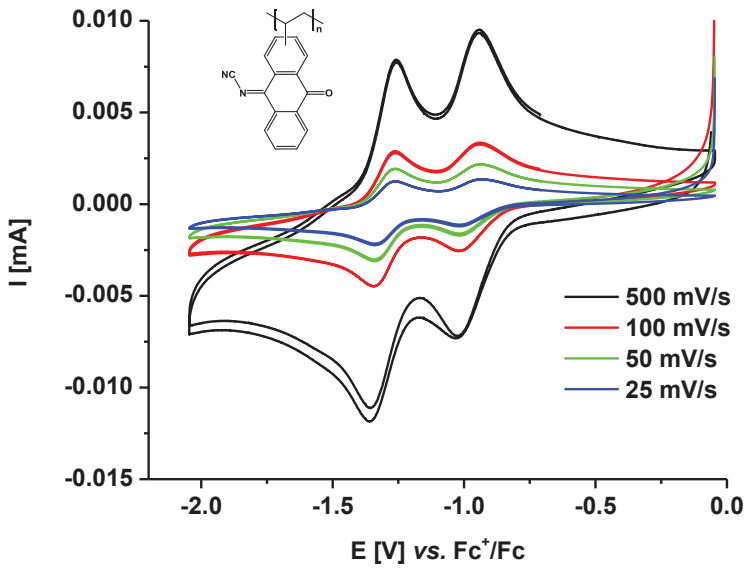

FIGURE S3 Cyclic voltammograms of polymer **4c** in DMF, 0.1 M $LiClO_4$ at different scan rates (WE: GC; RE: $AgNO_3$/Ag, in CH_3CN, CE: Pt), c = 0.2 mg mL^{-1}, 1st and 2nd cycle.

TABLE S2 Peak split of the cyclic voltammograms of polymer **4c** in DMF 0.1 M $LiClO_4$.

Scan rate (mV s^{-1})	Peak split [$E^1_{1/2}$ = -0.99 V *vs.* Fc^+/Fc] (mV)	Peak split [$E^1_{1/2}$ = -1.31 V *vs.* Fc^+/Fc] (mV)
500	94	101
100	76	82
50	76	79
25	81	77

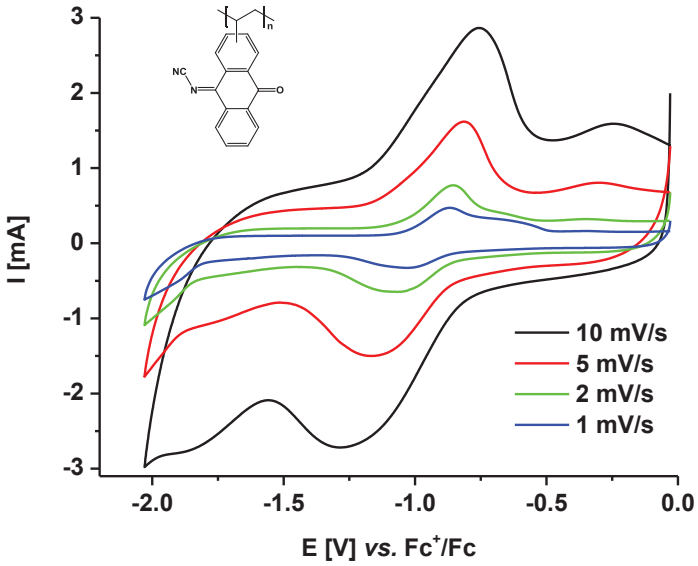

FIGURE S4 Cyclic voltammograms of composite electrode (**4h**/PVDF/MWCNT 1/1/8 (*w*/*w*/*w*)) in EC/DMC 1/4 (*v*/*v*), 1 M $LiClO_4$ at different scan rates (WE: GC; RE: $AgNO_3$/Ag, in CH_3CN, CE: Pt), c = 0.2 mg mL^{-1}, 1st cycle.

TABLE S3 Peak split of the cyclic voltammograms of composite electrode (**4h**/PVDF/MWCNT 1/1/8 (*w*/*w*/*w*)) in EC/DMC 1/4 (*v*/*v*), 1 M $LiClO_4$.

Scan rate ($mV\ s^{-1}$)	Peak split (mV)
10	530
5	350
2	210
1	160

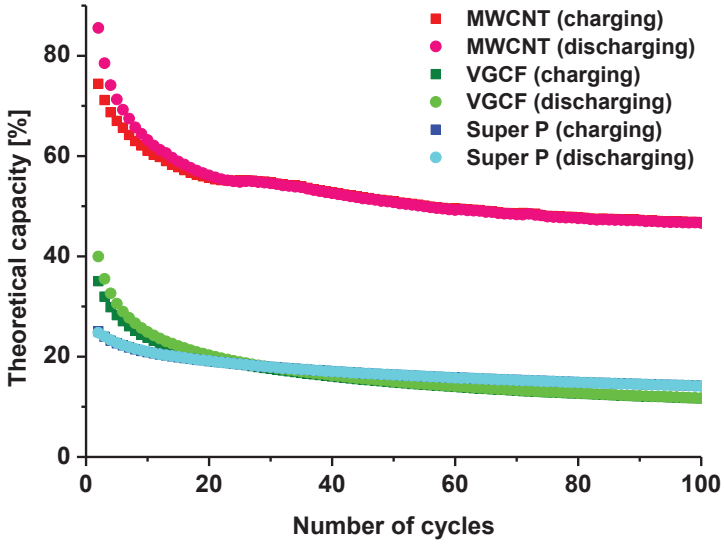

FIGURE S5 Charge/discharge cycles of a lithium organic battery of polymer **4c** in EC/DMC 1/4 (*v*/*v*), 1 M $LiClO_4$ (100 cycles, 5C). The anode is lithium metal, the cathode is a composite of **4c**/PVDF/carbon material 1/1/8 (*w*/*w*/*w*). The carbon material is MWCNT (red), vapor grown carbon fibers (green) and carbon black (Super P, blue).

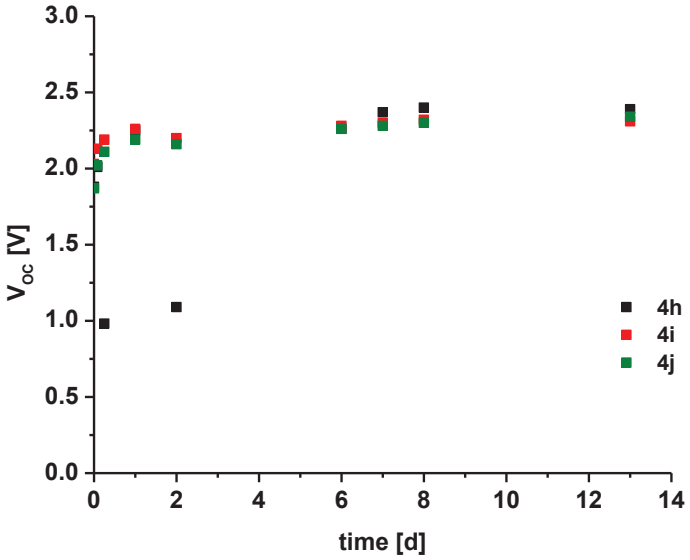

FIGURE S6 Open-circuit voltage of the lithium organic battery of polymer **4h**, **4i** and **4j** in EC/DMC 1/4 (*v*/*v*), 1 M $LiClO_4$ at room temperature.

Electrochemical impedance spectroscopy (EIS)

The potential difference between the plateaus corresponds to the characteristic overpotential of the coin cell. The overpotential during charge/discharge is defined as the difference between the measured potential and the equilibrium potential at a certain state of charge of the battery. It represents the inner resistance of the coin cell. However, due to a certain amount of self-discharge it is difficult and accompanied by a significant error to determine the overpotential and the corresponding ohmic resistance from the charge/discharge experiments. Therefore, impedance measurements have been performed in a frequency range from 600 kHz to 500 mHz. Two half circles were observed, where the first one is seen at the highest frequencies and is small compared to the second one (Figure S7). The second half circle ends up in a straight line. This is the typical behavior of a Randles circuit, which can be represented by a capacitance in parallel to a series circuit of an ohmic resistance and a Warburg impedance[S1]. The capacitance describes the double layer capacitance, the ohmic resistance corresponds to the charge transfer kinetics and the Warburg element describes the mass transfer at one electrode. Since the coin cell consists of two different types of electrodes it is reasonable to assume two Randles circuits in series to describe the processes at both electrodes. On that basis, an equivalent circuit for the system was chosen as shown in Figure S7b. Instead of a pure capacitance, a constant phase element (CPE) was chosen which accounts for an imperfect capacitor. Imperfections may arise from several sources, such as non-uniform electrode film properties, which are very likely due to the preparation procedure of the composite electrodes[S2]. The single series resistance in the equivalent circuit represents the ohmic resistance of the electrolyte and electronic periphery (i.e. wires, connectors, etc.). The equivalent circuit was fitted to the experimental data (Figure S7a). Table S4 shows the fit parameters. The total ohmic resistance causing the observed overpotential in the charging/discharging experiments is the sum of all ohmic contributions, which results in (218 ± 19) Ω. Since the Warburg coefficient of the second circuit is zero, it can be marked that mass transfer overpotential can be neglected for one electrode. The charge transfer resistance of the second electrode is small compared to the first. It is very likely that the small values can be attributed to the lithium half-cell of the coin cell. Thus, the polymer composite electrode gives the main contribution to the overpotential of the battery. Similar impedance behavior has already been reported for other polymer composite electrodes.[S3,S4]

TABLE S4 Fit parameters of the EIS.

Parameter	Fit value
R_S	17.37 Ω
$Q_{0,CPE1}$	18.98 µF $s^{(n-1)}$
n_{CPE1}	0.764
R_1	196.80 Ω
s_{W1}	173.8 Ω $s^{-1/2}$
$Q_{0,CPE2}$	1.056 µF $s^{(n-1)}$
n_{CPE2}	0.978
R_2	3.276 Ω
s_{W2}	0 Ω $s^{-1/2}$

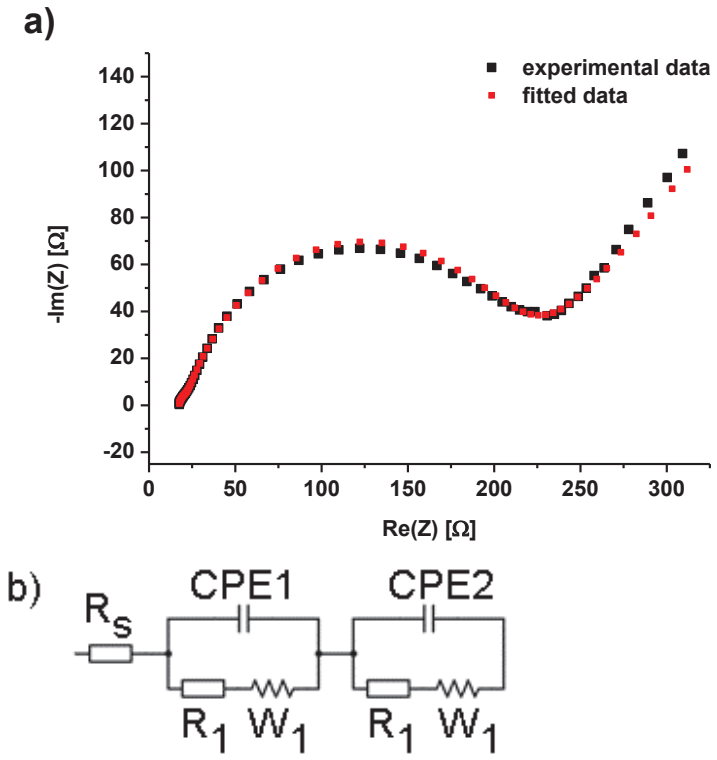

FIGURE S7 Electrochemical impedance spectroscopy data of a lithium organic battery of polymer **4h** in EC/DMC 1/4 (*v*/*v*), 1 M $LiClO_4$ (a) and the equivalent circuit (b) used to fit the experimental data.

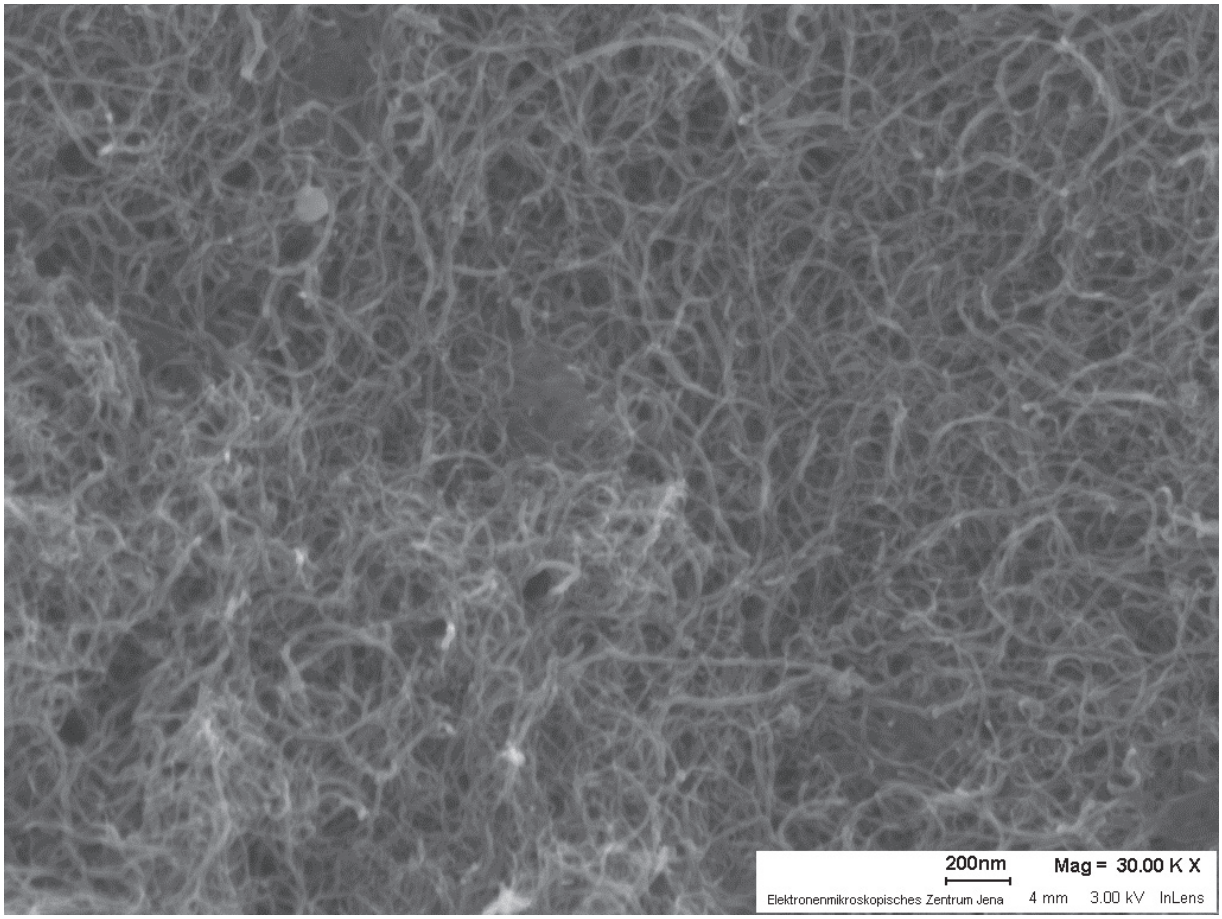

FIGURE S 8 SEM picture of a composite electrode (**4h**/PVDF/MWCNT 1/1/8 (*w*/*w*/*w*)).

REFERENCES AND NOTES

S1 J. E. B. Randles, *Discuss. Faraday Soc.* **1947**, 1, 11-19..

S2 J. R. Macdonald, ed., "Impedance Spectroscopy: Theory, Experiment, and Applications", *John Wiley* **1987**.

S3 S. Yoshihara, H. Isozumi, M. Kasai, H. Yonehara, Y. Ando, K. Oyaizu, H. Nishide, *J. Phys. Chem. B* **2010**, 114, 8335-8340.

S4 S. Yoshihara, H. Katsuta, H.Isozumi, M.Kasai, K. Oyaizu, H. Nishide, *J. Power Sources* **2011**, 196, 7806-7811.